Martin Neumüller

Space-Time Methods

Monographic Series TU Graz

Computation in Engineering and Science

Series Editors

Monographic Series TU Graz

Computation in Engineering and Science **Volume 20**

Martin Neumüller

Space-Time Methods

Fast Solvers and Applications

This work is based on the dissertation *"Space-Time Methods: Fast Solvers and Applications"*, presented by Martin Neumüller at Graz University of Technology, Institute of Computational Mathematics in June 2013.
Supervisor: O. Steinbach (Graz University of Technology)
Reviewer: G. Wittum (Goethe-University, Frankfurt am Main)

Bibliographic information published by Die Deutsche Bibliothek.
Die Deutsche Bibliothek lists this publication in the Deutsche Nationalbibliografie; detailed bibliographic data are available at http://dnb.ddb.de.

Cover photo	Vier-Spezies-Rechenmaschine by courtesy of the Gottfried Wilhelm Leibniz Bibliothek – Niedersächsische Landesbibliothek Hannover
Layout	Wolfgang Karl, TU Graz / Universitätsbibliothek Christina Fraueneder, TU Graz / Büro des Rektorates
Printed	by TU Graz / Büroservice

Verlag der Technischen Universität Graz

www.ub.tugraz.at/Verlag

ISBN: 978-3-85125-290-3 (print)
ISBN: 978-3-85125-291-0 (e-book)

DOI: 10.3217/978-3-85125-290-3

CONTENTS

1 INTRODUCTION

The philosophy of space-time methods is, to treat the time direction as an additional spatial coordinate. For the numerical solution of time dependent problems we therefore have to discretize the problem in the space-time domain or on so called space-time slabs. A simple way to derive a space-time method is, to use a standard finite element discretization in space combined with a discontinuous Galerkin time stepping scheme in time. This leads to a discretization scheme, where the space-time domain is decomposed by tensor product space-time elements. For this type of space-time methods a global time step size with respect to the spatial discretization is used. Such methods have been applied and analyzed for several problems in [24,25,27,49,50,77,78,97,105]. Space-time methods based on other discretization schemes, like least square methods are considered for example in [10,60,65,92–95] and wavelet space-time methods have been studied for example in [2,37,84].

In this work we will focus on space-time discretization schemes based on discontinuous Galerkin methods [36,48,52,66,67,91,100,104]. The original discontinuous Galerkin method was introduced in [75] to solve the neutron transport equation. Here we will apply an interior penalty approach in space [5,9,79], and an upwind technique in time [86,97]. This results in a flexible method, where almost arbitrary space-time elements can be used for the decomposition of the space-time domain.

One big advantage of space-time methods is, that they can treat moving domains in a natural way, because the moving boundary is continuously given with respect to time and therefore no projections between two different deformed meshes have to be computed. This allows the construction of conservative methods in space and time. In [92–95] least square space-time methods are used to solve flow problems for moving domains, whereas discontinuous Galerkin methods are used in [52,100].

Another big advantage of space-time methods is, that it is possible to apply local refinements in the space-time domain to resolve the local behaviour of the exact solution. Such local singularities may occur when problems with moving boundaries have to be solved or when problems with non-linearities are considered, like it is the case for flow problems. In [2,6,37,76,84] adaptive wavelet space-time methods are considered for parabolic problems and in [26,62] discontinuous Galerkin methods based on tensor product space-time elements are used

for an adaptive space-time approach. For hyperbolic problems adaptive discontinuous Galerkin methods are applied in [1,15,96] where unstructured space-time elements are used to resolve the moving shock fronts.

For discontinuous Galerkin methods it is possible to derive hybrid methods by introducing additional Lagrange multipliers on the sceleton of the mesh or on the interface between different subdomains to couple the local degrees of freedom, see also [17,21,22,68]. In this work we will apply this hybridization technique to derive a hybrid space-time formulation, which allows to eliminate the local degrees of freedom on the element level or to apply domain decomposition methods in space and time.

For space-time decompositions which form so called space-time slabs, we will derive a multigrid method in space and time for solving the upcoming linear systems. Multigrid methods for solving parabolic problems were first considered in [38] and were further developed in [44, 45, 47, 57, 101, 102, 107]. The big advantage of these methods is, that they can be applied in parallel with respect to time. Another method to solve time dependent problems parallel in time is for example the parareal algorithm, which have been introduced in [55] and has been analyzed in [7, 33, 58, 59, 87]. A lot of applications can be found, for example, in [30, 31, 34, 35, 80]. Multiple shooting methods [51, 71] can be also used in parallel with respect to time. In this work we will focus on a multigrid approach which will be analyzed by using the local Fourier mode analysis. This type of analysis was introduced in [12] and the rigorous analysis was done in [13]. The local Fourier mode analysis has been used for a large class of problems, see for example [90, 99, 108] and is regarded to special model problems, namely those with periodic boundary conditions on rectangular domains. For general boundary conditions this type of analysis can be used to study the local behavior of the two-grid algorithm, therefore it is also called local Fourier mode analysis.

For two-dimensional spatial domains the space-time domain is given by a three-dimensional object, which can be decomposed in unstructured space-time elements by applying standard three-dimensional meshing tools, like [85]. For complicated three-dimensional spatial domains, one has to construct a four-dimensional decomposition of the space-time domain into finite elements. If the domain is not moving with respect to time, the easiest way to get a space-time decomposition, is to use tensor product space-time elements. But for moving three-dimensional spatial domains one has to generate a four-dimensional unstructured space-time decomposition. In [10] four-dimensional simplex space-time elements are generated by using the Delaunay method. In [64] unstructured four-dimensional space-time meshes are generated by using the Tent-Pitcher algorithm to solve hyperbolic problems in the space-time domain, see also [111].

Outline:

For the heat equation, as a model problem, a discontinuous Galerkin space-time discretization is introduced in Chapter 2 for unstructured space-time decompositions. For this model problem an error analysis will be given by showing the boundedness and the stability of the discontinuous Galerkin method. At the end of Chapter 2 numerical examples will be given, which confirm the proven error estimates.

Based on the space-time method of Chapter 2, a hybrid space-time discretization scheme will be presented in Chapter 3 by subdividing the space-time domain into non-overlapping subdomains. The equivalent system of linear algebraic equations of this method allows the use of parallel solution algorithms, as they are used in domain decomposition methods. Moreover, an error analysis will be given, which will be confirmed by some numerical examples at the end of Chapter 3.

In Chapter 4 a space-time multigrid method will be introduced, which is based on the use of space-time slabs. The two-grid cycle of this method will be analyzed by using the local Fourier mode analysis. First this analysis will be applied to an ordinary differential equation and the results will be used to analyze the full space-time two-grid cycle. To show the robustness with respect to the discretization parameters several numerical examples will be given at the end of Chapter 4. Moreover, the parallel performance of this approach will be shown at the end of the chapter.

Applications of this space-time approaches to the Navier-Stokes equations will be given in Chapter 5. First the discontinuous Galerkin approach will be introduced and afterwards a hybridization technique will be applied. Numerical examples will show the expected convergence of this approaches. Moreover, to show the advantage of this approach, the flow in a two-dimensional pump will be simulated at the end of Chapter 5.

In the last chapter conclusions will be given and possible future work will be discussed.

2 SPACE-TIME DISCRETIZATIONS

In this chapter a space-time discretization for the heat equation, as a model problem, will be presented and analyzed. This discretization scheme is based on a discontinuous Galerkin approach in space and time, see also [66, 67]. This approach allows the use of arbitrary elements in space and time which has advantages when we have to deal with moving domains or if we need to do local refinements in the space-time domain. For other discontinuous Galerkin discretization schemes in space and time, where the discretization is based on so called space-time slabs and where the finite space-time elements are based on a tensor product structure, see for example [36, 52, 91, 100, 104]. In this work, we will allow unstructered decompositions for the space-time domain. Other space-time methods which are not based on discontinuous Galerkin methods are for example least square methods, which are considered in [10, 60, 65, 92–95].

Let $T > 0$ be a given simulation end time. For $t \in [0,T]$ we consider a bounded Lipschitz domain $\Omega(t) \subset \mathbb{R}^d$, $d = 1,2,3$ with boundary $\partial\Omega = \overline{\Gamma}_D \cup \overline{\Gamma}_N$, $\Gamma_D \cap \Gamma_N = \emptyset$. As a model problem we will study the heat equation

$$\begin{aligned} \partial_t u(x,t) - \Delta u(x,t) &= f(x,t) && \text{for } (x,t) \in Q := \Omega \times (0,T), \\ u(x,t) &= 0 && \text{for } (x,t) \in \Sigma_D := \Gamma_D \times (0,T), \\ n_x(x,t) \cdot \nabla_x u(x,t) &= g_N(x,t) && \text{for } (x,t) \in \Sigma_N := \Gamma_N \times (0,T), \\ u(x,0) &= u_0(x) && \text{for } (x,t) \in \Sigma_0 := \Omega(0) \times \{0\}. \end{aligned} \tag{2.1}$$

In view of [56, chapter 4] we assume $f \in L_2(Q)$, $g_N \in L_2(\Sigma_N)$ and $u_0 \in H^{\frac{1}{2}}(\Omega(0))$. An example for a possible space-time domain Q is given in Figure 2.1(a) for $d = 1$. In Section 2.1 the space-time discretization scheme for the model problem (2.1) will be presented and the numerical analysis for this approach will be given in Section 2.2. Finally numerical examples will be presented in Section 2.3.

2.1 Discretization

In this section a discrete variational formulation for the model problem (2.1) will be presented. The idea of this approach is to discretize the time dependent problem (2.1) in the entire space-time domain $Q = \Omega \times (0,T)$ at once. To do so,

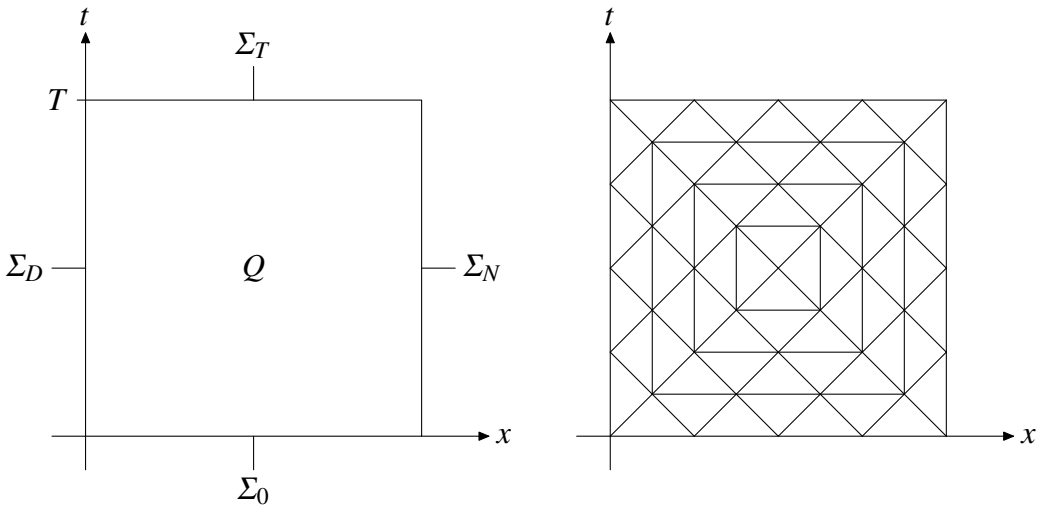

(a) Space-time domain Q. (b) Decomposition $\mathcal{T}_N$.

Figure 2.1: Space-time domain Q for $d = 1$ with a possible decomposition $\mathcal{T}_N$.

we need a decomposition of the space-time domain Q into $N \in \mathbb{N}$ simplices τ_ℓ of mesh size $h_\ell = \sqrt[d+1]{|\tau_\ell|}$

$$\overline{Q} = \overline{\mathcal{T}_N} := \bigcup_{\ell=1}^{N} \overline{\tau}_\ell.$$

For $d = 1$ an example for a possible decomposition $\mathcal{T}_N$ is given in Figure 2.1(b). Here we consider the simplest finite elements which are triangles for $d = 1$, tetrahedra for $d = 2$ and pentatopes for $d = 3$. To avoid additional numerical errors we assume that the space-time domain Q has a polygonal ($d = 1$), a polyhedral ($d = 2$), or a polychoral ($d = 3$) boundary ∂Q. Otherwise, one has to take the additional variational crimes into account.

Definition 2.1.1 (Interior facet)**.** *Let $\mathcal{T}_N$ be a decomposition of the space-time domain Q into finite elements τ_ℓ, $\ell = 1, \ldots, N$. For two neighboring elements $\tau_k, \tau_\ell \in \mathcal{T}_N$ the interior facet $\Gamma_{k\ell}$ is given by*

$$\Gamma_{k\ell} := \overline{\tau}_k \cap \overline{\tau}_\ell,$$

if the set $\Gamma_{k\ell}$ forms a d-dimensional manifold. The set of all interior facets of the decomposition $\mathcal{T}_N$ will be denoted by $\mathcal{I}_N$.

To derive a discrete variational formulation for the model problem (2.1), we need to have the following definitions for a function on an interior facet $\Gamma_{k\ell}$.

Definition 2.1.2 (Jump, average, upwind)**.** *Let $\Gamma_{k\ell} \in \mathcal{I}_N$ be an interior facet with the outer unit normal vector $n_k = (n_{k,x}, n_{k,t})^\top$ with respect to τ_k and with*

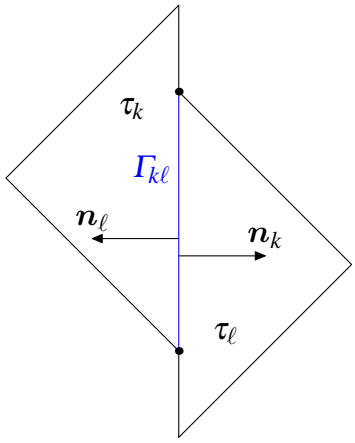

Figure 2.2: Interior facet $\Gamma_{k\ell}$ with normal vectors $\boldsymbol{n}_k$ and $\boldsymbol{n}_\ell$ for $d = 1$.

the outer unit normal vector $\boldsymbol{n}_\ell = -\boldsymbol{n}_k$ with respect to τ_ℓ, see also Figure 2.2. For a given function v the jump across the interior facet $\Gamma_{k\ell}$ is defined by

$$[v]_{\Gamma_{k\ell}}(\boldsymbol{x},t) := v_{|\tau_k}(\boldsymbol{x},t)\,\boldsymbol{n}_k + v_{|\tau_\ell}(\boldsymbol{x},t)\,\boldsymbol{n}_\ell \quad \text{for } (\boldsymbol{x},t) \in \Gamma_{k\ell}.$$

The jump in space direction is given by

$$[v]_{\Gamma_{k\ell},\boldsymbol{x}}(\boldsymbol{x},t) := v_{|\tau_k}(\boldsymbol{x},t)\,\boldsymbol{n}_{k,\boldsymbol{x}} + v_{|\tau_\ell}(\boldsymbol{x},t)\,\boldsymbol{n}_{\ell,\boldsymbol{x}} \quad \text{for } (\boldsymbol{x},t) \in \Gamma_{k\ell},$$

whereas the jump in time direction is defined by

$$[v]_{\Gamma_{k\ell},t}(\boldsymbol{x},t) := v_{|\tau_k}(\boldsymbol{x},t)\,n_{k,t} + v_{|\tau_\ell}(\boldsymbol{x},t)\,n_{\ell,t} \quad \text{for } (\boldsymbol{x},t) \in \Gamma_{k\ell}.$$

The average of a function v on the interior facet $\Gamma_{k\ell}$ is

$$\langle v \rangle_{\Gamma_{k,\ell}}(\boldsymbol{x},t) := \frac{1}{2}\left[v_{|\tau_k}(\boldsymbol{x},t) + v_{|\tau_\ell}(\boldsymbol{x},t)\right] \quad \text{for } (\boldsymbol{x},t) \in \Gamma_{k\ell},$$

and the upwind in time direction is given by

$$\{v\}^{\mathrm{up}}_{\Gamma_{k\ell}}(\boldsymbol{x},t) := \begin{cases} v_{|\tau_k}(\boldsymbol{x},t) & \text{for } n_{k,t} > 0, \\ 0 & \text{for } n_{k,t} = 0, \\ v_{|\tau_\ell}(\boldsymbol{x},t) & \text{for } n_{k,t} < 0, \end{cases} \quad \text{for } (\boldsymbol{x},t) \in \Gamma_{k\ell}.$$

Remark 2.1.3. *In Definition 2.1.2 the jumps, averages and upwind values for a given function v on an interior facet $\Gamma_{k\ell}$ are independent from the ordering of the finite elements τ_k and τ_ℓ.*

Definition 2.1.4 (Broken Sobolev space)**.** *Let $\mathcal{T}_N$ be a decomposition of the space-time domain Q. For $s \geq 0$ the broken Sobolev space is given by*

$$H^s(\mathcal{T}_N) := \left\{ v \in L_2(Q) : v_{|\tau_\ell} \in H^s(\tau_\ell) \text{ for all } \tau_\ell \in \mathcal{T}_N \right\}.$$

For a given decomposition $\mathcal{T}_N$ of the space-time domain Q into finite elements we introduce the discrete function space of piecewise polynomials of degree p by

$$S_h^p(\mathcal{T}_N) := \left\{ v_h \in L_2(Q) : v_{h|\tau_\ell} \in \mathbb{P}_p(\tau_\ell) \text{ for all } \tau_\ell \in \mathcal{T}_N \text{ and } v_h = 0 \text{ on } \Sigma_D \right\}.$$

We now assume that we have a classical solution u of the heat equation (2.1). If we multiply the first equation of (2.1) with a test function $v_h \in S_h^p(\mathcal{T}_N)$ and apply integration by parts for the time derivative $\partial_t u$ and the Laplacian Δu we end up with the discrete variational problem:

Find $u_h \in S_h^p(\mathcal{T}_N)$ such that

$$A(u_h, v_h) = \langle f, v_h \rangle_Q + \langle u_0, v_h \rangle_{\Sigma_0} + \langle g_N, v_h \rangle_{\Sigma_N} \tag{2.2}$$

for all $v_h \in S_h^p(\mathcal{T}_N)$.

In (2.2) the bilinear form $A(\cdot,\cdot)$ is given by

$$A(u_h, v_h) := b(u_h, v_h) + a(u_h, v_h), \tag{2.3}$$

where the bilinear form $a(\cdot,\cdot)$ results from an interior penalty Galerkin approximation for the Laplacian Δu

$$\begin{aligned} a(u_h, v_h) := & \sum_{\ell=1}^{N} \int_{\tau_\ell} \nabla_{\boldsymbol{x}} u_h(\boldsymbol{x},t) \cdot \nabla_{\boldsymbol{x}} v_h(\boldsymbol{x},t) \mathrm{d}(\boldsymbol{x},t) \\ & - \sum_{\Gamma_{k\ell} \in \mathcal{I}_N} \int_{\Gamma_{k\ell}} \langle \nabla_{\boldsymbol{x}} u_h \rangle_{\Gamma_{k\ell}} (\boldsymbol{x},t) \cdot [v_h]_{\Gamma_{k\ell},\boldsymbol{x}} (\boldsymbol{x},t) \mathrm{d}s_{(\boldsymbol{x},t)} \\ & - \sum_{\Gamma_{k\ell} \in \mathcal{I}_N} \int_{\Gamma_{k\ell}} [u_h]_{\Gamma_{k\ell},\boldsymbol{x}} (\boldsymbol{x},t) \cdot \langle \nabla_{\boldsymbol{x}} v_h \rangle_{\Gamma_{k\ell}} (\boldsymbol{x},t) \mathrm{d}s_{(\boldsymbol{x},t)} \\ & + \sum_{\Gamma_{k\ell} \in \mathcal{I}_N} \frac{\sigma}{\overline{h}_{k\ell}} \int_{\Gamma_{k\ell}} [u_h]_{\Gamma_{k\ell},\boldsymbol{x}} \cdot [v_h]_{\Gamma_{k\ell},\boldsymbol{x}} \mathrm{d}s_{(\boldsymbol{x},t)}, \end{aligned} \tag{2.4}$$

with the average mesh size $\overline{h}_{k\ell} := \frac{1}{2}(h_k + h_\ell)$ for an interior facet $\Gamma_{k\ell}$ and the stabilization parameter $\sigma > 0$, which has to be chosen appropriately. In addition the bilinear form $b(\cdot,\cdot)$ results from an approximation of the time derivative $\partial_t u$

$$\begin{aligned} b(u_h, v_h) := & - \sum_{\ell=1}^{N} \int_{\tau_\ell} u_h(\boldsymbol{x},t) \partial_t v_h(\boldsymbol{x},t) \mathrm{d}(\boldsymbol{x},t) + \int_{\Sigma_T} u_h(\boldsymbol{x},t) v_h(\boldsymbol{x},t) \mathrm{d}s_{(\boldsymbol{x},t)} \\ & + \sum_{\Gamma_{k\ell} \in \mathcal{I}_N} \int_{\Gamma_{k\ell}} \{u_h\}_{\Gamma_{k\ell}}^{\mathrm{up}} (\boldsymbol{x},t) \, [v_h]_{\Gamma_{k\ell},t} (\boldsymbol{x},t) \mathrm{d}s_{(\boldsymbol{x},t)}, \end{aligned} \tag{2.5}$$

with $\Sigma_T := \Omega(T) \times \{T\}$.

Remark 2.1.5. *For the bilinear form $a(\cdot,\cdot)$ we use the symmetric interior penalty Galerkin method, where the penalty parameter σ is a positive constant and depends on the polynomial degree p, see also [5, 20, 79]. As a different stabilization method, one may use a lifting operator as it is used for the Bassi-Rebay stabilization, see [4, 5, 8, 91].*

Remark 2.1.6. *By integrating by parts, the bilinear form $b(\cdot,\cdot)$ can be also written in the form*

$$b(u_h,v_h) = \sum_{\ell=1}^{N} \int_{\tau_\ell} \partial_t u_h(\boldsymbol{x},t) v_h(\boldsymbol{x},t) \mathrm{d}(\boldsymbol{x},t) + \int_{\Sigma_0} u_h(\boldsymbol{x},t) v_h(\boldsymbol{x},t) \mathrm{d}s_{(\boldsymbol{x},t)} - \sum_{\Gamma_{k\ell}\in\mathcal{I}_N} \int_{\Gamma_{k\ell}} [u_h]_{\Gamma_{k\ell},t}(\boldsymbol{x},t) \{v_h\}^{\mathrm{down}}_{\Gamma_{k\ell}}(\boldsymbol{x},t) \mathrm{d}s_{(\boldsymbol{x},t)}$$

for all $u_h, v_h \in S_h^p(\mathcal{T}_N)$. Note that the downwind value on an interior facet $\Gamma_{k\ell}$ is given by

$$\{v\}^{\mathrm{down}}_{\Gamma_{k\ell}}(\boldsymbol{x},t) := \begin{cases} v_{|\tau_\ell}(\boldsymbol{x},t) & \text{for } n_{k,t} > 0, \\ 0 & \text{for } n_{k,t} = 0, \\ v_{|\tau_k}(\boldsymbol{x},t) & \text{for } n_{k,t} < 0 \end{cases} \quad \text{for } (\boldsymbol{x},t) \in \Gamma_{k\ell}.$$

This alternative representation of the bilinear form $b(\cdot,\cdot)$ can be also derived by interpreting the time derivative $\partial_t u$ and the initial condition in the weak sense.

Remark 2.1.7. *Let $u \in H^s(\mathcal{T}_N)$ with $s > \frac{3}{2}$ be the exact solution of the model problem (2.1). Further let $u_h \in S_h^p(\mathcal{T}_N)$ be the solution of the discrete problem (2.2), then the Galerkin orthogonality*

$$A(u - u_h, v_h) = 0 \qquad \text{for all } v_h \in S_h^p(\mathcal{T}_N) \tag{2.6}$$

is satisfied. The Galerkin orthogonality can be proven by applying integration by parts, see also [20, 66, 79].

Remark 2.1.8. *Inhomogeneous Dirichlet boundary conditions can be easily imposed by an extension or by adding penalty terms, see [79, 91].*

Let φ_j, $j = 1,\dots,M$ be a basis of the discrete function space $S_h^p(\mathcal{T}_N)$, i.e.

$$S_h^p(\mathcal{T}_N) = \operatorname{span}\left\{\varphi_j\right\}_{j=1}^{M}, \qquad u_h(\boldsymbol{x},t) = \sum_{j=1}^{M} \boldsymbol{u}[j]\varphi_j(\boldsymbol{x},t) \quad \text{for } u_h \in S_h^p(\mathcal{T}_N).$$

Then the discrete variational problem (2.2) is equivalent to the system of linear algebraic equations

$$A_h \boldsymbol{u} = \boldsymbol{f} \tag{2.7}$$

with

$$A_h[i,j] := A(\varphi_j,\varphi_i) \qquad \text{and} \qquad \boldsymbol{f}[i] = \langle f,\varphi_i\rangle_Q + \langle u_0,\varphi_i\rangle_{\Sigma_0} + \langle g_N,\varphi_i\rangle_{\Sigma_N}$$

for $i,j = 1,\dots,M$.

2.2 Numerical analysis

In this section the discrete problem (2.2) will be analyzed. First the boundedness and the stability of the two bilinear forms $a(\cdot,\cdot)$ and $b(\cdot,\cdot)$ will be investigated. After that, the stability and boundedness of the bilinear form $A(\cdot,\cdot)$ will be proven, by following the ideas as used in the work [21]. At the end of this section related error estimates will be given.

First we need to make some assumptions on the triangulation $\mathcal{T}_N$.

Assumption 2.2.1 (Shape regularity)**.** *For the family of space-time decompositions $\mathcal{T}_N$ we assume shape regularity. For the measure of an element boundary $\partial\tau_\ell$ this assumption implies a lower and an upper bound with respect to the mesh size h_ℓ*

$$c_{R_1} h_\ell^d \leq |\partial\tau_\ell| \leq c_{R_2} h_\ell^d \qquad \text{for all } \tau_\ell \in \mathcal{T}_N.$$

For the measure of an element τ_ℓ we have by definition

$$|\tau_\ell| = h_\ell^{d+1} \qquad \text{for all } \tau_\ell \in \mathcal{T}_N.$$

Assumption 2.2.2 (Local mesh grading)**.** *For two neighbouring elements $\tau_k, \tau_\ell \in \mathcal{T}_N$ with interior facet $\Gamma_{k\ell}$ we assume local mesh grading, i.e.*

$$\tilde{c}_G^{-1} \leq \frac{h_k}{h_\ell} \leq \tilde{c}_G \qquad \text{with } \tilde{c}_G \geq 1.$$

This assumption implies also lower and upper bounds for the average mesh size $\overline{h}_{k\ell} = \frac{1}{2}(h_k + h_\ell)$

$$c_G^{-1} \leq \frac{\overline{h}_{k\ell}}{h_k} \leq c_G, \qquad c_G^{-1} \leq \frac{\overline{h}_{k\ell}}{h_\ell} \leq c_G \qquad \text{with } c_G \geq 1.$$

Lemma 2.2.3 (Inverse inequalities)**.** *For any discrete function $v_h \in S_h^p(\mathcal{T}_N)$ there holds for all interior facets $\Gamma_{k\ell} \in \mathcal{I}_N$ the inverse inequalities*

$$\|v_h\|_{L_2(\Gamma_{k\ell})} \leq c_I \, |\Gamma_{k\ell}|^{\frac{1}{2}} \, |\tau_\ell|^{-\frac{1}{2}} \, \|v_h\|_{L_2(\tau_\ell)}, \tag{2.8}$$

$$\|\nabla_{\boldsymbol{x}} v_h\|_{[L_2(\Gamma_{k\ell})]^d} \leq c_I \, |\Gamma_{k\ell}|^{\frac{1}{2}} \, |\tau_\ell|^{-\frac{1}{2}} \, \|\nabla_{\boldsymbol{x}} v_h\|_{[L_2(\tau_\ell)]^d}. \tag{2.9}$$

$$\|v_h\|_{H^1(\Gamma_{k\ell})} \leq c_I \overline{h}_{k\ell}^{-1} \, \|v_h\|_{L_2(\Gamma_{k\ell})}. \tag{2.10}$$

For all $\tau_\ell \in \mathcal{T}_N$ there also holds

$$\|v_h\|_{H^1(\tau_\ell)} \leq c_I h_\ell^{-1} \|v_h\|_{L_2(\tau_\ell)}, \tag{2.11}$$

Proof. The proof of (2.8) and (2.9) can be found in [20]. For the inverse inequality (2.11) see [20, 89]. The proof of the inequality (2.10) can be found in [110]. For arbitrary simplices see also [106]. ∎

Remark 2.2.4. *The constants of the inverse inequalities (2.8)–(2.11) depend on the polynomial degree p. For the inequalities (2.8) and (2.9) the constant c_I depend linearly on the polynomial degree p, i.e. $c_I = c_I(p)$ and for the inequalities (2.10) and (2.11) we have $c_I = c_I(p^2)$.*

Lemma 2.2.5 (Young's inequality)**.** *Let $x, y \in \mathbb{R}$, then there holds*

$$xy \leq \frac{\varepsilon}{2}x^2 + \frac{1}{2\varepsilon}y^2, \qquad \text{for any } \varepsilon > 0.$$

Proof. The statement of the lemma follows by using the inequality of arithmetic and geometric means

$$xy = \left(\varepsilon^{\frac{1}{2}}x\right)\left(\varepsilon^{-\frac{1}{2}}y\right) \leq \frac{1}{2}\left[\varepsilon x^2 + \varepsilon^{-1}y^2\right].$$

∎

In the following we are going to analyze the properties of the bilinear form $A(\cdot,\cdot)$. To do so, we first have to define energy norms with respect to the bilinear form $a(\cdot,\cdot)$. For a function $u \in H^s(\mathcal{T}_N)$ with $s > \frac{3}{2}$ we define

$$\begin{aligned}
\|u\|_A^2 &:= \sum_{\ell=1}^{N} \|\nabla_{\boldsymbol{x}} u\|^2_{[L_2(\tau_\ell)]^d} + \sum_{\Gamma_{k\ell}\in\mathcal{I}_N} \frac{\sigma}{\overline{h}_{k\ell}} \left\| [u]_{\Gamma_{k\ell},\boldsymbol{x}} \right\|^2_{[L_2(\Gamma_{k\ell})]^d}, \\
\|u\|_{A,*}^2 &:= \|u\|_A^2 + \sum_{\Gamma_{k\ell}\in\mathcal{I}_N} \overline{h}_{k\ell} \left\| \langle \nabla_{\boldsymbol{x}} u \rangle_{\Gamma_{k\ell}} \right\|^2_{[L_2(\Gamma_{k\ell})]^d}.
\end{aligned}$$

To analyze the bilinear form $b(\cdot,\cdot)$ we will use the following two norms for functions $u \in H^s(\mathcal{T}_N)$ with $s \geq 1$

$$\begin{aligned}
\|u\|_B^2 &:= \sum_{\ell=1}^{N} h_\ell \|\partial_t u\|^2_{L_2(\tau_\ell)} + \|u\|^2_{\Sigma_0} + \|u\|^2_{\Sigma_T} + \sum_{\Gamma_{k\ell}\in\mathcal{I}_N} \left\| [u]_{\Gamma_{k\ell},t} \right\|^2_{L_2(\Gamma_{k\ell})}, \\
\|u\|_{B,*}^2 &:= \sum_{\ell=1}^{N} h_\ell^{-1} \|u\|^2_{L_2(\tau_\ell)} + \|u\|^2_{\Sigma_T} + \sum_{\Gamma_{k\ell}\in\mathcal{I}_N} \left\| \{u\}^{\mathrm{up}}_{\Gamma_{k\ell}} \right\|^2_{L_2(\Gamma_{k\ell})}.
\end{aligned}$$

The next lemma will be used to give a bound for the bilinear form $a(\cdot,\cdot)$.

Lemma 2.2.6. *For all $u_h \in S_h^p(\mathcal{T}_N)$ there holds the estimate*

$$\sum_{\Gamma_{k\ell}\in\mathcal{I}_N} \overline{h}_{k\ell} \left\| \langle \nabla_{\boldsymbol{x}} u_h \rangle_{\Gamma_{k\ell}} \right\|^2_{[L_2(\Gamma_{k\ell})]^d} \leq c_K \sum_{\ell=1}^N \|\nabla_{\boldsymbol{x}} u_h\|^2_{[L_2(\tau_\ell)]^d},$$

with the constant $c_K = c_K(c_I, c_G, c_{R_2})$.

Proof. For $u_h \in S_h^p(\mathcal{T}_N)$ we have

$$\begin{aligned}\sum_{\Gamma_{k\ell}\in\mathcal{I}_N} \overline{h}_{k\ell} \left\| \langle \nabla_{\boldsymbol{x}} u_h \rangle_{\Gamma_{k\ell}} \right\|^2_{[L_2(\Gamma_{k\ell})]^d} &= \sum_{\Gamma_{k\ell}\in\mathcal{I}_N} \overline{h}_{k\ell} \left\| \frac{1}{2} \left[\nabla_{\boldsymbol{x}} u_{h|\tau_k} + \nabla_{\boldsymbol{x}} u_{h|\tau_\ell} \right] \right\|^2_{[L_2(\Gamma_{k\ell})]^d} \\ &\leq \sum_{\Gamma_{k\ell}\in\mathcal{I}_N} \overline{h}_{k\ell} \left[\left\| \nabla_{\boldsymbol{x}} u_{h|\tau_k} \right\|^2_{[L_2(\Gamma_{k\ell})]^d} + \left\| \nabla_{\boldsymbol{x}} u_{h|\tau_\ell} \right\|^2_{[L_2(\Gamma_{k\ell})]^d} \right].\end{aligned}$$

Applying the inverse inequality (2.9) leads to the estimate

$$\leq \sum_{\Gamma_{k\ell}\in\mathcal{I}_N} \overline{h}_{k\ell} c_I^2 |\Gamma_{k\ell}| \left[|\tau_k|^{-1} \|\nabla_{\boldsymbol{x}} u_h\|^2_{[L_2(\tau_k)]^d} + |\tau_\ell|^{-1} \|\nabla_{\boldsymbol{x}} u_h\|^2_{[L_2(\tau_\ell)]^d} \right].$$

If we rewrite the sum over all interior facets we get

$$\begin{aligned}&= c_I^2 \sum_{\ell=1}^N \sum_{\substack{\Gamma_{k\ell}\in\mathcal{I}_N \\ \Gamma_{k\ell}\subset\partial\tau_\ell}} \overline{h}_{k\ell} |\Gamma_{k\ell}| \, |\tau_\ell|^{-1} \|\nabla_{\boldsymbol{x}} u_h\|^2_{[L_2(\tau_\ell)]^d} \\ &= c_I^2 \sum_{\ell=1}^N |\tau_\ell|^{-1} \|\nabla_{\boldsymbol{x}} u_h\|^2_{[L_2(\tau_\ell)]^d} \sum_{\substack{\Gamma_{k\ell}\in\mathcal{I}_N \\ \Gamma_{k\ell}\subset\partial\tau_\ell}} \overline{h}_{k\ell} |\Gamma_{k\ell}|.\end{aligned}$$

With Assumption 2.2.2 we further obtain the estimate

$$\begin{aligned}&\leq c_I^2 \sum_{\ell=1}^N |\tau_\ell|^{-1} \|\nabla_{\boldsymbol{x}} u_h\|^2_{[L_2(\tau_\ell)]^d} c_G h_\ell \sum_{\substack{\Gamma_{k\ell}\in\mathcal{I}_N \\ \Gamma_{k\ell}\subset\partial\tau_\ell}} |\Gamma_{k\ell}| \\ &\leq c_I^2 c_G \sum_{\ell=1}^N |\tau_\ell|^{-1} h_\ell |\partial\tau_\ell| \, \|\nabla_{\boldsymbol{x}} u_h\|^2_{[L_2(\tau_\ell)]^d}.\end{aligned}$$

The statement of the lemma follows if we use Assumption 2.2.1 and $|\tau_\ell| = h_\ell^{d+1}$

$$\leq c_I^2 c_G c_{R_2} \sum_{\ell=1}^N \|\nabla_{\boldsymbol{x}} u_h\|^2_{[L_2(\tau_\ell)]^d}.$$

■

Lemma 2.2.7. *The bilinear form $a(\cdot,\cdot)$ as defined in (2.4) is bounded, i.e.*

$$a(u,v_h) \leq c_2^a \, \|u\|_{A,*} \|v_h\|_A,$$

for all $u \in H^s(\mathcal{T}_N)$ with $s > \frac{3}{2}$ and for all $v_h \in S_h^p(\mathcal{T}_N)$ with an h-independent constant $c_2^a > 0$.

Proof. For a function $u \in H^s(\mathcal{T}_N)$ and a function $v_h \in S_h^p(\mathcal{T}_N)$ we can estimate the bilinear form $a(\cdot,\cdot)$ by using the Cauchy–Schwarz inequality

$$\begin{aligned} a(u,v_h) \leq & \sum_{\ell=1}^{N} \|\nabla_{\boldsymbol{x}} u\|_{[L_2(\tau_\ell)]^d} \|\nabla_{\boldsymbol{x}} v_h\|_{[L_2(\tau_\ell)]^d} \\ & + \sum_{\Gamma_{k\ell} \in \mathcal{I}_N} \left\| \langle \nabla_{\boldsymbol{x}} u \rangle_{\Gamma_{k\ell}} \right\|_{[L_2(\tau_\ell)]^d} \left\| [v_h]_{\Gamma_{k\ell},\boldsymbol{x}} \right\|_{[L_2(\tau_\ell)]^d} \\ & + \sum_{\Gamma_{k\ell} \in \mathcal{I}_N} \left\| [u]_{\Gamma_{k\ell},\boldsymbol{x}} \right\|_{[L_2(\tau_\ell)]^d} \left\| \langle \nabla_{\boldsymbol{x}} v_h \rangle_{\Gamma_{k\ell}} \right\|_{[L_2(\tau_\ell)]^d} \\ & + \sum_{\Gamma_{k\ell} \in \mathcal{I}_N} \frac{\sigma}{\overline{h}_{k\ell}} \left\| [u]_{\Gamma_{k\ell},\boldsymbol{x}} \right\|_{[L_2(\tau_\ell)]^d} \left\| [v_h]_{\Gamma_{k\ell},\boldsymbol{x}} \right\|_{[L_2(\tau_\ell)]^d}. \end{aligned}$$

Using the Hölder inequality leads to the estimate

$$\begin{aligned} \leq & \left[\sum_{\ell=1}^{N} \|\nabla_{\boldsymbol{x}} u\|^2_{[L_2(\tau_\ell)]^d} \right]^{\frac{1}{2}} \left[\sum_{\ell=1}^{N} \|\nabla_{\boldsymbol{x}} v_h\|^2_{[L_2(\tau_\ell)]^d} \right]^{\frac{1}{2}} \\ & + \left[\sum_{\Gamma_{k\ell} \in \mathcal{I}_N} \frac{\overline{h}_{k\ell}}{\sigma} \left\| \langle \nabla_{\boldsymbol{x}} u \rangle_{\Gamma_{k\ell}} \right\|^2_{[L_2(\tau_\ell)]^d} \right]^{\frac{1}{2}} \left[\sum_{\Gamma_{k\ell} \in \mathcal{I}_N} \frac{\sigma}{\overline{h}_{k\ell}} \left\| [v_h]_{\Gamma_{k\ell},\boldsymbol{x}} \right\|^2_{[L_2(\tau_\ell)]^d} \right]^{\frac{1}{2}} \\ & + \left[\sum_{\Gamma_{k\ell} \in \mathcal{I}_N} \frac{\sigma}{\overline{h}_{k\ell}} \left\| [u]_{\Gamma_{k\ell},\boldsymbol{x}} \right\|^2_{[L_2(\tau_\ell)]^d} \right]^{\frac{1}{2}} \left[\sum_{\Gamma_{k\ell} \in \mathcal{I}_N} \frac{\overline{h}_{k\ell}}{\sigma} \left\| \langle \nabla_{\boldsymbol{x}} v_h \rangle_{\Gamma_{k\ell}} \right\|^2_{[L_2(\tau_\ell)]^d} \right]^{\frac{1}{2}} \\ & + \left[\sum_{\Gamma_{k\ell} \in \mathcal{I}_N} \frac{\sigma}{\overline{h}_{k\ell}} \left\| [u]_{\Gamma_{k\ell},\boldsymbol{x}} \right\|^2_{[L_2(\tau_\ell)]^d} \right]^{\frac{1}{2}} \left[\sum_{\Gamma_{k\ell} \in \mathcal{I}_N} \frac{\sigma}{\overline{h}_{k\ell}} \left\| [v_h]_{\Gamma_{k\ell},\boldsymbol{x}} \right\|^2_{[L_2(\tau_\ell)]^d} \right]^{\frac{1}{2}}. \end{aligned}$$

Applying Lemma 2.2.6 to the third term containing the test function v_h gives the stated bound for the bilinear form $a(\cdot,\cdot)$

$$\leq \sqrt{2 \max\{\sigma^{-1}, 1 + c_K \sigma^{-1}\}} \, \|u\|_{A,*} \|v_h\|_A.$$

■

Lemma 2.2.8. *The bilinear form $b(\cdot,\cdot)$ as given in (2.5) is bounded, i.e.*

$$b(u,v_h) \le \|u\|_{B,*}\|v_h\|_B,$$

for all $u \in H^s(\mathcal{T}_N)$ with $s \ge 1$ and for all $v_h \in S_h^p(\mathcal{T}_N)$.

Proof. Using the Cauchy–Schwarz inequality and the Hölder inequality we end up with the bound for the bilinear form $b(\cdot,\cdot)$

$$\begin{aligned}
b(u,v_h) &\le \sum_{\ell=1}^{N} \|u\|_{L_2(\tau_\ell)}\|\partial_t v_h\|_{L_2(\tau_\ell)} + \|u\|_{\Sigma_T}\|v_h\|_{\Sigma_T} \\
&\quad + \sum_{\Gamma_{k\ell}\in\mathcal{I}_N} \left\|\{u\}^{\mathrm{up}}_{\Gamma_{k\ell}}\right\|_{L_2(\Gamma_{k\ell})} \left\|[v_h]_{\Gamma_{k\ell},t}\right\|_{L_2(\Gamma_{k\ell})} \\
&\le \left[\sum_{\ell=1}^{N} h_\ell^{-1}\|u\|^2_{L_2(\tau_\ell)}\right]^{\frac{1}{2}} \left[\sum_{\ell=1}^{N} h_\ell \|\partial_t v_h\|^2_{L_2(\tau_\ell)}\right]^{\frac{1}{2}} + \|u\|_{\Sigma_T}\|v_h\|_{\Sigma_T} \\
&\quad + \left[\sum_{\Gamma_{k\ell}\in\mathcal{I}_N} \left\|\{u\}^{\mathrm{up}}_{\Gamma_{k\ell}}\right\|^2_{L_2(\Gamma_{k\ell})}\right]^{\frac{1}{2}} \left[\sum_{\Gamma_{k\ell}\in\mathcal{I}_N} \left\|[v_h]_{\Gamma_{k\ell},t}\right\|^2_{L_2(\Gamma_{k\ell})}\right]^{\frac{1}{2}} \\
&\le \|u\|_{B,*}\|v_h\|_B.
\end{aligned}$$

■

In the next lemma we will prove a lower bound for the bilinear form $a(\cdot,\cdot)$.

Lemma 2.2.9. *Let $\sigma \ge 4c_K$, with the constant c_K from Lemma 2.2.6, then for the bilinear form $a(\cdot,\cdot)$ as defined in (2.4) there holds the bound from below*

$$a(u_h,u_h) \ge \frac{1}{2}\|u_h\|_A^2 \qquad \text{for all } u_h \in S_h^p(\mathcal{T}_N).$$

Proof. For a function $u_h \in S_h^p(\mathcal{T}_N)$ we have by using the definition of $a(\cdot,\cdot)$

$$\begin{aligned}
a(u_h,u_h) &= \sum_{\ell=1}^{N} \|\nabla_{\boldsymbol{x}} u_h\|^2_{[L_2(\tau_\ell)]^d} - 2\sum_{\Gamma_{k\ell}\in\mathcal{I}_N}\int_{\Gamma_{k\ell}} \langle\nabla_{\boldsymbol{x}} u_h\rangle_{\Gamma_{k\ell}}(\boldsymbol{x},t)\cdot[u_h]_{\Gamma_{k\ell},\boldsymbol{x}}(\boldsymbol{x},t)\mathrm{d}s_{(\boldsymbol{x},t)} \\
&\quad + \sum_{\Gamma_{k\ell}\in\mathcal{I}_N} \frac{\sigma}{\overline{h}_{k\ell}} \left\|[u_h]_{\Gamma_{k\ell},\boldsymbol{x}}\right\|^2_{[L_2(\tau_\ell)]^d}.
\end{aligned}$$

Applying the Cauchy–Schwarz and the Hölder inequality gives the bound

$$\ge \|u_h\|_A^2 - 2\sum_{\Gamma_{k\ell}\in\mathcal{I}_N} \left\|\langle\nabla_{\boldsymbol{x}} u_h\rangle_{\Gamma_{k\ell}}\right\|_{[L_2(\tau_\ell)]^d} \left\|[u_h]_{\Gamma_{k\ell},\boldsymbol{x}}\right\|_{[L_2(\tau_\ell)]^d}$$

$$\geq \|u_h\|_A^2 - 2\left[\sum_{\Gamma_{k\ell}\in\mathcal{I}_N} \frac{\overline{h}_{k\ell}}{\sigma}\left\|\langle\nabla_{\boldsymbol{x}} u_h\rangle_{\Gamma_{k\ell}}\right\|^2_{[L_2(\tau_\ell)]^d}\right]^{\frac{1}{2}}\left[\sum_{\Gamma_{k\ell}\in\mathcal{I}_N}\frac{\sigma}{\overline{h}_{k\ell}}\left\|[u_h]_{\Gamma_{k\ell},\boldsymbol{x}}\right\|^2_{[L_2(\tau_\ell)]^d}\right]^{\frac{1}{2}}.$$

By using Lemma 2.2.6 we get the estimate

$$\geq \|u_h\|_A^2 - 2c_k^{\frac{1}{2}}\sigma^{-\frac{1}{2}}\left[\sum_{\ell=1}^{N}\|\nabla_{\boldsymbol{x}} u_h\|^2_{[L_2(\tau_\ell)]^d}\right]^{\frac{1}{2}}\left[\sum_{\Gamma_{k\ell}\in\mathcal{I}_N}\frac{\sigma}{\overline{h}_{k\ell}}\left\|[u_h]_{\Gamma_{k\ell},\boldsymbol{x}}\right\|^2_{[L_2(\tau_\ell)]^d}\right]^{\frac{1}{2}}.$$

Applying Young's inequality with some $\varepsilon\in\mathbb{R}_+$ gives

$$\geq \|u_h\|_A^2 - \varepsilon\sum_{\ell=1}^{N}\|\nabla_{\boldsymbol{x}} u_h\|^2_{[L_2(\tau_\ell)]^d} - \frac{c_K}{\varepsilon\sigma}\sum_{\Gamma_{k\ell}\in\mathcal{I}_N}\frac{\sigma}{\overline{h}_{k\ell}}\left\|[u_h]_{\Gamma_{k\ell},\boldsymbol{x}}\right\|^2_{[L_2(\tau_\ell)]^d},$$

and by using the assumption $\sigma\geq 4c_K$ and $\varepsilon=\frac{1}{2}$ the statement of the lemma follows with

$$\geq \frac{1}{2}\|u_h\|_A^2.$$

■

Lemma 2.2.10. *Let $\Gamma_{k\ell}\in\mathcal{I}_N$ be an interior facet and $u_h\in S_h^p(\mathcal{T}_N)$. Then the following relation holds*

$$\{u_h\}^{\mathrm{up}}_{\Gamma_{k\ell}}(\boldsymbol{x},t)\,[u_h]_{\Gamma_{k\ell},t}(\boldsymbol{x},t) - \frac{1}{2}\left[u_h^2\right]_{\Gamma_{k\ell},t}(\boldsymbol{x},t) = \frac{1}{2}\left|n_{k,t}\right|\left([u_h]_{\Gamma_{k\ell}}(\boldsymbol{x},t)\right)^2$$

for all $(\boldsymbol{x},t)\in\Gamma_{k\ell}$.

Proof. The statement of the lemma easily follows by using the Definition 2.1.2, see also [66]. ■

Lemma 2.2.11. *The bilinear form $b(\cdot,\cdot)$ as given in (2.5) is bounded from below with*

$$b(u_h,u_h)\geq\frac{1}{2}\left[\|u_h\|^2_{L_2(\Sigma_0)} + \|u_h\|^2_{L_2(\Sigma_T)} + \sum_{\Gamma_{k\ell}\in\mathcal{I}_N}\left\|[u_h]_{\Gamma_{k\ell},t}\right\|^2_{L_2(\Gamma_{k\ell})}\right]$$

for all $u_h\in S_h^p(\mathcal{T}_N)$.

Proof. Let $u_h\in S_h^p(\mathcal{T}_N)$. With the definition of the bilinear form $b(\cdot,\cdot)$ we have

$$b(u_h,u_h) = -\sum_{\ell=1}^{N}\int_{\tau_\ell} u_h(\boldsymbol{x},t)\partial_t u_h(\boldsymbol{x},t)\mathrm{d}(\boldsymbol{x},t) + \|u_h\|^2_{L_2(\Sigma_T)}$$

$$+\sum_{\Gamma_{k\ell}\in\mathcal{I}_N}\int_{\Gamma_{k\ell}}\{u_h\}^{\mathrm{up}}_{\Gamma_{k\ell}}(\boldsymbol{x},t)\,[u_h]_{\Gamma_{k\ell},t}(\boldsymbol{x},t)\mathrm{d}s_{(\boldsymbol{x},t)}.$$

Rewriting the first sum and using Gauss's theorem we obtain

$$\begin{aligned}
&=-\sum_{\ell=1}^{N}\int_{\tau_\ell}\frac{1}{2}\partial_t\left(u_h(\boldsymbol{x},t)\right)^2\mathrm{d}(\boldsymbol{x},t)+\|u_h\|^2_{L_2(\Sigma_T)}\\
&\quad+\sum_{\Gamma_{k\ell}\in\mathcal{I}_N}\int_{\Gamma_{k\ell}}\{u_h\}^{\mathrm{up}}_{\Gamma_{k\ell}}(\boldsymbol{x},t)\,[u_h]_{\Gamma_{k\ell},t}(\boldsymbol{x},t)\mathrm{d}s_{(\boldsymbol{x},t)}\\
&=-\frac{1}{2}\sum_{\ell=1}^{N}\int_{\partial\tau_\ell}n_{\ell,t}\left(u_h(\boldsymbol{x},t)\right)^2\mathrm{d}s_{(\boldsymbol{x},t)}+\|u_h\|^2_{L_2(\Sigma_T)}\\
&\quad+\sum_{\Gamma_{k\ell}\in\mathcal{I}_N}\int_{\Gamma_{k\ell}}\{u_h\}^{\mathrm{up}}_{\Gamma_{k\ell}}(\boldsymbol{x},t)\,[u_h]_{\Gamma_{k\ell},t}(\boldsymbol{x},t)\mathrm{d}s_{(\boldsymbol{x},t)}.
\end{aligned}$$

Summing up over all interior facets and over the boundaries Σ_0 and Σ_T leads to

$$\begin{aligned}
&=\frac{1}{2}\left[\|u_h\|^2_{L_2(\Sigma_0)}+\|u_h\|^2_{L_2(\Sigma_T)}\right]\\
&\quad+\sum_{\Gamma_{k\ell}\in\mathcal{I}_N}\int_{\Gamma_{k\ell}}\left[\{u_h\}^{\mathrm{up}}_{\Gamma_{k\ell}}(\boldsymbol{x},t)\,[u_h]_{\Gamma_{k\ell},t}(\boldsymbol{x},t)-\frac{1}{2}\left[u_h^2\right]_{\Gamma_{k\ell},t}(\boldsymbol{x},t)\right]\mathrm{d}s_{(\boldsymbol{x},t)}.
\end{aligned}$$

With Lemma 2.2.10 and by using $\left|n_{k,t}\right|\geq\left|n_{k,t}\right|^2$, we obtain the result of the lemma by

$$\begin{aligned}
&=\frac{1}{2}\left[\|u_h\|^2_{L_2(\Sigma_0)}+\|u_h\|^2_{L_2(\Sigma_T)}+\sum_{\Gamma_{k\ell}\in\mathcal{I}_N}\int_{\Gamma_{k\ell}}\left|n_{k,t}\right|\left([u_h]_{\Gamma_{k\ell}}(\boldsymbol{x},t)\right)^2\mathrm{d}s_{(\boldsymbol{x},t)}\right]\\
&\geq\frac{1}{2}\left[\|u_h\|^2_{L_2(\Sigma_0)}+\|u_h\|^2_{L_2(\Sigma_T)}+\sum_{\Gamma_{k\ell}\in\mathcal{I}_N}\left\|[u_h]_{\Gamma_{k\ell},t}\right\|^2_{L_2(\Gamma_{k\ell})}\right].
\end{aligned}$$

■

For $\sigma\geq 4c_K$ and $u_h\in S^p_h(\mathcal{T}_N)$ we can estimate the bilinear form $A(\cdot,\cdot)$ as defined in (2.3) from below by using Lemma 2.2.9 and Lemma 2.2.11 with

$$A(u_h,u_h)\geq\frac{1}{2}\left[\|u_h\|^2_A+\|u_h\|^2_{L_2(\Sigma_0)}+\|u_h\|^2_{L_2(\Sigma_T)}+\sum_{\Gamma_{k\ell}\in\mathcal{I}_N}\left\|[u_h]_{\Gamma_{k\ell},t}\right\|^2_{L_2(\Gamma_{k\ell})}\right].$$

This motivates the definition of the energy norm

$$\|u_h\|^2_{\widetilde{\mathrm{DG}}} := \|u_h\|^2_A + \|u_h\|^2_{L_2(\Sigma_0)} + \|u_h\|^2_{L_2(\Sigma_T)} + \sum_{\Gamma_{k\ell}\in\mathcal{I}_N} \left\| [u_h]_{\Gamma_{k\ell},t} \right\|^2_{L_2(\Gamma_{k\ell})}. \tag{2.12}$$

If the Dirichlet boundary Γ_D has non-zero measure $|\Gamma_D| > 0$, then it is easy to see that

$$\|u_h\|_{\widetilde{\mathrm{DG}}} = 0 \quad \text{implies} \quad u_h = 0$$

for $u_h \in S^p_h(\mathcal{T}_N)$. Therefore the energy norm $\|\cdot\|_{\widetilde{\mathrm{DG}}}$ implies a full norm with respect to the discrete function space $S^p_h(\mathcal{T}_N)$. Hence, for $\sigma \geq 4c_K$, the bilinear form $A(\cdot,\cdot)$ is elliptic on the space $S^p_h(\mathcal{T}_N)$ with respect to the energy norm $\|\cdot\|_{\widetilde{\mathrm{DG}}}$, i.e.

$$A(u_h,u_h) \geq \frac{1}{2}\|u_h\|^2_{\widetilde{\mathrm{DG}}} \qquad \text{for all } u_h \in S^p_h(\mathcal{T}_N). \tag{2.13}$$

Since (2.2) is a linear problem in finite dimension, the ellipticity estimate (2.13) implies the existence and uniqueness of a solution $u_h \in S^P_h(\mathcal{T}_N)$ of the discrete variational problem (2.2). In the case of a pure Neumann boundary value problem, i.e. $|\Gamma_D| = 0$, the next theorem guarantees the uniqueness of a discrete solution $u_h \in S^P_h(\mathcal{T}_N)$ of the variational problem (2.2).

Theorem 2.2.12. *Let $\sigma \geq 4c_K$, then the bilinear form $A(\cdot,\cdot)$ is injective, i.e. for $u_h \in S^p_h(\mathcal{T}_N)$ the condition*

$$A(u_h,v_h) = 0 \quad \textit{for all } v_h \in S^p_h(\mathcal{T}_N)$$

implies $u_h = 0$.

Proof. Let $u_h \in S^p_h(\mathcal{T}_N)$. The ellipticity estimate (2.13) implies

$$0 = A(u_h,u_h) \geq \frac{1}{2}\|u_h\|^2_{\widetilde{\mathrm{DG}}}$$

and therefore $\|u_h\|_{\widetilde{\mathrm{DG}}} = 0$. Hence we have

$$\nabla_{\boldsymbol{x}} u_{h|\tau_\ell} = 0 \quad \text{for all } \tau_\ell \in \mathcal{T}_N, \qquad u_h = 0 \text{ on } \Sigma_0 \cup \Sigma_T \quad \text{and} \quad u_h \in \mathcal{C}(\mathcal{T}_N). \tag{2.14}$$

Testing with the test function $v_h = \partial_t u_h \in S^p_h(\mathcal{T}_N)$ and using the alternative representation of the bilinear form $b(\cdot,\cdot)$ as given in Remark 2.1.6, we have, due to the properties (2.14), that

$$0 = A(u_h,\partial_t u_h) = \sum_{\ell=1}^{N} \|\partial_t u_h\|^2_{L_2(\tau_\ell)}.$$

This implies that $\partial_t u_{h|\tau_\ell} = 0$ for all $\tau_\ell \in \mathcal{T}_N$ and with (2.14) we conclude that $u_h = 0$. ∎

With Theorem 2.2.12 we conclude that the discrete variational problem (2.2) omits a unique solution $u_h \in S_h^p(\mathcal{T}_N)$. In view of Theorem 2.2.12 we will use special test functions with a weighted time derivative to derive a priori error estimates in some energy norm. To do so, we define the following piecewise linear weight function.

Definition 2.2.13 (Mesh function)**.** *Let $\overline{h}$ be a piecewise linear function on $\mathcal{T}_N$, i.e. $\overline{h}_{|\tau_\ell} \in \mathbb{P}^1(\tau_\ell)$ for all $\tau_\ell \in \mathcal{T}_N$, with the property*

$$c_g^{-1} h_\ell \leq \overline{h}(\boldsymbol{x},t) \leq c_g h_\ell \quad \text{for all } (\boldsymbol{x},t) \in \overline{\tau}_\ell \quad \text{and} \quad c_g \geq 1, \tag{2.15}$$

then $\overline{h}$ is called a mesh function.

For a given function $u_h \in S_h^p(\mathcal{T}_N)$ and a given mesh function $\overline{h}$ we define the new function $w_h \in S_h^p(\mathcal{T}_N)$ as

$$w_{h|\tau_\ell} := \overline{h}_{|\tau_\ell} \partial_t u_{h|\tau_\ell} \in \mathbb{P}^p(\tau_\ell) \qquad \text{for all } \tau_\ell \in \mathcal{T}_N. \tag{2.16}$$

The following techniques follow the ideas as used in the work [21].

Lemma 2.2.14. *For $u_h \in S_h^p(\mathcal{T}_N)$ let $w_h \in S_h^p(\mathcal{T}_N)$ be defined as in (2.16). Then for $\delta = (c_g^{-1} + 2c_I^2 c_{R_2} c_g^3)^{-1}$ there exists a constant $c_1^b > 0$, which is independent of the function u_h, such that the estimate*

$$b(u_h, u_h + \delta w_h) \geq c_1^b \|u_h\|_B^2$$

holds.

Proof. Let $u_h \in S_h^p(\mathcal{T}_N)$ be a given discrete function and $w_h \in S_h^p(\mathcal{T}_N)$ be defined as in (2.16). By using the representation of the bilinear form $b(\cdot,\cdot)$ as given in Remark 2.1.6 we have

$$\begin{aligned}
b(u_h, w_h) &= \sum_{\ell=1}^N \int_{\tau_\ell} \partial_t u_h(\boldsymbol{x},t) w_h(\boldsymbol{x},t) \mathrm{d}(\boldsymbol{x},t) + \int_{\Sigma_0} u_h(\boldsymbol{x},t) w_h(\boldsymbol{x},t) \mathrm{d}s_{(\boldsymbol{x},t)} \\
&\quad - \sum_{\Gamma_{k\ell} \in \mathcal{I}_N} \int_{\Gamma_{k\ell}} [u_h]_{\Gamma_{k\ell},t}(\boldsymbol{x},t) \{w_h\}_{\Gamma_{k\ell}}^{\text{down}}(\boldsymbol{x},t) \mathrm{d}s_{(\boldsymbol{x},t)} \\
&= \sum_{\ell=1}^N \int_{\tau_\ell} \overline{h}(\boldsymbol{x},t) \left(\partial_t u_h(\boldsymbol{x},t)\right)^2 \mathrm{d}(\boldsymbol{x},t) + \int_{\Sigma_0} u_h(\boldsymbol{x},t) w_h(\boldsymbol{x},t) \mathrm{d}s_{(\boldsymbol{x},t)} \\
&\quad - \sum_{\Gamma_{k\ell} \in \mathcal{I}_N} \int_{\Gamma_{k\ell}} [u_h]_{\Gamma_{k\ell},t}(\boldsymbol{x},t) \{w_h\}_{\Gamma_{k\ell}}^{\text{down}}(\boldsymbol{x},t) \mathrm{d}s_{(\boldsymbol{x},t)}.
\end{aligned}$$

With Definition 2.2.13 and by using the Cauchy–Schwarz inequality and the Hölder inequality we obtain the estimates

$$\begin{aligned}
&\geq c_g^{-1} \sum_{\ell=1}^{N} h_\ell \|\partial_t u_h\|^2_{L_2(\tau_\ell)} - \|u_h\|_{L_2(\Sigma_0)} \|w_h\|_{L_2(\Sigma_0)} \\
&\quad - \sum_{\Gamma_{k\ell} \in \mathcal{I}_N} \left\| [u_h]_{\Gamma_{k\ell},t} \right\|_{L_2(\Gamma_{k\ell})} \left\| \{w_h\}^{\text{down}}_{\Gamma_{k\ell}} \right\|_{L_2(\Gamma_{k\ell})} \\
&\geq c_g^{-1} \sum_{\ell=1}^{N} h_\ell \|\partial_t u_h\|^2_{L_2(\tau_\ell)} - \|u_h\|_{L_2(\Sigma_0)} \|w_h\|_{L_2(\Sigma_0)} \\
&\quad - \left[\sum_{\Gamma_{k\ell} \in \mathcal{I}_N} \left\| [u_h]_{\Gamma_{k\ell},t} \right\|^2_{L_2(\Gamma_{k\ell})} \right]^{\frac{1}{2}} \left[\sum_{\Gamma_{k\ell} \in \mathcal{I}_N} \left\| \{w_h\}^{\text{down}}_{\Gamma_{k\ell}} \right\|^2_{L_2(\Gamma_{k\ell})} \right]^{\frac{1}{2}}.
\end{aligned}$$

Now we estimate the function w_h on the boundary Σ_0. We first sum over all elements $\tau_\ell \in \mathcal{T}_N$ which are intersecting with the boundary Σ_0. Then we use the inverse inequality (2.8) to end up with the estimates

$$\begin{aligned}
\|w_h\|^2_{L_2(\Sigma_0)} &= \sum_{\substack{\tau_\ell \in \mathcal{T}_N \\ \partial\tau_\ell \cap \Sigma_0 \neq \emptyset}} \|w_h\|^2_{L_2(\partial\tau_\ell \cap \Sigma_0)} \leq c_I^2 \sum_{\substack{\tau_\ell \in \mathcal{T}_N \\ \partial\tau_\ell \cap \Sigma_0 \neq \emptyset}} |\partial\tau_\ell| \, |\tau_\ell|^{-1} \|w_h\|^2_{L_2(\tau_\ell)} \\
&\leq c_I^2 \sum_{\ell=1}^{N} |\partial\tau_\ell| \, |\tau_\ell|^{-1} \|w_h\|^2_{L_2(\tau_\ell)}.
\end{aligned}$$

With the shape regularity Assumption 2.2.1 and with the definition of the mesh function (2.15) we get for $|\tau_\ell| = h_\ell^{d+1}$ the estimate

$$\leq c_I^2 c_{R_2} \sum_{\ell=1}^{N} h_\ell^{-1} \left\| \overline{h} \, \partial_t u_h \right\|^2_{L_2(\tau_\ell)} \leq c_I^2 c_{R_2} c_g^2 \sum_{\ell=1}^{N} h_\ell \|\partial_t u_h\|^2_{L_2(\tau_\ell)}.$$

Next we estimate the downwind value of w_h on the interior facets $\Gamma_{k\ell} \in \mathcal{I}_N$. We first estimate the downwind value w_h with

$$\sum_{\Gamma_{k\ell} \in \mathcal{I}_N} \left\| \{w_h\}^{\text{down}}_{\Gamma_{k\ell}} \right\|^2_{L_2(\Gamma_{k\ell})} \leq \sum_{\Gamma_{k\ell} \in \mathcal{I}_N} \left[\left\| w_{h|\tau_k} \right\|^2_{L_2(\Gamma_{k\ell})} + \left\| w_{h|\tau_\ell} \right\|^2_{L_2(\Gamma_{k\ell})} \right].$$

Then we rewrite the sum over the interior facets as the sum over all elements

$$= \sum_{\ell=1}^{N} \sum_{\substack{\Gamma_{k\ell} \in \mathcal{I}_N \\ \Gamma_{k\ell} \subset \partial\tau_\ell}} \|w_h\|^2_{L_2(\Gamma_{k\ell})}.$$

By using the inverse estimate (2.8) and the shape regularity Assumption 2.2.1 we end up with the following estimates

$$\leq c_I^2 \sum_{\ell=1}^{N} \sum_{\substack{\Gamma_{k\ell} \in \mathcal{I}_N \\ \Gamma_{k\ell} \subset \partial\tau_\ell}} |\Gamma_{k\ell}| \, |\tau_\ell|^{-1} \|w_h\|^2_{L_2(\tau_\ell)}$$

$$\leq c_I^2 \sum_{\ell=1}^{N} |\partial\tau_\ell| \, |\tau_\ell|^{-1} \, \|w_h\|^2_{L_2(\tau_\ell)}$$
$$\leq c_I^2 c_{R_2} \sum_{\ell=1}^{N} h_\ell^{-1} \|w_h\|^2_{L_2(\tau_\ell)}.$$

Using the definition of w_h, see (2.16), we obtain the result

$$\leq c_I^2 c_{R_2} c_g^2 \sum_{\ell=1}^{N} h_\ell \|\partial_t u_h\|^2_{L_2(\tau_\ell)}.$$

With these estimates we have the following result for the bilinear form $b(\cdot,\cdot)$

$$b(u_h, w_h) \geq c_g^{-1} \sum_{\ell=1}^{N} h_\ell \|\partial_t u_h\|^2_{L_2(\tau_\ell)} - \|u_h\|_{L_2(\Sigma_0)} \left[c_I^2 c_{R_2} c_g^2 \sum_{\ell=1}^{N} h_\ell \|\partial_t u_h\|^2_{L_2(\tau_\ell)} \right]^{\frac{1}{2}}$$
$$- \left[\sum_{\Gamma_{k\ell} \in \mathcal{I}_N} \left\| [u_h]_{\Gamma_{k\ell},t} \right\|^2_{L_2(\Gamma_{k\ell})} \right]^{\frac{1}{2}} \left[c_I^2 c_{R_2} c_g^2 \sum_{\ell=1}^{N} h_\ell \|\partial_t u_h\|^2_{L_2(\tau_\ell)} \right]^{\frac{1}{2}}.$$

Using two times Young's inequality with some $\varepsilon_1, \varepsilon_2 \in \mathbb{R}_+$ results in the estimate

$$\geq \left(c_g^{-1} - c_I^2 c_{R_2} c_g^2 \frac{\varepsilon_1}{2} - c_I^2 c_{R_2} c_g^2 \frac{\varepsilon_2}{2} \right) \sum_{\ell=1}^{N} h_\ell \|\partial_t u_h\|^2_{L_2(\tau_\ell)} - \frac{1}{2\varepsilon_1} \|u_h\|^2_{L_2(\Sigma_0)}$$
$$- \frac{1}{2\varepsilon_2} \sum_{\Gamma_{k\ell} \in \mathcal{I}_N} \left\| [u_h]_{\Gamma_{k\ell},t} \right\|^2_{L_2(\Gamma_{k\ell})}.$$

Choosing $\varepsilon_1 = \varepsilon_2 = (2c_I^2 c_{R_2} c_g^3)^{-1}$ we have the estimate

$$\geq \frac{c_g^{-1}}{2} \sum_{\ell=1}^{N} h_\ell \|\partial_t u_h\|^2_{L_2(\tau_\ell)} - c_I^2 c_{R_2} c_g^3 \left[\|u_h\|^2_{L_2(\Sigma_0)} + \sum_{\Gamma_{k\ell} \in \mathcal{I}_N} \left\| [u_h]_{\Gamma_{k\ell},t} \right\|^2_{L_2(\Gamma_{k\ell})} \right].$$

Combining this estimate with the estimate from Lemma 2.2.11 we have

$$b(u_h, u_h + \delta w_h) \geq \frac{\delta c_g^{-1}}{2} \sum_{\ell=1}^{N} h_\ell \|\partial_t u_h\|^2_{L_2(\tau_\ell)} + \frac{1}{2} \|u_h\|^2_{L_2(\Sigma_T)}$$
$$+ \left(\frac{1}{2} - c_I^2 c_{R_2} c_g^3 \delta \right) \left[\|u_h\|^2_{L_2(\Sigma_0)} + \sum_{\Gamma_{k\ell} \in \mathcal{I}_N} \left\| [u_h]_{\Gamma_{k\ell},t} \right\|^2_{L_2(\Gamma_{k\ell})} \right].$$

For $c_1^b(\delta) := \frac{1}{2} \min\left\{1, \delta c_g^{-1}, 1 - 2c_I^2 c_{R_2} c_g^3 \delta\right\}$ we obtain

$$\geq c_1^b(\delta) \Big[\sum_{\ell=1}^{N} h_\ell \|\partial_t u_h\|^2_{L_2(\tau_\ell)} + \|u_h\|^2_{L_2(\Sigma_0)}$$

$$+ \|u_h\|^2_{L_2(\Sigma_T)} + \sum_{\Gamma_{k\ell}\in\mathcal{I}_N} \left\| [u_h]_{\Gamma_{k\ell},t} \right\|^2_{L_2(\Gamma_{k\ell})} \Big]$$
$$= c_1^b(\delta)\|u_h\|_B^2.$$

By choosing $\delta = \delta^* = (c_g^{-1} + 2c_I^2 c_{R_2} c_g^3)^{-1}$ we get

$$c_1^b(\delta^*) = \frac{1}{2}\min\left\{1, \frac{1}{1+2c_I^2 c_{R_2} c_g^4}\right\} > 0,$$

which completes the proof. ∎

Lemma 2.2.15. *For $u_h \in S_h^p(\mathcal{T}_N)$ let the discrete function $w_h \in S_h^p(\mathcal{T}_N)$ be defined as in (2.16). Then there holds*

$$\|w_h\|_B \le c_I^b \|u_h\|_B, \qquad \text{with } c_I^b > 0.$$

Proof. Let $u_h \in S_h^p(\mathcal{T}_N)$ and $w_h \in S_h^p(\mathcal{T}_N)$ be defined as in (2.16). Then we have

$$\|w_h\|_B^2 = \sum_{\ell=1}^N h_\ell \|\partial_t w_h\|^2_{L_2(\tau_\ell)} + \|w_h\|^2_{\Sigma_0} + \|w_h\|^2_{\Sigma_T} + \sum_{\Gamma_{k\ell}\in\mathcal{I}_N} \left\| [w_h]_{\Gamma_{k\ell},t} \right\|^2_{L_2(\Gamma_{k\ell})}.$$

The first term can be estimated by using the inverse inequality (2.11)

$$\sum_{\ell=1}^N h_\ell \|\partial_t w_h\|^2_{L_2(\tau_\ell)} \le c_I^2 \sum_{\ell=1}^N h_\ell^{-1} \|w_h\|^2_{L_2(\tau_\ell)} = c_I^2 \sum_{\ell=1}^N h_\ell^{-1} \left\|\overline{h}\,\partial_t u_h\right\|^2_{L_2(\tau_\ell)}.$$

Because $\overline{h}$ is a mesh function we get with (2.15) the estimate

$$\le c_I^2 c_g^2 \sum_{\ell=1}^N h_\ell \|\partial_t u_h\|^2_{L_2(\tau_\ell)}.$$

For the remaining terms we have by using the same arguments as in Lemma 2.2.14

$$\|w_h\|^2_{L_2(\Sigma_0\cup\Sigma_T)} = \sum_{\substack{\tau_\ell\in\mathcal{T}_N \\ \partial\tau_\ell\cap(\Sigma_0\cup\Sigma_T)\neq\emptyset}} \|w_h\|^2_{L_2(\partial\tau_\ell\Sigma_0\cup\Sigma_T)} \le c_I^2 c_{R_2} c_g^2 \sum_{\ell=1}^N h_\ell \|\partial_t u_h\|^2_{L_2(\tau_\ell)}$$

and

$$\sum_{\Gamma_{k\ell}\in\mathcal{I}_N} \left\| [w_h]_{\Gamma_{k\ell},t} \right\|^2_{L_2(\Gamma_{k\ell})} \le 2 \sum_{\Gamma_{k\ell}\in\mathcal{I}_N} \left[\left\| w_{h|\tau_k} \right\|^2_{L_2(\Gamma_{k\ell})} + \left\| w_{h|\tau_\ell} \right\|^2_{L_2(\Gamma_{k\ell})} \right]$$

$$\leq 2c_I^2 c_{R_2} c_g^2 \sum_{\ell=1}^{N} h_\ell \|\partial_t u_h\|^2_{L_2(\tau_\ell)}.$$

Hence we have

$$\|w_h\|_B \leq c_I c_g \sqrt{1+3c_{R_2}} \left[\sum_{\ell=1}^{N} h_\ell \|\partial_t u_h\|^2_{L_2(\tau_\ell)} \right]^{\frac{1}{2}} \leq c_I c_g \sqrt{1+3c_{R_2}} \|u_h\|_B,$$

which completes the proof. ∎

With Lemma 2.2.14 and Lemma 2.2.15 the following stability estimate for the bilinear $b(\cdot,\cdot)$ can be proven.

Theorem 2.2.16. *For the bilinear form $b(\cdot,\cdot)$ as defined in (2.5) the following stability estimate holds*

$$\sup_{0 \neq v_h \in S_h^p(\mathcal{T}_N)} \frac{b(u_h, v_h)}{\|v_h\|_B} \geq c_S^b \|u_h\|_B \qquad \text{for all } u_h \in S_h^p(\mathcal{T}_N).$$

Proof. For $u_h \in S_h^p(\mathcal{T}_N)$ and the special test function $v_h = u_h + \delta w_h$ where $w_h \in S_h^p(\mathcal{T}_N)$ is defined as in (2.16) the stability estimate follows by using the estimate of Lemma 2.2.14 and by using the boundedness estimate of Lemma 2.2.15

$$\begin{aligned} \sup_{0 \neq v_h \in S_h^p(\mathcal{T}_N)} \frac{b(u_h, v_h)}{\|v_h\|_B} &\geq \frac{b(u_h, u_h + \delta w_h)}{\|u_h + \delta w_h\|_B} \geq \frac{b(u_h, u_h + \delta w_h)}{\|u_h\|_B + \delta \|w_h\|_B} \\ &\geq \frac{c_1^b \|u_h\|_B^2}{(1 + \delta c_I^b)\|u_h\|_B} = c_S^b \|u_h\|_B. \end{aligned}$$

∎

Remark 2.2.17. *Let $\mathcal{T}_N$ be a decomposition of the intervall $(0,T)$ into finite elements. With the stability estimate of Theorem 2.2.16 and the boundedness estimate of Lemma 2.2.8 we have unique solvability of the discrete variational problem:*

Find $u_h \in S_h^p(\mathcal{T}_N)$ such that

$$b(u_h, v_h) = \langle f, v_h \rangle_{(0,T)} + u_0 v_h(0) \tag{2.17}$$

for all $v_h \in S_h^p(\mathcal{T}_N)$.

The unique solution $u_h \in S_h^p(\mathcal{T}_N)$ describes an approximate solution for the ordinary differential equation

$$\partial_t u(t) = f(t) \quad \text{for } t \in (0,T), \qquad u(0) = u_0.$$

An error estimate in the energy norm $\|u - u_h\|_B$ can be shown by applying standard techniques. A comprehensive analysis for the discrete problem (2.17) can be found for example in [97].

Next we combine all the previous estimates to prove a stability and a boundedness estimate for the bilinear form $A(\cdot,\cdot)$. To do so we define for $u \in H^s(\mathcal{T}_N)$, $s > \frac{3}{2}$ the following energy norms with respect to the bilinear form $A(\cdot,\cdot)$

$$\|u\|_{\mathrm{DG}}^2 := \|u\|_A^2 + \|u\|_B^2,$$
$$\|u\|_{\mathrm{DG},*}^2 := \|u\|_{A,*}^2 + \|u\|_{B,*}^2.$$

Lemma 2.2.18. *The bilinear form $A(\cdot,\cdot)$ as given in (2.3) is bounded, i.e.*

$$A(u, v_h) \leq c_2^A \|u\|_{\mathrm{DG},*} \|v_h\|_{\mathrm{DG}}$$

for all $u \in H^s(\mathcal{T}_N)$ with $s > \frac{3}{2}$ and for all $v_h \in S_h^p(\mathcal{T}_N)$ with an h-independent constant $c_2^A > 0$.

Proof. By using the boundedness estimates of Lemma 2.2.7 and Lemma 2.2.8 we get the boundedness estimate for the bilinear form $A(\cdot,\cdot)$ with

$$\begin{aligned} A(u, v_h) = a(u, v_h) + b(u, v_h) &\leq c_2^a \|u\|_{A,*} \|v_h\|_A + \|u\|_{B,*} \|v_h\|_B \\ &\leq \max\{1, c_2^a\} \, \|u\|_{\mathrm{DG},*} \|v_h\|_{\mathrm{DG}}. \end{aligned}$$

■

Lemma 2.2.19. *Let $\mathcal{T}_N$ be a quasi-uniform decomposition, i.e. for all $\tau_\ell \in \mathcal{T}_N$ there holds $c_q^{-1} h \leq h_\ell \leq c_q h$ with $c_q \geq 1$ and $h > 0$. For $u_h \in S_h^p(\mathcal{T}_N)$ let the discrete function $w_h \in S_h^p(\mathcal{T}_N)$ be defined as in (2.16) with the mesh function*

$$\overline{h} = \frac{1}{N} \sum_{\ell=1}^{N} h_\ell \in \mathbb{R}. \tag{2.18}$$

Then there holds

$$\|w_h\|_A \leq c_I^a \|u_h\|_A, \qquad \text{with } c_I^a > 0.$$

Proof. The function $\overline{h}$ is indeed a mesh function, because the condition that the decomposition $\mathcal{T}_N$ is quasi-uniform, i.e. $c_q h \le h_\ell \le c_q h$, implies for all $\tau_\ell \in \mathcal{T}_N$

$$c_g^{-1} h_\ell \le \overline{h} \le c_g h_\ell \quad \text{with } c_g = c_q^2. \tag{2.19}$$

Let $u_h \in S_h^p(\mathcal{T}_N)$ and $w_h \in S_h^p(\mathcal{T}_N)$ be defined as in (2.16). Then we have

$$\|w_h\|_A^2 = \sum_{\ell=1}^N \|\nabla_{\boldsymbol{x}} w_h\|_{[L_2(\tau_\ell)]^d}^2 + \sum_{\Gamma_{k\ell}\in\mathcal{I}_N} \frac{\sigma}{\overline{h}_{k\ell}} \left\| [w_h]_{\Gamma_{k\ell},\boldsymbol{x}} \right\|_{[L_2(\Gamma_{k\ell})]^d}^2. \tag{2.20}$$

For the first term of (2.20) we have due to the fact, that $\overline{h}$ is constant

$$\sum_{\ell=1}^N \|\nabla_{\boldsymbol{x}} w_h\|_{[L_2(\tau_\ell)]^d}^2 = \sum_{\ell=1}^N \left\|\nabla_{\boldsymbol{x}} (\overline{h}\partial_t u_h)\right\|_{[L_2(\tau_\ell)]^d}^2 = \sum_{\ell=1}^N \overline{h}^2 \|\nabla_{\boldsymbol{x}} \partial_t u_h\|_{[L_2(\tau_\ell)]^d}^2.$$

With (2.19) we further obtain

$$\le c_g^2 \sum_{\ell=1}^N h_\ell^2 \|\nabla_{\boldsymbol{x}} \partial_t u_h\|_{[L_2(\tau_\ell)]^d}^2 = c_g^2 \sum_{\ell=1}^N h_\ell^2 \sum_{i=1}^d \|\partial_t(\partial_{\boldsymbol{x}_i} u_h)\|_{L_2(\tau_\ell)}^2.$$

With the inverse inequality (2.11) we get the estimate

$$\le c_g^2 c_I^2 \sum_{\ell=1}^N h_\ell^2 \sum_{i=1}^d h_\ell^{-2} \|\partial_{\boldsymbol{x}_i} u_h\|_{L_2(\tau_\ell)}^2 = c_g^2 c_I^2 \sum_{\ell=1}^N \|\nabla_{\boldsymbol{x}} u_h\|_{[L_2(\tau_\ell)]^d}^2.$$

For the second term of (2.20) we have for $\Gamma_{k\ell} \in \mathcal{I}_N$

$$\begin{aligned} [w_h]_{\Gamma_{k\ell},\boldsymbol{x}} &= w_{h|\tau_k} \boldsymbol{n}_{k,\boldsymbol{x}} + w_{h|\tau_\ell} \boldsymbol{n}_{\ell,\boldsymbol{x}} = \left(w_{h|\tau_k} - w_{h|\tau_\ell}\right) \boldsymbol{n}_{k,\boldsymbol{x}} \\ &= \overline{h}\,\partial_t \left(u_{h|\tau_k} - u_{h|\tau_\ell}\right) \boldsymbol{n}_{k,\boldsymbol{x}} = \overline{h}\,\partial_t z_h\, \boldsymbol{n}_{k,\boldsymbol{x}}, \end{aligned}$$

with $z_h := u_{h|\tau_k} - u_{h|\tau_\ell}$. Hence we have

$$\left\| [w_h]_{\Gamma_{k\ell},\boldsymbol{x}} \right\|_{[L_2(\Gamma_{k\ell})]^d} = \overline{h} \left\| \partial_t z_h\, \boldsymbol{n}_{k,\boldsymbol{x}} \right\|_{[L_2(\Gamma_{k\ell})]^d} \le c_g \overline{h}_{k\ell} \left\| \partial_t z_h\, \boldsymbol{n}_{k,\boldsymbol{x}} \right\|_{[L_2(\Gamma_{k\ell})]^d}.$$

For $\left|\boldsymbol{n}_{k,\boldsymbol{x}}\right| = 1$, i.e. $\boldsymbol{n}_{k,t} = 0$ we conclude, that $\partial_t z_h$ is exactly the tangential derivative of z_h on the interior facet $\Gamma_{k\ell}$. Hence we obtain by using the inverse inequality (2.10)

$$\begin{aligned} \left\| [w_h]_{\Gamma_{k\ell},\boldsymbol{x}} \right\|_{[L_2(\Gamma_{k\ell})]^d} &\le c_g \overline{h}_{k\ell} \|\partial_t z_h\|_{L_2(\Gamma_{k\ell})} \le c_g c_I \|z_h\|_{L_2(\Gamma_{k\ell})} \\ &= c_g c_I \left\| [u_h]_{\Gamma_{k\ell},\boldsymbol{x}} \right\|_{[L_2(\Gamma_{k\ell})]^d}. \end{aligned}$$

For $\left|\boldsymbol{n}_{k,\boldsymbol{x}}\right| = 0$ we clearly have

$$0 = \left\| [w_h]_{\Gamma_{k\ell},\boldsymbol{x}} \right\|_{[L_2(\Gamma_{k\ell})]^d} \leq c_g c_I \left\| [u_h]_{\Gamma_{k\ell},\boldsymbol{x}} \right\|_{[L_2(\Gamma_{k\ell})]^d}.$$

For $0 < \left|\boldsymbol{n}_{k,\boldsymbol{x}}\right| < 1$ we will decompose the derivative $\partial_t z_h \boldsymbol{n}_{k,\boldsymbol{x}}$ into a tangential part and a part containing only space derivatives. To do so, we introduce for the normal vector $\boldsymbol{n}_k = (\boldsymbol{n}_{k,\boldsymbol{x}}, n_{k,t})^\top$ with $\boldsymbol{n}_{k,\boldsymbol{x}} = (n_{k,x_1}, \ldots, n_{k,x_d})^\top$ the tangential vectors $\boldsymbol{t}_i \in \mathbb{R}^{d+1}$ for $i = 1, \ldots, d$ as

$$\boldsymbol{t}_i[d+1] = n_{k,x_i}, \qquad \boldsymbol{t}_i[i] = -n_{k,t}, \qquad \boldsymbol{t}_i[j] = 0 \quad \text{for } j \neq i \text{ and } j \neq d+1.$$

Because we study the case $0 < \left|\boldsymbol{n}_{k,\boldsymbol{x}}\right| < 1$ we have $n_{k,t} \neq 0$ and we can compute the normalized tangential vectors $\tilde{\boldsymbol{t}}_i := (n_{k,x_i}^2 + n_{k,t}^2)^{-\frac{1}{2}} \boldsymbol{t}_i$. For the i-th tangential derivative of z_h we then obtain

$$\nabla z_h \cdot \boldsymbol{t}_i = -n_{k,t} \partial_{x_i} z_h + n_{k,x_i} \partial_t z_h.$$

Hence we have

$$n_{k,x_i} \partial_t z_h = \nabla z_h \cdot \boldsymbol{t}_i + n_{k,t} \partial_{x_i} z_h \qquad \text{for } i = 1, \ldots, d.$$

With this relation we have

$$\begin{aligned}
\left\| [w_h]_{\Gamma_{k\ell},\boldsymbol{x}} \right\|^2_{[L_2(\Gamma_{k\ell})]^d} &\leq c_g^2 \overline{h}_{k\ell}^2 \left\| \partial_t z_h \boldsymbol{n}_{k,\boldsymbol{x}} \right\|^2_{[L_2(\Gamma_{k\ell})]^d} = c_g^2 \overline{h}_{k\ell}^2 \sum_{i=1}^d \left\| n_{k,x_i} \partial_t z_h \right\|^2_{L_2(\Gamma_{k\ell})} \\
&= c_g^2 \overline{h}_{k\ell}^2 \sum_{i=1}^d \left\| \nabla z_h \cdot \boldsymbol{t}_i + n_{k,t} \partial_{x_i} z_h \right\|^2_{L_2(\Gamma_{k\ell})} \\
&\leq 2 c_g^2 \overline{h}_{k\ell}^2 \sum_{i=1}^d \left[\| \nabla z_h \cdot \boldsymbol{t}_i \|^2_{L_2(\Gamma_{k\ell})} + \left\| n_{k,t} \partial_{x_i} z_h \right\|^2_{L_2(\Gamma_{k\ell})} \right].
\end{aligned}$$

Using the normalized tangentials $\tilde{\boldsymbol{t}}_i$ results in

$$= 2 c_g^2 \overline{h}_{k\ell}^2 \sum_{i=1}^d \left[(n_{k,x_i}^2 + n_{k,t}^2) \left\| \nabla z_h \cdot \tilde{\boldsymbol{t}}_i \right\|^2_{L_2(\Gamma_{k\ell})} + \left\| n_{k,t} \partial_{x_i} z_h \right\|^2_{L_2(\Gamma_{k\ell})} \right].$$

Because $\nabla z_h \cdot \tilde{\boldsymbol{t}}_i$ is the tangential derivative of z_h on the interior facet $\Gamma_{k\ell}$ we obtain by using the inverse inequality (2.10)

$$\begin{aligned}
&\leq 2 c_I^2 c_g^2 \sum_{i=1}^d (n_{k,x_i}^2 + n_{k,t}^2) \| z_h \|^2_{L_2(\Gamma_{k\ell})} + 2 c_g^2 \overline{h}_{k\ell}^2 \| \nabla_{\boldsymbol{x}} z_h \|^2_{[L_2(\Gamma_{k\ell})]^d} \\
&\leq 2 c_I^2 c_g^2 (1 + d c_n^{-1}) \left\| [u_h]_{\Gamma_{k\ell},\boldsymbol{x}} \right\|^2_{[L_2(\Gamma_{k\ell})]^d} + 2 c_g^2 \overline{h}_{k\ell}^2 \| \nabla_{\boldsymbol{x}} z_h \|^2_{[L_2(\Gamma_{k\ell})]^d},
\end{aligned}$$

with the positive constant

$$c_n = \min\{\left|\boldsymbol{n}_{k,\boldsymbol{x}}\right| > 0 : \boldsymbol{n}_k = (\boldsymbol{n}_{k,\boldsymbol{x}}, n_{k,t})^\top \text{ is a normal vector of } \Gamma_{k\ell} \in \mathcal{I}_N\} > 0.$$

Hence we have

$$\sum_{\Gamma_{k\ell}\in\mathcal{I}_N} \frac{\sigma}{\overline{h}_{k\ell}} \left\| [w_h]_{\Gamma_{k\ell},\boldsymbol{x}} \right\|^2_{[L_2(\Gamma_{k\ell})]^d} \leq 2c_I^2 c_g^2 (1 + dc_n^{-1}) \sum_{\Gamma_{k\ell}\in\mathcal{I}_N} \frac{\sigma}{\overline{h}_{k\ell}} \left\| [u_h]_{\Gamma_{k\ell},\boldsymbol{x}} \right\|^2_{[L_2(\Gamma_{k\ell})]^d} + 2c_g^2 \sigma \sum_{\Gamma_{k\ell}\in\mathcal{I}_N} \overline{h}_{k\ell} \|\nabla_{\boldsymbol{x}} z_h\|^2_{[L_2(\Gamma_{k\ell})]^d}.$$

It remains to estimate

$$\sum_{\Gamma_{k\ell}\in\mathcal{I}_N} \overline{h}_{k\ell} \|\nabla_{\boldsymbol{x}} z_h\|^2_{[L_2(\Gamma_{k\ell})]^d} \leq 2 \sum_{\Gamma_{k\ell}\in\mathcal{I}_N} \overline{h}_{k\ell} \left[\left\| \nabla_{\boldsymbol{x}} u_{h|\tau_k} \right\|^2_{[L_2(\Gamma_{k\ell})]^d} + \left\| \nabla_{\boldsymbol{x}} u_{h|\tau_\ell} \right\|^2_{[L_2(\Gamma_{k\ell})]^d} \right].$$

With the same techniques as in the proof of Lemma 2.2.6 we obtain the estimate

$$\leq 2c_I^2 c_G c_{R_2} \sum_{\ell=1}^{N} \|\nabla_{\boldsymbol{x}} u_h\|^2_{[L_2(\tau_\ell)]^d}.$$

Overall we have

$$\|w_h\|_A^2 \leq c_I^2 (c_g^2 + 2c_G c_{R_2}) \sum_{\ell=1}^{N} \|\nabla_{\boldsymbol{x}} u_h\|^2_{[L_2(\tau_\ell)]^d} + 2c_I^2 c_g^2 (1 + dc_n^{-1}) \sum_{\Gamma_{k\ell}\in\mathcal{I}_N} \frac{\sigma}{\overline{h}_{k\ell}} \left\| [u_h]_{\Gamma_{k\ell},\boldsymbol{x}} \right\|^2_{[L_2(\Gamma_{k\ell})]^d},$$

which completes the proof. ∎

Remark 2.2.20. *Note, that the constant c_I^a of the boundedness estimate in Lemma 2.2.19 depends on the mesh constant c_n^{-1}. To ensure, that the constant c_n is bounded away from zero, i.e. $c_n \geq c_0 > 0$ we have to assume, that the space-time decomposition $\mathcal{T}_N$ fulfils an angle condition with respect to time.*

Next we will prove a stability estimate for the bilinear form $A(\cdot,\cdot)$. by combining the estimates from above.

Theorem 2.2.21. *Let $\mathcal{T}_N$ be a quasi-uniform decomposition and let $\sigma \geq 4c_K$, then for the bilinear form $A(\cdot,\cdot)$ the following stability estimate holds*

$$\sup_{0\neq v_h\in S_h^p(\mathcal{T}_N)} \frac{A(u_h, v_h)}{\|v_h\|_{\mathrm{DG}}} \geq c_S^A \|u_h\|_{\mathrm{DG}} \qquad \text{for all } u_h \in S_h^p(\mathcal{T}_N).$$

Proof. For $u_h \in S_h^p(\mathcal{T}_N)$ we use the special test function $v_h = u_h + \delta w_h$ where $w_h \in S_h^p(\mathcal{T}_N)$ is defined as given in (2.16) with the special mesh function (2.18). Then we obtain the estimate

$$\sup_{0\neq v_h\in S_h^p(\mathcal{T}_N)} \frac{A(u_h,v_h)}{\|v_h\|_{\mathrm{DG}}} \geq \frac{A(u_h,u_h+\delta w_h)}{\|u_h+\delta w_h\|_{\mathrm{DG}}}$$
$$= \frac{a(u_h,u_h)+\delta a(u_h,w_h)+b(u_h,u_h+\delta w_h)}{\|u_h+\delta w_h\|_{\mathrm{DG}}}.$$

By using the boundedness estimate of Lemma 2.2.7 for $u_h \in S_h^p(\mathcal{T}_N) \subset H^s(\mathcal{T}_N)$, $s > \frac{3}{2}$, and the stability estimate of Lemma 2.2.14 with the δ-dependent constant $c_1^b(\delta) := \frac{1}{2}\min\{1, \delta c_g^{-1}, 1 - 2c_I^2 c_{R_2} c_g^3 \delta\}$ as given in the proof of Lemma 2.2.14 we have the estimate

$$\geq \frac{\frac{1}{2}\|u_h\|_A^2 - c_2^a \delta \|u_h\|_{A,*}\|w_h\|_A + c_1^b(\delta)\|u_h\|_B^2}{\|u_h+\delta w_h\|_{\mathrm{DG}}}.$$

For discrete functions $u_h \in S_h^p(\mathcal{T}_N)$ the norm $\|u_h\|_{A,*}$ can be estimated by using Lemma 2.2.6, i.e. $\|u_h\|_{A,*} \leq \sqrt{1+c_K}\|u_h\|_A$. By using Lemma 2.2.15 and Lemma 2.2.19, we obtain the estimate

$$\geq \frac{\frac{1}{2}\|u_h\|_A^2 - c_2^a\sqrt{1+c_K} c_I^a \delta \|u_h\|_A^2 + c_1^b(\delta)\|u_h\|_B^2}{(1+c_I^A\delta)\|u_h\|_{\mathrm{DG}}},$$

with $c_I^A := \max\{c_I^a, c_I^b\}$. Further manipulations lead to

$$= \frac{(\frac{1}{2} - c_2^a\sqrt{1+c_K} c_I^a \delta)\|u_h\|_A^2 + c_1^b(\delta)\|u_h\|_B^2}{(1+c_I^A\delta)\|u_h\|_{\mathrm{DG}}}$$
$$\geq \frac{\min\{1, \delta c_g^{-1}, 1 - 2c_2^a\sqrt{1+c_K} c_I^a \delta, 1 - 2c_I^2 c_{R_2} c_g^3 \delta\}}{2(1+c_I^A\delta)}\|u_h\|_{\mathrm{DG}}.$$

By choosing a fixed $\delta = \delta^*$ as

$$\delta^* := \min\left\{\frac{1}{c_g^{-1} + 2c_I^2 c_{R_2} c_g^3}, \frac{1}{c_g^{-1} + 2c_2^a\sqrt{1+c_K} c_I^a}\right\} > 0$$

we obtain the stability estimate

$$\sup_{0\neq v_h\in S_h^p(\mathcal{T}_N)} \frac{A(u_h,v_h)}{\|v_h\|_{\mathrm{DG}}} \geq \frac{\min\{1, \delta^* c_g^{-1}\}}{2(1+c_I^A\delta^*)}\|u_h\|_{\mathrm{DG}} = c_s^A\|u_h\|_{\mathrm{DG}}.$$

■

By using the stability estimate of Theorem 2.2.21 and the boundedness estimate of Lemma 2.2.18 we can prove an error estimate in the energy norm $\|\cdot\|_{\mathrm{DG}}$.

Theorem 2.2.22. *Let $\mathcal{T}_N$ be a quasi-uniform decomposition and let $u \in H^s(\mathcal{T}_N)$, $s > \frac{3}{2}$, be the exact solution of the model problem (2.1). For $\sigma \geq 4c_K$ let $u_h \in S_h^p(\mathcal{T}_N)$ be the solution of the discrete variational problem (2.2). Then the following error estimate holds*

$$\|u - u_h\|_{\mathrm{DG}} \leq \inf_{z_h \in S_h^p(\mathcal{T}_N)} \left[\|u - z_h\|_{\mathrm{DG}} + \frac{c_2^A}{c_S^A} \|u - z_h\|_{\mathrm{DG},*} \right].$$

Proof. By using the stability estimate of Theorem 2.2.21 we have for any discrete function $z_h \in S_h^p(\mathcal{T}_N)$ the bound in the energy norm

$$c_S^A \|z_h - u_h\|_{\mathrm{DG}} \leq \sup_{0 \neq v_h \in S_h^p(\mathcal{T}_N)} \frac{A(z_h - u_h, v_h)}{\|v_h\|_{\mathrm{DG}}}.$$

By inserting the exact solution u and by using the Galerkin orthogonality (2.6) we have

$$\begin{aligned} &= \sup_{0 \neq v_h \in S_h^p(\mathcal{T}_N)} \frac{A(u - u_h - (u - z_h), v_h)}{\|v_h\|_{\mathrm{DG}}} \\ &= \sup_{0 \neq v_h \in S_h^p(\mathcal{T}_N)} \frac{A(z_h - u, v_h)}{\|v_h\|_{\mathrm{DG}}}. \end{aligned}$$

With the boundedness property of Lemma 2.2.18 we get the estimate

$$\|z_h - u_h\|_{\mathrm{DG}} \leq \frac{c_2^A}{c_S^A} \|u - z_h\|_{\mathrm{DG},*}.$$

Using the above estimate with the triangle inequality completes the error estimate of this theorem

$$\begin{aligned} \|u - u_h\|_{\mathrm{DG}} &\leq \|u - z_h\|_{\mathrm{DG}} + \|z_h - u_h\|_{\mathrm{DG}} \\ &\leq \|u - z_h\|_{\mathrm{DG}} + \frac{c_2^A}{c_S^A} \|u - z_h\|_{\mathrm{DG},*}. \end{aligned}$$

■

Lemma 2.2.23. *Let $\mathcal{T}_N$ be a decomposition of the space-time domain Q. For an element $\tau_\ell \in \mathcal{T}_N$ let $u \in H^s(\tau_\ell)$, $s \geq 0$, be a given function. By $Q_\ell u \in \mathbb{P}_p(\tau_\ell)$ we denote the local L_2-projection on τ_ℓ as*

$$\langle Q_\ell u, v_h \rangle_{L_2(\tau_\ell)} = \langle u, v_h \rangle_{L_2(\tau_\ell)} \qquad \text{for all } v_h \in \mathbb{P}^p(\tau_\ell).$$

Then the following error estimates for the local L_2-projection hold:

For $s \in \mathbb{N}_0$ and $0 \leq \mu \leq s$ there holds

$$|u - Q_\ell u|_{H^\mu(\tau_\ell)} \leq c h_\ell^{\min\{s,p+1\}-\mu} |u|_{H^s(\tau_\ell)}. \tag{2.21}$$

For $s \in \mathbb{N}$ there holds the L_2-error estimate on the boundary

$$\|u - Q_\ell u\|_{L_2(\partial\tau_\ell)} \leq c h_\ell^{\min\{s,p+1\}-\frac{1}{2}} |u|_{H^s(\tau_\ell)}. \tag{2.22}$$

For $s \in \mathbb{N}$ with $s \geq 2$ the L_2-error on the boundary $\partial\tau_\ell$ for the gradient can be estimated by

$$\|\nabla_{\boldsymbol{x}} (u - Q_\ell u)\|_{[L_2(\tau_\ell)]^d} \leq c h_\ell^{\min\{s,p+1\}-\frac{3}{2}} |u|_{H^s(\tau_\ell)}. \tag{2.23}$$

Proof. The proofs can be found in [20] for example. ∎

To prove explicit h-dependent error estimates we define the global L_2-projection $Q_{\mathcal{T}_N} u \in S_h^p(\mathcal{T}_N)$ such that

$$Q_{\mathcal{T}_N} u_{|\tau_\ell} := Q_\ell u \qquad \text{for all } \tau_\ell \in \mathcal{T}_N.$$

Lemma 2.2.24. *For $u \in H^s(\mathcal{T}_N)$ with $s \geq 1$ the following error estimate in the energy norm $\|\cdot\|_A$ holds*

$$\|u - Q_{\mathcal{T}_N} u\|_A \leq c \left[\sum_{\ell=1}^N h_\ell^{2\min\{s,p+1\}-2} |u|^2_{H^s(\tau_\ell)} \right]^{\frac{1}{2}}.$$

Proof. By using the definition of the energy norm $\|\cdot\|_A$ we have for $u \in H^s(\mathcal{T}_N)$

$$\|u - Q_{\mathcal{T}_N} u\|_A^2 = \sum_{\ell=1}^N \|\nabla_{\boldsymbol{x}}(u - Q_{\mathcal{T}_N} u)\|^2_{[L_2(\tau_\ell)]^d} + \sum_{\Gamma_{k\ell} \in \mathcal{I}_N} \frac{\sigma}{\overline{h}_{k\ell}} \left\| [u - Q_{\mathcal{T}_N} u]_{\Gamma_{k\ell}, \boldsymbol{x}} \right\|^2_{[L_2(\Gamma_{k\ell})]^d}.$$

With the error estimate (2.21) and by using the triangle inequality we have

$$\begin{aligned} &\leq c^2 \sum_{\ell=1}^N h_\ell^{2\min\{s,p+1\}-2} |u|^2_{H^s(\tau_\ell)} \\ &\quad + 2 \sum_{\Gamma_{k\ell} \in \mathcal{I}_N} \frac{\sigma}{\overline{h}_{k\ell}} \left[\|u - Q_k u\|^2_{[L_2(\Gamma_{k\ell})]^d} + \|u - Q_\ell u\|^2_{[L_2(\Gamma_{k\ell})]^d} \right]. \end{aligned}$$

Rewriting the sum over all interior facets as a sum over all elements and by using Assumption 2.2.2 we get the estimate

$$= c^2 \sum_{\ell=1}^N h_\ell^{2\min\{s,p+1\}-2} |u|^2_{H^s(\tau_\ell)} + 2 \sum_{\ell=1}^N \sum_{\substack{\Gamma_{k\ell} \in \mathcal{I}_N \\ \Gamma_{k\ell} \subset \partial\tau_\ell}} \frac{\sigma}{\overline{h}_{k\ell}} \|u - Q_\ell u\|^2_{[L_2(\Gamma_{k\ell})]^d}$$

$$\leq c^2 \sum_{\ell=1}^{N} h_\ell^{2\min\{s,p+1\}-2} |u|^2_{H^s(\tau_\ell)} + 2\sigma c_G \sum_{\ell=1}^{N} h_\ell^{-1} \|u - Q_\ell u\|^2_{[L_2(\partial\tau_\ell)]^d}.$$

Applying the error estimate (2.22) leads to the estimate

$$\leq c^2 (1 + 2\sigma c_G) \sum_{\ell=1}^{N} h_\ell^{2\min\{s,p+1\}-2} |u|^2_{H^s(\tau_\ell)}.$$

■

Lemma 2.2.25. *For $u \in H^s(\mathcal{T}_N)$ with $s \geq 2$ the following error estimate in the energy norm $\|\cdot\|_{A,*}$ holds*

$$\|u - Q_{\mathcal{T}_N} u\|_{A,*} \leq c \left[\sum_{\ell=1}^{N} h_\ell^{2\min\{s,p+1\}-2} |u|^2_{H^s(\tau_\ell)} \right]^{\frac{1}{2}}.$$

Proof. Using the definition of the norm $\|\cdot\|_{A,*}$ with the error estimate of Lemma 2.2.24 and by applying the triangle inequality we get the estimate

$$\begin{aligned}
\|u - Q_{\mathcal{T}_N} u\|^2_{A,*} &= \|u - Q_{\mathcal{T}_N} u\|^2_A + \sum_{\Gamma_{k\ell} \in \mathcal{I}_N} \overline{h}_{k\ell} \left\| \langle \nabla_{\boldsymbol{x}} (u - Q_{\mathcal{T}_N} u) \rangle_{\Gamma_{k\ell}} \right\|^2_{[L_2(\Gamma_{k\ell})]^d} \\
&\leq c^2 \sum_{\ell=1}^{N} h_\ell^{2\min\{s,p+1\}-2} |u|^2_{H^s(\tau_\ell)} \\
&\quad + \sum_{\Gamma_{k\ell} \in \mathcal{I}_N} \overline{h}_{k\ell} \left[\|\nabla_{\boldsymbol{x}} (u - Q_k u)\|^2_{[L_2(\Gamma_{k\ell})]^d} + \|\nabla_{\boldsymbol{x}} (u - Q_\ell u)\|^2_{[L_2(\Gamma_{k\ell})]^d} \right].
\end{aligned}$$

As in the proof of Lemma 2.2.24 we rewrite the sum over all interior facets as a sum over all elements. By using Assumption 2.2.2 we get

$$\begin{aligned}
&= c^2 \sum_{\ell=1}^{N} h_\ell^{2\min\{s,p+1\}-2} |u|^2_{H^s(\tau_\ell)} + \sum_{\ell=1}^{N} \sum_{\substack{\Gamma_{k\ell} \in \mathcal{I}_N \\ \Gamma_{k\ell} \subset \partial\tau_\ell}} \overline{h}_{k\ell} \|\nabla_{\boldsymbol{x}} (u - Q_\ell u)\|^2_{[L_2(\Gamma_{k\ell})]^d} \\
&\leq c^2 \sum_{\ell=1}^{N} h_\ell^{2\min\{s,p+1\}-2} |u|^2_{H^s(\tau_\ell)} + c_G \sum_{\ell=1}^{N} h_\ell \|\nabla_{\boldsymbol{x}} (u - Q_\ell u)\|^2_{[L_2(\partial\tau_\ell)]^d}.
\end{aligned}$$

With the error estimate (2.23) we obtain

$$\leq c^2 (1 + c_G) \sum_{\ell=1}^{N} h_\ell^{2\min\{s,p+1\}-2} |u|^2_{H^s(\tau_\ell)}.$$

■

Remark 2.2.26. *The regularity assumption $u \in H^s(\mathcal{T}_N)$, $s \geq 2$, for Lemma 2.2.25 is needed to estimate the error of the gradients on the interior facets $\Gamma_{k\ell} \in \mathcal{I}_N$. This assumption can be relaxed by assuming $u \in W_p^2(\mathcal{T}_N)$ with $p \in (\frac{2d}{d+2}, 2]$, see [19, 109].*

Lemma 2.2.27. *For $u \in H^s(\mathcal{T}_N)$ with $s \geq 1$ the following error estimates in the energy norms $\|\cdot\|_B$ and $\|\cdot\|_{B,*}$ hold*

$$\|u - Q_{\mathcal{T}_N} u\|_B \leq c \left[\sum_{\ell=1}^{N} h_\ell^{2\min\{s,p+1\}-1} \, |u|^2_{H^s(\tau_\ell)} \right]^{\frac{1}{2}},$$

$$\|u - Q_{\mathcal{T}_N} u\|_{B,*} \leq c \left[\sum_{\ell=1}^{N} h_\ell^{2\min\{s,p+1\}-1} \, |u|^2_{H^s(\tau_\ell)} \right]^{\frac{1}{2}}.$$

Proof. Let $u \in H^s(\mathcal{T}_N)$ with $s \geq 1$. We start by estimating the L_2-errors on the boundary Σ_0 and on the boundary Σ_T. If we sum over all elements we have

$$\|u - Q_{\mathcal{T}_N} u\|^2_{L_2(\Sigma_0)} + \|u - Q_{\mathcal{T}_N} u\|^2_{L_2(\Sigma_T)} = \sum_{\substack{\tau_\ell \in \mathcal{T}_N \\ \partial\tau_\ell \cap (\Sigma_0 \cup \Sigma_T) \neq \emptyset}} \|u - Q_{\mathcal{T}_N} u\|^2_{L_2(\partial\tau_\ell \cap (\Sigma_0 \cup \Sigma_T))}.$$

With the error estimate (2.22) we conclude

$$\begin{aligned} &\leq \sum_{\ell=1}^{N} \|u - Q_{\mathcal{T}_N} u\|^2_{L_2(\partial\tau_\ell)} \\ &\leq c^2 \sum_{\ell=1}^{N} h_\ell^{2\min\{s,p+1\}-1} \, |u|^2_{H^s(\tau_\ell)}. \end{aligned}$$

Next we will estimate the error of the jump in time direction. Using the triangle inequality and by rewriting the sum over the interior facets we get the estimates

$$\begin{aligned} \sum_{\Gamma_{k\ell} \in \mathcal{I}_N} \left\| [u - Q_{\mathcal{T}_N} u]_{\Gamma_{k\ell},t} \right\|^2_{L_2(\Gamma_{k\ell})} &\leq 2 \sum_{\Gamma_{k\ell} \in \mathcal{I}_N} \left[\|u - Q_k u\|^2_{L_2(\Gamma_{k\ell})} + \|u - Q_\ell u\|^2_{L_2(\Gamma_{k\ell})} \right] \\ &= 2 \sum_{\ell=1}^{N} \sum_{\substack{\Gamma_{k\ell} \in \mathcal{I}_N \\ \Gamma_{k\ell} \subset \partial\tau_\ell}} \|u - Q_\ell u\|^2_{L_2(\Gamma_{k\ell})} \\ &\leq 2 \sum_{\ell=1}^{N} \|u - Q_\ell u\|^2_{L_2(\partial\tau_\ell)}. \end{aligned}$$

With the error estimate (2.22) we end up with the estimate

$$\leq 2c^2 \sum_{\ell=1}^{N} h_\ell^{2\min\{s,p+1\}-1} \, |u|^2_{H^s(\tau_\ell)}.$$

Using the same techniques as above we can estimate the L_2-error of the upwind values in time directions

$$\begin{aligned}\sum_{\Gamma_{k\ell}\in\mathcal{I}_N}\left\|\{u-Q_{\mathcal{T}_N}u\}^{\mathrm{up}}_{\Gamma_{k\ell}}\right\|^2_{L_2(\Gamma_{k\ell})} &\le \sum_{\Gamma_{k\ell}\in\mathcal{I}_N}\left[\|u-Q_k u\|^2_{L_2(\Gamma_{k\ell})}+\|u-Q_\ell u\|^2_{L_2(\Gamma_{k\ell})}\right]\\ &\le \sum_{\ell=1}^{N}\sum_{\substack{\Gamma_{k\ell}\in\mathcal{I}_N\\ \Gamma_{k\ell}\subset\partial\tau_\ell}}\|u-Q_\ell u\|^2_{L_2(\Gamma_{k\ell})}\\ &\le \sum_{\ell=1}^{N}\|u-Q_\ell u\|^2_{L_2(\partial\tau_\ell)}\\ &\le c^2\sum_{\ell=1}^{N}h_\ell^{2\min\{s,p+1\}-1}\,|u|^2_{H^s(\tau_\ell)}\,.\end{aligned}$$

With the error estimates above we can now estimate the error of the L_2-projection $Q_{\mathcal{T}_N}u$ in the energy norm $\|\cdot\|_B$. By definition we have

$$\|u-Q_{\mathcal{T}_N}u\|^2_B \le \sum_{\ell=1}^{N}h_\ell\|\partial_t(u-Q_\ell u)\|^2_{L_2(\tau_\ell)}+3c^2\sum_{\ell=1}^{N}h_\ell^{2\min\{s,p+1\}-1}\,|u|^2_{H^s(\tau_\ell)}\,.$$

By using the error estimate (2.21) for $\mu=1$ we derive the first error estimate of the lemma

$$\le 4c^2\sum_{\ell=1}^{N}h_\ell^{2\min\{s,p+1\}-1}\,|u|^2_{H^s(\tau_\ell)}\,.$$

For the error in the energy norm $\|\cdot\|_{B,*}$ we also use the estimate (2.21) and we conclude

$$\begin{aligned}\|u-Q_{\mathcal{T}_N}u\|^2_{B,*} &\le \sum_{\ell=1}^{N}h_\ell^{-1}\|u-Q_\ell u\|^2_{L_2(\tau_\ell)}+2c^2\sum_{\ell=1}^{N}h_\ell^{2\min\{s,p+1\}-1}\,|u|^2_{H^s(\tau_\ell)}\\ &\le 3c^2\sum_{\ell=1}^{N}h_\ell^{2\min\{s,p+1\}-1}\,|u|^2_{H^s(\tau_\ell)}\,.\end{aligned}$$

■

Now it is possible to give a bound of the error in the energy norm $\|\cdot\|_{\mathrm{DG}}$ for the discrete solution $u_h\in S_h^p(\mathcal{T}_N)$ of the variational problem (2.2).

Theorem 2.2.28. *Let $\mathcal{T}_N$ be a quasi-uniform decomposition and let $u\in H^s(\mathcal{T}_N)$, $s\ge 2$, be the exact solution of the model problem (2.1) and for $\sigma\ge 4c_K$ let $u_h\in S_h^p(\mathcal{T}_N)$ be the solution of the discrete variational problem (2.2). Then the following error estimate holds*

$$\|u-u_h\|_{\mathrm{DG}} \le ch^{\min\{s,p+1\}-1}\,|u|_{H^s(\mathcal{T}_N)}\,.$$

Proof. By applying the estimate of Theorem 2.2.22 and by using the global L_2-projection $Q_{\mathcal{T}_N} u \in S_h^p(\mathcal{T}_N)$ we get the estimate

$$\begin{aligned}\|u-u_h\|_{\mathrm{DG}} &\leq \inf_{z_h \in S_h^p(\mathcal{T}_N)} \left[\|u-z_h\|_{\mathrm{DG}} + \frac{c_2^A}{c_S^A} \|u-z_h\|_{\mathrm{DG},*} \right] \\ &\leq \|u-Q_{\mathcal{T}_N} u\|_{\mathrm{DG}} + \frac{c_2^A}{c_S^A} \|u-Q_{\mathcal{T}_N} u\|_{\mathrm{DG},*}.\end{aligned}$$

With Lemmata 2.2.24–2.2.27 we conclude the error estimate

$$\begin{aligned}&= \left[\|u-Q_{\mathcal{T}_N} u\|_A^2 + \|u-Q_{\mathcal{T}_N} u\|_B^2 \right]^{\frac{1}{2}} \\ &\quad + \frac{c_2^A}{c_S^A} \left[\|u-Q_{\mathcal{T}_N} u\|_{A,*}^2 + \|u-Q_{\mathcal{T}_N} u\|_{B,*}^2 \right]^{\frac{1}{2}} \\ &\leq c \left(1 + \frac{c_2^A}{c_S^A} \right) \left[\sum_{\ell=1}^N (1+h_\ell) h_\ell^{2\min\{s,p+1\}-2} \, |u|_{H^s(\tau_\ell)}^2 \right]^{\frac{1}{2}} \\ &\leq c \left(1 + \frac{c_2^A}{c_S^A} \right) \left[\sum_{\ell=1}^N h_\ell^{2\min\{s,p+1\}-2} \, |u|_{H^s(\tau_\ell)}^2 \right]^{\frac{1}{2}}.\end{aligned}$$

The assumption that the decomposition $\mathcal{T}_N$ is quasi-uniform implies the estimate

$$\leq c c_g \left(1 + \frac{c_2^A}{c_S^A} \right) h^{\min\{s,p+1\}-1} \, |u|_{H^s(\mathcal{T}_N)}.$$

■

2.3 Numerical examples

In this section numerical examples will be presented which show the performance of the presented space-time method. The first example shows the convergence behavior for a regular solution with respect to different polynomial degrees. For the second and third example the convergence of the space-time method for solutions with singularities will be considered. The third example shows the convergence for higher dimensional problems. In the last example the use of continuous approximations will be studied and compared with respect to discontinuous approximations.

In all the numerical examples the estimated order of convergence

$$\mathrm{eoc} := \frac{\log(\left\|u-u_{h_\ell}\right\|_{\mathrm{DG}}) - \log(\left\|u-u_{h_{\ell+1}}\right\|_{\mathrm{DG}})}{\log(h_\ell) - \log(h_{\ell+1})}$$

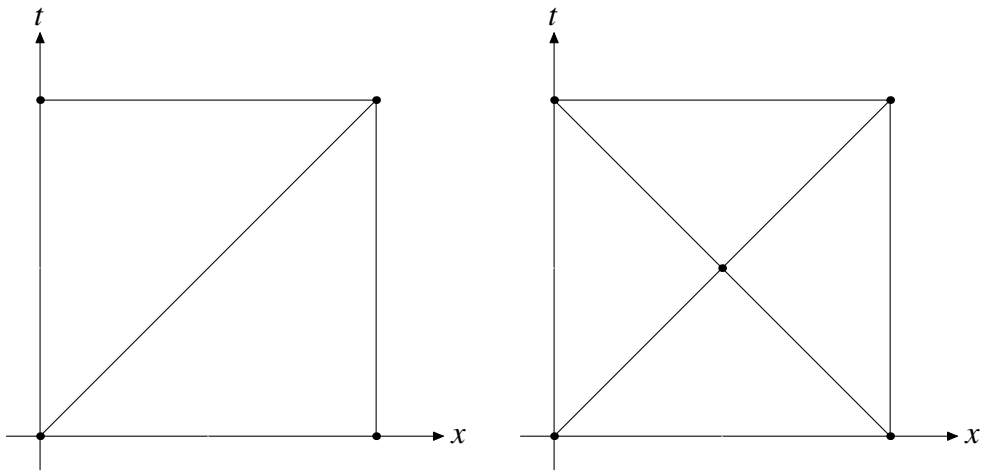

(a) Initial triangulation with $N = 2$. (b) Initial triangulation with $N = 4$.

Figure 2.3: Two initial space-time meshes.

will be used to compare the experimental results with the theoretical estimates.

Example 2.3.1 (Regular solution)**.** We consider the one dimensional spatial domain $\Omega = (0,1)$ and the simulation interval $(0,T)$ with $T = 1$. On the boundary $\Sigma_D = \partial\Omega \times (0,T)$ we apply homogeneous Dirichlet boundary conditions. The given data f and u_0 are chosen such that the solution is given by the regular function

$$u(x,t) = \cos(\pi t)\sin(\pi x).$$

As an initial triangulation for the space-time domain $Q = (0,1)^2$ we use two triangles of the same size, see also Figure 2.3(a). To analyze the convergence behavior of the presented space-time method we consider a sequence of several uniform refinement steps. Further we will use different polynomial degrees $p \in \{1,2,3,4\}$ to compare the numerical results with the analysis of the previous section. As a stabilization parameter for the space-time method we will use $\sigma = 10p^2$, where the additional scaling with the polynomial degree comes from the local inverse inequalities, as mentioned in Remark 2.2.4. The arising linear systems are solved with the solver package PARDISO, see [82, 83].

In Table 2.1–2.2 the numerical errors in the energy norm $\|u - u_h\|_{\mathrm{DG}}$ for different polynomial degrees and different uniform mesh refinements are given. The presented results confirm the numerical analysis presented in Section 2.2. In particular the numerical results agree with the error estimate of Theorem 2.2.28. Only for $p = 4$ and for the refinement level 8 the resulting error in the energy norm is bigger due to round off errors.

		$p=1$			$p=2$		
level	elements	dof	$\|u-u_h\|_{\mathrm{DG}}$	eoc	dof	$\|u-u_h\|_{\mathrm{DG}}$	eoc
0	2	2	$2.5100+0$	–	6	$1.3885+0$	–
1	8	16	$1.2482+0$	1.01	36	$3.7080-1$	1.90
2	32	80	$6.5025-1$	0.94	168	$9.4582-2$	1.97
3	128	352	$3.2824-1$	0.99	720	$2.2839-2$	2.05
4	512	1 472	$1.6442-1$	1.00	2 976	$5.4760-3$	2.06
5	2 048	6 016	$8.2210-2$	1.00	12 096	$1.3253-3$	2.05
6	8 192	24 320	$4.1089-2$	1.00	48 768	$3.2452-4$	2.03
7	32 768	97 792	$2.0537-2$	1.00	195 840	$8.0170-5$	2.02
8	131 072	392 192	$1.0267-2$	1.00	784 896	$1.9914-5$	2.01
Theory:				1.00			2.00

Table 2.1: Numerical results for polynomial degree $p=1$ and $p=2$.

		$p=3$			$p=4$		
level	elements	dof	$\|u-u_h\|_{\mathrm{DG}}$	eoc	dof	$\|u-u_h\|_{\mathrm{DG}}$	eoc
0	2	12	$4.6587-1$	–	20	$2.7556-1$	–
1	8	64	$8.9955-2$	2.37	100	$1.7229-2$	4.00
2	32	288	$1.1065-2$	3.02	440	$1.0214-3$	4.08
3	128	1 216	$1.2973-3$	3.09	1 840	$5.8403-5$	4.13
4	512	4 992	$1.5205-4$	3.09	7 520	$3.3506-6$	4.12
5	2 048	20 224	$1.8067-5$	3.07	30 400	$1.9604-7$	4.10
6	8 192	81 408	$2.1840-6$	3.05	122 240	$1.1732-8$	4.06
7	32 768	326 656	$2.6767-7$	3.03	490 240	$7.1379-10$	4.04
8	131 072	1 308 672	$3.3098-8$	3.02	1 963 520	$1.1881-10$	2.59
Theory:				3.00			4.00

Table 2.2: Numerical results for polynomial degree $p=3$ and $p=4$.

level	elements	dof	$\|u-u_h\|_{\mathrm{DG}}$	eoc
0	4	18	$3.2689-1$	–
1	16	84	$1.3925-1$	1.23
2	64	360	$9.2011-2$	0.60
3	256	1 488	$6.2846-2$	0.55
4	1 024	6 048	$4.3657-2$	0.53
5	4 096	24 384	$3.0589-2$	0.51
6	16 384	97 920	$2.1529-2$	0.51
7	65 536	392 448	$1.5188-2$	0.50
8	262 144	1 571 328	$1.0727-2$	0.50
9	1 048 576	6 288 384	$7.5806-3$	0.50
10	4 194 304	25 159 680	$5.3587-3$	0.50
Theory:				0.50

Table 2.3: Numerical results for the singular solution I.

Example 2.3.2 (Singular solution I)**.** As in the previous example we consider the one dimensional spatial domain $\Omega = (0,1)$ and the simulation interval $(0,T)$ with $T = 1$. On the boundary $\Sigma_D = \partial\Omega \times (0,T)$ we apply Dirichlet boundary conditions. The given data f and u_0 and the Dirichlet boundary conditions are chosen such that the solution is given by the function

$$u(x,t) = \left[x^2 + \left(t - \frac{1}{2} \right)^2 \right]^{\frac{1}{4}}.$$

The exact solution u omits a point singularity at $x = 0$ and $t = \frac{1}{2}$. Hence the exact solution is contained in the Sobolev space

$$u \in H^{\frac{3}{2}-\varepsilon}(Q), \quad \text{for } \varepsilon > 0.$$

As an initial triangulation for the space-time domain $Q = (0,1)^2$ we use four triangles of same size, see also Figure 2.3(b). As in the previous example we consider a sequence of several uniform refinement steps. Hence we can apply Theorem 2.2.28 and we end up with the a priori error estimate

$$\|u-u_h\|_{\mathrm{DG}} \leq c h^{\frac{1}{2}-\varepsilon} |u|_{H^{\frac{3}{2}-\varepsilon}(\mathcal{T}_N)} \quad \text{for } p \geq 1 \text{ and } \varepsilon > 0.$$

Due to the point singularity we can not expect better convergence rates for higher polynomial degrees. But to get faster in the asymptotic range we use for our numerical experiment a uniform polynomial degree $p = 2$. For the stabilization parameter we use $\sigma = 40$. As before we solve the arising linear systems with the solver package PARDISO.

In Table 2.3 the errors in the energy norm $\|u-u_h\|_{\mathrm{DG}}$ are given for different refinement levels. As predicted from the theory we see the expected order of convergence of $\mathrm{eoc} = \frac{1}{2}$. The convergence rate for singular solutions can be improved by using adaptive space-time elements as presented in Chapter 6.

Example 2.3.3 (Singular solution II)**.** We again consider the one dimensional spatial domain $\Omega = (0,1)$ and the simulation interval $(0,T)$ with $T = 1$. As in the first example we apply homogeneous Dirichlet boundary conditions. Now we consider the exact solution with a line singularity at $t = 1$

$$u(x,t) = (1-t)^{\alpha} \sin(\pi x) \quad \text{with } \alpha \in (0,1).$$

Due to the line singularity at $t = 1$ the exact solution is contained in the Sobolev space

$$u \in H^{\alpha+\frac{1}{2}-\varepsilon}(Q) \quad \text{for } \varepsilon > 0.$$

For the initial triangulation of the space-time domain $Q = (0,1)^2$ we again use the space-time mesh with four triangles as shown in Figure 2.3(b). Again we apply several uniform refinement steps to estimate the convergence behavior for the error in the energy norm $\|u-u_h\|_{\mathrm{DG}}$. We apply the space-time method for two different choices of the regularity parameter $\alpha \in \left\{\frac{1}{2}, \frac{3}{4}\right\}$. If we apply the error estimate of Theorem 2.2.28 to the given exact solution we get

$$\|u-u_h\|_{\mathrm{DG}} \leq c h^{\alpha-\frac{1}{2}-\varepsilon} \, |u|_{H^{\alpha+\frac{1}{2}-\varepsilon}(\mathcal{T}_N)} \quad \text{for } p \geq 1 \text{ and } \varepsilon > 0. \tag{2.24}$$

As in the previous example we choose a polynomial degree $p = 2$ to reach the asymptotic range faster. For the stabilization parameter we again use $\sigma = 40$.

In Table 2.4 the results for different mesh refinements are given for the regularity parameter $\alpha = \frac{1}{2}$ and $\alpha = \frac{3}{4}$. From the error estimate (2.24) we expect a convergence rate of $\mathrm{eoc} = 0.00$ for $\alpha = \frac{1}{2}$ and $\mathrm{eoc} = 0.25$ for $\alpha = \frac{3}{4}$. In both cases the numerical results show a better convergence rate as predicted from the theory. This behavior can be explained by the fact that the exact solution has a line singularity at $t = 1$. For any time $t \in [0,T]$ the exact solution u has full regularity in space. Using Lemma 2.2.27 for uniform meshes, we have the following error estimate for the L_2-projection

$$\|u - Q_{\mathcal{T}_N} u\|_B + \|u - Q_{\mathcal{T}_N} u\|_{B,*} \leq c h^{\min\{s,p+1\}-\frac{1}{2}} \, |u|_{H^s(\mathcal{T}_N)} .$$

Hence we loose only $\frac{1}{2}$ order in time for the energy error. Since we have full regularity in space for any time $t \in [0,T]$ we do not lose one order for the error in the energy norm as predicted in Theorem 2.2.28. This additional convergence rate of $\frac{1}{2}$ can be observed in Table 2.4. The full algebraic convergences rates can be obtained by using anistropic mesh refinement, see [3].

			$\alpha = 0.5$		$\alpha = 0.75$	
level	elements	dof	$\|u-u_h\|_{\mathrm{DG}}$	eoc	$\|u-u_h\|_{\mathrm{DG}}$	eoc
0	4	18	$5.5930-1$	–	$2.7264-1$	–
1	16	84	$3.3948-1$	0.72	$9.3966-2$	1.54
2	64	360	$2.3452-1$	0.53	$4.0622-2$	1.21
3	256	1 488	$1.6766-1$	0.48	$2.2667-2$	0.84
4	1 024	6 048	$1.1994-1$	0.48	$1.3535-2$	0.74
5	4 096	24 384	$8.5442-2$	0.49	$8.1292-3$	0.74
6	16 384	97 920	$6.0664-2$	0.49	$4.8659-3$	0.74
7	65 536	392 448	$4.2988-2$	0.50	$2.9040-3$	0.74
8	262 144	1 571 328	$3.0430-2$	0.50	$1.7300-3$	0.75
9	1 048 576	6 288 384	$2.1529-2$	0.50	$1.0297-3$	0.75
10	4 194 304	25 159 680	$1.5228-2$	0.50	$6.1256-4$	0.75
Theory:				0.00		0.25

Table 2.4: Numerical results for the singular solution II with regularity parameter $\alpha = 0.5$ and $\alpha = 0.75$.

Example 2.3.4 (Higher dimensions)**.** We consider for the spatial domain the two and three dimensional unit cube $\Omega = (0,1)^d$, $d = 2,3$ with homogeneous Dirichlet boundary conditions. The simulation interval is chosen to be $[0,T]$ with $T = 1$. The given data f and u_0 are chosen such that the exact solution is given by

$$u(\boldsymbol{x},t) = \cos(\pi t)\prod_{i=1}^{d}\sin(\pi x_i).$$

For $d = 2$ the space-time domain is given by the three dimensional unit cube $Q = (0,1)^3$ which is decomposed into 6 tetrahedrons for the initial triangulation, see also Figure 2.4(a). For $d = 3$ the space-time domain is given by the four dimensional unit cube $Q = (0,1)^4$ which is decomposed into 96 pentatopes of the same size. A projection of a pentatope is shown in Figure 2.4(b). For details how to decompose a four dimensional unit cube into pentatopes and how to refine these four dimensional simplices see [11, 32, 66, 67, 72]. These initial triangulations are refined uniformly several times to analyze the convergence behavior of the presented space-time method. The arising linear systems are solved with a geometric space-time multigrid method with a relative error reduction of $\varepsilon = 10^{-8}$. This multigrid solver is explained in Chapter 4. For $p = 1$ and a stabilization parameter $\sigma = 15$ the errors in the energy norm are given in Tables 2.5–2.6. As predicted from the theory the expected order of convergence can be observed.

Example 2.3.5 (Continuous approximation)**.** In this example we study the presented space-time method for the case when continuous approximations are used instead of discontinuous ones. To do so we repeat Example 2.3.1 and Example

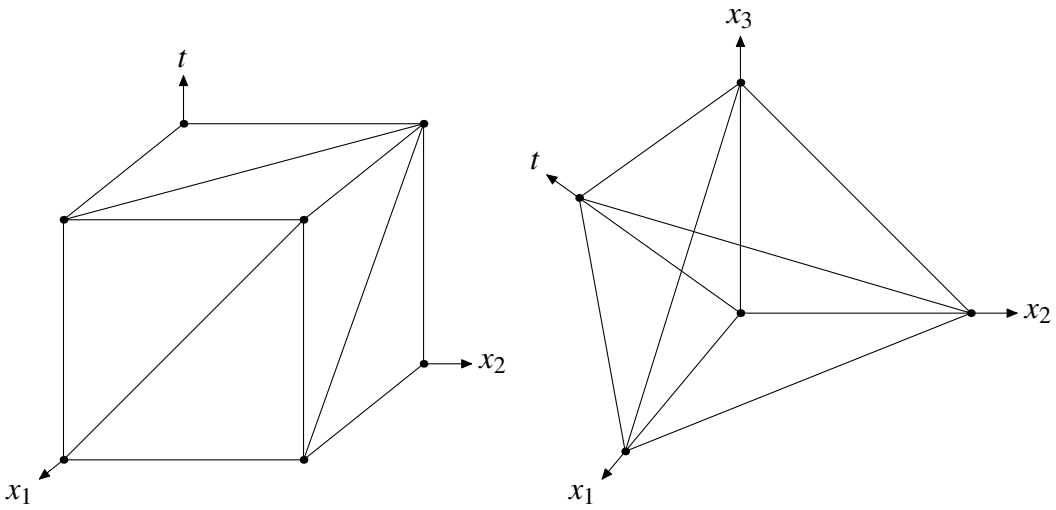

(a) Initial triangulation with $N = 6$. (b) Four dimensional simplex, pentatope.

Figure 2.4: Three dimensional triangulation and a four dimensional simplex.

level	elements	dof	$\|u - u_h\|_{\mathrm{DG}}$	eoc
0	6	4	$1.9019 + 0$	–
1	48	104	$1.3615 + 0$	0.48
2	384	1 168	$7.7764 - 1$	0.81
3	3 072	10 784	$4.0785 - 1$	0.93
4	24 576	92 224	$2.0889 - 1$	0.97
5	196 608	761 984	$1.0607 - 1$	0.98
6	1 572 864	6 193 408	$5.3588 - 2$	0.98
7	12 582 912	49 938 944	$2.6979 - 2$	0.99
Theory:				1.00

Table 2.5: Numerical results for $d = 2$.

level	elements	dof	$\|u - u_h\|_{\mathrm{DG}}$	eoc
0	96	192	$1.2027 + 0$	–
1	1 536	5 376	$8.7542 - 1$	0.46
2	24 576	104 448	$5.0831 - 1$	0.78
3	393 216	1 818 624	$2.6943 - 1$	0.92
4	6 291 456	30 277 632	$1.3775 - 1$	0.97
Theory:				1.00

Table 2.6: Numerical results for $d = 3$.

		$p=1$			$p=2$		
level	elements	dof	$\|u-u_h\|_{\mathrm{DG}}$	eoc	dof	$\|u-u_h\|_{\mathrm{DG}}$	eoc
0	2	0	$2.1707+0$	–	3	$1.4015+0$	–
1	8	3	$1.2779+0$	0.76	15	$3.9261-1$	1.84
2	32	15	$6.5150-1$	0.97	63	$1.1578-1$	1.76
3	128	63	$3.1981-1$	1.03	255	$3.5071-2$	1.72
4	512	255	$1.5736-1$	1.02	1 023	$1.1148-2$	1.65
5	2 8	1 023	$7.7932-2$	1.01	4 095	$3.6972-3$	1.59
6	8 192	4 095	$3.8765-2$	1.01	16 383	$1.2616-3$	1.55
7	32 768	16 383	$1.9331-2$	1.00	65 535	$4.3779-4$	1.53
8	131 072	65 535	$9.6519-3$	1.00	262 143	$1.5330-4$	1.51
Observed:				1.00			1.50

Table 2.7: Numerical results for polynomial degree $p=1$ and $p=2$.

2.3.3 with continuous approximations. According to Example 2.3.1 the results for different polynomial degrees are presented in Table 2.7–2.8. Here it can be observed, that for odd polynomial degrees the same convergence rates are obtained when continuous approximations are used instead of discontinuous approximations. For even polynomial degrees one observes that the convergence rates are reduced by a factor of $\frac{1}{2}$ when continuous approximations are used. However the number of unknowns for the arising linear systems is much smaller for continuouse approximations.

According to Example 2.3.3 we also compute the errors in the energy norm, when continuous approximations are used. The results are given in Table 2.9. Here we obtain, that the order of convergence is also reduced by a factor of $\frac{1}{2}$ compared to the discontinuous case. For the regularity parameter $\alpha=\frac{1}{2}$ the error in the energy norm is not reduced when the space-time mesh is refined uniformly.
This example shows, that discontinuous approximations are necessary to obtain the right convergence rates. However, the use of continuous approximations leads to smaller linear systems which have to be solved.

		$p=3$			$p=4$		
level	elements	dof	$\|u-u_h\|_{\mathrm{DG}}$	eoc	dof	$\|u-u_h\|_{\mathrm{DG}}$	eoc
0	2	8	$4.8007-1$	–	15	$2.8608-1$	–
1	8	35	$9.9193-2$	2.27	63	$1.7684-2$	4.02
2	32	143	$1.1997-2$	3.05	255	$1.2267-3$	3.85
3	128	575	$1.3506-3$	3.15	1 023	$9.5546-5$	3.68
4	512	2 303	$1.5800-4$	3.10	4 095	$7.8633-6$	3.60
5	2 048	9 215	$1.8981-5$	3.06	16 383	$6.6826-7$	3.56
6	8 192	36 863	$2.3199-6$	3.03	65 535	$5.7799-8$	3.53
7	32 768	147 455	$2.8651-7$	3.02	262 143	$4.9009-9$	3.56
8	131 072	589 823	$3.5594-8$	3.01	1 048 575	$1.2465-9$	2.87
Observed:				3.00			3.50

Table 2.8: Numerical results for polynomial degree $p=3$ and $p=4$.

			$\alpha=0.5$		$\alpha=0.75$	
level	elements	dof	$\|u-u_h\|_{\mathrm{DG}}$	eoc	$\|u-u_h\|_{\mathrm{DG}}$	eoc
0	4	7	$6.1358-1$	–	$3.1058-1$	–
1	16	31	$3.4246-1$	0.84	$9.8628-2$	1.65
2	64	127	$2.3648-1$	0.53	$4.1484-2$	1.25
3	256	511	$1.8187-1$	0.38	$2.5638-2$	0.69
4	1 024	2 047	$1.5262-1$	0.25	$1.9305-2$	0.41
5	4 096	8 191	$1.3731-1$	0.15	$1.5663-2$	0.30
6	16 384	32 767	$1.2951-1$	0.08	$1.3038-2$	0.26
7	65 536	131 071	$1.2559-1$	0.04	$1.0942-2$	0.25
8	262 144	524 287	$1.2365-1$	0.02	$9.2025-3$	0.25
9	1 048 576	2 097 151	$1.2452-1$	0.01	$7.7428-3$	0.25
10	4 194 304	8 388 607	$1.2406-1$	0.01	$6.5139-3$	0.25
Observed:				0.00		0.25

Table 2.9: Numerical results for regularity parameter $\alpha=0.5$ and $\alpha=0.75$.

3 HYBRID SPACE-TIME DISCRETIZATIONS

In this chapter we will derive a hybrid space-time discretization scheme by using the space-time method introduced in the previous chapter. In the first section we will introduce the hybrid discretization scheme by subdividing the space-time domain into non-overlapping subdomains and we will introduce the finite element discretization and the corresponding linear system. Moreover, we will discuss some solution algorithms. In Section 3.2 we will analyze this hybrid formulation and derive some a priori error estimates. Finally, numerical examples will be given in Section 3.3, which confirm the proven error estimates of Section 3.2. The main ideas of this chapter come from [17, 21, 68].

3.1 Discretization

We introduce a decomposition of the space-time domain $Q \subset \mathbb{R}^{d+1}$ into non-overlapping subdomains Q_i for $i = 1, \ldots, P$

$$\overline{Q} = \bigcup_{i=1}^{P} \overline{Q}_i, \qquad Q_i \cap Q_j = \emptyset \quad \text{for } i \neq j.$$

For this space-time decomposition we define the interface between the space-time subdomains Q_i as

$$\Sigma := \bigcup_{i=1}^{P} \Sigma_i \quad \text{with } \Sigma_i := \overline{\partial Q_i \setminus \partial Q}.$$

For each space-time subdomain Q_i we introduce a decomposition

$$\overline{Q}_i = \overline{\mathcal{T}}_{N_i} := \bigcup_{\ell=1}^{N_i} \overline{\tau}_\ell^i$$

into N_i simplices. For these decompositions $\mathcal{T}_{N_i}$ we assume the shape regularity Assumption 2.2.1 and the mesh grading Assumption 2.2.2. If we sum up all elements of each decomposition $\mathcal{T}_{N_i}$ for $i = 1 \ldots, P$ we obtain a decomposition of the space-time domain Q

$$\overline{Q} = \overline{\mathcal{T}}_N := \bigcup_{i=1}^{P} \bigcup_{\tau_\ell^i \in \mathcal{T}_{N_i}} \overline{\tau}_\ell^i$$

into finite elements, with the set of all interior facets $\mathcal{I}_N$. With $\mathcal{I}_{N_i}$, $i = 1,\dots,P$ we denote the interior facets of the decomposition $\mathcal{T}_{N_i}$. On the interface Σ we define the set of all facets

$$\Sigma_h := \mathcal{I}_N \setminus \bigcup_{i=1}^{P} \mathcal{I}_{N_i}, \qquad \text{i.e. } \overline{\Sigma} = \bigcup_{\Gamma_{k\ell}\in\Sigma_h} \overline{\Sigma}_{k\ell}.$$

A possible configuration for $d = 1$ is given in Figure 3.1. On the interface Σ we introduce the discrete function space of piecewise polynomials of degree p as

$$S_h^p(\Sigma_h) := \left\{ \mu_h \in L_2(\Sigma) : \mu_{h|\Gamma_{k\ell}} \in \mathbb{P}_p(\Gamma_{k\ell}) \text{ for all } \Gamma_{k\ell} \in \Sigma_h \right\}.$$

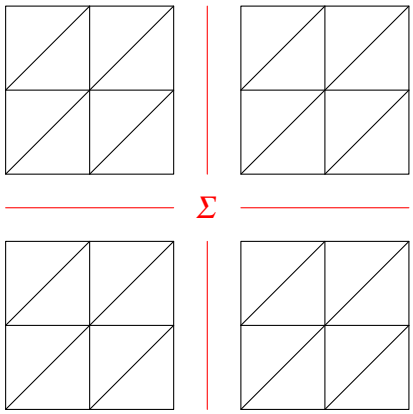

Figure 3.1: Space-time domain decomposition for $d = 1$ into four subdomains with interface Σ.

Using the decomposition $\mathcal{T}_N$ one can now use the space-time formulation (2.2) introduced in Chapter 2 to solve for a discrete solution $u_h \in S_h^p(\mathcal{T}_N)$, hence we have to solve the following discrete problem:

Find $u_h \in S_h^p(\mathcal{T}_N)$ such that

$$A(u_h, v_h) = \langle f, v_h\rangle_Q + \langle u_0, v_h\rangle_{\Sigma_0} + \langle g_N, v_h\rangle_{\Sigma_N} \tag{3.1}$$

for all $v_h \in S_h^p(\mathcal{T}_N)$.

With respect to each space-time subdomain Q_i we apply the space-time discretization (3.1). To do so, we define for $u_h^i, v_h^i \in S_h^p(\mathcal{T}_{N_i})$ the local bilinear form

$$A^{(i)}(u_h^i, v_h^i) := a^{(i)}(u_h^i, v_h^i) + b^{(i)}(u_h^i, v_h^i)$$

with the bilinear form

$$a^{(i)}(u_h^i, v_h^i) := \sum_{\ell=1}^{N_i} \int_{\tau_\ell^i} \nabla_{\boldsymbol{x}} u_h^i(\boldsymbol{x},t) \cdot \nabla_{\boldsymbol{x}} v_h^i(\boldsymbol{x},t) \mathrm{d}(\boldsymbol{x},t)$$

$$
\begin{aligned}
&- \sum_{\Gamma_{k\ell}\in\mathcal{I}_{N_i}} \int_{\Gamma_{k\ell}} \left\langle \nabla_{\boldsymbol{x}} u_h^i \right\rangle_{\Gamma_{k\ell}} (\boldsymbol{x},t) \cdot \left[v_h^i \right]_{\Gamma_{k\ell},\boldsymbol{x}} (\boldsymbol{x},t) \mathrm{d}s_{(\boldsymbol{x},t)} \\
&- \sum_{\Gamma_{k\ell}\in\mathcal{I}_{N_i}} \int_{\Gamma_{k\ell}} \left[u_h^i \right]_{\Gamma_{k\ell},\boldsymbol{x}} (\boldsymbol{x},t) \cdot \left\langle \nabla_{\boldsymbol{x}} v_h^i \right\rangle_{\Gamma_{k\ell}} (\boldsymbol{x},t) \mathrm{d}s_{(\boldsymbol{x},t)} \\
&+ \sum_{\Gamma_{k\ell}\in\mathcal{I}_{N_i}} \frac{\sigma}{\overline{h}_{k\ell}} \int_{\Gamma_{k\ell}} \left[u_h^i \right]_{\Gamma_{k\ell},\boldsymbol{x}} (\boldsymbol{x},t) \cdot \left[v_h^i \right]_{\Gamma_{k\ell},\boldsymbol{x}} (\boldsymbol{x},t) \mathrm{d}s_{(\boldsymbol{x},t)},
\end{aligned}
$$

and with the bilinear form

$$
\begin{aligned}
b^{(i)}(u_h^i, v_h^i) := &- \sum_{\ell=1}^{N_i} \int_{\tau_\ell^i} u_h^i(\boldsymbol{x},t) \partial_t v_h^i(\boldsymbol{x},t) \mathrm{d}(\boldsymbol{x},t) + \int_{\Sigma_T \cap \partial Q_i} u_h^i(\boldsymbol{x},t) v_h^i(\boldsymbol{x},t) \mathrm{d}s_{(\boldsymbol{x},t)} \\
&+ \sum_{\Gamma_{k\ell}\in\mathcal{I}_{N_i}} \int_{\Gamma_{k\ell}} \left\{ u_h^i \right\}_{\Gamma_{k\ell}}^{\mathrm{up}} (\boldsymbol{x},t) \left[v_h^i \right]_{\Gamma_{k\ell},t} (\boldsymbol{x},t) \mathrm{d}s_{(\boldsymbol{x},t)}
\end{aligned}
$$

for all $i = 1, \ldots, P$. We also define the local right hand sides

$$
F^{(i)}(v_h^i) := \left\langle f, v_h^i \right\rangle_{Q_i} + \left\langle u_0, v_h^i \right\rangle_{\Sigma_0 \cap \partial Q_i} + \left\langle g_N, v_h^i \right\rangle_{\Sigma_N \cap \partial Q_i},
$$

for $i = 1, \ldots, P$. With these definitions and by using the fact that $u_h^i = u_{h|Q_i}$ we can split the bilinear form $A(\cdot,\cdot)$ in a sum over all local bilinear forms $A^{(i)}(\cdot,\cdot)$ and into four different coupling parts on the interface Σ_h

$$
\begin{aligned}
A(u_h, v_h) = &\sum_{i=1}^{P} A^{(i)}(u_h, v_h) \\
&- \sum_{\Gamma_{k\ell}\in\Sigma_h} \int_{\Gamma_{k\ell}} \left\langle \nabla_{\boldsymbol{x}} u_h \right\rangle_{\Gamma_{k\ell}} (\boldsymbol{x},t) \cdot \left[v_h \right]_{\Gamma_{k\ell},\boldsymbol{x}} (\boldsymbol{x},t) \mathrm{d}s_{(\boldsymbol{x},t)} \\
&- \sum_{\Gamma_{k\ell}\in\Sigma_h} \int_{\Gamma_{k\ell}} \left[u_h \right]_{\Gamma_{k\ell},\boldsymbol{x}} (\boldsymbol{x},t) \cdot \left\langle \nabla_{\boldsymbol{x}} v_h \right\rangle_{\Gamma_{k\ell}} (\boldsymbol{x},t) \mathrm{d}s_{(\boldsymbol{x},t)} \\
&+ \sum_{\Gamma_{k\ell}\in\Sigma_h} \frac{\sigma}{\overline{h}_{k\ell}} \int_{\Gamma_{k\ell}} \left[u_h \right]_{\Gamma_{k\ell},\boldsymbol{x}} (\boldsymbol{x},t) \cdot \left[v_h \right]_{\Gamma_{k\ell},\boldsymbol{x}} (\boldsymbol{x},t) \mathrm{d}s_{(\boldsymbol{x},t)} \\
&+ \sum_{\Gamma_{k\ell}\in\Sigma_h} \int_{\Gamma_{k\ell}} \left\{ u_h \right\}_{\Gamma_{k\ell}}^{\mathrm{up}} (\boldsymbol{x},t) \left[v_h \right]_{\Gamma_{k\ell},t} (\boldsymbol{x},t) \mathrm{d}s_{(\boldsymbol{x},t)}.
\end{aligned}
\tag{3.2}
$$

To reduce the coupling on the interface Σ we rewrite the four coupling terms. Following the approach in [17, 21, 68] we introduce a new variable $\lambda_h \in S_h^p(\Sigma_h)$ on the interface Σ

$$
\lambda_{h|\Gamma_{k\ell}}(\boldsymbol{x},t) := \langle u_h \rangle_{\Gamma_{k\ell}} (\boldsymbol{x},t) = \frac{1}{2} \left[u_{h|\tau_k}(\boldsymbol{x},t) + u_{h|\tau_\ell}(\boldsymbol{x},t) \right] \quad \text{for all } (\boldsymbol{x},t) \in \Gamma_{k\ell}.
$$

In the next definition we introduce the jumps on the interface Σ between functions on the interface and function on the space-time subdomains.

Definition 3.1.1 (Hybrid jump)**.** *Let $\Gamma_{k\ell} \in \Sigma_h$ be a facet on the interface Σ with the outer unit normal vector $\boldsymbol{n}_k = (\boldsymbol{n}_{k,\boldsymbol{x}}, n_{k,t})^\top$ with respect to the element τ_k. For a given function $u \in H^s(\mathcal{T}_N)$, $s \geq 1$ and a function $\lambda \in L_2(\Sigma_h)$ the hybrid jump in space direction for the element τ_k is given by*

$$[u/\lambda]_{\partial\tau_k,\boldsymbol{x}}(\boldsymbol{x},t) := \left[u_{|\tau_k}(\boldsymbol{x},t) - \lambda(\boldsymbol{x},t)\right]\boldsymbol{n}_{k,\boldsymbol{x}} \quad \text{for } (\boldsymbol{x},t) \in \Gamma_{k\ell} \quad a.e.$$

The hybrid jump in time direction for the element τ_k is defined as

$$[u/\lambda]_{\partial\tau_k,t}(\boldsymbol{x},t) := \left[u_{|\tau_k}(\boldsymbol{x},t) - \lambda(\boldsymbol{x},t)\right]n_{k,t} \quad \text{for } (\boldsymbol{x},t) \in \Gamma_{k\ell} \quad a.e.$$

For a function $u_h \in S_h^p(\mathcal{T}_N)$ we now can use the definition of λ_h to rewrite the jump in space direction on a facet $\Gamma_{k\ell} \in \Sigma_h$

$$\begin{aligned}
[u_h]_{\Gamma_{k\ell},\boldsymbol{x}}(\boldsymbol{x},t) &= u_{h|\tau_k}(\boldsymbol{x},t)\boldsymbol{n}_{k,\boldsymbol{x}} + u_{h|\tau_\ell}(\boldsymbol{x},t)\boldsymbol{n}_{\ell,\boldsymbol{x}} \\
&= u_{h|\tau_k}(\boldsymbol{x},t)\boldsymbol{n}_{k,\boldsymbol{x}} + \left[2\lambda_{h|\Gamma_{k\ell}}(\boldsymbol{x},t) - u_{h|\tau_k}(\boldsymbol{x},t)\right]\boldsymbol{n}_{\ell,\boldsymbol{x}} \\
&= 2\left[u_{h|\tau_k}(\boldsymbol{x},t) - \lambda_{h|\Gamma_{k\ell}}(\boldsymbol{x},t)\right]\boldsymbol{n}_{k,\boldsymbol{x}} \\
&= 2\,[u_h/\lambda_h]_{\partial\tau_k,\boldsymbol{x}}(\boldsymbol{x},t)
\end{aligned} \tag{3.3}$$

or by using the other representation

$$\begin{aligned}
[u_h]_{\Gamma_{k\ell},\boldsymbol{x}}(\boldsymbol{x},t) &= u_{h|\tau_k}(\boldsymbol{x},t)\boldsymbol{n}_{k,\boldsymbol{x}} + u_{h|\tau_\ell}(\boldsymbol{x},t)\boldsymbol{n}_{\ell,\boldsymbol{x}} \\
&= \left[2\lambda_{h|\Gamma_{k\ell}}(\boldsymbol{x},t) - u_{h|\tau_\ell}(\boldsymbol{x},t)\right]\boldsymbol{n}_{k,\boldsymbol{x}} + u_{h|\tau_\ell}(\boldsymbol{x},t)\boldsymbol{n}_{\ell,\boldsymbol{x}} \\
&= 2\left[u_{h|\tau_\ell}(\boldsymbol{x},t) - \lambda_{h|\Gamma_{k\ell}}(\boldsymbol{x},t)\right]\boldsymbol{n}_{\ell,\boldsymbol{x}} \\
&= 2\,[u_h/\lambda_h]_{\partial\tau_\ell,\boldsymbol{x}}(\boldsymbol{x},t).
\end{aligned} \tag{3.4}$$

With these two representations (3.3) and (3.4) we can express for $u_h \in S_h^p(\mathcal{T}_N)$ the jump on a facet $\Gamma_{k\ell} \in \Sigma_h$ with the two hybrid jumps. For the second coupling term in (3.2) we get the following relation

$$\begin{aligned}
[u_h]_{\Gamma_{k\ell},\boldsymbol{x}}(\boldsymbol{x},t) \cdot \langle \nabla_{\boldsymbol{x}} v_h \rangle_{\Gamma_{k\ell}}(\boldsymbol{x},t) &= [u_h]_{\Gamma_{k\ell},\boldsymbol{x}}(\boldsymbol{x},t) \cdot \frac{1}{2}\left[\nabla_{\boldsymbol{x}} v_{h|\tau_k}(\boldsymbol{x},t) + \nabla_{\boldsymbol{x}} v_{h|\tau_\ell}(\boldsymbol{x},t)\right] \\
&= \frac{1}{2}\,[u_h]_{\Gamma_{k\ell},\boldsymbol{x}}(\boldsymbol{x},t) \cdot \nabla_{\boldsymbol{x}} v_{h|\tau_k}(\boldsymbol{x},t) + \frac{1}{2}\,[u_h]_{\Gamma_{k\ell},\boldsymbol{x}}(\boldsymbol{x},t) \cdot \nabla_{\boldsymbol{x}} v_{h|\tau_\ell}(\boldsymbol{x},t) \\
&= [u_h/\lambda_h]_{\partial\tau_k,\boldsymbol{x}}(\boldsymbol{x},t) \cdot \nabla_{\boldsymbol{x}} v_{h|\tau_k}(\boldsymbol{x},t) + [u_h/\lambda_h]_{\partial\tau_\ell,\boldsymbol{x}}(\boldsymbol{x},t) \cdot \nabla_{\boldsymbol{x}} v_{h|\tau_\ell}(\boldsymbol{x},t).
\end{aligned}$$

Using this relation above we can split the sum over the interface facets into the local sums over the space-time subdomains

$$\sum_{\Gamma_{k\ell} \in \Sigma_h} \int_{\Gamma_{k\ell}} [u_h]_{\Gamma_{k\ell},\boldsymbol{x}}(\boldsymbol{x},t) \cdot \langle \nabla_{\boldsymbol{x}} v_h \rangle_{\Gamma_{k\ell}}(\boldsymbol{x},t) \mathrm{d}s_{(\boldsymbol{x},t)}$$

$$
\begin{aligned}
&= \sum_{\Gamma_{k\ell}\in\Sigma_h} \int_{\Gamma_{k\ell}} \Big[[u_h/\lambda_h]_{\partial\tau_k,\boldsymbol{x}}(\boldsymbol{x},t)\cdot\nabla_{\boldsymbol{x}} v_{h|\tau_k}(\boldsymbol{x},t) \\
&\qquad\qquad + [u_h/\lambda_h]_{\partial\tau_\ell,\boldsymbol{x}}(\boldsymbol{x},t)\cdot\nabla_{\boldsymbol{x}} v_{h|\tau_\ell}(\boldsymbol{x},t)\Big] \mathrm{d}s_{(\boldsymbol{x},t)} \\
&= \sum_{i=1}^{P}\sum_{\ell=1}^{N_i} \sum_{\substack{\Gamma_{k\ell}\in\Sigma_h \\ \Gamma_{k\ell}\subset\partial\tau_\ell^i}} \int_{\Gamma_{k\ell}} [u_h/\lambda_h]_{\partial\tau_\ell^i,\boldsymbol{x}}(\boldsymbol{x},t)\cdot\nabla_{\boldsymbol{x}} v_{h|\tau_\ell^i}(\boldsymbol{x},t)\mathrm{d}s_{(\boldsymbol{x},t)}.
\end{aligned}
$$

If we introduce for the test function $v_h \in S_h^p(\mathcal{T}_N)$ also a new variable $\mu_h \in S_h^p(\Sigma_h)$ on the interface Σ

$$
\mu_{h|\Gamma_{k\ell}}(\boldsymbol{x},t) := \langle v_h\rangle_{\Gamma_{k\ell}}(\boldsymbol{x},t) = \frac{1}{2}\left[v_{h|\tau_k}(\boldsymbol{x},t) + v_{h|\tau_k}(\boldsymbol{x},t)\right] \quad \text{for all } (\boldsymbol{x},t)\in\Gamma_{k\ell},
$$

we can rewrite the first coupling part of (3.2) in the same way

$$
\begin{aligned}
&\sum_{\Gamma_{k\ell}\in\Sigma_h} \int_{\Gamma_{k\ell}} \langle\nabla_{\boldsymbol{x}} u_h\rangle_{\Gamma_{k\ell}}(\boldsymbol{x},t)\cdot[v_h]_{\Gamma_{k\ell},\boldsymbol{x}}(\boldsymbol{x},t)\mathrm{d}s_{(\boldsymbol{x},t)} = \\
&\qquad \sum_{i=1}^{P}\sum_{\ell=1}^{N_i} \sum_{\substack{\Gamma_{k\ell}\in\Sigma_h \\ \Gamma_{k\ell}\subset\partial\tau_\ell^i}} \int_{\Gamma_{k\ell}} \nabla_{\boldsymbol{x}} u_{h|\tau_\ell^i}(\boldsymbol{x},t)\cdot[v_h/\mu_h]_{\partial\tau_\ell^i,\boldsymbol{x}}(\boldsymbol{x},t)\mathrm{d}s_{(\boldsymbol{x},t)}.
\end{aligned}
$$

Next we will focus on the third coupling part of (3.2). We use the two relations (3.3) and (3.4) to rewrite the stabilization terms on the interface

$$
\begin{aligned}
&[u_h]_{\Gamma_{k\ell},\boldsymbol{x}}(\boldsymbol{x},t)\cdot[v_h]_{\Gamma_{k\ell},\boldsymbol{x}}(\boldsymbol{x},t) \\
&\qquad = \frac{1}{2}[u_h]_{\Gamma_{k\ell},\boldsymbol{x}}(\boldsymbol{x},t)\cdot[v_h]_{\Gamma_{k\ell},\boldsymbol{x}}(\boldsymbol{x},t) + \frac{1}{2}[u_h]_{\Gamma_{k\ell},\boldsymbol{x}}(\boldsymbol{x},t)\cdot[v_h]_{\Gamma_{k\ell},\boldsymbol{x}}(\boldsymbol{x},t) \\
&\qquad = 2[u_h/\lambda_h]_{\partial\tau_k,\boldsymbol{x}}(\boldsymbol{x},t)\cdot[v_h/\mu_h]_{\partial\tau_k,\boldsymbol{x}}(\boldsymbol{x},t) \\
&\qquad\quad + 2[u_h/\lambda_h]_{\partial\tau_\ell,\boldsymbol{x}}(\boldsymbol{x},t)\cdot[v_h/\mu_h]_{\partial\tau_\ell,\boldsymbol{x}}(\boldsymbol{x},t).
\end{aligned}
$$

With this new representation above the third coupling term of (3.2) can be expressed in the following way

$$
\begin{aligned}
&\sum_{\Gamma_{k\ell}\in\Sigma_h} \frac{\sigma}{\overline{h}_{k\ell}} \int_{\Gamma_{k\ell}} [u_h]_{\Gamma_{k\ell},\boldsymbol{x}}(\boldsymbol{x},t)\cdot[v_h]_{\Gamma_{k\ell},\boldsymbol{x}}(\boldsymbol{x},t)\mathrm{d}s_{(\boldsymbol{x},t)} \\
&\quad = \sum_{\Gamma_{k\ell}\in\Sigma_h} \frac{2\sigma}{\overline{h}_{k\ell}} \int_{\Gamma_{k\ell}} \Big[[u_h/\lambda_h]_{\partial\tau_k,\boldsymbol{x}}(\boldsymbol{x},t)\cdot[v_h/\mu_h]_{\partial\tau_k,\boldsymbol{x}}(\boldsymbol{x},t) \\
&\qquad\qquad + [u_h/\lambda_h]_{\partial\tau_\ell,\boldsymbol{x}}(\boldsymbol{x},t)\cdot[v_h/\mu_h]_{\partial\tau_\ell,\boldsymbol{x}}(\boldsymbol{x},t)\Big] \mathrm{d}s_{(\boldsymbol{x},t)} \\
&\quad = \sum_{i=1}^{P}\sum_{\ell=1}^{N_i} \sum_{\substack{\Gamma_{k\ell}\in\Sigma_h \\ \Gamma_{k\ell}\subset\partial\tau_\ell^i}} \frac{2\sigma}{\overline{h}_{k\ell}} \int_{\Gamma_{k\ell}} [u_h/\lambda_h]_{\partial\tau_\ell^i,\boldsymbol{x}}(\boldsymbol{x},t)\cdot[v_h/\mu_h]_{\partial\tau_\ell^i,\boldsymbol{x}}(\boldsymbol{x},t)\mathrm{d}s_{(\boldsymbol{x},t)}.
\end{aligned}
$$

For the fourth coupling part of (3.2), the coupling in time direction, we introduce a new upwind term between functions on the interface and functions on the local space-time subdomains.

Definition 3.1.2 (Hybrid upwind)**.** *Let $\Gamma_{k\ell} \in \Sigma_h$ be a facet on the interface Σ with the outer unit normal vector $\boldsymbol{n}_k = (\boldsymbol{n}_{k,\boldsymbol{x}}, n_{k,t})^\top$ with respect to the element τ_k. For a given function $u \in H^s(\mathcal{T}_N)$, $s \geq 1$ and a function $\lambda \in L_2(\Sigma_h)$ the hybrid upwind in time direction for the element τ_k is given by*

$$\{u/\lambda\}^{\text{up}}_{\partial\tau_k}(\boldsymbol{x},t) := \begin{cases} u_{|\tau_k}(\boldsymbol{x},t) & \text{for } n_{k,t} > 0, \\ 0 & \text{for } n_{k,t} = 0, \\ \lambda(\boldsymbol{x},t) & \text{for } n_{k,t} < 0 \end{cases} \quad \text{for } (\boldsymbol{x},t) \in \Gamma_{k\ell}.$$

With this new definition of the hybrid upwind, we reformulate the standard upwind term in the following way. First we split the upwind in time direction into two parts

$$\{u_h\}^{\text{up}}_{\Gamma_{k\ell}}(\boldsymbol{x},t) = \frac{1}{2}\{u_h\}^{\text{up}}_{\Gamma_{k\ell}}(\boldsymbol{x},t) + \frac{1}{2}\{u_h\}^{\text{up}}_{\Gamma_{k\ell}}(\boldsymbol{x},t).$$

Next we use the definition of the upwind term, where we use for the first part the normal vector of the element τ_k and for the second part we use the normal vector of the element τ_ℓ

$$= \frac{1}{2}\begin{cases} u_{h|\tau_k}(\boldsymbol{x},t) & \text{for } n_{k,t} > 0, \\ 0 & \text{for } n_{k,t} = 0, \\ u_{h|\tau_\ell}(\boldsymbol{x},t) & \text{for } n_{k,t} < 0 \end{cases} + \frac{1}{2}\begin{cases} u_{h|\tau_\ell}(\boldsymbol{x},t) & \text{for } n_{\ell,t} > 0, \\ 0 & \text{for } n_{\ell,t} = 0, \\ u_{h|\tau_k}(\boldsymbol{x},t) & \text{for } n_{\ell,t} < 0. \end{cases}$$

Adding and subtracting the interface variable λ_h leads to

$$= \frac{1}{2}\begin{cases} u_{h|\tau_k}(\boldsymbol{x},t) & \text{for } n_{k,t} > 0, \\ 0 & \text{for } n_{k,t} = 0, \\ \lambda_h(\boldsymbol{x},t) & \text{for } n_{k,t} < 0 \end{cases} + \frac{1}{2}\begin{cases} u_{h|\tau_\ell}(\boldsymbol{x},t) & \text{for } n_{\ell,t} > 0, \\ 0 & \text{for } n_{\ell,t} = 0, \\ \lambda_h(\boldsymbol{x},t) & \text{for } n_{\ell,t} < 0 \end{cases}$$
$$+ \frac{1}{2}\begin{cases} u_{h|\tau_k}(\boldsymbol{x},t) - \lambda_h(\boldsymbol{x},t) & \text{for } n_{k,t} > 0, \\ 0 & \text{for } n_{k,t} = 0, \\ u_{h|\tau_\ell}(\boldsymbol{x},t) - \lambda_h(\boldsymbol{x},t) & \text{for } n_{k,t} < 0. \end{cases}$$

With the definition of the hybrid jump we end up with another representation for the upwind term in time direction

$$= \frac{1}{2}\{u_h/\lambda_h\}^{\text{up}}_{\partial\tau_k}(\boldsymbol{x},t) + \frac{1}{2}\{u_h/\lambda_h\}^{\text{up}}_{\partial\tau_\ell}(\boldsymbol{x},t)$$

$$+\frac{1}{2}\begin{cases} u_{h|\tau_k}(\boldsymbol{x},t)-\lambda_h(\boldsymbol{x},t) & \text{for } n_{k,t}>0,\\ 0 & \text{for } n_{k,t}=0,\\ u_{h|\tau_\ell}(\boldsymbol{x},t)-\lambda_h(\boldsymbol{x},t) & \text{for } n_{k,t}<0. \end{cases}$$

For a classical, i.e. continuous, solution of the model problem (2.1) we obtain for an interior facet $\Gamma_{k\ell}\in\Sigma_h$ the relations

$$\lambda(\boldsymbol{x},t):=\langle u\rangle_{\Gamma_{k\ell}}(\boldsymbol{x},t)=u_{|\tau_k}(\boldsymbol{x},t)=u_{|\tau_\ell}(\boldsymbol{x},t)\quad\text{for } (\boldsymbol{x},t)\in\Gamma_{k\ell}.$$

For the exact solution of (2.1) we therefore have the following representation for the upwind term in time on an interior facet $\Gamma_{k\ell}\in\Sigma_h$

$$\{u\}^{\mathrm{up}}_{\Gamma_{k\ell}}(\boldsymbol{x},t)=\frac{1}{2}\{u/\lambda\}^{\mathrm{up}}_{\partial\tau_k}(\boldsymbol{x},t)+\frac{1}{2}\{u/\lambda\}^{\mathrm{up}}_{\partial\tau_\ell}(\boldsymbol{x},t)\quad\text{for } (\boldsymbol{x},t)\in\Gamma_{k\ell}. \tag{3.5}$$

This motivates to use on the interface Σ also for the discrete case the representation (3.5) for the upwind in time direction. Using the same manipulations as above and replacing the upwind in time direction by (3.5) we replace the fourth coupling part of (3.2)

$$\sum_{\Gamma_{k\ell}\in\Sigma_h}\int_{\Gamma_{k\ell}}\{u_h\}^{\mathrm{up}}_{\Gamma_{k\ell}}(\boldsymbol{x},t)\,[v_h]_{\Gamma_{k\ell},t}(\boldsymbol{x},t)\mathrm{d}s_{(\boldsymbol{x},t)}$$

with the coupling term

$$\sum_{i=1}^{P}\sum_{\ell=1}^{N_i}\sum_{\substack{\Gamma_{k\ell}\in\Sigma_h\\ \Gamma_{k\ell}\subset\partial\tau_\ell^i}}\int_{\Gamma_{k\ell}}\{u_h/\lambda_h\}^{\mathrm{up}}_{\partial\tau_\ell^i}(\boldsymbol{x},t)\,[v_h/\mu_h]_{\partial\tau_\ell^i,\boldsymbol{x}}(\boldsymbol{x},t)\mathrm{d}s_{(\boldsymbol{x},t)}.$$

Now we can define for each space-time subdomain Q_i the local bilinear form

$$\begin{aligned} c^{(i)}(u_h,\lambda_h;v_h,\mu_h):=&-\sum_{\ell=1}^{N_i}\sum_{\substack{\Gamma_{k\ell}\in\Sigma_h\\ \Gamma_{k\ell}\subset\partial\tau_\ell^i}}\int_{\Gamma_{k\ell}}[u_h/\lambda_h]_{\partial\tau_\ell^i,\boldsymbol{x}}(\boldsymbol{x},t)\cdot\nabla_{\boldsymbol{x}}v_{h|\tau_\ell^i}(\boldsymbol{x},t)\mathrm{d}s_{(\boldsymbol{x},t)}\\ &-\sum_{\ell=1}^{N_i}\sum_{\substack{\Gamma_{k\ell}\in\Sigma_h\\ \Gamma_{k\ell}\subset\partial\tau_\ell^i}}\int_{\Gamma_{k\ell}}\nabla_{\boldsymbol{x}}u_{h|\tau_\ell^i}(\boldsymbol{x},t)\cdot[v_h/\mu_h]_{\partial\tau_\ell^i,\boldsymbol{x}}(\boldsymbol{x},t)\mathrm{d}s_{(\boldsymbol{x},t)}\\ &+\sum_{\ell=1}^{N_i}\sum_{\substack{\Gamma_{k\ell}\in\Sigma_h\\ \Gamma_{k\ell}\subset\partial\tau_\ell^i}}\frac{2\sigma}{\overline{h}_{k\ell}}\int_{\Gamma_{k\ell}}[u_h/\lambda_h]_{\partial\tau_\ell^i,\boldsymbol{x}}(\boldsymbol{x},t)\cdot[v_h/\mu_h]_{\partial\tau_\ell^i,\boldsymbol{x}}(\boldsymbol{x},t)\mathrm{d}s_{(\boldsymbol{x},t)}\\ &+\sum_{\ell=1}^{N_i}\sum_{\substack{\Gamma_{k\ell}\in\Sigma_h\\ \Gamma_{k\ell}\subset\partial\tau_\ell^i}}\int_{\Gamma_{k\ell}}\{u_h/\lambda_h\}^{\mathrm{up}}_{\partial\tau_\ell^i}(\boldsymbol{x},t)\,[v_h/\mu_h]_{\partial\tau_\ell^i,\boldsymbol{x}}(\boldsymbol{x},t)\mathrm{d}s_{(\boldsymbol{x},t)}. \end{aligned} \tag{3.6}$$

With the local coupling parts (3.6) we are now able to formulate the hybrid space-time discretization.

Find $u_h \in S_h^p(\mathcal{T}_N)$ and $\lambda_h \in S_h^p(\Sigma_h)$ such that

$$\sum_{i=1}^{P} \left[A^{(i)}(u_h, v_h) + c^{(i)}(u_h, \lambda_h; v_h, \mu_h) \right] = \sum_{i=1}^{P} F^{(i)}(v_h) \tag{3.7}$$

is satisfied for all $v_h \in S_h^p(\mathcal{T}_N)$ and $\mu_h \in S_h^p(\Sigma_h)$.

Remark 3.1.3. *A solution $u_h \in S_h^p(\mathcal{T}_N)$ of the hybrid formulation (3.7) is in general not a solution of the discrete problem (2.2), because in the hybrid formulation (3.7) a different upwind term in time is used.*

Remark 3.1.4. *In the hybrid formulation (3.7) everything is local with respect to each space-time subdomain Q_i, $i = 1, \ldots, P$. Therefore it is possible to use different approximation schemes on different subdomains. Hence this hybrid formulation allows the coupling of finite element methods with boundary element methods or the coupling with standard finite difference schemes, like the implicit Euler time stepping scheme for example.*

Next we introduce the equivalent linear system for the discrete variational problem (3.7). For each space-time decomposition $\mathcal{T}_{N_i}$, $i = 1, \ldots, P$, let φ_ℓ^i, $\ell = 1, \ldots, M_i$ be a basis of the discrete function space $S_h^p(\mathcal{T}_{N_i})$, i.e.

$$S_h^p(\mathcal{T}_{N_i}) = \operatorname{span}\left\{ \varphi_\ell^i \right\}_{\ell=1}^{M_i}, \qquad u_h^i(\boldsymbol{x}, t) = \sum_{\ell=1}^{M_i} \boldsymbol{u}_I^{(i)}[\ell] \varphi_\ell^i(\boldsymbol{x}, t) \quad \text{for } u_h^i \in S_h^p(\mathcal{T}_{N_i}).$$

Further let ψ_n, $n = 1, \ldots, M_\Sigma$ be a basis of the discrete function space $S_h^p(\Sigma_h)$, i.e.

$$S_h^p(\Sigma_h) = \operatorname{span}\{\psi_n\}_{n=1}^{M_\Sigma}, \qquad \lambda_h(\boldsymbol{x}, t) = \sum_{n=1}^{M_\Sigma} \boldsymbol{\lambda}_\Sigma[n] \psi_n(\boldsymbol{x}, t) \quad \text{for } \lambda_h \in S_h^p(\Sigma_h).$$

Next we define for each space-time decomposition $\mathcal{T}_{N_i}$, $i = 1, \ldots, P$, the local matrices

$$\begin{aligned}
A_{II}^{(i)}[k, \ell] &:= A^{(i)}(\varphi_\ell^i, \varphi_k^i) + c^{(i)}(\varphi_\ell^i, 0; \varphi_k^i, 0) && \text{for } k, \ell = 1, \ldots, M_i, \\
A_{I\Sigma}^{(i)}[k, n] &:= c^{(i)}(0, \psi_n; \varphi_k^i, 0) && \text{for } k = 1, \ldots, M_i \text{ and } n = 1, \ldots, M_\Sigma, \\
A_{\Sigma I}^{(i)}[m, \ell] &:= c^{(i)}(\varphi_\ell^i, 0; 0, \psi_m) && \text{for } m = 1, \ldots, M_\Sigma \text{ and } \ell = 1, \ldots, M_i
\end{aligned}$$

and the local right hand sides

$$\boldsymbol{f}_I^{(i)}[k] := F^{(i)}(\varphi_k^i) \qquad \text{for } k = 1, \ldots, M_i.$$

For the decomposition of the interface Σ_h we define the matrix

$$A_{\Sigma\Sigma}[m, n] := \sum_{i=1}^{P} c^{(i)}(0, \psi_n; 0, \psi_m) \qquad \text{for } m, n = 1, \ldots, M_\Sigma.$$

Then the discrete variational problem (3.7) is equivalent to the system of linear algebraic equations

$$\begin{pmatrix} A_{II}^{(1)} & & & & A_{I\Sigma}^{(1)} \\ & A_{II}^{(2)} & & & A_{I\Sigma}^{(2)} \\ & & \ddots & & \vdots \\ & & & A_{II}^{(P)} & A_{I\Sigma}^{(P)} \\ A_{\Sigma I}^{(1)} & A_{\Sigma I}^{(2)} & \cdots & A_{\Sigma I}^{(P)} & A_{\Sigma\Sigma} \end{pmatrix} \begin{pmatrix} \boldsymbol{u}_I^{(1)} \\ \boldsymbol{u}_I^{(2)} \\ \vdots \\ \boldsymbol{u}_I^{(P)} \\ \boldsymbol{\lambda}_\Sigma \end{pmatrix} = \begin{pmatrix} \boldsymbol{f}_I^{(1)} \\ \boldsymbol{f}_I^{(2)} \\ \vdots \\ \boldsymbol{f}_I^{(P)} \\ \boldsymbol{0} \end{pmatrix}. \tag{3.8}$$

Remark 3.1.5. *The linear system (3.8) has the same structure as the linear systems arising from general domain decomposition approaches, like FETI methods for example. Therefore the same implementation framework and algorithms can be used to assemble and solve the linear system (3.8). For an introduction to domain decomposition methods see [61, 73, 74, 98] for example.*

In Section 3.2 an ellipticity estimate for the local bilinear forms

$$A^{(i)}(u_h^i, u_h^i) + c^{(i)}(u_h^i, 0; u_h^i, 0) > 0 \qquad \text{for all } 0 \neq u_h^i \in S_h^p(\mathcal{T}_{N_i}) \tag{3.9}$$

is shown in Theorem 3.2.5. Hence the local matrices $A_{II}^{(i)}$ are invertible for any space-time subdomain Q_i, $i = 1, \ldots, P$. Therefore we obtain from the global linear system (3.8) the Schur complement system

$$\left[A_{\Sigma\Sigma} - \sum_{i=1}^{P} A_{\Sigma I}^{(i)} \left(A_{II}^{(i)} \right)^{-1} A_{I\Sigma}^{(i)} \right] \boldsymbol{\lambda}_\Sigma = - \sum_{i=1}^{P} A_{\Sigma I}^{(i)} \left(A_{II}^{(i)} \right)^{-1} \boldsymbol{f}_I^{(i)}, \tag{3.10}$$

where the local solutions are given by

$$\boldsymbol{u}_I^{(i)} = \left(A_{II}^{(i)} \right)^{-1} \left[\boldsymbol{f}_I^{(i)} - A_{I\Sigma}^{(i)} \boldsymbol{\lambda}_\Sigma \right] \qquad \text{for } i = 1, \ldots, P. \tag{3.11}$$

The Schur complement system (3.10) is in general non-symmetric, since the model problem itself is non-symmetric. For the solution of the Schur complement system (3.10) we can use for example the GMRES method [81,88], where the inversion of the local matrices $A_{II}^{(i)}$ can be done in parallel either by using a direct approach, or by a suitable iterative scheme. After solving for the Lagrange multipliers $\boldsymbol{\lambda}_\Sigma$ one can compute the solutions on each space-time subdomain in parallel by using the equation (3.11).

Remark 3.1.6 (Static condensation)**.** *If any element $\tau_\ell \in \mathcal{T}_N$ is assumed to be a single subdomain Q_ℓ, $\ell = 1, \ldots, N$, then the Schur complement system (3.10) can be easily set up by computing the inverse of the small local problems $A_{II}^{(i)}$ exactly. Then the Schur complement system (3.10) preserves also the sparse structure. With this approach we arrive in a pure hybrid setting where the unknowns of the Schur complement system (3.10) are located on the element facets $\mathcal{I}_N$. This approach has advantages for example when higher polynomial ansatz functions are used. For hybrid methods applied to other model problems see [21, 22, 54, 63, 69, 70].*

3.2 Numerical analysis

In this section the presented hybrid space-time method will be analyzed. Here we also assume that Assumption 2.2.1 and Assumption 2.2.2 are satisfied. First we focus on the local bilinear forms, where we show an ellipticity estimate, which guarantees unique solvability of the local space-time problems. After that, we will show an stability estimate for the whole hybrid method. At the end a priori error estimates in some energy norm will be derived.

With the same arguments as in Chapter 2 it is possible to bound the local bilinear forms $a^{(i)}(\cdot,\cdot)$ from above.

Lemma 3.2.1. *Let the stabilization parameter be large enough, i.e.* $\sigma \geq 4c_K$. *Further let* $\mathcal{T}_{N_i}$ *be a given space-time decomposition. Then the following estimate holds*

$$a^{(i)}(u_h^i, u_h^i) \geq \frac{1}{2}\left[\sum_{\ell=1}^{N_i} \left\|\nabla_{\boldsymbol{x}} u_h^i\right\|^2_{[L_2(\tau_\ell^i)]^d} + \sum_{\Gamma_{k\ell}\in\mathcal{I}_{N_i}} \frac{\sigma}{\overline{h}_{k\ell}} \left\| \left[u_h^i\right]_{\Gamma_{k\ell},\boldsymbol{x}} \right\|^2_{[L_2(\Gamma_{k\ell})]^d}\right]$$

for all $u_h^i \in S_h^p(\mathcal{T}_{N_i})$.

Proof. The estimate is a direct consequence of Lemma 2.2.9. ∎

For the next lemma we define the following sets of interior facets. First we define the set of all interface facets which belong to the space-time subdomain decomposition $\mathcal{T}_{N_i}$

$$\Sigma_{N_i} := \left\{\Gamma_{k\ell} \in \Sigma_N : \Gamma_{k\ell} \subset \partial\tau_k^i \text{ with } \tau_k^i \in \mathcal{T}_{N_i}\right\}.$$

Next we split the set of all interface facets Σ_{N_i} into two parts. The set

$$\Sigma_{N_i}^+ := \left\{\Gamma_{k\ell} \in \Sigma_{N_i} : n_{k,t} \geq 0\right\}$$

contains all interior facets where the outer unit normal vector $\boldsymbol{n}_k$ is pointing to the future. Furthermore, we define the set

$$\Sigma_{N_i}^- := \left\{\Gamma_{k\ell} \in \Sigma_{N_i} : n_{k,t} < 0\right\} = \Sigma_{N_i} \setminus \Sigma_{N_i}^+$$

with all interior facets where the outer unit normal vector $\boldsymbol{n}_k$ is pointing to the past. With these sets of interface facets we can give the following lemma.

Lemma 3.2.2. *For the local bilinear forms $b^{(i)}(\cdot,\cdot)$ the following estimate holds*

$$\begin{aligned} b^{(i)}(u_h^i,u_h^i) \geq \frac{1}{2}\left[\left\|u_h^i\right\|^2_{L_2(\Sigma_0\cap\partial Q_i)} + \left\|u_h^i\right\|^2_{L_2(\Sigma_T\cap\partial Q_i)} + \sum_{\Gamma_{k\ell}\in\mathcal{I}_{N_i}}\left\|\left[u_h^i\right]_{\Gamma_{k\ell},t}\right\|^2_{L_2(\Gamma_{k\ell})}\right] \\ + \frac{1}{2}\sum_{\Gamma_{k\ell}\in\Sigma^-_{N_i}}\left\|\left[u_h^i/0\right]_{\partial\tau_k^i,t}\right\|^2_{L_2(\Gamma_{k\ell})} \\ - \frac{1}{2}\sum_{\Gamma_{k\ell}\in\Sigma^+_{N_i}}\int_{\Gamma_{k\ell}}\left|n_{\ell,t}\right|\left(\left[u_h^i\right]_{\Gamma_{k\ell},t}(\boldsymbol{x},t)\right)^2 \mathrm{d}s_{(\boldsymbol{x},t)} \end{aligned}$$

for all $u_h^i \in S_h^p(\mathcal{T}_{N_i})$.

Proof. Let $u_h^i \in S_h^p(\mathcal{T}_{N_i})$. Using the definition of the local bilinear form $b^{(i)}(\cdot,\cdot)$ we have

$$\begin{aligned} b^{(i)}(u_h^i,u_h^i) = -\sum_{\ell=1}^{N_i}\int_{\tau_\ell^i} u_h^i(\boldsymbol{x},t)\partial_t u_h^i(\boldsymbol{x},t)\mathrm{d}(\boldsymbol{x},t) + \left\|u_h^i\right\|^2_{L_2(\Sigma_T\cap\partial Q_i)} \\ + \sum_{\Gamma_{k\ell}\in\mathcal{I}_{N_i}}\int_{\Gamma_{k\ell}}\left\{u_h^i\right\}^{\mathrm{up}}_{\Gamma_{k\ell}}(\boldsymbol{x},t)\left[u_h^i\right]_{\Gamma_{k\ell},t}(\boldsymbol{x},t)\mathrm{d}s_{(\boldsymbol{x},t)}. \end{aligned}$$

Rewriting the first term and applying Gauss's theorem leads to

$$\begin{aligned} &= -\sum_{\ell=1}^{N_i}\int_{\tau_\ell^i}\frac{1}{2}\partial_t\left(u_h^i(\boldsymbol{x},t)\right)^2\mathrm{d}(\boldsymbol{x},t) + \left\|u_h^i\right\|^2_{L_2(\Sigma_T\cap\partial Q_i)} \\ &\quad + \sum_{\Gamma_{k\ell}\in\mathcal{I}_{N_i}}\int_{\Gamma_{k\ell}}\left\{u_h^i\right\}^{\mathrm{up}}_{\Gamma_{k\ell}}(\boldsymbol{x},t)\left[u_h^i\right]_{\Gamma_{k\ell},t}(\boldsymbol{x},t)\mathrm{d}s_{(\boldsymbol{x},t)} \\ &= -\frac{1}{2}\sum_{\ell=1}^{N_i}\int_{\partial\tau_\ell^i} n_{\ell,t}\left(u_h^i(\boldsymbol{x},t)\right)^2\mathrm{d}s_{(\boldsymbol{x},t)} + \left\|u_h^i\right\|^2_{L_2(\Sigma_T\cap\partial Q_i)} \\ &\quad + \sum_{\Gamma_{k\ell}\in\mathcal{I}_{N_i}}\int_{\Gamma_{k\ell}}\left\{u_h^i\right\}^{\mathrm{up}}_{\Gamma_{k\ell}}(\boldsymbol{x},t)\left[u_h^i\right]_{\Gamma_{k\ell},t}(\boldsymbol{x},t)\mathrm{d}s_{(\boldsymbol{x},t)}. \end{aligned}$$

Now we can reorder the sum over all elements to a sum over all interior facets and a sum over the boundaries Σ_0 and Σ_T and we get

$$= \frac{1}{2}\left[\left\|u_h^i\right\|^2_{L_2(\Sigma_0\cap\partial Q_i)} + \left\|u_h^i\right\|^2_{L_2(\Sigma_T\cap\partial Q_i)}\right]$$

$$
\begin{aligned}
&+\sum_{\Gamma_{k\ell}\in\mathcal{I}_{N_i}}\int_{\Gamma_{k\ell}}\left[\{u_h^i\}^{\mathrm{up}}_{\Gamma_{k\ell}}(\boldsymbol{x},t)\left[u_h^i\right]_{\Gamma_{k\ell},t}(\boldsymbol{x},t)-\frac{1}{2}\left[(u_h^i)^2\right]_{\Gamma_{k\ell},t}(\boldsymbol{x},t)\right]\mathrm{d}s_{(\boldsymbol{x},t)}\\
&+\frac{1}{2}\sum_{\Gamma_{k\ell}\in\Sigma^-_{N_i}}\int_{\Gamma_{k\ell}}\left|n_{k,t}\right|\left(\left[u_h^i\right]_{\Gamma_{k\ell},t}(\boldsymbol{x},t)\right)^2\mathrm{d}s_{(\boldsymbol{x},t)}\\
&-\frac{1}{2}\sum_{\Gamma_{k\ell}\in\Sigma^+_{N_i}}\int_{\Gamma_{k\ell}}\left|n_{k,t}\right|\left(\left[u_h^i\right]_{\Gamma_{k\ell},t}(\boldsymbol{x},t)\right)^2\mathrm{d}s_{(\boldsymbol{x},t)}.
\end{aligned}
$$

Next we use Lemma 2.2.10 and we obtain

$$
\begin{aligned}
&=\frac{1}{2}\left[\left\|u_h^i\right\|^2_{L_2(\Sigma_0\cap\partial Q_i)}+\left\|u_h^i\right\|^2_{L_2(\Sigma_T\cap\partial Q_i)}\right]\\
&+\frac{1}{2}\sum_{\Gamma_{k\ell}\in\mathcal{I}_{N_i}}\int_{\Gamma_{k\ell}}\left|n_{k,t}\right|\left(\left[u_h^i\right]_{\Gamma_{k\ell},t}(\boldsymbol{x},t)\right)^2\mathrm{d}s_{(\boldsymbol{x},t)}\\
&+\frac{1}{2}\sum_{\Gamma_{k\ell}\in\Sigma^-_{N_i}}\int_{\Gamma_{k\ell}}\left|n_{k,t}\right|\left(\left[u_h^i\right]_{\Gamma_{k\ell},t}(\boldsymbol{x},t)\right)^2\mathrm{d}s_{(\boldsymbol{x},t)}\\
&-\frac{1}{2}\sum_{\Gamma_{k\ell}\in\Sigma^+_{N_i}}\int_{\Gamma_{k\ell}}\left|n_{k,t}\right|\left(\left[u_h^i\right]_{\Gamma_{k\ell},t}(\boldsymbol{x},t)\right)^2\mathrm{d}s_{(\boldsymbol{x},t)}.
\end{aligned}
$$

The estimate of this lemma follows by using the inequality $\left|n_{k,t}\right|\geq\left|n_{k,t}\right|^2$

$$
\begin{aligned}
&\geq\frac{1}{2}\left[\left\|u_h^i\right\|^2_{L_2(\Sigma_0\cap\partial Q_i)}+\left\|u_h^i\right\|^2_{L_2(\Sigma_T\cap\partial Q_i)}+\sum_{\Gamma_{k\ell}\in\mathcal{I}_{N_i}}\left\|\left[u_h^i\right]_{\Gamma_{k\ell},t}\right\|^2_{L_2(\Gamma_{k\ell})}\right]\\
&+\frac{1}{2}\sum_{\Gamma_{k\ell}\in\Sigma^-_{N_i}}\left\|\left[u_h^i/0\right]_{\partial\tau_k^i,t}\right\|^2_{L_2(\Gamma_{k\ell})}\\
&-\frac{1}{2}\sum_{\Gamma_{k\ell}\in\Sigma^+_{N_i}}\int_{\Gamma_{k\ell}}\left|n_{\ell,t}\right|\left(\left[u_h^i\right]_{\Gamma_{k\ell},t}(\boldsymbol{x},t)\right)^2\mathrm{d}s_{(\boldsymbol{x},t)}.
\end{aligned}
$$

■

Analogously to Lemma 2.2.6 we can prove the following lemma.

Lemma 3.2.3. *Let $u_h^i\in S_h^p(\mathcal{T}_{N_i})$. Then the following estimate holds*

$$
\sum_{\ell=1}^{N_i}\sum_{\substack{\Gamma_{k\ell}\in\Sigma_h\\ \Gamma_{k\ell}\subset\partial\tau_\ell^i}}\overline{h}_{k\ell}\left\|\nabla_{\boldsymbol{x}}u^i_{h|\tau_\ell^i}\right\|^2_{[L_2(\Gamma_{k\ell})]^d}\leq c_K\sum_{\ell=1}^{N_i}\left\|\nabla_{\boldsymbol{x}}u_h^i\right\|^2_{[L_2(\tau_\ell^i)]^d},
$$

with a constant $c_K=c_K(c_I,c_G,c_{R_2})$.

Proof. Let $u_h^i \in S_h^p(\mathcal{T}_{N_i})$. Using the inverse inequality (2.9) gives the bound

$$\sum_{\ell=1}^{N_i} \sum_{\substack{\Gamma_{k\ell}\in\Sigma_h \\ \Gamma_{k\ell}\subset\partial\tau_\ell^i}} \overline{h}_{k\ell} \left\| \nabla_{\boldsymbol{x}} u_{h|\tau_\ell^i}^i \right\|_{[L_2(\Gamma_{k\ell})]^d}^2 \leq c_I^2 \sum_{\ell=1}^{N_i} \sum_{\substack{\Gamma_{k\ell}\in\Sigma_h \\ \Gamma_{k\ell}\subset\partial\tau_\ell^i}} |\Gamma_{k\ell}| \left|\tau_\ell^i\right|^{-1} \overline{h}_{k\ell} \left\| \nabla_{\boldsymbol{x}} u_h^i \right\|_{[L_2(\tau_\ell^i)]^d}^2.$$

With the local mesh grading Assumption 2.2.2 we further get

$$\begin{aligned} &\leq c_I^2 c_G \sum_{\ell=1}^{N_i} h_\ell^i \left|\tau_\ell^i\right|^{-1} \left\| \nabla_{\boldsymbol{x}} u_h^i \right\|_{[L_2(\tau_\ell^i)]^d}^2 \sum_{\substack{\Gamma_{k\ell}\in\Sigma_h \\ \Gamma_{k\ell}\subset\partial\tau_\ell^i}} |\Gamma_{k\ell}| \\ &\leq c_I^2 c_G \sum_{\ell=1}^{N_i} h_\ell^i \left|\partial\tau_\ell^i\right| \left|\tau_\ell^i\right|^{-1} \left\| \nabla_{\boldsymbol{x}} u_h^i \right\|_{[L_2(\tau_\ell^i)]^d}^2. \end{aligned}$$

Applying the shape regularity Assumption 2.2.1 and with $|\tau_\ell| = h_\ell^{d+1}$ we obtain the stated bound of this lemma

$$\leq c_I^2 c_G c_{R_2} \sum_{\ell=1}^{N_i} \left\| \nabla_{\boldsymbol{x}} u_h^i \right\|_{[L_2(\tau_\ell^i)]^d}^2.$$

■

Lemma 3.2.4. *Let us assume for the stabilization parameter $\sigma \geq 4c_K$, then the following estimate holds*

$$\begin{aligned} c^{(i)}(u_h^i, 0; u_h^i, 0) \geq -\frac{1}{4} \sum_{\ell=1}^{N_i} \left\| \nabla_{\boldsymbol{x}} u_h^i \right\|_{[L_2(\tau_\ell^i)]^d}^2 + \sum_{\Gamma_{k\ell}\in\Sigma_{N_i}} \frac{\sigma}{\overline{h}_{k\ell}} \left\| \left[u_h^i/0\right]_{\partial\tau_k^i,\boldsymbol{x}} \right\|_{[L_2(\Gamma_{k\ell})]^d}^2 \\ + \sum_{\Gamma_{k\ell}\in\Sigma_{N_i}^+} \int_{\Gamma_{k\ell}} \left|n_{\ell,t}\right| \left(\left[u_h^i\right]_{\Gamma_{k\ell},t}(\boldsymbol{x},t) \right)^2 \mathrm{d}s_{(\boldsymbol{x},t)} \end{aligned}$$

for all $u_h^i \in S_h^p(\mathcal{T}_{N_i})$.

Proof. Let $u_h^i \in S_h^p(\mathcal{T}_{N_i})$. Using the definition of the bilinear form $c(\cdot,0;\cdot,0)$ we have

$$\begin{aligned} c^{(i)}(u_h^i, 0; u_h^i, 0) = -2 \sum_{\ell=1}^{N_i} \sum_{\substack{\Gamma_{k\ell}\in\Sigma_h \\ \Gamma_{k\ell}\subset\partial\tau_\ell^i}} \int_{\Gamma_{k\ell}} [u_h/0]_{\partial\tau_\ell^i,\boldsymbol{x}}(\boldsymbol{x},t) \cdot \nabla_{\boldsymbol{x}} u_{h|\tau_\ell^i}(\boldsymbol{x},t) \mathrm{d}s_{(\boldsymbol{x},t)} \\ + \sum_{\ell=1}^{N_i} \sum_{\substack{\Gamma_{k\ell}\in\Sigma_h \\ \Gamma_{k\ell}\subset\partial\tau_\ell^i}} \frac{2\sigma}{\overline{h}_{k\ell}} \int_{\Gamma_{k\ell}} [u_h/0]_{\partial\tau_\ell^i,\boldsymbol{x}}(\boldsymbol{x},t) \cdot [u_h/0]_{\partial\tau_\ell^i,\boldsymbol{x}}(\boldsymbol{x},t) \mathrm{d}s_{(\boldsymbol{x},t)} \end{aligned}$$

$$+\sum_{\ell=1}^{N_i}\sum_{\substack{\Gamma_{k\ell}\in\Sigma_h\\ \Gamma_{k\ell}\subset\partial\tau_\ell^i}}\int_{\Gamma_{k\ell}}\{u_h/0\}^{\mathrm{up}}_{\partial\tau_\ell^i}(\boldsymbol{x},t)\,[u_h/0]_{\partial\tau_\ell^i,\boldsymbol{x}}(\boldsymbol{x},t)\mathrm{d}s_{(\boldsymbol{x},t)}.$$

Applying the Cauchy–Schwarz inequality gives the bound

$$\begin{aligned}
&\geq -2\sum_{\ell=1}^{N_i}\sum_{\substack{\Gamma_{k\ell}\in\Sigma_h\\ \Gamma_{k\ell}\subset\partial\tau_\ell^i}}\left\|[u_h/0]_{\partial\tau_\ell^i,\boldsymbol{x}}\right\|_{[L_2(\Gamma_{k\ell})]^d}\left\|\nabla_{\boldsymbol{x}}u_{h|\tau_\ell^i}\right\|_{[L_2(\Gamma_{k\ell})]^d}\\
&\quad+2\sum_{\ell=1}^{N_i}\sum_{\substack{\Gamma_{k\ell}\in\Sigma_h\\ \Gamma_{k\ell}\subset\partial\tau_\ell^i}}\frac{\sigma}{\overline{h}_{k\ell}}\left\|[u_h/0]_{\partial\tau_\ell^i,\boldsymbol{x}}\right\|^2_{[L_2(\Gamma_{k\ell})]^d}\\
&\quad+\sum_{\Gamma_{k\ell}\in\Sigma_{N_i}^+}\int_{\Gamma_{k\ell}}|n_{\ell,t}|\left(\left[u_h^i\right]_{\Gamma_{k\ell},t}(\boldsymbol{x},t)\right)^2\mathrm{d}s_{(\boldsymbol{x},t)}.
\end{aligned}$$

Using the Hölder inequality leads to the bound

$$\begin{aligned}
&\geq -2\left[\sum_{\ell=1}^{N_i}\sum_{\substack{\Gamma_{k\ell}\in\Sigma_h\\ \Gamma_{k\ell}\subset\partial\tau_\ell^i}}\frac{\sigma}{\overline{h}_{k\ell}}\left\|[u_h/0]_{\partial\tau_\ell^i,\boldsymbol{x}}\right\|^2_{[L_2(\Gamma_{k\ell})]^d}\right]^{\frac{1}{2}}\\
&\qquad\qquad\times\left[\sum_{\ell=1}^{N_i}\sum_{\substack{\Gamma_{k\ell}\in\Sigma_h\\ \Gamma_{k\ell}\subset\partial\tau_\ell^i}}\frac{\overline{h}_{k\ell}}{\sigma}\left\|\nabla_{\boldsymbol{x}}u_{h|\tau_\ell^i}\right\|^2_{[L_2(\Gamma_{k\ell})]^d}\right]^{\frac{1}{2}}\\
&\quad+2\sum_{\ell=1}^{N_i}\sum_{\substack{\Gamma_{k\ell}\in\Sigma_h\\ \Gamma_{k\ell}\subset\partial\tau_\ell^i}}\frac{\sigma}{\overline{h}_{k\ell}}\left\|[u_h/0]_{\partial\tau_\ell^i,\boldsymbol{x}}\right\|^2_{[L_2(\Gamma_{k\ell})]^d}\\
&\quad+\sum_{\Gamma_{k\ell}\in\Sigma_{N_i}^+}\int_{\Gamma_{k\ell}}|n_{\ell,t}|\left(\left[u_h^i\right]_{\Gamma_{k\ell},t}(\boldsymbol{x},t)\right)^2\mathrm{d}s_{(\boldsymbol{x},t)}.
\end{aligned}$$

Now we can apply Lemma 3.2.3 and we conclude the estimate

$$\begin{aligned}
&\geq -2\left[\sum_{\ell=1}^{N_i}\sum_{\substack{\Gamma_{k\ell}\in\Sigma_h\\ \Gamma_{k\ell}\subset\partial\tau_\ell^i}}\frac{\sigma}{\overline{h}_{k\ell}}\left\|[u_h/0]_{\partial\tau_\ell^i,\boldsymbol{x}}\right\|^2_{[L_2(\Gamma_{k\ell})]^d}\right]^{\frac{1}{2}}\left[\frac{c_K}{\sigma}\sum_{\ell=1}^{N_i}\|\nabla_{\boldsymbol{x}}u_h\|^2_{[L_2(\tau_\ell^i)]^d}\right]^{\frac{1}{2}}\\
&\quad+2\sum_{\ell=1}^{N_i}\sum_{\substack{\Gamma_{k\ell}\in\Sigma_h\\ \Gamma_{k\ell}\subset\partial\tau_\ell^i}}\frac{\sigma}{\overline{h}_{k\ell}}\left\|[u_h/0]_{\partial\tau_\ell^i,\boldsymbol{x}}\right\|^2_{[L_2(\Gamma_{k\ell})]^d}
\end{aligned}$$

$$+\sum_{\Gamma_{k\ell}\in\Sigma_{N_i}^{+}}\int_{\Gamma_{k\ell}}|n_{\ell,t}|\left(\left[u_h^i\right]_{\Gamma_{k\ell},t}(\boldsymbol{x},t)\right)^2\mathrm{d}s_{(\boldsymbol{x},t)}.$$

Using Young's inequality for some $\varepsilon\in\mathbb{R}_+$ results in

$$\begin{aligned}
&\geq -\varepsilon\frac{c_K}{\sigma}\sum_{\ell=1}^{N_i}\left\|\nabla_{\boldsymbol{x}}u_h\right\|^2_{\left[L_2(\tau_\ell^i)\right]^d}\\
&\quad+\left(2-\frac{1}{\varepsilon}\right)\sum_{\ell=1}^{N_i}\sum_{\substack{\Gamma_{k\ell}\in\Sigma_h\\ \Gamma_{k\ell}\subset\partial\tau_\ell^i}}\frac{\sigma}{\overline{h}_{k\ell}}\left\|\left[u_h/0\right]_{\partial\tau_\ell^i,\boldsymbol{x}}\right\|^2_{[L_2(\Gamma_{k\ell})]^d}\\
&\quad+\sum_{\Gamma_{k\ell}\in\Sigma_{N_i}^{+}}\int_{\Gamma_{k\ell}}|n_{\ell,t}|\left(\left[u_h^i\right]_{\Gamma_{k\ell},t}(\boldsymbol{x},t)\right)^2\mathrm{d}s_{(\boldsymbol{x},t)}.
\end{aligned}$$

With the assumption $\sigma\geq 4c_K$ and with the choice $\varepsilon=1$ this leads to the statement of this lemma

$$\begin{aligned}
&\geq -\frac{1}{4}\sum_{\ell=1}^{N_i}\left\|\nabla_{\boldsymbol{x}}u_h^i\right\|^2_{\left[L_2(\tau_\ell^i)\right]^d}+\sum_{\Gamma_{k\ell}\in\Sigma_{N_i}}\frac{\sigma}{\overline{h}_{k\ell}}\left\|\left[u_h^i/0\right]_{\partial\tau_k^i,\boldsymbol{x}}\right\|^2_{[L_2(\Gamma_{k\ell})]^d}\\
&\quad+\sum_{\Gamma_{k\ell}\in\Sigma_{N_i}^{+}}\int_{\Gamma_{k\ell}}|n_{\ell,t}|\left(\left[u_h^i\right]_{\Gamma_{k\ell},t}(\boldsymbol{x},t)\right)^2\mathrm{d}s_{(\boldsymbol{x},t)}.
\end{aligned}$$

■

For each space-time subdomain Q_i, $i=1,\ldots,P$, we define for a discrete function $u_h^i\in S_h^p(\mathcal{T}_{N_i})$ the following energy norm

$$\begin{aligned}
\left\|u_h^i\right\|^2_{\widetilde{\mathrm{HDG}},i}:=&\sum_{\ell=1}^{N_i}\left\|\nabla_{\boldsymbol{x}}u_h^i\right\|^2_{\left[L_2(\tau_\ell^i)\right]^d}+\sum_{\Gamma_{k\ell}\in\mathcal{I}_{N_i}}\frac{\sigma}{\overline{h}_{k\ell}}\left\|\left[u_h^i\right]_{\Gamma_{k\ell},\boldsymbol{x}}\right\|^2_{[L_2(\Gamma_{k\ell})]^d}\\
&+\sum_{\Gamma_{k\ell}\in\Sigma_{N_i}}\frac{\sigma}{\overline{h}_{k\ell}}\left\|\left[u_h^i/0\right]_{\partial\tau_k^i,\boldsymbol{x}}\right\|^2_{[L_2(\Gamma_{k\ell})]^d}\\
&+\left\|u_h^i\right\|^2_{L_2(\Sigma_0\cap\partial Q_i)}+\left\|u_h^i\right\|^2_{L_2(\Sigma_T\cap\partial Q_i)}+\sum_{\Gamma_{k\ell}\in\mathcal{I}_{N_i}}\left\|\left[u_h^i\right]_{\Gamma_{k\ell},t}\right\|^2_{L_2(\Gamma_{k\ell})}\\
&+\sum_{\Gamma_{k\ell}\in\Sigma_{N_i}}\left\|\left[u_h^i/0\right]_{\partial\tau_k^i,t}\right\|^2_{L_2(\Gamma_{k\ell})}.
\end{aligned}$$

This energy norm $\|\cdot\|_{\widetilde{\mathrm{HDG}},i}$ corresponds to the energy norm $\|\cdot\|_{\widetilde{\mathrm{DG}}}$ defined in (2.12) with the difference, that the energy norm $\|\cdot\|_{\widetilde{\mathrm{HDG}},i}$ contains the additional terms

$$\sum_{\Gamma_{k\ell}\in\Sigma_{N_i}}\frac{\sigma}{\overline{h}_{k\ell}}\left\|\left[u_h^i/0\right]_{\partial\tau_k^i,\boldsymbol{x}}\right\|^2_{[L_2(\Gamma_{k\ell})]^d}\quad\text{and}\quad\sum_{\Gamma_{k\ell}\in\Sigma_{N_i}}\left\|\left[u_h^i/0\right]_{\partial\tau_k^i,t}\right\|^2_{L_2(\Gamma_{k\ell})}.$$

With this additional term it is easy to see, that the energy norm $\|\cdot\|_{\widetilde{\mathrm{HDG}},i}$ describes a full norm on the discrete function space $S_h^p(\mathcal{T}_{N_i})$.

Combining all the lemmata above it is possible to prove the following ellipticity estimate.

Theorem 3.2.5. *Let the stabilization parameter be large enough, i.e.* $\sigma \geq 4c_K$. *Then the following ellipticity estimate holds*

$$A^{(i)}(u_h^i, u_h^i) + c^{(i)}(u_h^i, 0; u_h^i, 0) \geq \frac{1}{4}\left\|u_h^i\right\|^2_{\widetilde{\mathrm{HDG}},i}$$

for all $u_h^i \in S_h^p(\mathcal{T}_{N_i})$.

Proof. Let $u_h^i \in S_h^p(\mathcal{T}_{N_i})$. Combining Lemma 3.2.1 with Lemma 3.2.2 and Lemma 3.2.4 we get the ellipticity estimate of this theorem with

$$\begin{aligned}
A^{(i)}(u_h^i, u_h^i) + c^{(i)}(u_h^i, 0; u_h^i, 0) &= a^{(i)}(u_h^i, u_h^i) + b^{(i)}(u_h^i, u_h^i) + c^{(i)}(u_h^i, 0; u_h^i, 0) \\
&\geq \frac{1}{4}\sum_{\ell=1}^{N_i}\left\|\nabla_{\boldsymbol{x}} u_h^i\right\|^2_{\left[L_2(\tau_\ell^i)\right]^d} + \frac{1}{2}\sum_{\Gamma_{k\ell}\in\mathcal{I}_{N_i}}\frac{\sigma}{\overline{h}_{k\ell}}\left\|\left[u_h^i\right]_{\Gamma_{k\ell},\boldsymbol{x}}\right\|^2_{[L_2(\Gamma_{k\ell})]^d} \\
&\quad + \sum_{\Gamma_{k\ell}\in\Sigma_{N_i}}\frac{\sigma}{\overline{h}_{k\ell}}\left\|\left[u_h^i/0\right]_{\partial\tau_k^i,\boldsymbol{x}}\right\|^2_{[L_2(\Gamma_{k\ell})]^d} \\
&\quad + \frac{1}{2}\left[\left\|u_h^i\right\|^2_{L_2(\Sigma_0\cap\partial Q_i)} + \left\|u_h^i\right\|^2_{L_2(\Sigma_T\cap\partial Q_i)} + \sum_{\Gamma_{k\ell}\in\mathcal{I}_{N_i}}\left\|\left[u_h^i\right]_{\Gamma_{k\ell},t}\right\|^2_{L_2(\Gamma_{k\ell})}\right] \\
&\quad + \frac{1}{2}\sum_{\Gamma_{k\ell}\in\Sigma_{N_i}^-}\left\|\left[u_h^i/0\right]_{\partial\tau_k^i,t}\right\|^2_{L_2(\Gamma_{k\ell})} \\
&\quad + \frac{1}{2}\sum_{\Gamma_{k\ell}\in\Sigma_{N_i}^+}\int_{\Gamma_{k\ell}}|n_{\ell,t}|\left(\left[u_h^i\right]_{\Gamma_{k\ell},t}(\boldsymbol{x},t)\right)^2 \mathrm{d}s_{(\boldsymbol{x},t)} \\
&\geq \frac{1}{4}\left\|u_h^i\right\|^2_{\widetilde{\mathrm{HDG}},i}.
\end{aligned}$$

■

Since the energy norm $\|\cdot\|_{\widetilde{\mathrm{HDG}},i}$ implies a full norm on the discrete function space $S_h^p(\mathcal{T}_{N_i})$ the ellipticity estimate of Theorem 3.2.5 induces the injectivity of the local space-time problem (3.11). Hence the discrete local problems are always uniquely solvable.

According to Lemma 2.2.10 the following lemma shows a similar identity on the interface Σ with respect to the hybrid upwind in time.

Lemma 3.2.6. *Let $\Gamma_{k\ell} \in \Sigma_h$ be an interior facet on the interface, $u_h \in S_h^p(\mathcal{T}_N)$ and $\lambda_h \in S_h^p(\Sigma_h)$. Then the following identity holds*

$$\begin{aligned}
&\{u_h/\lambda_h\}^{\mathrm{up}}_{\partial\tau_k}(\boldsymbol{x},t)\,[u_h/\lambda_h]_{\partial\tau_k,t}(\boldsymbol{x},t) \\
&\qquad + \{u_h/\lambda_h\}^{\mathrm{up}}_{\partial\tau_\ell}(\boldsymbol{x},t)\,[u_h/\lambda_h]_{\partial\tau_\ell,t}(\boldsymbol{x},t) - \frac{1}{2}\left[u_h^2\right]_{\Gamma_{k\ell},t}(\boldsymbol{x},t) \\
&\quad = \frac{1}{2}\left[\left|n_{k,t}\right|\left(u_{h|\tau_k}(\boldsymbol{x},t) - \lambda_h(\boldsymbol{x},t)\right)^2 + \left|n_{\ell,t}\right|\left(u_{h|\tau_\ell}(\boldsymbol{x},t) - \lambda_h(\boldsymbol{x},t)\right)^2\right]
\end{aligned}$$

for all $(\boldsymbol{x},t) \in \Gamma_{k\ell}$.

Proof. Without loss of generality we assume that $n_{k,t} \geq 0$. Using the definition of the hybrid upwind we have

$$\begin{aligned}
&\{u_h/\lambda_h\}^{\mathrm{up}}_{\partial\tau_k}(\boldsymbol{x},t)\,[u_h/\lambda_h]_{\partial\tau_k,t}(\boldsymbol{x},t) \\
&\qquad + \{u_h/\lambda_h\}^{\mathrm{up}}_{\partial\tau_\ell}(\boldsymbol{x},t)\,[u_h/\lambda_h]_{\partial\tau_\ell,t}(\boldsymbol{x},t) - \frac{1}{2}\left[u_h^2\right]_{\Gamma_{k\ell},t}(\boldsymbol{x},t) \\
&= u_{h|\tau_k}(\boldsymbol{x},t)\left[u_{h|\tau_k}(\boldsymbol{x},t) - \lambda_h(\boldsymbol{x},t)\right] n_{k,t} + \lambda_h(\boldsymbol{x},t)\left[u_{h|\tau_\ell}(\boldsymbol{x},t) - \lambda_h(\boldsymbol{x},t)\right] n_{\ell,t} \\
&\qquad - \frac{1}{2}\left(u_{h|\tau_k}(\boldsymbol{x},t)\right)^2 n_{k,t} - \frac{1}{2}\left(u_{h|\tau_\ell}(\boldsymbol{x},t)\right)^2 n_{\ell,t}.
\end{aligned}$$

With the assumption $n_{k,t} \geq 0$ and some algebraic manipulations we get the statement of the lemma with

$$\begin{aligned}
&= \left|n_{k,t}\right|\left(u_{h|\tau_k}(\boldsymbol{x},t)\right)^2 - \left|n_{k,t}\right| u_{h|\tau_k}(\boldsymbol{x},t)\lambda_h(\boldsymbol{x},t) - \left|n_{\ell,t}\right|\lambda_h(\boldsymbol{x},t)u_{h|\tau_\ell}(\boldsymbol{x},t) \\
&\qquad + \left|n_{\ell,t}\right|\left(\lambda_h(\boldsymbol{x},t)\right)^2 - \frac{1}{2}\left|n_{k,t}\right|\left(u_{h|\tau_k}(\boldsymbol{x},t)\right)^2 + \frac{1}{2}\left|n_{\ell,t}\right|\left(u_{h|\tau_\ell}(\boldsymbol{x},t)\right)^2 \\
&= \frac{1}{2}\left|n_{k,t}\right|\Big[\left(u_{h|\tau_k}(\boldsymbol{x},t)\right)^2 - 2u_{h|\tau_k}(\boldsymbol{x},t)\lambda_h(\boldsymbol{x},t) + \left(\lambda_h(\boldsymbol{x},t)\right)^2 \\
&\qquad\qquad + \left(u_{h|\tau_\ell}(\boldsymbol{x},t)\right)^2 - 2u_{h|\tau_\ell}(\boldsymbol{x},t)\lambda_h(\boldsymbol{x},t) + \left(\lambda_h(\boldsymbol{x},t)\right)^2\Big] \\
&= \frac{1}{2}\left[\left|n_{k,t}\right|\left(u_{h|\tau_k}(\boldsymbol{x},t) - \lambda_h(\boldsymbol{x},t)\right)^2 + \left|n_{\ell,t}\right|\left(u_{h|\tau_\ell}(\boldsymbol{x},t) - \lambda_h(\boldsymbol{x},t)\right)^2\right].
\end{aligned}$$

■

For $u_h \in S_h^p(\mathcal{T}_N)$ and $\lambda_h \in S_h^p(\Sigma_h)$ we define the following energy norm

$$\begin{aligned}
\|(u_h,\lambda_h)\|^2_{\widetilde{\mathrm{HDG}}} := &\sum_{i=1}^{P}\sum_{\ell=1}^{N_i}\|\nabla_{\boldsymbol{x}} u_h\|^2_{[L_2(\tau_\ell^i)]^d} + \sum_{i=1}^{P}\sum_{\Gamma_{k\ell}\in\mathcal{I}_{N_i}}\frac{\sigma}{\overline{h}_{k\ell}}\left\|[u_h]_{\Sigma_{k\ell},\boldsymbol{x}}\right\|^2_{[L_2(\Gamma_{k\ell})]^d} \\
&+ \sum_{i=1}^{P}\sum_{\ell=1}^{N_i}\sum_{\substack{\Gamma_{k\ell}\in\Sigma_h \\ \Gamma_{k\ell}\subset\partial\tau_\ell^i}}\frac{\sigma}{\overline{h}_{k\ell}}\left\|[u_h/\lambda_h]_{\partial\tau_\ell^i,\boldsymbol{x}}\right\|^2_{[L_2(\Gamma_{k\ell})]^d}
\end{aligned}$$

$$+\|u_h\|^2_{L_2(\Sigma_0)}+\|u_h\|^2_{L_2(\Sigma_T)}+\sum_{i=1}^{P}\sum_{\Gamma_{k\ell}\in\mathcal{I}_{N_i}}\left\|[u_h]_{\Gamma_{k\ell},t}\right\|^2_{L_2(\Gamma_{k\ell})}$$
$$+\sum_{i=1}^{P}\sum_{\ell=1}^{N_i}\sum_{\substack{\Gamma_{k\ell}\in\Sigma_h\\ \Gamma_{k\ell}\subset\partial\tau_\ell}}\left\|[u_h/\lambda_h]_{\partial\tau_\ell,t}\right\|^2_{L_2(\Gamma_{k\ell})}.$$

With this energy norm we can prove the following ellipticity estimate.

Theorem 3.2.7. *Let $u_h\in S_h^p(\mathcal{T}_N)$ and $\lambda_h\in S_h^p(\Sigma_h)$. Further we assume, that the stabilization parameter satisfies $\sigma\geq 4c_K$. Then the following ellipticity estimate holds*

$$\sum_{i=1}^{P}\left[A^{(i)}(u_h,u_h)+c^{(i)}(u_h,\lambda_h;u_h,\lambda_h)\right]\geq\frac{1}{4}\|(u_h,\lambda_h)\|^2_{\widetilde{\mathrm{HDG}}}.$$

Proof. Let $u_h\in S_h^p(\mathcal{T}_N)$ and $\lambda_h\in S_h^p(\Sigma_h)$. Applying Lemma 3.2.1 and by using the techniques as used in the proof of Lemma 3.2.4 we find the estimate

$$\begin{aligned}
&\sum_{i=1}^{P}\left[a^{(i)}(u_h,u_h)+c^{(i)}(u_h,\lambda_h;u_h,\lambda_h)\right]\\
&\quad\geq\frac{1}{4}\sum_{i=1}^{P}\sum_{\ell=1}^{N_i}\|\nabla_{\boldsymbol{x}}u_h\|^2_{[L_2(\tau_\ell^i)]^d}+\frac{1}{2}\sum_{i=1}^{P}\sum_{\Gamma_{k\ell}\in\mathcal{I}_{N_i}}\frac{\sigma}{\overline{h}_{k\ell}}\left\|[u_h]_{\Sigma_{k\ell,\boldsymbol{x}}}\right\|^2_{[L_2(\Gamma_{k\ell})]^d}\\
&\qquad+\sum_{i=1}^{P}\sum_{\ell=1}^{N_i}\sum_{\substack{\Gamma_{k\ell}\in\Sigma_h\\ \Gamma_{k\ell}\subset\partial\tau_\ell^i}}\frac{\sigma}{\overline{h}_{k\ell}}\left\|[u_h/\lambda_h]_{\partial\tau_\ell^i,\boldsymbol{x}}\right\|^2_{[L_2(\Gamma_{k\ell})]^d}\\
&\qquad+\sum_{i=1}^{P}\sum_{\ell=1}^{N_i}\sum_{\substack{\Gamma_{k\ell}\in\Sigma_h\\ \Gamma_{k\ell}\subset\partial\tau_\ell^i}}\int_{\Gamma_{k\ell}}\{u_h/\lambda\}^{\mathrm{up}}_{\partial\tau_\ell^i}(\boldsymbol{x},t)\,[u_h/\lambda_h]_{\partial\tau_\ell^i,\boldsymbol{x}}(\boldsymbol{x},t)\mathrm{d}s_{(\boldsymbol{x},t)}.
\end{aligned}$$

For the sum over the local bilinear forms $b^{(i)}(\cdot,\cdot)$ we have by definition

$$\begin{aligned}
\sum_{i=1}^{P}b^{(i)}(u_h,u_h)&=-\sum_{i=1}^{P}\sum_{\ell=1}^{N_i}\int_{\tau_\ell^i}u_h(\boldsymbol{x},t)\partial_t u_h(\boldsymbol{x},t)\mathrm{d}(\boldsymbol{x},t)+\|u_h\|^2_{L_2(\Sigma_T)}\\
&\qquad+\sum_{i=1}^{P}\sum_{\Gamma_{k\ell}\in\mathcal{I}_{N_i}}\int_{\Gamma_{k\ell}}\{u_h\}^{\mathrm{up}}_{\Gamma_{k\ell}}(\boldsymbol{x},t)\,[u_h]_{\Gamma_{k\ell},t}(\boldsymbol{x},t)\mathrm{d}s_{(\boldsymbol{x},t)}.
\end{aligned}$$

Applying Gauss's theorem we find, by rewriting the sum over all elements analogously to Lemma 2.2.11, the estimate

$$\geq\frac{1}{2}\left[\|u_h\|^2_{L_2(\Sigma_0)}+\|u_h\|^2_{L_2(\Sigma_T)}+\sum_{i=1}^{P}\sum_{\Gamma_{k\ell}\in\mathcal{I}_{N_i}}\left\|[u_h]_{\Gamma_{k\ell},t}\right\|^2_{L_2(\Gamma_{k\ell})}\right]$$

$$- \frac{1}{2} \sum_{i=1}^{P} \sum_{\ell=1}^{N_i} \sum_{\substack{\Gamma_{k\ell} \in \Sigma_h \\ \Gamma_{k\ell} \subset \partial \tau_\ell^i}} \int_{\Gamma_{k\ell}} n_{\ell,t} \left(u_h(\boldsymbol{x},t) \right)^2 \mathrm{d}s_{(\boldsymbol{x},t)}.$$

With the definition of the jump in time direction we further have

$$= \frac{1}{2} \left[\|u_h\|^2_{L_2(\Sigma_0)} + \|u_h\|^2_{L_2(\Sigma_T)} + \sum_{i=1}^{P} \sum_{\Gamma_{k\ell} \in \mathcal{I}_{N_i}} \left\| [u_h]_{\Gamma_{k\ell},t} \right\|^2_{L_2(\Gamma_{k\ell})} \right] - \frac{1}{2} \sum_{\Gamma_{k\ell} \in \Sigma_h} \int_{\Gamma_{k\ell}} \left[u_h^2 \right]_{\Gamma_{k\ell},t} (\boldsymbol{x},t) \mathrm{d}s_{(\boldsymbol{x},t)}.$$

Combining these two estimates we obtain

$$\begin{aligned}
&\sum_{i=1}^{P} \left[A^{(i)}(u_h,u_h) + c^{(i)}(u_h,\lambda_h;u_h,\lambda_h) \right] \\
&\quad \geq \frac{1}{4} \sum_{i=1}^{P} \sum_{\ell=1}^{N_i} \left\| \nabla_{\boldsymbol{x}} u_h \right\|^2_{\left[L_2(\tau_\ell^i)\right]^d} + \frac{1}{2} \sum_{i=1}^{P} \sum_{\Gamma_{k\ell} \in \mathcal{I}_{N_i}} \frac{\sigma}{\overline{h}_{k\ell}} \left\| [u_h]_{\Sigma_{k\ell},\boldsymbol{x}} \right\|^2_{[L_2(\Gamma_{k\ell})]^d} \\
&\qquad + \sum_{i=1}^{P} \sum_{\ell=1}^{N_i} \sum_{\substack{\Gamma_{k\ell} \in \Sigma_h \\ \Gamma_{k\ell} \subset \partial \tau_\ell^i}} \frac{\sigma}{\overline{h}_{k\ell}} \left\| [u_h/\lambda_h]_{\partial \tau_\ell^i,\boldsymbol{x}} \right\|^2_{[L_2(\Gamma_{k\ell})]^d} \\
&\qquad + \frac{1}{2} \left[\|u_h\|^2_{L_2(\Sigma_0)} + \|u_h\|^2_{L_2(\Sigma_T)} + \sum_{i=1}^{P} \sum_{\Gamma_{k\ell} \in \mathcal{I}_{N_i}} \left\| [u_h]_{\Gamma_{k\ell},t} \right\|^2_{L_2(\Gamma_{k\ell})} \right] \\
&\qquad - \frac{1}{2} \sum_{\Gamma_{k\ell} \in \Sigma_h} \int_{\Gamma_{k\ell}} \left[u_h^2 \right]_{\Gamma_{k\ell},t} (\boldsymbol{x},t) \mathrm{d}s_{(\boldsymbol{x},t)} \\
&\qquad + \sum_{i=1}^{P} \sum_{\ell=1}^{N_i} \sum_{\substack{\Gamma_{k\ell} \in \Sigma_h \\ \Gamma_{k\ell} \subset \partial \tau_\ell^i}} \int_{\Gamma_{k\ell}} \left\{ u_h/\lambda \right\}^{\mathrm{up}}_{\partial \tau_\ell^i} (\boldsymbol{x},t) \left[u_h/\lambda_h \right]_{\partial \tau_\ell^i,\boldsymbol{x}} (\boldsymbol{x},t) \mathrm{d}s_{(\boldsymbol{x},t)}.
\end{aligned}$$

Rewriting the sum of the last term leads to the identity

$$\begin{aligned}
&= \frac{1}{4} \sum_{i=1}^{P} \sum_{\ell=1}^{N_i} \left\| \nabla_{\boldsymbol{x}} u_h \right\|^2_{\left[L_2(\tau_\ell^i)\right]^d} + \frac{1}{2} \sum_{i=1}^{P} \sum_{\Gamma_{k\ell} \in \mathcal{I}_{N_i}} \frac{\sigma}{\overline{h}_{k\ell}} \left\| [u_h]_{\Sigma_{k\ell},\boldsymbol{x}} \right\|^2_{[L_2(\Gamma_{k\ell})]^d} \\
&\quad + \sum_{i=1}^{P} \sum_{\ell=1}^{N_i} \sum_{\substack{\Gamma_{k\ell} \in \Sigma_h \\ \Gamma_{k\ell} \subset \partial \tau_\ell^i}} \frac{\sigma}{\overline{h}_{k\ell}} \left\| [u_h/\lambda_h]_{\partial \tau_\ell^i,\boldsymbol{x}} \right\|^2_{[L_2(\Gamma_{k\ell})]^d}
\end{aligned}$$

$$
\begin{aligned}
&+\frac{1}{2}\left[\|u_h\|^2_{L_2(\Sigma_0)}+\|u_h\|^2_{L_2(\Sigma_T)}+\sum_{i=1}^{P}\sum_{\Gamma_{k\ell}\in\mathcal{I}_{N_i}}\left\|[u_h]_{\Gamma_{k\ell},t}\right\|^2_{L_2(\Gamma_{k\ell})}\right]\\
&+\sum_{\Gamma_{k\ell}\in\Gamma_N}\int_{\Gamma_{k\ell}}\Big[-\frac{1}{2}\left[u_h^2\right]_{\Gamma_{k\ell},t}(\boldsymbol{x},t)+\{u_h/\lambda_h\}^{\mathrm{up}}_{\partial\tau_k}(\boldsymbol{x},t)\,[u_h/\lambda_h]_{\partial\tau_k,t}(\boldsymbol{x},t)\\
&\qquad\qquad+\{u_h/\lambda_h\}^{\mathrm{up}}_{\partial\tau_\ell}(\boldsymbol{x},t)\,[u_h/\lambda_h]_{\partial\tau_\ell,t}(\boldsymbol{x},t)\Big]\mathrm{d}s_{(\boldsymbol{x},t)}.
\end{aligned}
$$

With Lemma 3.2.6 we further obtain

$$
\begin{aligned}
&=\frac{1}{4}\sum_{i=1}^{P}\sum_{\ell=1}^{N_i}\|\nabla_{\boldsymbol{x}}u_h\|^2_{[L_2(\tau_\ell^i)]^d}+\frac{1}{2}\sum_{i=1}^{P}\sum_{\Gamma_{k\ell}\in\mathcal{I}_{N_i}}\frac{\sigma}{\overline{h}_{k\ell}}\left\|[u_h]_{\Sigma_{k\ell,\boldsymbol{x}}}\right\|^2_{[L_2(\Gamma_{k\ell})]^d}\\
&\quad+\sum_{i=1}^{P}\sum_{\ell=1}^{N_i}\sum_{\substack{\Gamma_{k\ell}\in\Sigma_h\\ \Gamma_{k\ell}\subset\partial\tau_\ell^i}}\frac{\sigma}{\overline{h}_{k\ell}}\left\|[u_h/\lambda_h]_{\partial\tau_\ell^i,\boldsymbol{x}}\right\|^2_{[L_2(\Gamma_{k\ell})]^d}\\
&\quad+\frac{1}{2}\left[\|u_h\|^2_{L_2(\Sigma_0)}+\|u_h\|^2_{L_2(\Sigma_T)}+\sum_{i=1}^{P}\sum_{\Gamma_{k\ell}\in\mathcal{I}_{N_i}}\left\|[u_h]_{\Gamma_{k\ell},t}\right\|^2_{L_2(\Gamma_{k\ell})}\right]\\
&\quad+\frac{1}{2}\sum_{\Gamma_{k\ell}\in\Sigma_h}\int_{\Gamma_{k\ell}}\Big[\left|n_{k,t}\right|\left(u_{h|\tau_k}(\boldsymbol{x},t)-\lambda_h(\boldsymbol{x},t)\right)^2\\
&\qquad\qquad+\left|n_{\ell,t}\right|\left(u_{h|\tau_\ell}(\boldsymbol{x},t)-\lambda_h(\boldsymbol{x},t)\right)^2\Big]\mathrm{d}s_{(\boldsymbol{x},t)}.
\end{aligned}
$$

The statement of the theorem follows by applying the definition of the hybrid jump and by summing up over all elements

$$
\begin{aligned}
&\geq\frac{1}{4}\sum_{i=1}^{P}\sum_{\ell=1}^{N_i}\|\nabla_{\boldsymbol{x}}u_h\|^2_{[L_2(\tau_\ell^i)]^d}+\frac{1}{2}\sum_{i=1}^{P}\sum_{\Gamma_{k\ell}\in\mathcal{I}_{N_i}}\frac{\sigma}{\overline{h}_{k\ell}}\left\|[u_h]_{\Sigma_{k\ell,\boldsymbol{x}}}\right\|^2_{[L_2(\Gamma_{k\ell})]^d}\\
&\quad+\sum_{i=1}^{P}\sum_{\ell=1}^{N_i}\sum_{\substack{\Gamma_{k\ell}\in\Sigma_h\\ \Gamma_{k\ell}\subset\partial\tau_\ell^i}}\frac{\sigma}{\overline{h}_{k\ell}}\left\|[u_h/\lambda_h]_{\partial\tau_\ell^i,\boldsymbol{x}}\right\|^2_{[L_2(\Gamma_{k\ell})]^d}\\
&\quad+\frac{1}{2}\left[\|u_h\|^2_{L_2(\Sigma_0)}+\|u_h\|^2_{L_2(\Sigma_T)}+\sum_{i=1}^{P}\sum_{\Gamma_{k\ell}\in\mathcal{I}_{N_i}}\left\|[u_h]_{\Gamma_{k\ell},t}\right\|^2_{L_2(\Gamma_{k\ell})}\right]\\
&\quad+\frac{1}{2}\sum_{i=1}^{P}\sum_{\ell=1}^{N_i}\sum_{\substack{\Gamma_{k\ell}\in\Sigma_h\\ \Gamma_{k\ell}\subset\partial\tau_\ell^i}}\left\|[u_h/\lambda_h]_{\partial\tau_\ell^i,t}\right\|^2_{L_2(\Gamma_{k\ell})}
\end{aligned}
$$

■

Using Theorem 3.2.7 we now can show the injectivity of the discrete variational problem (3.7).

Theorem 3.2.8. *Let the assumptions of Theorem 3.2.7 be fulfilled. If the function $u_h \in S_h^p(\mathcal{T}_N)$ and $\lambda_h \in S_h^p(\Sigma_h)$ satisfy*

$$\sum_{i=1}^{P} \left[A^{(i)}(u_h, v_h) + c^{(i)}(u_h, \lambda_h; v_h, \mu_h) \right] = 0$$

for all $v_h \in S_h^p(\mathcal{T}_N)$ and $\mu_h \in S_h^p(\Sigma_h)$, then this implies $u_h = 0$ and $\lambda_h = 0$.

Proof. Let $u_h \in S_h^p(\mathcal{T}_N)$ and $\lambda_h \in S_h^p(\Sigma_h)$. The ellipticity estimate of Theorem 3.2.7 implies

$$0 = \sum_{i=1}^{P} \left[A^{(i)}(u_h, u_h) + c^{(i)}(u_h, \lambda_h; u_h, \lambda_h) \right] \geq \frac{1}{4} \|(u_h, \lambda_h)\|_{\widetilde{\text{HDG}}}^2 \geq 0$$

and therefore $\|(u_h, \lambda_h)\|_{\widetilde{\text{HDG}}} = 0$. Hence there holds

$$\nabla_{\boldsymbol{x}} u_{h|\tau_\ell} = 0 \quad \text{for all } \tau_\ell \in \mathcal{T}_N, \qquad u_h = 0 \text{ on } \Sigma_0 \cup \Sigma_T \quad \text{and} \quad u_h \in \mathcal{C}(\mathcal{T}_N), \tag{3.12}$$

with $u_{h|\Sigma} = \lambda_h$. As in the proof of Theorem 2.2.12 we can use an alternative representation for the local bilinear forms $b^{(i)}(\cdot,\cdot)$. Further we use the test function $v_h = \partial_t u_h \in S_h^p(\mathcal{T}_N)$ and the properties (3.12) to derive the identity

$$0 = \sum_{i=1}^{P} \left[A^{(i)}(u_h, \partial_t u_h) + c^{(i)}(u_h, \lambda_h; \partial_t u_h, 0) \right] = \sum_{\ell=1}^{N} \|\partial_t u_h\|_{L_2(\tau_\ell)}^2 \geq 0.$$

Hence we have $\partial_t u_{h|\partial\tau_\ell} = 0$ for all $\tau_\ell \in \mathcal{T}_N$ and with the above properties (3.12) we conclude that $u_h = 0$. With $u_{h|\Sigma} = \lambda_h$ we also have that $\lambda_h = 0$. ∎

Theorem 3.2.8 implies that the discrete variational problem (3.7) omits a unique solution $u_h \in S_h^p(\mathcal{T}_N)$ and $\lambda_h \in S_h^p(\Sigma_h)$.

Next we will derive a priori error estimates. To do so, we need to introduce the following two energy norms for functions $u \in H^s(\mathcal{T}_N)$, $s > \frac{3}{2}$, and functions $\lambda \in L_2(\Sigma_h)$:

$$\|(u,\lambda)\|_{\text{HDG}}^2 := \|(u,\lambda)\|_{\widetilde{\text{HDG}}}^2 + \sum_{i=1}^{P} \sum_{\ell=1}^{N_i} h_\ell^i \|\partial_t u\|_{L_2(\tau_\ell^i)}^2,$$

$$\|(u,\lambda)\|_{\text{HDG},*}^2 := \|(u,\lambda)\|_{\widetilde{\text{HDG}}}^2 + \sum_{i=1}^{P} \sum_{\ell=1}^{N_i} \left(h_\ell^i\right)^{-1} \|u\|_{L_2(\tau_\ell^i)}^2$$

$$+\sum_{i=1}^{P}\sum_{\Gamma_{k\ell}\in\mathcal{I}_{N_i}}\overline{h}_{k\ell}\left\|\langle\nabla_{\boldsymbol{x}}u\rangle_{\Gamma_{k\ell}}\right\|^2_{[L_2(\Gamma_{k\ell})]^d}$$
$$+\sum_{i=1}^{P}\sum_{\ell=1}^{N_i}\sum_{\substack{\Gamma_{k\ell}\in\Sigma_h\\ \Gamma_{k\ell}\subset\partial\tau_\ell^i}}\overline{h}_{k\ell}\left\|\nabla_{\boldsymbol{x}}u_{|\tau_\ell^i}\right\|^2_{[L_2(\Gamma_{k\ell})]^d}.$$

With respect to these energy norms the following boundedness estimate holds.

Theorem 3.2.9. *Let $u\in H^s(\mathcal{T}_N)$, $s>\frac{3}{2}$, and $\lambda\in L_2(\Sigma_h)$. Further let $v_h\in S_h^p(\mathcal{T}_N)$ and $\mu_h\in S_h^p(\Sigma_h)$. Then the boundedness estimate holds*

$$\sum_{i=1}^{P}\left[A^{(i)}(u,v_h)+c^{(i)}(u,\lambda;v_h,\mu_h)\right]\leq c_2^A\|(u,\lambda)\|_{\mathrm{HDG},*}\|(v_h,\mu_h)\|_{\mathrm{HDG}}.$$

Proof. As in Chapter 2, see Lemma 2.2.7 and Lemma 2.2.8 the estimate follows by using the Cauchy–Schwarz inequality and by applying Lemma 3.2.3 and Lemma 2.2.6. ∎

Theorem 3.2.10. *Let $\mathcal{T}_N$ be a quasi-uniform decomposition and let $\sigma\geq 4c_K$, then the following stability estimate holds*

$$\sup_{(0,0)\neq(v_h,\mu_h)\in S_h^p(\mathcal{T}_N)\times S_h^p(\Sigma_h)}\frac{\sum_{i=1}^{P}\left[A^{(i)}(u_h,v_h)+c^{(i)}(u_h,\lambda_h;v_h,\mu_h)\right]}{\|(v_h,\mu_h)\|_{\mathrm{HDG}}}\geq c_S^A\|(u_h,\lambda_h)\|_{\mathrm{HDG}}$$

for all $u_h\in S_h^p(\mathcal{T}_N)$ and $\lambda_h\in S_h^p(\Sigma_h)$.

Proof. The stability estimate follows exactly in the same way as the stability estimate of Theorem 2.2.22. The main difference is the ellipticity estimate, which is proven in Theorem 3.2.7. ∎

Theorem 3.2.11. *Let $\mathcal{T}_N$ be a quasi-uniform decomposition and let $u\in H^s(\mathcal{T}_N)$, $s\geq 2$, be the exact solution of the model problem (2.1). Further let $u_h\in S_h^p(\mathcal{T}_N)$ and $\lambda_h\in S_h^p(\Sigma_h)$ be the exact solution of the discrete variational problem (3.7) with $\sigma\geq 4c_K$. Then the following error estimate in the energy norm holds*

$$\|(u-u_h,u-\lambda_h)\|_{\mathrm{HDG}}\leq ch^{\min\{s,p+1\}-1}\,|u|_{H^s(\mathcal{T}_N)}.$$

Proof. The main ingredients for the proof are the Galerkin orthogonality (2.6), Theorem 3.2.10 and Theorem 3.2.11 combined with standard arguments as it was done for the proof of Theorem 2.2.28. ∎

3.3 Numerical examples

In this section numerical examples for the presented hybrid space-time discretization will be presented to show the performance of this method.

Example 3.3.1. In this example we consider the spatial domains $\Omega = (0,1)^d$ for $d = 1,2,3$ and the simulation end time $T = 1$. Hence the space-time domains are given by the $(d+1)$ unit cubes $Q = (0,1)^{d+1}$. On the boundary $\Sigma_D = \partial\Omega \times (0,T)$ we assume homogeneous Dirichlet boundary conditions and the given data f and u_0 are chosen such that the exact solutions are given by

$$u(\boldsymbol{x},t) = \cos(\pi t)\prod_{i=1}^{d}\sin(\pi x_i).$$

Further we decompose the space-time domains Q into several space-time subdomains Q_i, $i = 1,\dots,P$. Where for $d = 1$ we use $P = 16$, for $d = 2$ we use $P = 24$ and for $d = 3$ we use $P = 96$ space-time subdomains. For $d = 1$ and $d = 2$ these decompositions are shown in Figure 3.2. The initial triangulation for $d = 1$ is given by 32 triangles, by simply using two triangles for each space-time subdomain. For $d = 2,3$ the space-time subdomains itself are considered as initial triangulations. To analyze the convergence behavior of the presented hybrid space-time method we apply several uniform refinement steps. For the stabilization parameter we choose $\sigma = 10p^2$ for the polynomial degrees $p \in \{1,2\}$.

For the iterative solution of the Schur complement system (3.10) we use the GMRES method without any preconditioning with a relative error reduction of $\varepsilon_{\text{GMRES}} = 10^{-8}$. The local problems $A_{II}^{(i)}$, $i = 1,\dots,P$ are solved in parallel by using the solver package PARDISO or by applying the GMRES method, where a simple multigrid preconditioner is used.

In Tables 3.1–3.6 the number of required iterations and the errors in the energy norm $\|u - u_h\|_{\text{HDG}}$ are given. We observe that the number of required iterations for solving the Schur complement system (3.10) are growing slightly indicating the need of using an appropriate preconditioner. Further, the expected convergence rates with respect to the energy norm for linear and quadratic ansatz functions can be observed.

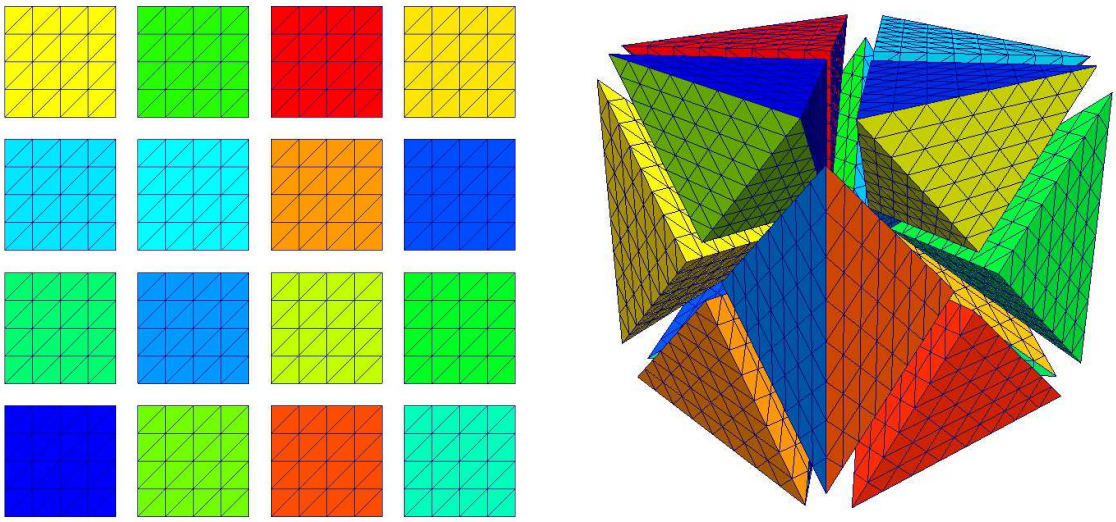

(a) Decomposition into $P = 16$ subdomains. (b) Decomposition into $P = 24$ subdomains.

Figure 3.2: Space-time decompositions for $d = 1$ and $d = 2$.

level	elements	dof u_h	dof λ_h	$\|(u-u_h, u-\lambda_h)\|_{\mathrm{HDG}}$	eoc	iter
0	32	80	48	$5.9010-1$	–	28
1	128	352	96	$2.9501-1$	1.00	38
2	512	1 472	192	$1.4660-1$	1.01	50
3	2 048	6 016	384	$7.2877-2$	1.01	65
4	8 192	24 320	768	$3.6289-2$	1.01	84
5	32 768	97 792	1 536	$1.8098-2$	1.00	110
6	131 072	392 192	3 072	$9.0362-3$	1.00	135
7	524 288	1 570 816	6 144	$4.5147-3$	1.00	166
8	2 097 152	6 287 360	12 288	$2.2564-3$	1.00	209
Theory:					1.00	

Table 3.1: Numerical results for $d = 1$, $p = 1$ and $P = 16$ subdomains.

level	elements	dof u_h	dof λ_h	$\|(u-u_h, u-\lambda_h)\|_{\mathrm{HDG}}$	eoc	iter
0	32	168	72	$9.6081-2$	–	40
1	128	720	144	$2.3273-2$	2.05	58
2	512	2 976	288	$5.5544-3$	2.07	76
3	2 048	12 096	576	$1.3358-3$	2.06	98
4	8 192	48 768	1 152	$3.2540-4$	2.04	116
5	32 768	195 840	2 304	$8.0120-5$	2.02	142
6	131 072	784 896	4 608	$1.9863-5$	2.01	172
7	524 288	3 142 656	9 216	$4.9440-6$	2.01	198
8	2 097 152	12 576 768	18 432	$1.2333-6$	2.00	236
Theory:					2.00	

Table 3.2: Numerical results for $d=1$, $p=2$ and $P=16$ subdomains.

level	elements	dof u_h	dof λ_h	$\|(u-u_h, u-\lambda_h)\|_{\mathrm{HDG}}$	eoc	iter
0	24	48	108	$1.4177+0$	–	25
1	192	576	432	$9.1732-1$	0.63	82
2	1 536	5 376	1 728	$4.8790-1$	0.91	127
3	12 288	46 080	6 912	$2.4827-1$	0.97	209
4	98 304	380 928	27 648	$1.2480-1$	0.99	365
5	786 432	3 096 576	110 592	$6.2508-2$	1.00	635
6	6 291 456	24 969 216	442 368	$3.1276-2$	1.00	1075
Theory:					1.00	

Table 3.3: Numerical results for $d=2$, $p=1$ and $P=24$ subdomains.

level	elements	dof u_h	dof λ_h	$\|(u-u_h, u-\lambda_h)\|_{\mathrm{HDG}}$	eoc	iter
0	24	144	216	$6.4591-1$	–	107
1	192	1 536	864	$1.6417-1$	1.98	273
2	1 536	13 824	3 456	$4.4846-2$	1.87	370
3	12 288	116 736	13 824	$1.1423-2$	1.97	509
4	98 304	958 464	55 296	$2.8653-3$	2.00	746
5	786 432	7 766 016	221 184	$7.1658-4$	2.00	1 125
Theory:					2.00	

Table 3.4: Numerical results for $d=2$, $p=2$ with $P=24$ subdomains.

level	elements	dof u_h	dof λ_h	$\|(u-u_h, u-\lambda_h)\|_{\mathrm{HDG}}$	eoc	iter
0	96	192	768	$1.1669+0$	–	70
1	1 536	5 376	6 144	$8.2292-1$	0.50	145
2	24 576	104 448	49 152	$4.7452-1$	0.79	207
3	393 216	1 818 624	393 216	$2.5066-1$	0.92	323
4	6 291 456	30 277 632	3 145 728	$1.2797-1$	0.97	551
Theory:					1.00	

Table 3.5: Numerical results for $d=3$, $p=1$ with $P=96$ subdomains.

level	elements	dof u_h	dof λ_h	$\|(u-u_h, u-\lambda_h)\|_{\mathrm{HDG}}$	eoc	iter
0	96	720	1 920	$7.2073-1$	–	391
1	1 536	17 280	15 360	$2.5149-1$	1.52	680
2	24 576	322 560	122 880	$7.3177-2$	1.78	889
3	393 216	5 529 600	983 040	$1.9496-2$	1.91	1 134
Theory:					2.00	

Table 3.6: Numerical results for $d=3$, $p=2$ with $P=96$ subdomains.

4 SPACE-TIME MULTIGRID METHODS

In this chapter a multigrid approach for the space-time discretization (2.2) introduced in Chapter 2 will be presented. Here we assume that the space-time decompositions form so called space-time slabs. Two examples for space-time meshes with space-time slabs are given in Figure 4.1 for $d = 1$.

For $0 = t_0 < t_1 < \cdots < t_{N-1} < t_N = T$ let $\mathcal{T}_{N_n}$, $n = 1, \ldots, N$ be the decomposition of the n-th space-time slab into finite elements, i.e.

$$\overline{Q}_n = \bigcup_{\tau_\ell^n \in \mathcal{T}_{N_n}} \overline{\tau}_\ell^n, \qquad \text{with} \quad Q_n := \Omega \times (t_{n-1}, t_n).$$

For each space-time slab we consider the discrete function space $S_h^p(\mathcal{T}_{N_n})$ and by $A_n(\cdot,\cdot)$ we denote the bilinear form (2.3) with respect to the space-time slab Q_n and the initial boundary $\Sigma_n := \Omega(t_{n-1}) \times \{t_{n-1}\}$. Then the linear system (2.7) introduced in Chapter 2 is given by the following equations

$$\begin{pmatrix} A_{\tau,h}^1 & & & & \\ B_{\tau,h}^{2,1} & A_{\tau,h}^2 & & & \\ & B_{\tau,h}^{3,2} & A_{\tau,h}^3 & & \\ & & \ddots & \ddots & \\ & & & B_{\tau,h}^{N,N-1} & A_{\tau,h}^N \end{pmatrix} \begin{pmatrix} \boldsymbol{u}_1 \\ \boldsymbol{u}_2 \\ \boldsymbol{u}_3 \\ \vdots \\ \boldsymbol{u}_N \end{pmatrix} = \begin{pmatrix} \boldsymbol{f}_1 \\ \boldsymbol{f}_2 \\ \boldsymbol{f}_3 \\ \vdots \\ \boldsymbol{f}_N \end{pmatrix}. \tag{4.1}$$

For $n = 1, \ldots, N$ the matrices of (4.1) are given by

$$\begin{aligned} A_{\tau,h}^n[j,i] &:= A_n(\varphi_j^n, \varphi_i^n) && \text{for } \varphi_i^n, \varphi_j^n \in S_h^p(\mathcal{T}_{N_n}), \\ B_{\tau,h}^{n+1,n}[k,j] &:= -\left\langle \varphi_j^n, \varphi_k^{n+1} \right\rangle_{\Sigma_{n+1}} && \text{for } \varphi_j^n \in S_h^p(\mathcal{T}_{N_n}), \varphi_k^{n+1} \in S_h^p(\mathcal{T}_{N_{n+1}}). \end{aligned}$$

Moreover, the vectors on the right hand side of (4.1) are defined as

$$\boldsymbol{f}_n[i] := \langle f, \varphi_i^n \rangle_{Q_n} + \langle g_N, \varphi_i^n \rangle_{\Sigma_N \cap \partial Q_n} \quad \text{for } \varphi_j^n \in S_h^p(\mathcal{T}_{N_n}).$$

With the solution vectors $\boldsymbol{u}_n$ for $n = 1, \ldots, N$ of the linear system (4.1) we obtain an approximate solution on each space-time slab Q_n.

To solve the linear system (4.1) one can simply apply a forward substitution with respect to the blocks corresponding to a space-time slab. Hence one has to invert the matrix $A_{\tau,h}^n$ for each space-time slab Q_n, where for example a multigrid solver can be applied. This is the usual way how time dependent problems are

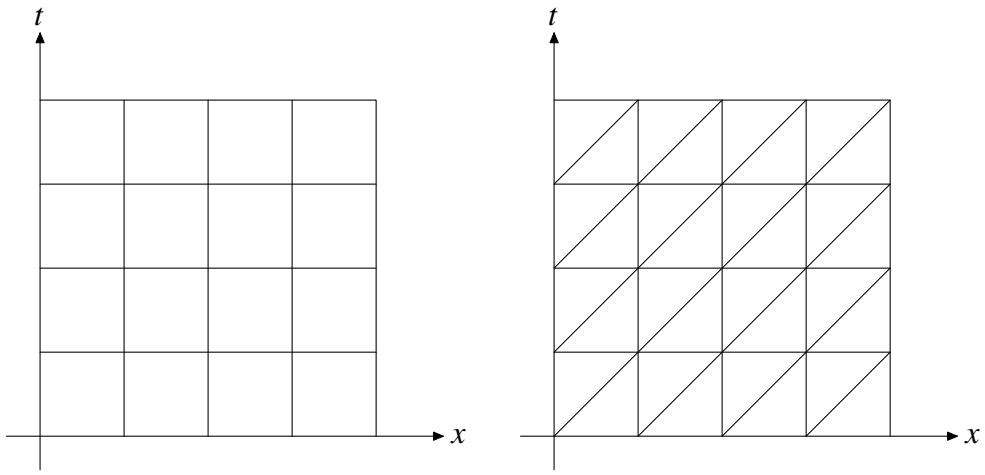

(a) Tensor product space-time mesh. (b) Simplex space-time mesh.

Figure 4.1: Space-time meshes with space-time slaps for $d = 1$.

solved when implicit schemes are used [41, 42, 97]. But in this chapter we want to apply a space-time multigrid scheme to solve the global linear system (4.1) at once. Space-time multigrid methods have been studied earlier in [38, 44, 45, 107]. Other methods to solve the global linear system (4.1) are for example waveform relaxation methods, which have been considered in [46, 47].

Next we will study the case when tensor product space-time meshes are used, like in Figure 4.1(a). For an easier notation we assume, that we have a uniform partition of the time interval $(0,T)$ into subintervals (t_{n-1},t_n) for $n = 1,\dots,N$, i.e. $t_n = n\tau$ with $\tau > 0$. For tensor product space-time meshes the approximate solution on the space-time slab Q_n is then given by the ansatz

$$u_h^n(\boldsymbol{x},t) = \sum_{\ell=1}^{N_t} \sum_{j=1}^{N_x} u_{\ell,j}^n \, \varphi_j(\boldsymbol{x}) \, \psi_\ell(t), \quad \text{with } u_{\ell,j}^n := \boldsymbol{u}_n[jN_t + \ell], \tag{4.2}$$

and with basis functions

$$u_h^n \in S_h^{\boldsymbol{p}}(\mathcal{T}_{N_n}) = \operatorname{span}\{\varphi_j\}_{j=1}^{N_x} \otimes \operatorname{span}\{\psi_\ell\}_{\ell=1}^{N_t}. \tag{4.3}$$

For the tensor product case different polynomial degrees with respect to space and time can be used, i.e. $\boldsymbol{p} := (p_x, p_t)$. For the space-time discretization (2.2) the ansatz (4.2) leads to the following matrices

$$A_{\tau,h}^n = A_{\tau,h} := M_h \otimes K_\tau + K_h \otimes M_\tau, \qquad B_{\tau,h}^{n+1,n} = B_{\tau,h} := -M_h \otimes N_\tau,$$

with the mass and stiffness matrix

$$M_h[i,j] := \int_\Omega \varphi_j(\boldsymbol{x})\varphi_i(\boldsymbol{x})\mathrm{d}\boldsymbol{x}, \quad K_h[i,j] := \tilde{a}(\varphi_j,\varphi_i)$$

for $i,j=1,\ldots,N_x$. Note that the bilinear form $\tilde{a}(\cdot,\cdot)$ results from the bilinear form $a(\cdot,\cdot)$ by integrating only over the spatial domain Ω. The matrices with respect to the time discretization are given by

$$K_\tau[k,\ell] := -\int_{t_{n-1}}^{t_n} \psi_\ell(t)\partial_t\psi_k(t)\mathrm{d}t + \psi_\ell(t_n)\psi_k(t_n), \tag{4.4}$$

$$M_\tau[k,\ell] := \int_{t_{n-1}}^{t_n} \psi_\ell(t)\psi_k(t)\mathrm{d}t, \quad N_\tau[k,\ell] := \psi_\ell(t_n)\psi_k(t_{n-1}) \tag{4.5}$$

for $k,\ell=1,\ldots,N_t$. Note that for the coupling matrix N_τ we have to evaluate the ansatz function ψ_ℓ at the time t_n, because we have $\psi_\ell^{n-1}(t_{n-1}) = \psi_\ell^n(t_n) = \psi_\ell(t_n)$. Further for $n=1,\ldots,N$ the right hand sides are given by

$$\boldsymbol{f}_n[jN_t+\ell] := \int_{t_{n-1}}^{t_n}\int_\Omega f(\boldsymbol{x},t)\varphi_j(\boldsymbol{x})\psi_\ell(t)\mathrm{d}\boldsymbol{x}\mathrm{d}t$$

for $j=1,\ldots,N_x$ and $\ell=1,\ldots,N_t$. If for the spatial ansatz functions continuous basis functions are used, then the stiffness matrix K_h reduces to the standard finite element stiffness matrix

$$K_h[i,j] := \int_\Omega \nabla\varphi_j(\boldsymbol{x})\cdot\nabla\varphi_i(\boldsymbol{x})\mathrm{d}\boldsymbol{x} \qquad \text{for } i,j=1,\ldots,N_x.$$

Hence, for tensor product space-time meshes we conclude, that the use of continuous ansatz functions in space leads to a standard finite element discretization in space combined with a discontinuous Galerkin time stepping scheme in time. This type of discretizations has been analyzed for example in [97].

4.1 Multigrid method

In this section a space-time multigrid method to solve the linear system (4.1) will be introduced. For an introduction to multigrid methods see for example [39,99,103,108]. For an easier notation we now write the linear system (4.1) as

$$\mathcal{L}_{\tau,h}\boldsymbol{x} = \boldsymbol{f}. \tag{4.6}$$

To solve the linear system (4.6) with a multigrid technique, a hierarchical sequence of space-time meshes $\mathcal{T}_{N_L}$ is needed for $L=0,\ldots,M_L$. This space-time hierarchy has to be chosen in an appropriate way and will depend on the discretization, see Section 4.3. For each space-time decomposition $\mathcal{T}_{N_L}$ we can compute the system

matrix $\mathcal{L}_{\tau_L,h_L}$ for $L=0,\ldots,M_L$. On the last level M_L we have to solve the linear system (4.6) and therefore we have $\mathcal{L}_{\tau_{M_L},h_{M_L}}=\mathcal{L}_{\tau,h}$.

With $\mathcal{S}^{\nu}_{\tau_L,h_L}$ we denote the smoother, where $\nu\in\mathbb{N}$ is the number of smoothing steps which are used. For the smoothing operator we consider the damped block Jacobi iteration

$$\boldsymbol{x}^{k+1}=\boldsymbol{x}^k+\omega_l(\widetilde{D}_{\tau_L,h_L})^{-1}\left[\boldsymbol{f}-\mathcal{L}_{\tau_L,h_L}\boldsymbol{x}^k\right]. \tag{4.7}$$

By $\widetilde{D}^{-1}_{\tau_L,h_L}$ we denote an approximation of the inverse of the block diagonal matrix $D_{\tau_L,h_L}:=\mathrm{diag}\{A^n_{\tau_L,h_L}\}_{n=1}^{N_L}$ where a block $A^n_{\tau_L,h_L}$ corresponds to the space-time slab Q_n. For the approximation of $(D_{\tau_L,h_L})^{-1}$ we apply one space multigrid iteration for each space-time slab. When tensor product space-time meshes are used we have to apply a multigrid solver on each space-time slab, where the system matrix is given by

$$A_{\tau_L,h_L}:=M_{h_L}\otimes K_{\tau_L}+K_{h_L}\otimes M_{\tau_L}.$$

In this case the matrix A_{τ_L,h_L} has tensor product structure, hence we can use a standard tensor product multigrid, like in [14] to approximate the inverse of the block diagonal matrix D_{τ_L,h_L}. To get an approximation for the inverse of the block diagonal matrix D_{τ_L,h_L} for general simplex space-time slabs, like in Figure 4.1(b), we apply an algebraic multigrid solver to the system matrix A_{τ_L,h_L}, as implemented in the package *hypre*, see [28, 29].

For the prolongation operator $\mathcal{P}^L$ we use the standard interpolation from coarse space-time grids to the next fine space-time grids. Therefore the prolongation operator will depend on the chosen space-time hierarchy. The restriction operator is defined as the adjoint of the prolongation operator $\mathcal{R}^L=(\mathcal{P}^L)^\top$.

The definition of one complete multigrid cycle is given in Algorithm 4.2. With $\nu_1,\nu_2\in\mathbb{N}$ we denote the number of pre- and post smoothing steps. Further $\gamma\in\mathbb{N}$ defines the cycle index, where a typical choice is $\gamma\in\{1,2\}$. For $\gamma=1$ the multigrid cycle in Algorithm 4.2 is the classical V-cycle, whereas for $\gamma=2$ we have the so called W-cycle. On the coarse level $L=0$ we solve the linear system exactly by using a LU-factorization for the system matrix $\mathcal{L}_{\tau_0,h_0}$. For a given initial guess we apply the space-time multigrid cycle of Algorithm 4.2 several times, until we have reached a given relative error reduction $\varepsilon_{\mathrm{MG}}$.

To prove convergence of the presented space-time multigrid method, we will use the local Fourier mode analysis. First we will apply this type of analysis to the simpler ODE case and afterwards we will use these results to analyze the space-time two-grid cycle.

MGCycle($\boldsymbol{x}$, $\boldsymbol{f}$, L)
if $L = 0$ **then**
  Coarse grid solver: $\boldsymbol{x} = (\mathcal{L}_{\tau_L,h_L})^{-1}\boldsymbol{f}$
else

  Pre-smoothing: $\boldsymbol{x} = \mathcal{S}^{\nu_1}_{\tau_L,h_L}(\boldsymbol{x},\boldsymbol{f})$
  Compute defect: $\boldsymbol{d} = \boldsymbol{f} - \mathcal{L}_{\tau_L,h_L}\boldsymbol{x}$
  Restriction: $\boldsymbol{d}_{L-1} = \mathcal{R}^L\boldsymbol{d}$
  Initialize: $\boldsymbol{w}_{L-1} = 0$

  for all $i = 1,\ldots,\gamma$ **do**
    MGCycle($\boldsymbol{w}_{L-1}$, $\boldsymbol{d}_{L-1}$, $L-1$)
  end for

  Prolongation: $\boldsymbol{w} = \mathcal{P}^L\boldsymbol{w}_{L-1}$
  Correction: $\boldsymbol{x} = \boldsymbol{x} + \boldsymbol{w}$
  Post-smoothing: $\boldsymbol{x} = \mathcal{S}^{\nu_2}_{\tau_L,h_L}(\boldsymbol{x},\boldsymbol{f})$

end if

Algorithm 4.2: Space-time multigrid cycle.

4.2 Time analysis

In this section we will consider for $T > 0$ the one-dimensional model problem

$$\begin{aligned} \partial_t u(t) + u(t) &= f(t) \qquad \text{for } t \in (0,T), \\ u(0) &= u_0. \end{aligned} \tag{4.8}$$

For the discretization of the model problem (4.8) we will use the discontinuous Galerkin approach as introduced at the beginning of this chapter. To solve the related linear system we will apply the multigrid idea presented above. We will see, that the analysis of the two-grid cycle for this simple one-dimensional problem is strongly connected to the analysis of the more complicated space-time two-grid cycle.

In what follows we first subdivide the simulation interval $[0,T]$ into $N \in \mathbb{N}$ uniform subintervals

$$0 = t_0 < t_1 < \cdots < t_{N-1} < t_N = T, \qquad t_n = n\,\tau,$$

with the time step size $\tau = \frac{T}{N}$, see also Figure 4.3. By introducing the continuity condition $u^n_\tau(t_{n-1}) = u^{n-1}_\tau(t_{n-1})$ in the weak sense we obtain for the time interval (t_{n-1},t_n) the following discrete variational problem:

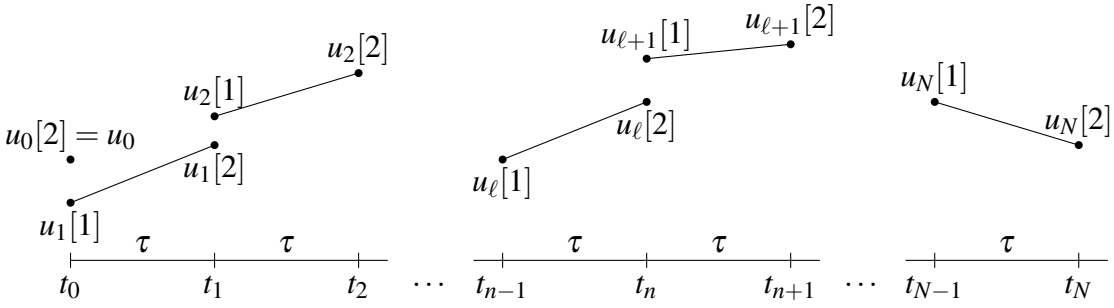

Figure 4.3: DG time stepping scheme for $p_t = 1$.

Find $u_\tau^n \in \mathbb{P}^{p_t}(t_{n-1}, t_n)$ such that

$$\begin{aligned} -\int_{t_{n-1}}^{t_n} u_\tau^n(t)\partial_t v_\tau^n(t)\mathrm{d}t + u_\tau^n(t_n)v_\tau^n(t_n) + \int_{t_{n-1}}^{t_n} u_\tau^n(t)v_\tau^n(t)\mathrm{d}t \\ = \int_{t_{n-1}}^{t_n} f(t)v_\tau^n(t)\mathrm{d}t + u_\tau^{n-1}(t_{n-1})v_\tau^n(t_{n-1}) \end{aligned} \tag{4.9}$$

is fulfilled for all $v_\tau^n \in \mathbb{P}^{p_t}(t_{n-1}, t_n)$.

Using the basis functions

$$\mathbb{P}^{p_t}(t_{n-1}, t_n) = \operatorname{span}\{\psi_\ell\}_{\ell=1}^{N_t}, \qquad N_t = p_t + 1,$$

the discrete variational problem (4.9) is equivalent to the system of linear algebraic equations

$$[K_\tau + M_\tau]\,\boldsymbol{u}_n = \boldsymbol{f}_n + N_\tau \boldsymbol{u}_{n-1},$$

with the matrices K_τ, M_τ and N_τ as defined in (4.4)–(4.5). Moreover, the right hand side is given by

$$\boldsymbol{f}_n[\ell] := \int_{t_{n-1}}^{t_n} f(t)\psi_\ell(t)\mathrm{d}t, \qquad \ell = 1, \ldots, N_t.$$

On the time interval $[t_{n-1}, t_n]$ we therefore can define the approximation

$$u_\tau^n(t) = \sum_{\ell=1}^{N_t} u_n[\ell]\psi_\ell(t).$$

Overall we have to solve the linear system

$$\begin{pmatrix} K_\tau + M_\tau & & & & \\ -N_\tau & K_\tau + M_\tau & & & \\ & -N_\tau & K_\tau + M_\tau & & \\ & & \ddots & \ddots & \\ & & & -N_\tau & K_\tau + M_\tau \end{pmatrix} \begin{pmatrix} \boldsymbol{u}_1 \\ \boldsymbol{u}_2 \\ \boldsymbol{u}_3 \\ \vdots \\ \boldsymbol{u}_N \end{pmatrix} = \begin{pmatrix} \boldsymbol{f}_1 \\ \boldsymbol{f}_2 \\ \boldsymbol{f}_3 \\ \vdots \\ \boldsymbol{f}_N \end{pmatrix}. \tag{4.10}$$

The linear system (4.10) is closely related to the linear system (4.1) corresponding to the full space-time discretization. Before we introduce the multigrid approach for solving the linear system (4.10), we will first study the properties of the discontinuous Galerkin discretization (4.9).

To do so, we consider for a function $f : (t_{n-1}, t_n) \to \mathbb{R}$ the Radau quadrature of order $2s-1$

$$\int_{t_{n-1}}^{t_n} f(t)\mathrm{d}t \approx \tau \sum_{k=1}^{s} b_k f(t_{n-1} + c_k \tau),$$

with the weights $b_k \in \mathbb{R}_+$ and the integration points $c_1 = 0$ and $c_2, \ldots, c_s \in [0,1]$, see also [42]. If the right hand side $\boldsymbol{f}_n$ of the discontinuous Galerkin discretization scheme (4.9) is approximated by the Radau quadrature of order $2p_t + 1$, i.e. $s = p_t + 1$, we can prove the following theorem.

Theorem 4.2.1. *The discontinuous Galerkin approximation (4.9) of the model problem (4.8), introduced above, is equivalent to the (p_t+1)-stage implicit Runge-Kutta scheme RADAU IA, if the integral of the right hand side is approximated by the Radau quadrature of order $2p_t+1$.*

Proof. Approximating the right hand side of (4.9) by the Radau quadrature rule of order $2p_t+1$ and by using integration by parts, the discontinuous Galerkin scheme (4.9) is given by to following variational problem:

Find $u_\tau^n \in \mathbb{P}^{p_t}(t_{n-1}, t_n)$ such that

$$\begin{aligned} &\int_{t_{n-1}}^{t_n} \partial_t u_\tau^n(t) v_\tau^n(t)\mathrm{d}t + u_\tau^n(t_{n-1}) v_\tau^n(t_{n-1}) + \int_{t_{n-1}}^{t_n} u_\tau^n(t) v_\tau^n(t)\mathrm{d}t \\ &\qquad = \tau \sum_{k=1}^{p_t+1} b_k f(t_{n-1} + c_k\tau) v_\tau^n(t_{n-1} + c_k\tau) + u_\tau^{n-1}(t_{n-1}) v_\tau^n(t_{n-1}) \end{aligned} \tag{4.11}$$

is fulfilled for all $v_\tau^n \in \mathbb{P}^{p_t}(t_{n-1}, t_n)$.

In what follows, we will also apply the discontinuous collocation method introduced in [40] to the model problem (4.8). Let $c_1 = 0$ and $c_2, \dots, c_{p_t+1} \in [0,1]$ be the integration points of the Radau quadrature of order $2p_t + 1$ with the weights $b_1, \dots, b_{p_t+1} \in \mathbb{R} \setminus \{0\}$. Then the discontinuous collocation method is given by:

Find $w_\tau^n \in \mathbb{P}^{p_t}(t_{n-1}, t_n)$ such that

$$\begin{aligned} w_\tau^n(t_{n-1}) - w_\tau^{n-1}(t_{n-1}) &= \tau b_1 \left[f(t_{n-1}) - \partial_t w_\tau^n(t_{n-1}) - w_\tau^n(t_{n-1}) \right], \\ \partial_t w_\tau^n(t_{n-1} + c_k\tau) + w_\tau^n(t_{n-1} + c_k\tau) &= f(t_{n-1} + c_k\tau) \end{aligned} \tag{4.12}$$

is fulfilled for all $k = 2, \dots, p_t + 1$.

In [40] it was shown, that the discontinuous collocation method (4.12) is equivalent to the (p_t+1)-stage implicit Runge-Kutta scheme RADAU IA. Hence it remains to show the equivalence of the discontinuous Galerkin method (4.11) with the discontinuous collocation method (4.12). First we observe that $\partial_t u_\tau^n v_\tau^n$ and $u_\tau^n v_\tau^n$ are polynomials of degree at most $2p_t$. Therefore we can replace the integrals on the left hand side of (4.11) with the Radau quadrature of order $2p_t + 1$. Hence we obtain

$$\begin{aligned} \tau \sum_{k=1}^{p_t+1} b_k \partial_t u_\tau^n(t_{n-1} + c_k\tau) v_\tau^n(t_{n-1} + c_k\tau) + u_\tau^n(t_{n-1}) v_\tau^n(t_{n-1}) & \\ + \tau \sum_{k=1}^{p_t+1} b_k u_\tau^n(t_{n-1} + c_k\tau) v_\tau^n(t_{n-1} + c_k\tau) & \\ = \tau \sum_{k=1}^{p_t+1} b_k f(t_{n-1} + c_k\tau) v_\tau^n(t_{n-1} + c_k\tau) + u_\tau^{n-1}(t_{n-1}) v_\tau^n(t_{n-1}), & \end{aligned} \tag{4.13}$$

with $v_\tau^n \in \mathbb{P}^{p_t}(t_{n-1}, t_n)$. As test functions v_τ^n we now consider the Lagrange polynomials

$$\ell_i^n(t) = \prod_{\substack{j=1 \\ j \neq i}}^{p_t+1} \frac{t - (t_{n-1} + c_j\tau)}{\tau(c_i - c_j)} \qquad \text{for } i = 1, \dots, p_t + 1.$$

Hence we have $\ell_i^n(t_{n-1} + c_j\tau) = 0$ for $i \neq j$ and $\ell_i^n(t_{n-1} + c_i\tau) = 1$ for $i = 1, \dots, p_t + 1$. First we use the test function $v_\tau^n = \ell_1^n$ in (4.13) and we obtain

$$\tau b_1 \partial_t u_\tau^n(t_{n-1}) + u_\tau^n(t_{n-1}) + \tau b_1 u_\tau^n(t_{n-1}) = \tau b_1 f(t_{n-1}) + u_\tau^{n-1}(t_{n-1}).$$

This implies, that the solution u_τ^n of (4.11) satisfies the first equation of (4.12). For the test function $v_\tau^n = \ell_k^n$, $k = 2, \dots, p_t + 1$ we further get

$$\tau b_k \partial_t u_\tau^n(t_{n-1} + c_k\tau) + \tau b_k u_\tau^n(t_{n-1} + c_k\tau) = \tau b_k f(t_{n-1} + c_k\tau).$$

Dividing this equation by the factor $\tau b_k \neq 0$ we obtain, that the solution u_τ^n of the discontinuous Galerkin scheme (4.11) also satisfies the second equation

of the discontinuous collocation method (4.12). Hence, the solution u_τ^n of the discontinuous Galerkin scheme (4.11) is a solution of the discontinuous collocation method (4.12). The other direction of the proof is obtained by reverting the arguments of above. ∎

Remark 4.2.2. *The RADAU IA scheme has been introduced in the PhD thesis [23] in 1969, see also [16]. Whereas the original discontinuous Galerkin method was introduced by Reed and Hill [75] in 1973 to solve the hyperbolic neutron transport equation. In [53] discontinuous Galerkin methods for ordinary differential equations are considered, see also [18].*

Remark 4.2.3. *In the proof of Theorem 4.2.1 it is shown, that the jump of the discrete solution at the time t_{n-1} is equal to the pointwise error multiplied with the time step size τ and the weight b_1, see equation (4.12). Hence the hight of the jump can be used as a simple error estimator for adaptive time stepping schemes.*

Remark 4.2.4. *We obtain by replacing the integrals of (4.11) with the Lobatto IIIC quadrature, see [42], the implicit Runge Kutta scheme Lobatto IIIC, which has a different stability behaviour as the RADAU IA method.*

Theorem 4.2.5. *For $s \in \mathbb{N}$ the s-stage RADAU IA scheme is of order $2s-1$ and the stability function $R(z)$ is given by the $(s-1,s)$ subdiagonal Padé approximation of the exponential function e^z. Furthermore the method is A-stable, i.e.*

$$|R(z)| < 1 \qquad \text{for } z \in \mathbb{C} \text{ with } \Re(z) < 0.$$

Proof. The proof can be found in [42]. ∎

Remark 4.2.6. *For $s \in \mathbb{N}$, the first $(s-1,s)$ subdiagonal Padé approximations $P_{s-1,s}(z)$ of the exponential function e^z are given by*

$$P_{0,1}(z) = \frac{1}{1-z}, \qquad P_{1,2}(z) = \frac{6+2z}{6-4z+z^2},$$
$$P_{2,3}(z) = \frac{60+24z+3z^2}{60-36z+9z^2-z^3}, \qquad P_{3,4}(z) = \frac{840+360z+60z^2+4z^3}{840-480z+120z^2-16z^3+z^4}.$$

Corollary 4.2.7. *The stability function $R(z)$ of the discontinuous Galerkin approximation with polynomial degree $p_t \in \mathbb{N}$ is given by the (p_t, p_t+1) subdiagonal Padé approximation of the exponential function e^z. Furthermore the method is A-stable, i.e.*

$$|R(z)| < 1 \qquad \text{for } z \in \mathbb{C} \text{ with } \Re(z) < 0.$$

Proof. For the Dahlquist test equation $\partial_t u = \lambda u, \lambda \in \mathbb{C}$ we obtain by Theorem 4.2.1 that the discontinuous Galerkin scheme is equivalent to the RADAU IA

method. Hence the two methods have the same stability function $R(z)$. Applying Theorem 4.2.5 completes the proof. ∎

In what follows, we will consider a global multigrid scheme, as introduced in Section 4.1, for the solution of (4.10). For an easier notation we write the linear system (4.10) as

$$[I_N \otimes (K_\tau + M_\tau) + U_N \otimes N_\tau]\, \boldsymbol{x} =: \mathcal{L}_\tau \boldsymbol{x} = \boldsymbol{f}, \tag{4.14}$$

with the matrix

$$U_N := \begin{pmatrix} 0 & & & & \\ -1 & 0 & & & \\ & -1 & 0 & & \\ & & \ddots & \ddots & \\ & & & -1 & 0 \end{pmatrix} \in \mathbb{R}^{N\times N}.$$

For the global multigrid scheme we assume a nested sequence of decompositions $\mathcal{T}_{N_L}$ with time step size τ_L for $L = 0,\dots,M_L$. Moreover we use the geometric restriction and prolongation operators $\mathcal{R}^L$ and $\mathcal{P}^L$. For the smoother we apply a fixed number $\nu \in \mathbb{N}$ of damped block Jacobi iterations

$$\boldsymbol{x}^{k+1} = \boldsymbol{x}^k + \omega_t D_{\tau_L}^{-1} \left[\boldsymbol{f} - \mathcal{L}_{\tau_L} \boldsymbol{x}^k\right], \tag{4.15}$$

with the block diagonal matrix $D_{\tau_L} := \mathrm{diag}\{K_{\tau_L} + M_{\tau_L}\}_{n=1}^{N_L}$ and with the damping parameter $\omega_t \in (0,2)$.

In what follows, we will study the two-grid cycle for solving the linear system (4.10). Using the definition of the smoother (4.15) we find for a given time step size τ_L that the error of the $(k+1)$-th Jacobi iteration for $\nu \in \mathbb{N}$ is given by

$$\boldsymbol{x} - \boldsymbol{x}^{k+1,\nu} =: \boldsymbol{e}^{k+1,\nu} = \left[I - \omega_t D_{\tau_L}^{-1} \mathcal{L}_{\tau_L}\right]^\nu \boldsymbol{e}^{k,\nu} =: \mathcal{S}_{\tau_L}^\nu \boldsymbol{e}^{k,\nu}. \tag{4.16}$$

Moreover the $(k+1)$-th error of the two-grid cycle is given by

$$\boldsymbol{x} - \boldsymbol{x}^{k+1} =: \boldsymbol{e}^{k+1} = \mathcal{S}_{\tau_L}^{\nu_2} \left[I - \mathcal{P}^L \mathcal{L}_{2\tau_L}^{-1} \mathcal{R}^L \mathcal{L}_{\tau_L}\right] \mathcal{S}_{\tau_L}^{\nu_1} \boldsymbol{e}^k =: \mathcal{M}_{\tau_L} \boldsymbol{e}^k. \tag{4.17}$$

To ensure mesh independent convergence of the two-grid cycle we need that the spectral radius of the iteration matrix $\mathcal{M}_{\tau_L}$ is smaller than one, i.e.

$$\rho(\mathcal{M}_{\tau_L}) \le q < 1,$$

with a constant q independent of the time step size. The computation of the spectral radius for arbitrary two-grid iteration matrices is in general not trivial, because the inverse of the coarse grid operator $\mathcal{L}_{2\tau_L}$ is involved. Moreover the

iteration matrix $\mathcal{M}_{\tau_L}$ is not symmetric in our case. To overcome this problem we transform the equation (4.14) into the frequency domain, where we apply the analysis based on exponential Fourier modes. This type of analysis was introduced in [12] where the rigorous analysis was done in [13] and it is used for a large class of problems, see for example [90, 99, 108]. The analysis is regarded to special model problems, namely those with periodic boundary conditions on rectangular domains. For general boundary conditions this type of analysis can be used to study the local behavior of the two-grid algorithm, therefore it is also called local Fourier mode analysis.

For time periodic solutions the problem (4.8) changes to

$$\partial_t u(t) + u(t) = f(t) \quad \text{for } t \in (0,t), \qquad u(0) = u(T). \tag{4.18}$$

For the discretization of the problem (4.18) with a discontinuous Galerkin time stepping method we therefore have to solve the linear system (4.14), i.e.

$$\left[I_N \otimes (K_\tau + M_\tau) + \tilde{U}_N \otimes N_\tau\right] \boldsymbol{x} = \boldsymbol{f},$$

where the matrix $\tilde{U}_N$ is given by the circulant matrix

$$\tilde{U}_N := \begin{pmatrix} 0 & & & & -1 \\ -1 & 0 & & & \\ & -1 & 0 & & \\ & & \ddots & \ddots & \\ & & & -1 & 0 \end{pmatrix} \in \mathbb{R}^{N\times N}. \tag{4.19}$$

4.2.1 Smoothing analysis

In this subsection we will use the local Fourier mode analysis to study the smoothing behavior of the iteration matrix $\mathcal{S}_{\tau_L}^{\nu}$. To transform the problem (4.14) into the frequency domain we need the following theorem.

Theorem 4.2.8 (Discrete Fourier transform)**.** *For $m \in \mathbb{N}$ let $\boldsymbol{u} \in \mathbb{R}^{2m}$, then there holds*

$$\boldsymbol{u} = \sum_{k=1-m}^{m} \hat{u}_k \boldsymbol{\varphi}(\theta_k), \qquad \boldsymbol{\varphi}(\theta_k)[\ell] := e^{\mathrm{i}\ell\theta_k}, \quad \ell = 1,\dots,2m, \qquad \theta_k := \frac{k\pi}{m},$$

with the coefficients

$$\hat{u}_k := \frac{1}{2m}(\boldsymbol{u}, \boldsymbol{\varphi}(-\theta_k))_2 = \frac{1}{2m}\sum_{\ell=1}^{2m} \boldsymbol{u}[\ell]\boldsymbol{\varphi}(-\theta_k)[\ell], \qquad \textit{for } k = 1-m,\dots,m.$$

Proof. The proof can be found in [108, Theorem 7.3.1] for example. ∎

Definition 4.2.9 (Fourier modes, Fourier frequencies)**.** *Let $N_L \in \mathbb{N}$. Then the vector valued function $\varphi(\theta_k)[\ell] := e^{i\ell\theta_k}$, $\ell = 1,\dots,N_L$ is called Fourier mode with frequency*

$$\theta_k \in \Theta_L := \left\{ \frac{2k\pi}{N_L} : k = 1 - \frac{N_L}{2},\dots,\frac{N_L}{2} \right\} \subset (-\pi,\pi].$$

The frequencies Θ_L are further separated into low and high frequencies

$$\Theta_L^{\text{low}} := \Theta_L \cap (-\frac{\pi}{2},\frac{\pi}{2}],$$
$$\Theta_L^{\text{high}} := \Theta_L \cap \Big((-\pi,-\frac{\pi}{2}] \cup (\frac{\pi}{2},\pi] \Big) = \Theta_L \setminus \Theta_L^{\text{low}}.$$

In the following we denote by $N_L \in \mathbb{N}$ the number of time steps for the level $L \in \mathbb{N}_0$ and by $N_t = p_t + 1 \in \mathbb{N}$ we denote the degrees of freedom with respect to one time step, see also (4.3). With the next lemma we transform a given vector corresponding to the problem (4.14) into the frequency domain.

Lemma 4.2.10. *The vector $\boldsymbol{u} = (\boldsymbol{u}_1, \boldsymbol{u}_2, \dots, \boldsymbol{u}_{N_L})^\top \in \mathbb{R}^{N_L N_t}$ for $N_{L-1}, N_t \in \mathbb{N}$ and $N_L = 2N_{L-1}$ can be written as*

$$\boldsymbol{u} = \sum_{k=1-N_{L-1}}^{N_{L-1}} \boldsymbol{\psi}^L(\theta_k, U) = \sum_{\theta_k \in \Theta_L} \boldsymbol{\psi}^L(\theta_k, U),$$

with the vectors

$$\boldsymbol{\psi}_n^L(\theta_k, U) := U\boldsymbol{\Phi}_n^L(\theta_k), \quad \boldsymbol{\Phi}_n^L(\theta_k)[\ell] := \varphi(\theta_k)[n] \quad \text{for } n = 1,\dots,N_L \text{ and } \ell = 1,\dots,N_t$$

and the coefficent matrix

$$U = \operatorname{diag}(\hat{u}_k[1],\dots,\hat{u}_k[N_t]) \in \mathbb{C}^{N_t \times N_t}$$

with the coefficients

$$\hat{u}_k[\ell] := \frac{1}{N_L} \sum_{i=1}^{N_L} u_i[\ell] \varphi(-\theta_k)[i] \qquad \text{for } k = 1 - N_{L-1},\dots,N_{L-1}.$$

Proof. For a fixed index $\ell \in \{1,\dots,N_t\}$ we apply Theorem 4.2.8 to the vector $\tilde{\boldsymbol{u}}_\ell \in \mathbb{R}^{N_L}$ with $\tilde{\boldsymbol{u}}_\ell[n] := \boldsymbol{u}_n[\ell]$, $n = 1,\dots,N_L$. Further by using the definition of the coefficient $\hat{u}_k[\ell]$ and the definition of the vector $\boldsymbol{\psi}_n^L(\theta_k)$ the statement of the lemma follows with

$$u_n[\ell] = \tilde{\boldsymbol{u}}_\ell[n] = \sum_{k=1-N_{L-1}}^{N_{L-1}} \hat{u}_k[\ell] \varphi(\theta_k)[n]$$

$$
\begin{aligned}
&= \sum_{k=1-N_{L-1}}^{N_{L-1}} \hat{u}_k[\ell]\boldsymbol{\Phi}_n^L(\theta_k)[\ell] \\
&= \sum_{k=1-N_{L-1}}^{N_{L-1}} U[\ell,\ell]\boldsymbol{\Phi}_n^L(\theta_k)[\ell] \\
&= \sum_{k=1-N_{L-1}}^{N_{L-1}} \boldsymbol{\psi}_n^L(\theta_k,U)[\ell] = \sum_{\theta_k\in\Theta_L} \boldsymbol{\psi}_n^L(\theta_k,U)[\ell].
\end{aligned}
$$

■

Remark 4.2.11. *Note that in Lemma 4.2.10 the vector $\boldsymbol{\psi}^L = \boldsymbol{\psi}^L(\theta_k,U)$ depends on the frequency $\theta_k \in \Theta_L$ and on the coefficent matrix $U \in \mathbb{C}^{N_t\times N_t}$, where the coefficent matrix U can be computed via the given vector $\boldsymbol{u} = (\boldsymbol{u}_1,\boldsymbol{u}_2,\ldots,\boldsymbol{u}_{N_L})^\top$. In the following we will study the mapping properties of the system matrix $\mathcal{L}_{\tau_L}$ and the smoother $\mathcal{S}_{\tau_L}^\nu$ with respect to the vector $\boldsymbol{\psi}^L = \boldsymbol{\psi}^L(\theta_k,U)$. Since the coefficent matrix U will be fixed and since we have to study the mapping properties of $\mathcal{L}_{\tau_L}$ and $\mathcal{S}_{\tau_L}^\nu$ with respect to the frequencies $\theta_k \in \Theta_L$ we will use the simpler notation $\boldsymbol{\psi}^L = \boldsymbol{\psi}^L(\theta_k)$. The dependence of the vector $\boldsymbol{\psi}^L$ with the coefficent matrix U is given in the following definition.*

Definition 4.2.12 (Fourier space)**.** *For $N_L,N_t \in \mathbb{N}$ let the vector $\boldsymbol{\Phi}^L(\theta_k) \in \mathbb{C}^{N_tN_L}$ be defined as in Lemma 4.2.10 with frequency $\theta_k \in \Theta_L$. Then we define the linear space of Fourier modes with frequency θ_k as*

$$
\begin{aligned}
\Psi_L(\theta_k) &:= \operatorname{span}\left\{\boldsymbol{\Phi}^L(\theta_k)\right\} \\
&= \left\{\boldsymbol{\psi}^L(\theta_k) \in \mathbb{C}^{N_tN_L} : \boldsymbol{\psi}_n^L(\theta_k) = U\boldsymbol{\Phi}_n^L(\theta_k),\ n=1,\ldots,N_L \text{ and } U \in \mathbb{C}^{N_t\times N_t}\right\}.
\end{aligned}
$$

Before we can study the mapping properties of the system matrix $\mathcal{L}_{\tau_L}$ and the smoother $\mathcal{S}_{\tau_L}^\nu$ we have to prove the following lemma.

Lemma 4.2.13. *For $N_L,N_t \in \mathbb{N}$ let $\boldsymbol{\psi}^L(\theta_k) \in \Psi_L(\theta_k)$. Then the following shifting equality holds true*

$$
\boldsymbol{\psi}_{n-1}^L(\theta_k) = e^{-\mathbb{i}\theta_k}\boldsymbol{\psi}_n^L(\theta_k) \qquad \text{for } n = 2,\ldots,N_L.
$$

Proof. By using the definition of the blockwise Fourier mode $\boldsymbol{\psi}^L(\theta_k) \in \Psi_L(\theta_k)$ we get the statement of the lemma for $n = 2,\ldots,N_L$ with

$$
\begin{aligned}
\boldsymbol{\psi}_{n-1}^L(\theta_k)[\ell] &= \sum_{i=1}^{N_t} U[\ell,i]\boldsymbol{\Phi}_{n-1}^L(\theta_k)[i] = \sum_{i=1}^{N_t} U[\ell,i]\boldsymbol{\varphi}(\theta_k)[n-1] = \sum_{i=1}^{N_t} U[\ell,i]e^{\mathbb{i}(n-1)\theta_k} \\
&= e^{-\mathbb{i}\theta_k}\sum_{i=1}^{N_t} U[\ell,i]e^{\mathbb{i}n\theta_k} = e^{-\mathbb{i}\theta_k}\sum_{i=1}^{N_t} U[\ell,i]\boldsymbol{\varphi}(\theta_k)[n]
\end{aligned}
$$

$$= e^{-\mathbb{i}\theta_k} \sum_{i=1}^{N_t} U[\ell,i]\boldsymbol{\Phi}_n^L(\theta_k)[i] = e^{-\mathbb{i}\theta_k}\boldsymbol{\psi}_n^L(\theta_k)[\ell]$$

for $\ell = 1,\dots,N_t$. ∎

For the system matrix $\mathcal{L}_{\tau_L}$ we are now able describe the Fourier symbol.

Lemma 4.2.14. *For $N_L, N_t \in \mathbb{N}$ let $\boldsymbol{\psi}^L(\theta_k) \in \Psi_L(\theta_k)$. Then for the system matrix $\mathcal{L}_{\tau_L}$ as defined in (4.14) there holds*

$$\left(\mathcal{L}_{\tau_L}\boldsymbol{\psi}^L(\theta_k)\right)_n = \left(K_{\tau_L} + M_{\tau_L} - \lambda_n N_{\tau_L}\right)\boldsymbol{\psi}_n^L(\theta_k) \qquad \text{for } n = 1,\dots,N_L,$$

with

$$\lambda_n := \begin{cases} e^{-\mathbb{i}\theta_k} & n \neq 1, \\ 0 & n = 1. \end{cases}$$

Proof. By using the representation (4.14) of the matrix $\mathcal{L}_{\tau_L}$ we get for a fixed but arbitrary $j = 1,\dots,N_t$

$$\begin{aligned}\left(\mathcal{L}_{\tau_L}\boldsymbol{\psi}^L(\theta_k)\right)_n[j] &= \sum_{m=1}^{N_L}\sum_{i=1}^{N_t}\left(I_{N_L}[n,m](K_{\tau_L}+M_{\tau_L})[j,i] + U_{N_L}[n,m]N_{\tau_L}[j,i]\right)\boldsymbol{\psi}_m^L(\theta_k)[i] \\ &= \sum_{i=1}^{N_t}(K_{\tau_L}+M_{\tau_L})[j,i]\boldsymbol{\psi}_n^L(\theta_k)[i] + \sum_{i=1}^{N_t} N_{\tau_L}[j,i]\sum_{m=1}^{N_L} U_{N_L}[n,m]\boldsymbol{\psi}_m^L(\theta_k)[i].\end{aligned}$$

With the definition of the matrix U_{N_L} we obtain for $n \neq 1$

$$= \sum_{i=1}^{N_t}(K_{\tau_L}+M_{\tau_L})[j,i]\boldsymbol{\psi}_n^L(\theta_k)[i] - \sum_{i=1}^{N_t} N_{\tau_L}[j,i]\boldsymbol{\psi}_{n-1}^L(\theta_k)[i].$$

Applying Lemma 4.2.13 gives the statment of this lemma for $n \neq 1$

$$\begin{aligned}&= \sum_{i=1}^{N_t}\left(K_{\tau_L}+M_{\tau_L}-e^{-\mathbb{i}\theta_k}N_{\tau_L}\right)[j,i]\boldsymbol{\psi}_n^L(\theta_k)[i] \\ &= \left(\left(K_{\tau_L}+M_{\tau_L}-\lambda_n N_{\tau_L}\right)\boldsymbol{\psi}_n^L(\theta_k)\right)[j].\end{aligned}$$

For $n = 1$ we observe that

$$\sum_{m=1}^{N_L} U_{N_L}[n,m]\boldsymbol{\psi}_m^L(\theta_k)[i] = 0,$$

and hence we conclude that

$$\left(\mathcal{L}_{\tau_L}\boldsymbol{\Phi}^k\right)_n[j] = \left(\left(K_{\tau_L}+M_{\tau_L}\right)\boldsymbol{\psi}_n^L(\theta_k)\right)[j].$$

∎

Remark 4.2.15. *Lemma 4.2.14 shows, that the system matrix $\mathcal{L}_{\tau_L}$ is not a self mapping on the Fourier space $\Psi_L(\theta_k)$, i.e.*

$$\mathcal{L}_{\tau_L} : \Psi_L(\theta_k) \nrightarrow \Psi_L(\theta_k),$$

since $K_{\tau_L} + M_{\tau_L} - \lambda_n N_{\tau_L} \in \mathbb{C}^{N_t \times N_t}$ is not constant with respect to n. But for periodic solutions, see (4.18) we have due to the circulant matrix $\tilde{U}_N$, see (4.19)

$$K_{\tau_L} + M_{\tau_L} - \lambda_n N_{\tau_L} = K_{\tau_L} + M_{\tau_L} - e^{-\mathbb{i}\theta_k} N_{\tau_L},$$

which implies that $\mathcal{L}_{\tau_L}$ is a self mapping on the Fourier space $\Psi_L(\theta_k)$ in this case. Since $\lambda_n = e^{-\mathbb{i}\theta_k}$ for all $n \neq 1$ the mapping $\mathcal{L}_{\tau_L}$ is closely related to the case with periodic solutions.

With the next lemma we will compute the Fourier symbol for the smoother $\mathcal{S}^{\nu}_{\tau_L}$ for $\nu = 1$.

Lemma 4.2.16. *For $N_L, N_t \in \mathbb{N}$ let $\psi^L(\theta_k) \in \Psi_L(\theta_k)$. Then for the smoother $\mathcal{S}^{\nu}_{\tau_L}$, there holds for $\nu = 1$ and $\omega_t \in \mathbb{R}$*

$$\left(\mathcal{S}^1_{\tau_L} \psi^L(\theta_k)\right)_n = S_n \psi^L_n(\theta_k) \qquad \text{for } n = 1, \ldots, N_L,$$

with the local iteration matrix

$$S_n := (1-\omega_t) I_{N_t} + \lambda_n \omega_t (K_{\tau_L} + M_{\tau_L})^{-1} N_{\tau_L}, \qquad \lambda_n := \begin{cases} e^{-\mathbb{i}\theta_k} & n \neq 1, \\ 0 & n = 1. \end{cases}$$

Proof. Let $\psi^L(\theta_k) \in \Psi_L(\theta_k)$. Then for $n = 1, \ldots, N_L$ we obtain

$$\left(\mathcal{S}^1_{\tau_L} \psi^L(\theta_k)\right)_n = \left(\left(I_{N_L N_t} - \omega_t D^{-1}_{\tau_L} \mathcal{L}_{\tau_L} \right) \psi^L(\theta_k) \right)_n.$$

Since $D^{-1}_{\tau_L}$ is a block diagonal matrix we obtain

$$= \psi^L_n(\theta_k) - \omega_t (K_{\tau_L} + M_{\tau_L})^{-1} \left(\mathcal{L}_{\tau_L} \psi^L(\theta_k)\right)_n.$$

Applying Lemma 4.2.14 leads to the statement of this lemma with

$$\begin{aligned} &= \psi^L_n(\theta_k) - \omega_t (K_{\tau_L} + M_{\tau_L})^{-1} \left(K_{\tau_L} + M_{\tau_L} - \lambda_n N_{\tau_L}\right) \psi^L_n(\theta_k) \\ &= \left((1-\omega_t) I_{N_t} + \lambda_n \omega_t (K_{\tau_L} + M_{\tau_L})^{-1} N_{\tau_L}\right) \psi^L_n(\theta_k). \end{aligned}$$

■

To analyze the smoothing behaviour of the damped block Jacobi smoother (4.15) we have to estimate the spectral radius of the local iteration matrix

$$S_n = (1-\omega_t) I_{N_t} + \lambda_n \omega_t (K_{\tau_L} + M_{\tau_L})^{-1} N_{\tau_L} \in \mathbb{C}^{N_t \times N_t}.$$

Hence, we have to compute the eigenvalues of the matrix $(K_{\tau_L} + M_{\tau_L})^{-1} N_{\tau_L}$.

Theorem 4.2.17. *The eigenvalues of the matrix* $(K_{\tau_L}+M_{\tau_L})^{-1}N_{\tau_L} \in \mathbb{R}^{N_t\times N_t}$ *are given by*

$$\sigma((K_{\tau_L}+M_{\tau_L})^{-1}N_{\tau_L}) = \{0,\alpha(\tau_L)\},$$

where $\alpha(\tau_L) = R(-\tau_L)$*, and* $R(z)$ *is the A-stability function of the given discontinuous Galerkin time stepping scheme.*

Proof. First we notice, that the eigenvalues of the matrix $(K_{\tau_L}+M_{\tau_L})^{-1}N_{\tau_L}$ are independent of the basis $\{\psi_k\}_{k=1}^{N_t}$ which is used to compute the matrices K_{τ_L}, M_{τ_L} and N_{τ_L}. Hence we will use special basis functions $\{\psi_k\}_{k=1}^{N_t}$ where the eigenvalues of the matrix $(K_{\tau_L}+M_{\tau_L})^{-1}N_{\tau_L}$ are easy to compute. In particular we use polynomials $\psi_k \in \mathbb{P}^p(0,\tau_L)$ with the property

$$\psi_k(\tau_L) = \begin{cases} 1 & k=1, \\ 0 & k\neq 1 \end{cases} \qquad \text{for } k=1,\dots,N_t.$$

In what follows, we will study the A-stability of the discontinuous Galerkin discretization. We therefore consider for $\lambda\in\mathbb{C}$ with $\Re(\lambda)<0$ the model problem

$$\partial_t u(t) = \lambda u(t), \quad t\in(0,\tau_L) \quad \text{and} \quad u(0)=u_0.$$

This leads to the linear system

$$(K_{\tau_L}-\lambda M_{\tau_L})\,\boldsymbol{u}_1 = u_0 N_{\tau_L}\boldsymbol{v},$$

with the vector $\boldsymbol{v}[1]=1$ and $\boldsymbol{v}[k]=0$ for $k=2,\dots,N_t$ and with the solution vector $\boldsymbol{u}_1\in\mathbb{R}^{N_t}$ for the first step. Therefore the value at the endpoint τ_L of the discrete solution is given by

$$u_1 = u_0\boldsymbol{v}^\top (K_{\tau_L}-\lambda M_{\tau_L})^{-1}N_{\tau_L}\boldsymbol{v}\in\mathbb{R}.$$

Hence the stability function $R(z)$ with $z=\lambda\tau_L$ is given by

$$R(z(\lambda,\tau_L)) = \boldsymbol{v}^\top (K_{\tau_L}-\lambda M_{\tau_L})^{-1}N_{\tau_L}\boldsymbol{v}. \tag{4.20}$$

Multiplying the equation (4.20) with the vector $\boldsymbol{v}$ results in

$$(K_{\tau_L}-\lambda M_{\tau_L})^{-1}N_{\tau_L}\boldsymbol{v} = R(z(\lambda,\tau_L))\boldsymbol{v}.$$

For $\lambda=-1$ this implies, that the vector $\boldsymbol{v}$ is an eigenvector with eigenvalue $\alpha(\tau_L)=R(-\tau_L)$ of the matrix $(K_{\tau_L}-\lambda M_{\tau_L})^{-1}N_{\tau_L}$. Since the matrix N_{τ_L} has rank one, all the other eigenvalues have to be zero. ∎

Remark 4.2.18. *Theorem 4.2.17 holds true for any single step method. Hence any single step method is A-stable if and only if*

$$|R(z(\lambda,\tau_L))| = \rho((K_{\tau_L}-\lambda M_{\tau_L})^{-1}N_{\tau_L}) < 1 \qquad \text{for all } z\in\mathbb{C} \text{ with } \Re(z)<0.$$

Now we are able to compute the spectral radius of the local iteration matrix $S_n = (1-\omega_t)I_{N_t} + \lambda_n\omega_t(K_{\tau_L}+M_{\tau_L})^{-1}N_{\tau_L} \in \mathbb{C}^{N_t\times N_t}$.

Lemma 4.2.19. *Let $p_t \in \mathbb{N}_0$. Then for the smoother $\mathcal{S}^{\nu}_{\tau_L}$ the spectral radius of the local iteration matrix $S_n = (1-\omega_t)I_{N_t} + \lambda_n\omega_t(K_{\tau_L}+M_{\tau_L})^{-1}N_{\tau_L}$ is given by*

$$\rho(S_n) = \begin{cases} |1-\omega_t| & n=1, \\ \max\left\{|1-\omega_t|, \hat{S}(\omega_t,\alpha(\tau_L),\theta_k)\right\} & n\neq 1, \end{cases}$$

with

$$\left(\hat{S}(\omega_t,\alpha,\theta_k)\right)^2 := (1-\omega_t)^2 + 2\omega_t(1-\omega_t)\alpha\cos(\theta_k) + \alpha^2\omega_t^2,$$

where $\alpha = \alpha(t)$ is the (p_t, p_t+1) subdiagonal Padé approximation of the exponential function e^{-t}.

Proof. For $n=1$ we have $\lambda_n = 0$ and therefore the eigenvalues are given by

$$\sigma(S_n) := \sigma\left((1-\omega_t)I_{N_t} + \lambda_n\omega_t(K_{\tau_L}+M_{\tau_L})^{-1}N_{\tau_L}\right) = \{1-\omega_t\}.$$

Hence the spectral radius is given by $\rho(S_n) = |1-\omega_t|$. For $n\neq 1$ we have $\lambda_n = e^{-\mathbb{i}\theta_k}$ and since I_{N_t} is the identity matrix the eigenvalues of the local iteration matrix S_n are given by

$$\sigma(S_n) = 1-\omega_t + e^{-\mathbb{i}\theta_k}\omega_t\sigma((K_{\tau_L}+M_{\tau_L})^{-1}N_{\tau_L}).$$

With Theorem 4.2.17 we are now able to compute the spectrum of the iteration matrix S_n

$$\sigma(S_n) = \left\{1-\omega_t, 1-\omega_t + e^{-\mathbb{i}\theta_k}\omega_t\alpha(\tau_L)\right\}.$$

Hence we obtain the spectral radius

$$\rho(S_n) = \max\left\{|1-\omega_t|, \left|1-\omega_t + e^{-\mathbb{i}\theta_k}\omega_t\alpha(\tau_L)\right|\right\}.$$

Simple calculations lead to

$$\left|1-\omega_t + e^{-\mathbb{i}\theta_k}\omega_t\alpha(\tau_L)\right|^2 = (1-\omega_t)^2 + 2\omega_t(1-\omega_t)\alpha(\tau_L)\cos(\theta_k) + (\alpha(\tau_L))^2\omega_t^2,$$

which completes the proof. ∎

To prove the convergence of the block Jacobi smoother introduced in (4.15), we will estimate the spectral radius of the local iteration matrix $S_n \in \mathbb{C}^{N_t\times N_t}$ with the following lemma.

Lemma 4.2.20. *Let $p_t \in \mathbb{N}_0$ and $\omega_t \in (0,1]$, then the spectral radius of the local iteration matrix $S_n = (1-\omega_t) I_{N_t} + \lambda_n \omega_t (K_{\tau_L} + M_{\tau_L})^{-1} N_{\tau_L}$ is strictly bounded by one, i.e.*

$$\rho(S_n) < 1.$$

Proof. In view of Lemma 4.2.19 we have to estimate for a fixed $n \in \{1,\dots,N_L\}$ the function

$$\max\left\{|1-\omega_t|, \hat{S}(\omega_t,\tau_L,\theta_k)\right\}.$$

For $\omega_t \in (0,1]$ we clearly have that $|1-\omega_t| < 1$. Furthermore we can estimate $\hat{S}(\omega_t,\tau_L,\theta_k)$ by

$$\begin{aligned}\left|\left(\hat{S}(\omega_t,\tau_L,\theta_k)\right)\right|^2 &= \left|(1-\omega_t)^2 + 2\omega_t(1-\omega_t)\alpha(\tau_L)\cos(\theta_k) + (\alpha(\tau_L))^2\omega_t^2\right| \\ &\le (1-\omega_t)^2 + 2\omega_t(1-\omega_t)\left|\alpha(\tau_L)\right| + \left|\alpha(\tau_L)\right|^2\omega_t^2.\end{aligned}$$

Since $\alpha(\tau_L) = R(-\tau_L)$ is the A-stability function for $z = -\tau_L$, see Theorem 4.2.17, and by using the fact that the discontinuous Galerkin scheme is A-stable, see Corollary 4.2.7, we have $|\alpha(\tau_L)| < 1$ for $\tau_L > 0$. Hence we obtain the statment of this lemma with

$$\begin{aligned}&< (1-\omega_t)^2 + 2\omega_t(1-\omega_t) + \omega_t^2 \\ &= (1-\omega_t+\omega_t)^2 = 1.\end{aligned}$$

■

Theorem 4.2.21. *For any damping parameter $\omega_t \in (0,1]$ the block Jacobi smoother introduced in (4.15) converges for any initial guess $\boldsymbol{x}^0$ to the exact solution of*

$$\mathcal{L}_{\tau_L}\boldsymbol{x} = \boldsymbol{f}.$$

Proof. For an arbitrary but fixed $n \in \{1,\dots,N_L\}$ the n-th error component $\boldsymbol{e}_n^1$ of the first damped block Jacobi iteration is given by

$$\boldsymbol{e}_n^1 = \left(\mathcal{S}_{\tau_L}^1 \boldsymbol{e}^0\right)_n,$$

with the initial error $\boldsymbol{e}^0 = \boldsymbol{x} - \boldsymbol{x}^0$. In what follows, we will transform the initial error $\boldsymbol{e}^0$ into the frequency domain by applying Lemma 4.2.10

$$= \left(\mathcal{S}_{\tau_L}^1 \left(\sum_{\theta_k \in \Theta_L} \boldsymbol{\psi}^L(\theta_k)\right)\right)_n,$$

where the Fourier vectors $\psi^L(\theta_k)$, $\theta_k \in \Theta_L$ depend on the constant coefficent matrix $U = U(e_0) \in \mathbb{C}^{N_t \times N_t}$ resulting from the initial vector e_0. Since $\mathcal{S}^\nu_{\tau_L}$, $\nu = 1$, is a linear operator we have

$$= \sum_{\theta_k \in \Theta_L} \left(\mathcal{S}^1_{\tau_L} \psi^L(\theta_k)\right)_n.$$

Using Lemma 4.2.16 leads to

$$\begin{aligned} &= \sum_{\theta_k \in \Theta_L} \left((1-\omega_t) I_{N_t} + \lambda_n \omega_t (K_{\tau_L} + M_{\tau_L})^{-1} N_{\tau_L}\right) \psi^L_n(\theta_k) \\ &= \sum_{\theta_k \in \Theta_L} S_n \psi^L_n(\theta_k). \end{aligned}$$

Further computations show that for $n \geq \nu$ we have

$$S^\nu_n = \left((1-\omega_t) I_{N_t} + e^{-\mathbb{i}\theta_k} \omega_t (K_{\tau_L} + M_{\tau_L})^{-1} N_{\tau_L}\right)^\nu.$$

As the spectral radius $\rho\left((1-\omega_t) I_{N_t} + e^{-\mathbb{i}\theta_k} \omega_t (K_{\tau_L} + M_{\tau_L})^{-1} N_{\tau_L}\right)$ is strictly smaller then one, see Lemma 4.2.20, we conclude, that S^ν_n contracts as $\nu \to n$. Furthermore for $n < \nu$ the local iteration matrix S^ν_n is given by

$$S^\nu_n = \sum_{j=0}^{n-1} \binom{\nu}{\nu-j} (1-\omega_t)^{\nu-j} \left(\omega_t e^{-\mathbb{i}\theta_k} (K_{\tau_L} + M_{\tau_L})^{-1} N_{\tau_L}\right)^j.$$

Hence we can estimate the spectral radius by

$$\begin{aligned} \rho(S^\nu_n) &= \rho\left(\sum_{j=0}^{n-1} \binom{\nu}{\nu-j} (1-\omega_t)^{\nu-j} \left(\omega_t e^{-\mathbb{i}\theta_k} (K_{\tau_L} + M_{\tau_L})^{-1} N_{\tau_L}\right)^j\right) \\ &\leq \sum_{j=0}^{n-1} \binom{\nu}{\nu-j} (1-\omega_t)^{\nu-j} \omega_t^j \rho\left(\left(e^{-\mathbb{i}\theta_k} (K_{\tau_L} + M_{\tau_L})^{-1} N_{\tau_L}\right)^j\right) \\ &\leq \sum_{j=0}^{n-1} \binom{\nu}{\nu-j} (1-\omega_t)^{\nu-j} \omega_t^j \left[\rho\left((K_{\tau_L} + M_{\tau_L})^{-1} N_{\tau_L}\right)\right]^j \\ &\leq \sum_{j=0}^{\nu} \binom{\nu}{\nu-j} (1-\omega_t)^{\nu-j} \omega_t^j \left[\rho\left((K_{\tau_L} + M_{\tau_L})^{-1} N_{\tau_L}\right)\right]^j \\ &= \left[1 - \omega_t + \omega_t \rho\left((K_{\tau_L} + M_{\tau_L})^{-1} N_{\tau_L}\right)\right]^\nu. \end{aligned}$$

Since $\rho\left((K_{\tau_L} + M_{\tau_L})^{-1} N_{\tau_L}\right) = |\alpha(\tau_L)| < 1$, see Theorem 4.2.17 we conclude that

$$\left|1 - \omega_t + \omega_t \rho\left((K_{\tau_L} + M_{\tau_L})^{-1} N_{\tau_L}\right)\right| < 1.$$

Hence we obtain

$$S^\nu_n \to 0 \quad \text{as} \quad \nu \to \infty.$$

This implies, that the n-th component e_n^ν of the ν-th Jacobi iteration converges to zero as ν tends to infinity, i.e.

$$e_n^\nu \to \mathbf{0} \qquad \text{for } \nu \to \infty.$$

Hence $x^\nu \to x$ as the number of iterations ν tends to infinity. ■

Remark 4.2.22. *In Theorem 4.2.21 the uniform convergence of the damped block Jacobi smoother with respect to the blocks is proven for $\omega_t \in (0,1]$. Otherwise, to prove convergence of the smoother one can simply compute the spectral radius of the iteration matrix*

$$\mathcal{S}_{\tau_L} = \begin{pmatrix} (1-\omega_t)I_{N_t} & & & \\ \omega_t(K_{\tau_L}+M_{\tau_L})^{-1}N_{\tau_L} & (1-\omega_t)I_{N_t} & & \\ & \ddots & \ddots & \\ & & \omega_t(K_{\tau_L}+M_{\tau_L})^{-1}N_{\tau_L} & (1-\omega_t)I_{N_t} \end{pmatrix},$$

which simply is

$$\rho(\mathcal{S}_{\tau_L}) = |1-\omega_t|.$$

Hence the damped block Jacobi smoother converges also for a damping parameter

$$\omega_t \in (0,2).$$

Choosing a damping parameter $\omega_t \in (1,2)$ leads to a convergent smoother but not to a uniform convergent one. This means that the error can grow for some blocks if we use a damping parameter $\omega_t \in (1,2)$. This implies that for a good smoother we have to use a damping parameter $\omega_t \in (0,1]$.

For a convergent multigrid scheme we need that the applied smoother reduces the error with respect to the high frequencies Θ^{high} fast. In view of Theorem 4.2.21 this motivates the following definition.

Definition 4.2.23 (Smoothing factor)**.** *For the damped block Jacobi iteration introduced in (4.15) we define the smoothing factor as*

$$\mu_S := \max\left\{\rho\left(S_n\right) : \theta_k \in \Theta_L^{\text{high}} \text{ and } n \in \{1,\ldots,N_L\}\right\}$$

with

$$S_n = (1-\omega_t)I_{N_t} + \lambda_n\omega_t(K_{\tau_L}+M_{\tau_L})^{-1}N_{\tau_L} \quad \text{and} \quad \lambda_n = \begin{cases} e^{-\mathrm{i}\theta_k} & n \neq 1, \\ 0 & n = 1. \end{cases}$$

To analyze the smoothing behavior, we have to prove the following lemma for an arbitrary $\alpha \in \mathbb{R}_+$.

Lemma 4.2.24. *Let $\alpha \in \mathbb{R}$ with $\alpha \geq -1$. Then for the function*

$$\left(\hat{S}(\omega_t, \alpha, \theta_k)\right)^2 = (1-\omega_t)^2 + 2\omega_t(1-\omega_t)\alpha\cos(\theta_k) + \alpha^2\omega_t^2$$

the following min-max principle holds true

$$\inf_{\omega_t \in (0,1]} \sup_{\theta_k \in [\frac{\pi}{2}, \pi]} \hat{S}(\omega_t, \alpha, \theta_k) = \begin{cases} \frac{\alpha}{\sqrt{1+\alpha^2}} & \alpha \geq 0, \\ |\alpha| & \alpha < 0 \end{cases} \in [0,1],$$

with the optimal parameter

$$\omega_t^* = \begin{cases} \frac{1}{1+\alpha^2} & \alpha \geq 0, \\ 1 & \alpha < 0 \end{cases} \quad \textit{and} \quad \theta^* = \begin{cases} \frac{\pi}{2} & \alpha \geq 0, \\ \pi & \alpha < 0. \end{cases}$$

Proof. Since $\hat{S}(\omega_t, \alpha, \theta_k) \geq 0$ we will study the function

$$\left(\hat{S}(\omega_t, \alpha, \theta_k)\right)^2 = (1-\omega_t)^2 + 2\omega_t(1-\omega_t)\alpha\cos(\theta_k) + \alpha^2\omega_t^2.$$

For $\omega_t \in (0,1]$ only the terms with α and $\cos(\theta_k)$ can get negative. Hence we first consider the case when α is positive, i.e. $\alpha \geq 0$. In this case we simply have

$$\operatorname*{argsup}_{\theta_k \in [\frac{\pi}{2}, \pi]} \hat{S}(\omega_t, \alpha, \theta_k) = \frac{\pi}{2} \qquad \text{for } \omega_t \in (0,1].$$

This gives for the case $\alpha \geq 0$

$$\inf_{\omega_t \in (0,1]} \sup_{\theta_k \in [\frac{\pi}{2}, \pi]} \hat{S}(\omega_t, \alpha, \theta_k) = \inf_{\omega_t \in (0,1]} \hat{S}(\omega_t, \alpha, \frac{\pi}{2}).$$

Since

$$\left(\hat{S}(\omega_t, \alpha, \frac{\pi}{2})\right)^2 = (1-\omega_t)^2 + \alpha^2\omega_t^2,$$

we find that

$$\operatorname*{arginf}_{\omega_t \in (0,1]} \hat{S}(\omega_t, \alpha, \frac{\pi}{2}) = \frac{1}{1+\alpha^2} \quad \text{and} \quad \hat{S}(\frac{1}{1+\alpha^2}, \alpha, \frac{\pi}{2}) = \frac{\alpha}{\sqrt{1+\alpha^2}}.$$

For the case $\alpha < 0$ we have

$$\operatorname*{argsup}_{\theta_k \in [\frac{\pi}{2}, \pi]} \hat{S}(\omega_t, \alpha, \theta_k) = \pi \qquad \text{for } \omega_t \in (0,1].$$

Because of

$$\left(\hat{S}(\omega_t, \alpha, \pi)\right)^2 = (1-\omega_t)^2 - 2\omega_t(1-\omega_t)|\alpha| + |\alpha|^2\omega_t^2 = (1-\omega_t(1+|\alpha|))^2$$

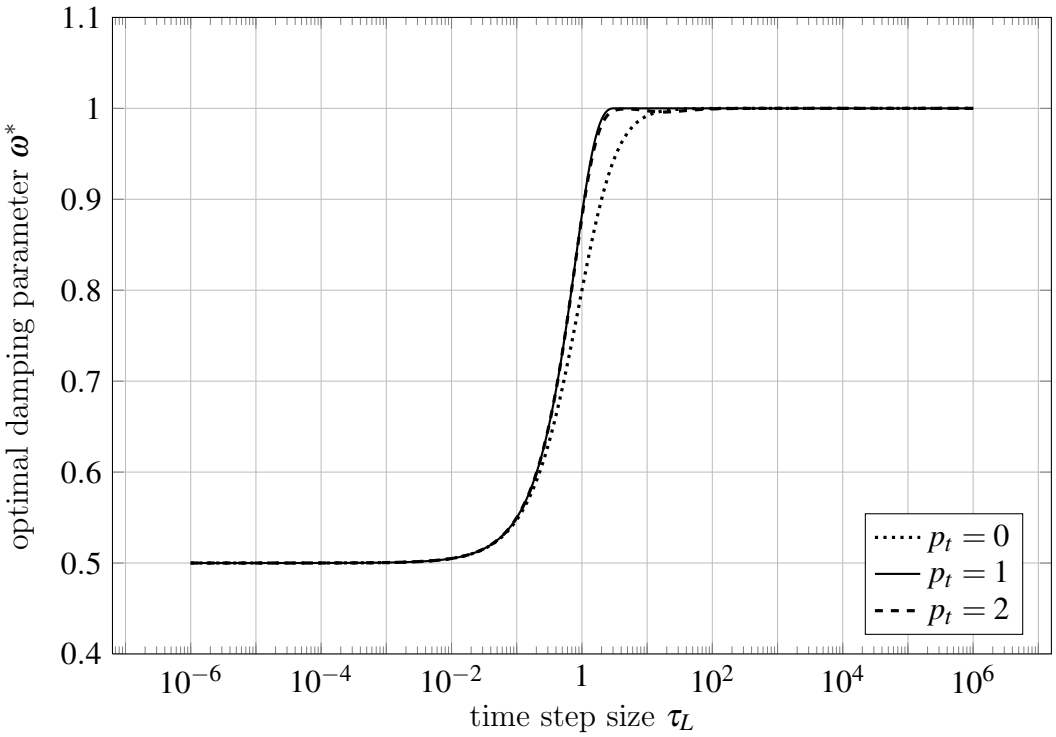

Figure 4.4: Optimal damping parameter $\omega^* = \omega^*(\tau_L)$ for different polynomial degrees p_t and different time step sizes τ_L.

we find that

$$\operatorname*{arginf}_{\omega_t \in (0,1]} \hat{S}(\omega_t, \alpha, \pi) = 1 \quad \text{and} \quad \hat{S}(1, \alpha, \pi) = |\alpha|,$$

which completes the proof. ∎

With the next lemma we will show, that the smoothing factor μ_S is strictly bounded by one, if we use the optimal damping parameter $\omega_t^* = \omega_t^*(\tau_L)$.

Lemma 4.2.25. *For the optimal choice of the damping parameter*

$$\omega_t^*(\tau_L) := \begin{cases} \frac{1}{1+(\alpha(\tau_L))^2} & \alpha(\tau_L) \geq 0, \\ 1 & \alpha(\tau_L) < 0 \end{cases}$$

the smoothing factor μ_S of the damped block Jacobi iteration (4.15) is bounded by

$$\mu_S \leq \frac{1}{\sqrt{2}}.$$

Proof. In view of Lemma 4.2.19 we have to estimate

$$\max_{\theta_k \in \Theta_L^{\text{high}}} \left\{ |1-\omega_t^*|, \hat{S}(\omega_t^*, \alpha(\tau_L), \theta_k) \right\}$$

with

$$\left(\hat{S}(\omega_t^*, \alpha, \theta_k)\right)^2 := (1-\omega_t^*)^2 + 2\omega_t^*(1-\omega_t^*)\alpha\cos(\theta_k) + \alpha^2(\omega_t^*)^2.$$

Since $\hat{S}(\omega_t^*, \alpha, \theta_k)$ is symmetric with respect to the frequencies θ_k, we only have to estimate the function $\hat{S}(\omega_t^*, \alpha, \theta_k)$ for the frequencies $\theta_k \in \Theta_L^{\text{high}} \cap [\frac{\pi}{2}, \pi]$. Applying Lemma 4.2.24 for $\alpha = \alpha(\tau_L)$ gives the estimate

$$\max_{\theta_k \in \Theta_L^{\text{high}}} \hat{S}(\omega_t^*, \alpha(\tau_L), \theta_k) \leq \sup_{\theta_k \in [\frac{\pi}{2}, \pi]} \hat{S}(\omega_t^*, \alpha(\tau_L), \theta_k) = \begin{cases} \frac{\alpha(\tau_L)}{\sqrt{1+(\alpha(\tau_L))^2}} & \alpha(\tau_L) \geq 0, \\ |\alpha(\tau_L)| & \alpha(\tau_L) < 0. \end{cases} \tag{4.21}$$

Since $\alpha(\tau_L)$ is the (p_t, p_t+1) subdiagonal Padé approximation of the exponential function, see Lemma 4.2.19, we have

$$-0.0980762 \approx \frac{5-3\sqrt{3}}{2} \leq \alpha(\tau_L) \leq 1 \qquad \text{for } \tau_L \geq 0.$$

Combining this estimate with the results of (4.21) we end up with

$$\max_{\theta_k \in \Theta_L^{\text{high}}} \hat{S}(\omega_t^*, \alpha, \theta_k) \leq \begin{cases} \frac{1}{\sqrt{2}} & \alpha \geq 0, \\ \frac{3\sqrt{3}-5}{2} & \alpha < 0 \end{cases} \leq \frac{1}{\sqrt{2}}.$$

Simple calculations show that

$$\sup_{\theta_k \in [\frac{\pi}{2}, \pi]} \hat{S}(\omega_t^*, \alpha, \theta_k) \geq |1-\omega_t^*|,$$

which completes the proof. ∎

Remark 4.2.26. *Because $\alpha(\tau_L)$ is the (p_t, p_t+1) subdiagonal Padé approximation of the exponential function e^{-t} we have that $\alpha(\tau_L) \to 1$ as $\tau_L \to 0$ and hence $\omega^* \approx \frac{1}{2}$ for τ_L close to zero, see also Figure 4.4. It turns out, that the estimate of Lemma 4.2.25 is also true for a uniform damping parameter $\omega^* = \frac{1}{2}$. But for large time steps τ_L a better smoothing behaviour is obtained when the optimal damping parameter $\omega^* = \omega^*(\tau_L)$ as given in Lemma 4.2.25 is used.*

To show the convergence behaviour of the damped block Jacobi smoother (4.15) with respect to the time step size τ_L, we will prove the following lemma for an arbitrary $\alpha \in \mathbb{R}$.

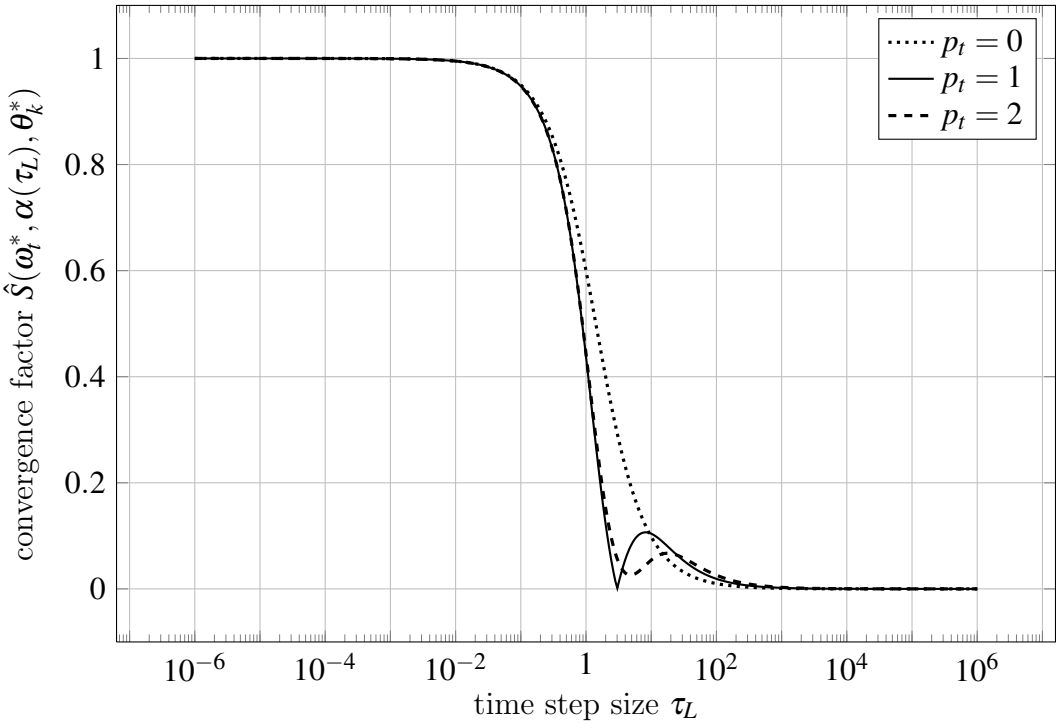

Figure 4.5: Convergence factor $\hat{S}(\omega_t^*, \alpha(\tau_L), \theta_k^*) = \frac{|\alpha(\tau_L)|(1+|\alpha(\tau_L)|)}{1+(\alpha(\tau_L))^2}$ of the damped block Jacobi for the optimal damping parameter ω^* and different polynomial degrees p_t plotted with respect to the time step sizes τ_L.

Lemma 4.2.27. *For $\alpha \in \mathbb{R}$ and the optimal choice for the damping parameter*

$$\omega_t^* = \begin{cases} \frac{1}{1+\alpha^2} & \alpha \geq 0, \\ 1 & \alpha < 0 \end{cases}$$

the following estimate holds true

$$\max_{\theta_k \in \Theta_L} \hat{S}(\omega_t^*, \alpha, \theta_k) \leq \frac{|\alpha|\,(1+|\alpha|)}{1+\alpha^2}.$$

Proof. For the optimal damping parameter ω_t^* we have

$$\left(\hat{S}(\omega_t^*, \alpha, \theta_k)\right)^2 = \frac{\alpha^2}{1+\alpha^2} + \frac{2\alpha^3}{(1+\alpha^2)^2}\cos(\theta_k).$$

For the case $\alpha \geq 0$ we therefore obtain

$$\operatorname*{argsup}_{\theta_k \in [0,\pi]} \hat{S}(\omega_t^*, \alpha, \theta_k) = 0.$$

Thus we have

$$\left(\hat{S}(\omega_t^*,\alpha,0)\right)^2 = \frac{\alpha^2+\alpha^4+2\alpha^3}{(1+\alpha^2)^2} = \frac{\alpha^2(1+\alpha)^2}{(1+\alpha^2)^2}.$$

For the case $\alpha < 0$ we find that

$$\operatorname*{argsup}_{\theta_k\in[0,\pi]} \hat{S}(\omega_t^*,\alpha,\theta_k) = \pi$$

and thus

$$\left(\hat{S}(\omega_t^*,\alpha,0)\right)^2 = \frac{\alpha^2+\alpha^4+2\,|\alpha|^3}{(1+\alpha^2)^2} = \frac{\alpha^2(1+|\alpha|)^2}{(1+\alpha^2)^2}.$$

The statement of this lemma follows with the fact that

$$\max_{\theta_k\in\Theta_L} \hat{S}(\omega_t^*,\alpha,\theta_k) \leq \sup_{\theta_k\in[0,\pi]} \hat{S}(\omega_t^*,\alpha,\theta_k).$$

■

Remark 4.2.28. *For sufficiently small values of $\alpha = \alpha(\tau_L)$, i.e. for sufficiently large time step sizes τ_L it is shown in Lemma 4.2.27, that the convergence factor $\hat{S}(\omega_t^*,\alpha(\tau_L),\theta_k^*)$ of the block Jacobi smoother (4.15) is close to zero, see also Figure 4.5. Hence the block Jacobi smoother (4.15) is already a very good iterative solver.*

Remark 4.2.29. *All the estimates above are valid for arbitrary polynomial degrees $p_t \in \mathbb{N}_0$. For the limit case $p_t \to \infty$ the function $\alpha(\tau_L)$ is given by*

$$\alpha(\tau_L) = e^{-\tau_L},$$

since $\alpha(t)$ is the (p_t, p_t+1) subdiagonal the Padé approximation of the exponential function e^{-t}. Hence, the choice of the best damping parameter ω^* and the smoothing factors converge also to a limit function.

4.2.2 Two-grid analysis

In this subsection we will analyze the two-grid cycle for solving the linear system (4.14). For the $(k+1)$-th two-grid iteration the error is given by

$$e^{k+1} = \mathcal{M}_{\tau_L} e^k := \mathcal{S}_{\tau_L}^{\nu_2}\left[I - \mathcal{P}^L \mathcal{L}_{2\tau_L}^{-1} \mathcal{R}^L \mathcal{L}_{\tau_L}\right] \mathcal{S}_{\tau_L}^{\nu_1} e^k. \tag{4.22}$$

In what follows, we will apply the local Fourier mode analysis to analyze the local convergence behaviour of the two-grid iteration matrix $\mathcal{M}_{\tau_L}$. This type of analysis will be exact, if we consider periodic solutions, see (4.18). To do so, we

will compute the Fourier symbol of the two-grid iteration matrix $\mathcal{M}_{\tau_L}$. In Lemma 4.2.14 we already derived the local Fourier symbol for the system matrix $\mathcal{L}_{\tau_L}$ as

$$\hat{\mathcal{L}}_{\tau_L}(\theta_k) := K_{\tau_L} + M_{\tau_L} - e^{-\mathbb{i}\theta_k} N_{\tau_L} \in \mathbb{C}^{N_t \times N_t}.$$

Whereas the local Fourier symbol for the smoother $\mathcal{S}_{\tau_L}^{\nu}$ is given by

$$\hat{\mathcal{S}}_{\tau_L}^{\nu}(\theta_k, \omega_t) := \left((1-\omega_t) I_{N_t} + e^{-\mathbb{i}\theta_k} \omega_t (K_{\tau_L} + M_{\tau_L})^{-1} N_{\tau_L} \right)^{\nu} \in \mathbb{C}^{N_t \times N_t},$$

see Lemma 4.2.16. For the local parts this motivates to use the so called stencil notation for the upcoming operators. For the system matrix $\mathcal{L}_{\tau_L}$ we therefore have the stencil

$$\widetilde{\mathcal{L}}_{\tau_L} := \begin{bmatrix} -N_{\tau_L} & K_{\tau_L} + M_{\tau_L} & 0 \end{bmatrix},$$

and one smoothing iteration $\mathcal{S}_{\tau_L}^{\nu}$, $\nu = 1$, is given in stencil notation by

$$\widetilde{\mathcal{S}}_{\tau_L}^{1} := \begin{bmatrix} -\omega_t (K_{\tau_L} + M_{\tau_L})^{-1} N_{\tau_L} & (1-\omega_t) I_{N_t} & 0 \end{bmatrix}.$$

For periodic solutions this leads to the following mapping properties

$$\mathcal{L}_{\tau_L} : \Psi_L(\theta_k) \to \Psi_L(\theta_k) \quad \text{and} \quad \mathcal{S}_{\tau_L}^{\nu} : \Psi_L(\theta_k) \to \Psi_L(\theta_k). \tag{4.23}$$

In what follows, we will analyze the mapping properties of the restriction and the prolongation operator. To do so, we first have to prove the following lemma.

Lemma 4.2.30. *The mapping* $\gamma : \Theta_L^{\text{low}} \to \Theta_L^{\text{high}}$ *with*

$$\gamma(\theta_k) := \theta_k - \text{sign}(\theta_k)\pi$$

is a one to one mapping.

Proof. Let $\theta_k \in \Theta_L^{\text{low}}$. By definition we have

$$\theta_k = \frac{2k\pi}{N_L} \qquad \text{with} \quad k \in \left\{ 1 - \frac{N_L}{4}, \ldots, \frac{N_L}{4} \right\}.$$

For the mapping γ we then obtain

$$\gamma(\theta_k) = \theta_k - \text{sign}(\theta_k)\pi = \frac{2k\pi}{N_L} - \text{sign}(\theta_k)\pi = \frac{2(k - \text{sign}(\theta_k)\frac{N_L}{2})\pi}{N_L} = \frac{2\hat{k}\pi}{N_L},$$

with

$$\hat{k} = k - \text{sign}(\theta_k)\frac{N_L}{2} \in \left\{ 1 - \frac{N_L}{2}, \ldots, -\frac{N_L}{4} \right\} \cup \left\{ \frac{N_L}{4} + 1, \ldots, \frac{N_L}{2} \right\}.$$

This implies that $\gamma(\theta_k) \in \Theta_L^{\text{high}}$ and that $\text{sign}(\gamma(\theta_k)) = -\text{sign}(\theta_k)$. Hence we have

$$\gamma(\gamma(\theta_k)) = \gamma(\theta_k) - \text{sign}(\gamma(\theta_k))\pi = \gamma(\theta_k) + \text{sign}(\theta_k)\pi = \theta_k.$$

which completes the proof. ∎

Lemma 4.2.31. *The vector* $\boldsymbol{u} = (\boldsymbol{u}_1, \boldsymbol{u}_2, \ldots, \boldsymbol{u}_{N_L})^\top \in \mathbb{R}^{N_L N_t}$ *for* $N_{L-1}, N_t \in \mathbb{N}$ *and* $N_L = 2N_{L-1}$ *can be written as*

$$\boldsymbol{u} = \sum_{\theta_k \in \theta_L^{\text{low}}} \left[\boldsymbol{\psi}^L(\theta_k) + \boldsymbol{\psi}^L(\gamma(\theta_k)) \right]$$

where the vector $\boldsymbol{\psi}^L(\theta_k) \in \mathbb{C}^{N_t N_L}$ *is defined as in Lemma 4.2.10.*

Proof. Applying Lemma 4.2.10 and Lemma 4.2.30 proves the statement of this lemma with

$$\begin{aligned} \boldsymbol{u} &= \sum_{\theta_k \in \Theta_L} \boldsymbol{\psi}^L(\theta_k) = \sum_{\theta_k \in \Theta_L^{\text{low}}} \boldsymbol{\psi}^L(\theta_k) + \sum_{\theta_k \in \Theta_L^{\text{high}}} \boldsymbol{\psi}^L(\theta_k) \\ &= \sum_{\theta_k \in \Theta_L^{\text{low}}} \boldsymbol{\psi}^L(\theta_k) + \sum_{\theta_k \in \Theta_L^{\text{low}}} \boldsymbol{\psi}^L(\gamma(\theta_k)) = \sum_{\theta_k \in \Theta_L^{\text{low}}} \left[\boldsymbol{\psi}^L(\theta_k) + \boldsymbol{\psi}^L(\gamma(\theta_k)) \right]. \end{aligned}$$

■

Lemma 4.2.31 motivates the following definition.

Definition 4.2.32 (Space of harmonics)**.** *For* $N_L, N_t \in \mathbb{N}$ *and for a low frequency* $\theta_k \in \Theta_L^{\text{low}}$ *let the vector* $\boldsymbol{\Phi}^L(\theta_k) \in \mathbb{C}^{N_t N_L}$ *be defined as in Lemma 4.2.10. Then the linear space of harmonics with frequency* θ_k *is given by*

$$\begin{aligned} \mathcal{E}_L(\theta_k) &:= \operatorname{span}\left\{ \boldsymbol{\Phi}^L(\theta_k), \boldsymbol{\Phi}^L(\gamma(\theta_k)) \right\} \\ &= \Big\{ \boldsymbol{\psi}^L(\theta_k) \in \mathbb{C}^{N_t N_L} : \boldsymbol{\psi}_n^L(\theta_k) = U_1 \boldsymbol{\Phi}_n^L(\theta_k) + U_2 \boldsymbol{\Phi}_n^L(\gamma(\theta_k)), \\ &\qquad\qquad n = 1, \ldots, N_L \text{ and } U_1, U_2 \in \mathbb{C}^{N_t \times N_t} \Big\}. \end{aligned}$$

Under the assumption of periodic solutions the mappings (4.23) imply the following mapping properties

$$\mathcal{L}_{\tau_L} : \mathcal{E}_L(\theta_k) \to \mathcal{E}_L(\theta_k) \quad \text{and} \quad \mathcal{S}_{\tau_L}^\nu : \mathcal{E}_L(\theta_k) \to \mathcal{E}_L(\theta_k), \tag{4.24}$$

with the mapping for the system matrix $\mathcal{L}_{\tau_L}$

$$\begin{pmatrix} U_1 \\ U_2 \end{pmatrix} \mapsto \begin{pmatrix} \hat{\mathcal{L}}_{\tau_L}(\theta_k) & 0 \\ 0 & \hat{\mathcal{L}}_{\tau_L}(\gamma(\theta_k)) \end{pmatrix} \begin{pmatrix} U_1 \\ U_2 \end{pmatrix} \tag{4.25}$$

and with the mapping for the smoother $\mathcal{S}_{\tau_L}^\nu$

$$\begin{pmatrix} U_1 \\ U_2 \end{pmatrix} \mapsto \begin{pmatrix} \hat{\mathcal{S}}_{\tau_L}^\nu(\theta_k, \omega_t) & 0 \\ 0 & \hat{\mathcal{S}}_{\tau_L}^\nu(\gamma(\theta_k), \omega_t) \end{pmatrix} \begin{pmatrix} U_1 \\ U_2 \end{pmatrix}. \tag{4.26}$$

In what follows, we will analyze the two-grid cycle on the space of harmonics $\mathcal{E}_L(\theta_k)$ for frequencies $\theta_k \in \Theta_L^{\text{low}}$. To do so, we further have to investigate the

mapping properties of the restriction and prolongation operators $\mathcal{R}^L$ and $\mathcal{P}^L$. The restriction operator is given by

$$\mathcal{R}^L := \begin{pmatrix} R_1 & R_2 & & & & \\ & & R_1 & R_2 & & \\ & & & \ddots & \ddots & \\ & & & & R_1 & R_2 \end{pmatrix} \in \mathbb{R}^{N_t N_L \times N_t N_{L-1}}, \tag{4.27}$$

whereas the prolongation operator is given by

$$\mathcal{P}^L := \begin{pmatrix} R_1^\top & & & \\ R_2^\top & & & \\ & R_1^\top & & \\ & R_2^\top & \ddots & \\ & & \ddots & R_1^\top \\ & & & R_2^\top \end{pmatrix} = (\mathcal{R}^L)^\top \in \mathbb{R}^{N_t N_{L-1} \times N_t N_L}, \tag{4.28}$$

with the local prolongation matrices

$$R_1^\top := M_{\tau_L}^{-1} \widetilde{M}_{\tau_L}^1 \quad \text{and} \quad R_2^\top := M_{\tau_L}^{-1} \widetilde{M}_{\tau_L}^2,$$

where for basis functions $\{\psi_k\}_{k=1}^{N_t} \subset \mathbb{P}^{p_t}(0,\tau_L)$ and $\{\widetilde{\psi}_k\}_{k=1}^{N_t} \subset \mathbb{P}^{p_t}(0,2\tau_L)$ the local projection matrices from coarse to fine grids are defined as

$$\widetilde{M}_{\tau_L}^1[k,\ell] := \int_0^{\tau_L} \widetilde{\psi}_\ell(t)\psi_k(t)\mathrm{d}t \quad \text{and} \quad \widetilde{M}_{\tau_L}^2[k,\ell] := \int_{\tau_L}^{2\tau_L} \widetilde{\psi}_\ell(t)\psi_k(t+\tau)\mathrm{d}t$$

for $k,\ell = 1,\dots,N_t$. To prove the mapping properties of the restriction operator $\mathcal{R}^L$ we need the following lemma.

Lemma 4.2.33. *Let $\boldsymbol{\psi}^L(\theta_k) \in \Psi_L(\theta_k)$ for $\theta_k \in \Theta_L$. Then there holds*

$$\psi_{2n}^L(\theta_k) = \psi_n^L(2\theta_k),$$

for $n = 1,\dots,N_{L-1}$.

Proof. Let $\boldsymbol{\psi}^L(\theta_k) \in \Psi_L(\theta_k)$. Hence we have $\boldsymbol{\psi}_n^L(\theta_k) = U\boldsymbol{\Phi}_n^L(\theta_k)$ for $n = 1,\dots,N_L$. Then for $\boldsymbol{\Phi}_{2n}^L(\theta_k)$ with $n \in \{1,\dots,N_{L-1}\}$ we obtain for $\ell = 1,\dots,N_t$ that

$$\boldsymbol{\Phi}_{2n}^L(\theta_k)[\ell] = \varphi_{2n}(\theta_k) = e^{\mathbb{i}2n\theta_k} = \varphi_n(2\theta_k) = \boldsymbol{\Phi}_n^L(2\theta_k)[\ell].$$

Hence we conclude the statement of this lemma with

$$\boldsymbol{\psi}_{2n}^L(\theta_k) = U\boldsymbol{\Phi}_{2n}^L(\theta_k) = U\boldsymbol{\Phi}_n^L(2\theta_k) = \boldsymbol{\psi}_n^L(2\theta_k).$$

■

The next lemma shows the mapping property of the restriction operator.

Lemma 4.2.34. *Let $\theta_k \in \Theta_L^{\text{low}}$. Then the following mapping property for the restriction operator $\mathcal{R}^L$ holds true*

$$\mathcal{R}^L : \mathcal{E}_L(\theta_k) \to \Psi_{L-1}(2\theta_k),$$

with the mapping

$$\begin{pmatrix} U_1 \\ U_2 \end{pmatrix} \mapsto \begin{pmatrix} \hat{\mathcal{R}}(\theta_k) & \hat{\mathcal{R}}(\gamma(\theta_k)) \end{pmatrix} \begin{pmatrix} U_1 \\ U_2 \end{pmatrix} \in \mathbb{C}^{N_t \times N_t}$$

and the Fourier symbol

$$\hat{\mathcal{R}}(\theta_k) := e^{-\mathbb{i}\theta_k} R_1 + R_2.$$

Proof. Let $\psi^L(\theta_k) \in \mathcal{E}_L(\theta_k)$ for some frequency $\theta_k \in \Theta_L^{\text{low}}$ with the linear combination $\psi_n^L(\theta_k) = U_1 \Phi_n^L(\theta_k) + U_2 \Phi_n^L(\gamma(\theta_k))$. Then for the Fourier mode $\Phi^L(\theta_\ell)$ with frequency $\theta_\ell \in \Theta_L$ there holds for a fixed $n \in \{1, \dots, N_{L-1}\}$ that

$$\left(\mathcal{R}^L \Phi^L(\theta_\ell)\right)_n = R_1 \Phi_{2n-1}^L(\theta_\ell) + R_2 \Phi_{2n}^L(\theta_\ell).$$

Since $\Phi^L(\theta_\ell) \in \Psi_L(\theta_\ell)$ we further obtain by using Lemma 4.2.13

$$= \left[e^{-\mathbb{i}\theta_\ell} R_1 + R_2 \right] \Phi_{2n}^L(\theta_\ell).$$

Applying Lemma 4.2.33 gives

$$= \left[e^{-\mathbb{i}\theta_\ell} R_1 + R_2 \right] \Phi_n^{L-1}(2\theta_\ell).$$

Using this result for the vector $\psi^L(\theta_k)$ leads to

$$\left(\mathcal{R}^L \psi^L(\theta_k)\right)_n = \hat{\mathcal{R}}(\theta_k) U_1 \Phi_n^{L-1}(2\theta_k) + \hat{\mathcal{R}}(\gamma(\theta_k)) U_2 \Phi_n^{L-1}(2\gamma(\theta_k)).$$

For $i = 1, \dots, N_t$ we further have that

$$\begin{aligned} \Phi_n^{L-1}(2\gamma(\theta_k))[i] = \varphi_n(2\gamma(\theta_k)) &= e^{\mathbb{i} n 2\gamma(\theta_k)} = e^{\mathbb{i} n 2\theta_k - \mathbb{i}\,\mathrm{sign}(\theta_k) 2\pi} \\ &= e^{\mathbb{i} n 2\theta_k} = \varphi_n(2\theta_k) = \Phi_n^{L-1}(2\theta_k)[i]. \end{aligned}$$

Hence we obtain

$$\left(\mathcal{R}^L \psi^L(\theta_k)\right)_n = \left[\hat{\mathcal{R}}(\theta_k) U_1 + \hat{\mathcal{R}}(\gamma(\theta_k)) U_2 \right] \Phi_n^{L-1}(2\theta_k),$$

which completes the proof. ∎

For the prolongation operator the mapping property will be proven in the following lemma.

Lemma 4.2.35. *Let $\theta_k \in \Theta_L^{\text{low}}$. Then the following mapping property for the prolongation operator $\mathcal{P}^L$ holds true*

$$\mathcal{P}^L : \Psi_{L-1}(2\theta_k) \to \mathcal{E}_L(\theta_k),$$

with the mapping

$$U \mapsto \begin{pmatrix} \hat{\mathcal{P}}(\theta_k) \\ \hat{\mathcal{P}}(\gamma(\theta_k)) \end{pmatrix} U \in \mathbb{C}^{2N_t \times N_t}$$

and the Fourier symbol

$$\hat{\mathcal{P}}(\theta_k) := \frac{1}{2}\left[e^{\mathbb{i}\theta_k} R_1^\top + R_2^\top\right].$$

Proof. For $\theta_k \in \Theta_L^{\text{low}}$ let $\boldsymbol{\psi}^{L-1}(2\theta_k) \in \Psi_{L-1}(2\theta_k)$ with $\boldsymbol{\psi}^{L-1}_{\hat{n}}(2\theta_k) = U\boldsymbol{\Phi}^{L-1}_{\hat{n}}(2\theta_k)$ for $\hat{n} \in \{1,\dots,N_{L-1}\}$. We then define $\boldsymbol{\psi}^L(\theta_k) \in \Psi_L(\theta_k)$ as $\boldsymbol{\psi}^L_n(\theta_k) = U\boldsymbol{\Phi}^L_n(\theta_k)$ for $n \in \{1,\dots,N_L\}$. Then we have

$$\left(\mathcal{P}^L \boldsymbol{\psi}^{L-1}(2\theta_k)\right)_{2\hat{n}-1} = R_1^\top \boldsymbol{\psi}^{L-1}_{\hat{n}}(2\theta_k).$$

With Lemma 4.2.33 we further obtain

$$= R_1^\top \boldsymbol{\psi}^L_{2\hat{n}}(\theta_k).$$

Applying Lemma 4.2.13 results in

$$= e^{\mathbb{i}\theta_k} R_1^\top \boldsymbol{\psi}^L_{2\hat{n}-1}(\theta_k).$$

Similar computations as above give

$$\left(\mathcal{P}^L \boldsymbol{\psi}^{L-1}(2\theta_k)\right)_{2\hat{n}} = R_2^\top \boldsymbol{\psi}^{L-1}_{\hat{n}}(2\theta_k) = R_2^\top \boldsymbol{\psi}^L_{2\hat{n}}(\theta_k).$$

Hence we have for $n \in \{1,\dots,N_L\}$

$$\left(\mathcal{P}^L \boldsymbol{\psi}^{L-1}(2\theta_k)\right)_n = \begin{cases} e^{\mathbb{i}\theta_k} R_1^\top \boldsymbol{\psi}^L_n(\theta_k) & n \text{ odd}, \\ R_2^\top \boldsymbol{\psi}^L_n(\theta_k) & n \text{ even} \end{cases} \in \mathbb{C}^{N_t}.$$

If the image of the prolongation operator $\mathcal{P}^L$ should be contained in $\mathcal{E}_L(\theta_k)$ we therefore have to fulfil the following equations

$$\begin{aligned} U_1\boldsymbol{\Phi}^L_n(\theta_k) + U_2\boldsymbol{\Phi}^L_n(\gamma(\theta_k)) &= e^{\mathbb{i}\theta_k} R_1^\top U\boldsymbol{\Phi}^L_n(\theta_k) && \text{for } n \text{ odd}, \\ U_1\boldsymbol{\Phi}^L_n(\theta_k) + U_2\boldsymbol{\Phi}^L_n(\gamma(\theta_k)) &= R_2^\top U\boldsymbol{\Phi}^L_n(\theta_k) && \text{for } n \text{ even} \end{aligned} \tag{4.29}$$

for $n = 1,\dots,N_L$. Further computations show for $\ell = 1,\dots,N_t$ that

$$\boldsymbol{\Phi}^L_n(\gamma(\theta_k))[\ell] = \varphi_n(\gamma(\theta_k)) = e^{\mathbb{i}n\gamma(\theta_k)} = e^{\mathbb{i}n\theta_k - \mathbb{i}\,\mathrm{sign}(\theta_k)n\pi} = \varphi_n(\theta_k) e^{\mathbb{i}\,\mathrm{sign}(\theta_k)n\pi}$$

$$= \boldsymbol{\Phi}_n^L(\theta_k)[\ell] \begin{cases} 1 & n \text{ even}, \\ -1 & n \text{ odd}. \end{cases}$$

Hence the equations (4.29) are equivalent to the system of linear equations

$$\begin{aligned} U_1 - U_2 &= e^{\mathbb{i}\theta_k} R_1^\top U, \\ U_1 + U_2 &= R_2^\top U. \end{aligned}$$

Solving for U_1 and U_2 results in

$$\begin{aligned} U_1 &= \frac{1}{2}\left[e^{\mathbb{i}\theta_k} R_1^\top + R_2^\top\right] = \hat{\mathcal{P}}(\theta_k) U, \\ U_2 &= \frac{1}{2}\left[-e^{\mathbb{i}\theta_k} R_1^\top + R_2^\top\right] = \frac{1}{2}\left[e^{\mathbb{i}(\theta_k - \operatorname{sign}(\theta_k)\pi)} R_1^\top + R_2^\top\right] \\ &= \frac{1}{2}\left[e^{\mathbb{i}\gamma(\theta_k)} R_1^\top + R_2^\top\right] = \hat{\mathcal{P}}(\gamma(\theta_k)) U, \end{aligned}$$

which completes the proof. ∎

Remark 4.2.36. *In view of Lemma 4.2.34 and Lemma 4.2.35 the stencil notations for the restriction and prolongation operator $\mathcal{R}^L$ and $\mathcal{P}^L$ are given by*

$$\widetilde{\mathcal{R}}^L := \begin{bmatrix} R_1 & R_2 & 0 \end{bmatrix} \quad \textit{and} \quad \widetilde{\mathcal{P}}^L := \frac{1}{2}\begin{bmatrix} 0 & R_2^\top & R_1^\top \end{bmatrix}.$$

For the two-grid operator $\mathcal{M}_{\tau_L}$ it now remains to prove the mapping property of the coarse grid operator $\mathcal{L}_{2\tau_L}^{-1}$. Under the assumption of periodic solutions we have for $\theta_k \in \Theta_{L-1}$ by using (4.23) that

$$\mathcal{L}_{2\tau_L}^{-1} : \Psi_{L-1}(\theta_k) \to \Psi_{L-1}(\theta_k),$$

with the Fourier symbol

$$\hat{\mathcal{L}}_{2\tau_L}^{-1}(\theta_k) = \left(K_{\tau_L} + M_{\tau_L} - e^{-\mathbb{i}\theta_k} N_{\tau_L}\right)^{-1} = (\hat{\mathcal{L}}_{2\tau_L}(\theta_k))^{-1} \in \mathbb{C}^{N_t \times N_t}.$$

Lemma 4.2.37. *The frequency mapping*

$$\beta : \Theta_L^{\text{low}} \to \Theta_{L-1} \qquad \textit{with} \qquad \theta_k \mapsto 2\theta_k$$

is a one to one mapping.

Proof. For $\theta_k \in \Theta_L^{\text{low}}$ we obtain

$$\beta(\theta_k) = 2\theta_k = 2\frac{2k\pi}{N_L} = \frac{2k\pi}{\frac{N_L}{2}} = \frac{2k\pi}{N_{L-1}} \in \Theta_{L-1}.$$

The proof of this lemma follows by using the identity

$$k \in \left\{1 - \frac{N_L}{4}, \ldots, \frac{N_L}{4}\right\} = \left\{1 - \frac{N_{L-1}}{2}, \ldots, \frac{N_{L-1}}{2}\right\}.$$

■

With Lemma 4.2.37 we now conclude for $\theta_k \in \Theta_L^{\text{low}}$ the following mapping property of the coarse grid operator

$$\mathcal{L}_{2\tau_L}^{-1} : \Psi_{L-1}(2\theta_k) \to \Psi_{L-1}(2\theta_k). \tag{4.30}$$

We are now able to prove the following theorem for the two-grid operator $\mathcal{M}_{\tau_L}$.

Theorem 4.2.38. *Let $\theta_k \in \Theta_L^{\text{low}}$. Under the assumption of periodic solutions the following mapping property for the two-grid operator $\mathcal{M}_{\tau_L}$ holds true*

$$\mathcal{M}_{\tau_L} : \mathcal{E}_L(\theta_k) \to \mathcal{E}_L(\theta_k),$$

with the mapping

$$\begin{pmatrix} U_1 \\ U_2 \end{pmatrix} \mapsto \hat{\mathcal{M}}(\theta_k) \begin{pmatrix} U_1 \\ U_2 \end{pmatrix}$$

and the iteration matrix

$$\hat{\mathcal{M}}(\theta_k) := \begin{pmatrix} \hat{\mathcal{S}}_{\tau_L}^{\nu_2}(\theta_k, \omega_t) & 0 \\ 0 & \hat{\mathcal{S}}_{\tau_L}^{\nu_2}(\gamma(\theta_k), \omega_t) \end{pmatrix} \mathcal{K}(\theta_k) \begin{pmatrix} \hat{\mathcal{S}}_{\tau_L}^{\nu_1}(\theta_k, \omega_t) & 0 \\ 0 & \hat{\mathcal{S}}_{\tau_L}^{\nu_1}(\gamma(\theta_k), \omega_t) \end{pmatrix}$$

with

$$\mathcal{K}(\theta_k) := I_{2N_t} - \begin{pmatrix} \hat{\mathcal{P}}(\theta_k) \\ \hat{\mathcal{P}}(\gamma(\theta_k)) \end{pmatrix} (\hat{\mathcal{L}}_{2\tau_L}(2\theta_k))^{-1} \begin{pmatrix} \hat{\mathcal{R}}(\theta_k)^\top \\ \hat{\mathcal{R}}(\gamma(\theta_k))^\top \end{pmatrix}^\top \begin{pmatrix} \hat{\mathcal{L}}_{\tau_L}(\theta_k) & 0 \\ 0 & \hat{\mathcal{L}}_{\tau_L}(\gamma(\theta_k)) \end{pmatrix}.$$

Proof. The statement of this theorem is a direct consequence of Lemma 4.2.34, Lemma 4.2.35 and the mapping properties (4.23) and (4.30). ■

We now write the initial error $\boldsymbol{e}^0 = \boldsymbol{x} - \boldsymbol{x}^0$ as

$$\boldsymbol{e}^0 = \sum_{\theta_k \in \Theta_L^{\text{low}}} \left[\boldsymbol{\psi}^L(\theta_k) + \boldsymbol{\psi}^L(\gamma(\theta_k))\right],$$

with $\boldsymbol{\psi}^L(\theta_k) + \boldsymbol{\psi}^L(\gamma(\theta_k)) \in \mathcal{E}_L(\theta_k)$ for all $\theta_k \in \Theta_L^{\text{low}}$, see Lemma 4.2.31. In view of Theorem 4.2.38 we can analyze the convergence of the two-grid cycle by simply computing the largest spectral radius of $\hat{\mathcal{M}}(\theta_k) \in \mathbb{C}^{2N_t \times 2N_t}$ with respect to the low frequencies $\theta_k \in \Theta_L^{\text{low}}$. This motivates the following definition.

Definition 4.2.39 (Two-grid convergence factor)**.** *For the two-grid iteration matrix $\mathcal{M}_{\tau_L}$ we define the asymptotic convergence factor as*

$$\rho(\mathcal{M}_{\tau_L}) := \max\left\{\rho\left(\hat{\mathcal{M}}(\theta_k)\right) : \theta_k \in \Theta_L^{\text{low}}\right\}.$$

For the simplest case, i.e. for the polynomial degree $p_t = 0$, we have to compute the spectral radius of the 2×2 iteration matrix $\hat{\mathcal{M}}(\theta_k)$. Using one pre and post smoothing step, i.e. $\nu_1 = \nu_2 = 1$, we find that the spectral radius of $\hat{\mathcal{M}}(\theta_k) \in \mathbb{C}^{2\times 2}$ is given by

$$\rho\left(\hat{\mathcal{M}}(\theta_k)\right) = \left|\frac{4(1+\tau_L)^2(\sin(\theta_k))^2 + \tau_L^2(1+2\tau_L - e^{2\mathbb{i}\theta_k})}{(2+\tau_L(2+\tau_L))^2\left((1+2\tau_L)e^{2\mathbb{i}\theta_k} - 1\right)}\right|.$$

Further calculations show that the maximum of $\rho\left(\hat{\mathcal{M}}(\theta_k)\right)$ with respect to the low frequencies $\theta_k \in \Theta_L^{\text{low}}$ is obtained for $\theta_k^* = \frac{\pi}{2}$. Hence for this simple case we can compute the asymptotic convergence factor as

$$\rho(\mathcal{M}_{\tau_L}) = \frac{1}{2+2\tau_l+\tau_L^2} \in [0, \frac{1}{2}] \qquad \text{for all } \tau_L \geq 0.$$

For periodic solutions we therefore conclude, that the two-grid cycle converges for any $\tau_L \geq 0$ to the exact solution, since $\rho(\mathcal{M}_{\tau_L}) \leq \frac{1}{2}$ for all $\tau_L \geq 0$. Furthermore we obtain, that the asymptotic convergence factor $\rho(\mathcal{M}_{\tau_L})$ gets very small for large time step sizes, i.e. $\rho(\mathcal{M}_{\tau_L}) = \mathcal{O}(\tau_L^{-2})$. This results from the fact, that the smoother itself is already an efficient iterative solver for large time step sizes.

For higher polynomial degrees p_t we have to compute the eigenvalues of the $2(p_t+1)\times 2(p_t+1)$ iteration matrix $\hat{\mathcal{M}}(\theta_k)$, which is in general not a trivial task. To overcome this problem we compute for all frequencies $\theta_k \in \Theta_L^{\text{low}}$ the eigenvalues of $\hat{\mathcal{M}}(\theta_k)$ numerically to find the asymptotic convergence factor $\rho\left(\hat{\mathcal{M}}(\theta_k)\right)$ for a given time step sizes τ_L.

With respect to the time step sizes $\tau_L \in [10^{-6}, 10^6]$ and for different polynomial degrees $p_t \in \{0,1,\ldots,5\}$ the theoretical average convergence factors $\rho\left(\hat{\mathcal{M}}(\theta_k)\right)$ are plotted as solid lines in the Figures 4.6–4.11. In each plot the convergence factors are compared for a different number of smoothing iterations $\nu_1 = \nu_2 = \nu$ with $\nu \in \{1,2,5\}$. It can be seen, that for higher polynomial degrees $p_t \geq 1$ the theoretical convergence rates are almost smaller by a factor of two compared to the theoretical convergence rates of the lowest order case $p_t = 0$. In addition we see, that the theoretical convergence factors are close to zero for large time step sizes τ_L. This results from the fact, that the smoother itself is already a good iterative solver for the given problem, see also Remark 4.2.28. Furthermore for odd polynomial degrees p_t we observe a peak in the plots for the theoretical convergence rates. This behaviour can be explained due to the fact, that for odd

polynomial degrees the (p_t, p_t+1) subdiagonal Padé approximation of e^{-t} has exactly one zero for $t>0$. Hence for one $\tau_L^*>0$ we have $\alpha(\tau_L^*)=0$ which implies for the smoothing factor $\mu_S=0$, see Lemma 4.2.27. Hence the application of only one smoothing iteration results in an exact solver.

Furthermore we compare the theoretical results of the local Fourier mode analysis with the numerical results for solving the equation

$$\mathcal{L}_{\tau_L}\boldsymbol{x}=\boldsymbol{f}$$

with the two-grid cycle. In particular we use $N_L=1024$ time steps with a zero right hand side, i.e. $\boldsymbol{f}=\boldsymbol{0}$. As an initial vector $\boldsymbol{x}^0$ we use a random vector with values between zero and one. The convergence of the two-grid cycle is measured with

$$\max_{k=1,\dots,N_{\text{iter}}} \frac{\left\|\boldsymbol{r}^{k+1}\right\|_2}{\left\|\boldsymbol{r}^{k}\right\|_2}, \quad \text{with } \boldsymbol{r}^k := \boldsymbol{f}-\mathcal{L}_{\tau_L}\boldsymbol{x}^k,$$

where $N_{\text{iter}}\in\mathbb{N}$, $N_{\text{iter}}\leq 250$ is the number of used two-grid iterations until we have reached a given relative error reduction of ε_{MG}. To measure the asymptotic behaviour of the two-grid cycle we have to use $\varepsilon_{\text{MG}}=10^{-140}$, since in the pre-asymptotic range the convergence rates of two-grid cycle are in the most cases smaller than in the asymptotic range. The measured convergence rates of the two-grid cycle are plotted as dots, triangles and squares in Figures 4.6–4.11. Here we observe that the theoretical results from the local Fourier mode analysis completely agree with the numerical results, even if the applied Fourier mode analysis is only a rigorous analysis when periodic solutions are assumed.

4.3 Space-time analysis

In this section we analyze the two-grid cycle for solving the discretized space-time problem (2.2) introduced at the beginning of this chapter. In particular we analyze the case when tensor product space-time elements are used. For simplicity we assume that Ω is a one-dimensional domain. The analysis for higher dimensions is more technical, but the techniques stay the same as for the one dimensional case. Hence we have to solve the linear system

$$\begin{pmatrix} A_{\tau,h} & & & & \\ B_{\tau,h} & A_{\tau,h} & & & \\ & B_{\tau,h} & A_{\tau,h} & & \\ & & \ddots & \ddots & \\ & & & B_{\tau,h} & A_{\tau,h} \end{pmatrix} \begin{pmatrix} \boldsymbol{u}_1 \\ \boldsymbol{u}_2 \\ \boldsymbol{u}_3 \\ \vdots \\ \boldsymbol{u}_N \end{pmatrix} = \begin{pmatrix} \boldsymbol{f}_1 \\ \boldsymbol{f}_2 \\ \boldsymbol{f}_3 \\ \vdots \\ \boldsymbol{f}_N \end{pmatrix}, \tag{4.31}$$

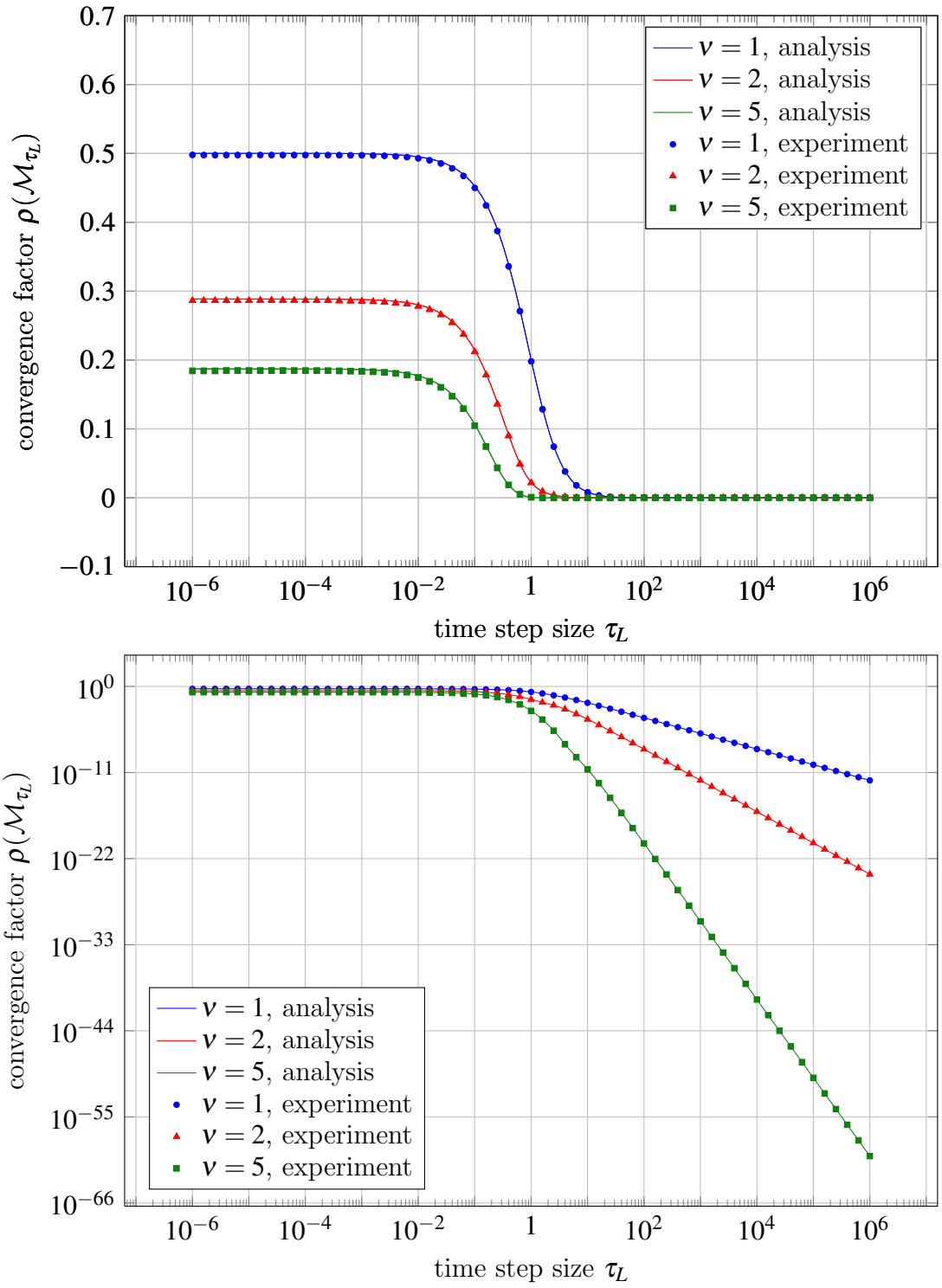

Figure 4.6: Average convergence factor $\rho(\mathcal{M}_{\tau_L})$ for different time step sizes τ_L, $p_t = 0$ and numerical convergence rates for $N_t = 1024$ time steps. Log-linear plot (top) and Log-log plot (bottom).

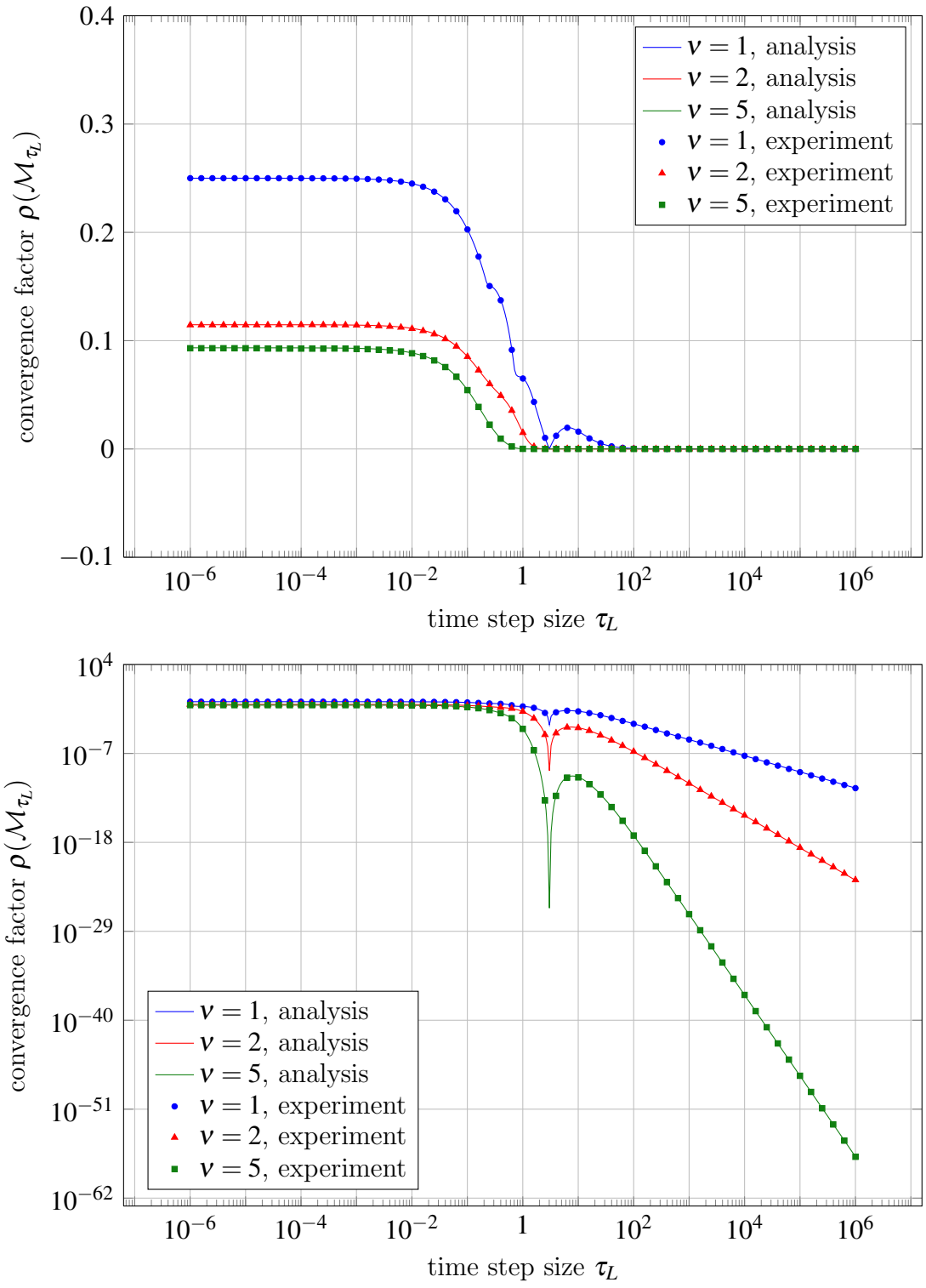

Figure 4.7: Average convergence factor $\rho(\mathcal{M}_{\tau_L})$ for different time step sizes τ_L, $p_t = 1$ and numerical convergence rates for $N_t = 1024$ time steps. Log-linear plot (top) and Log-log plot (bottom).

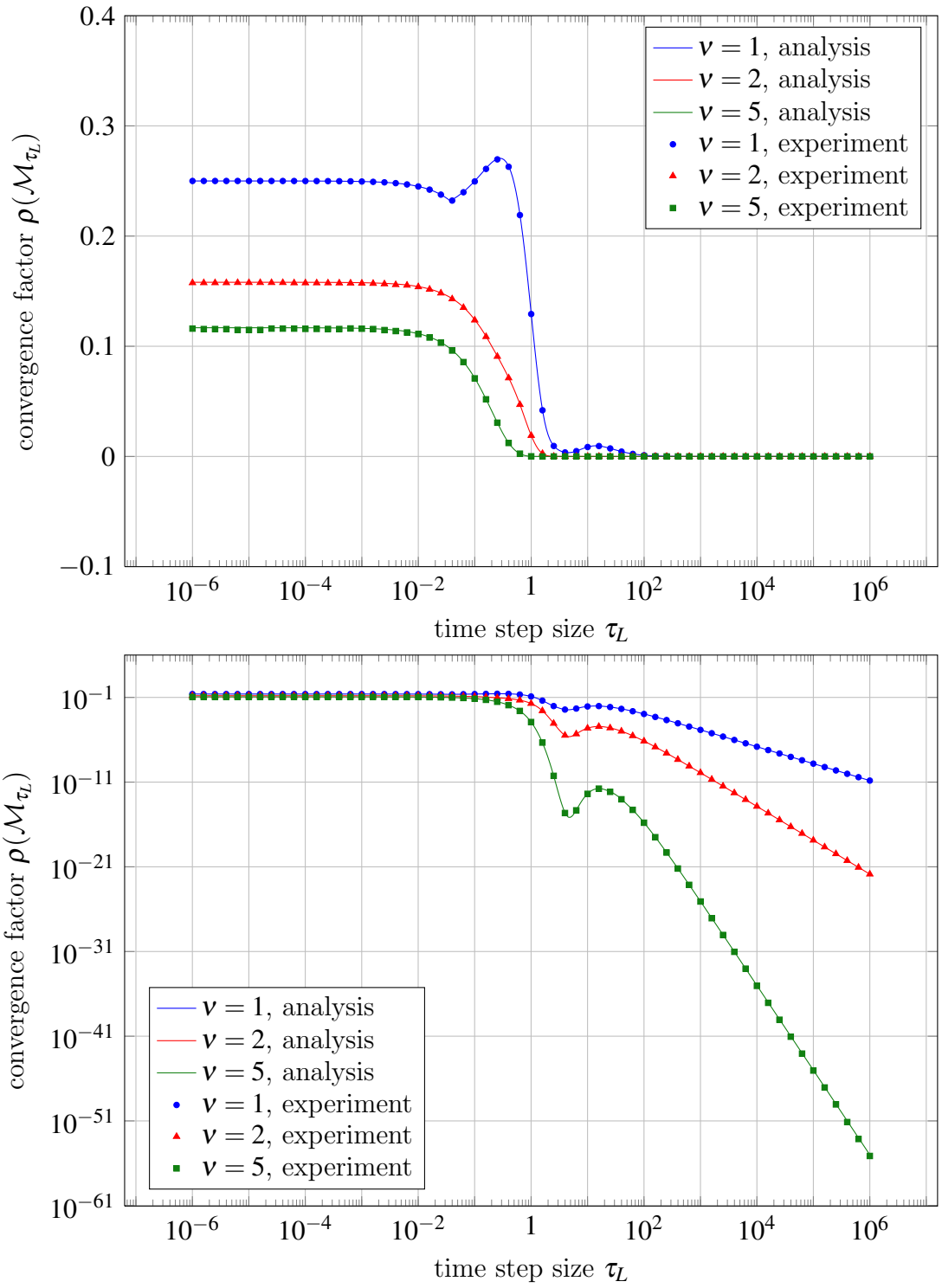

Figure 4.8: Average convergence factor $\rho(\mathcal{M}_{\tau_L})$ for different time step sizes τ_L, $p_t = 2$ and numerical convergence rates for $N_t = 1024$ time steps. Log-linear plot (top) and Log-log plot (bottom).

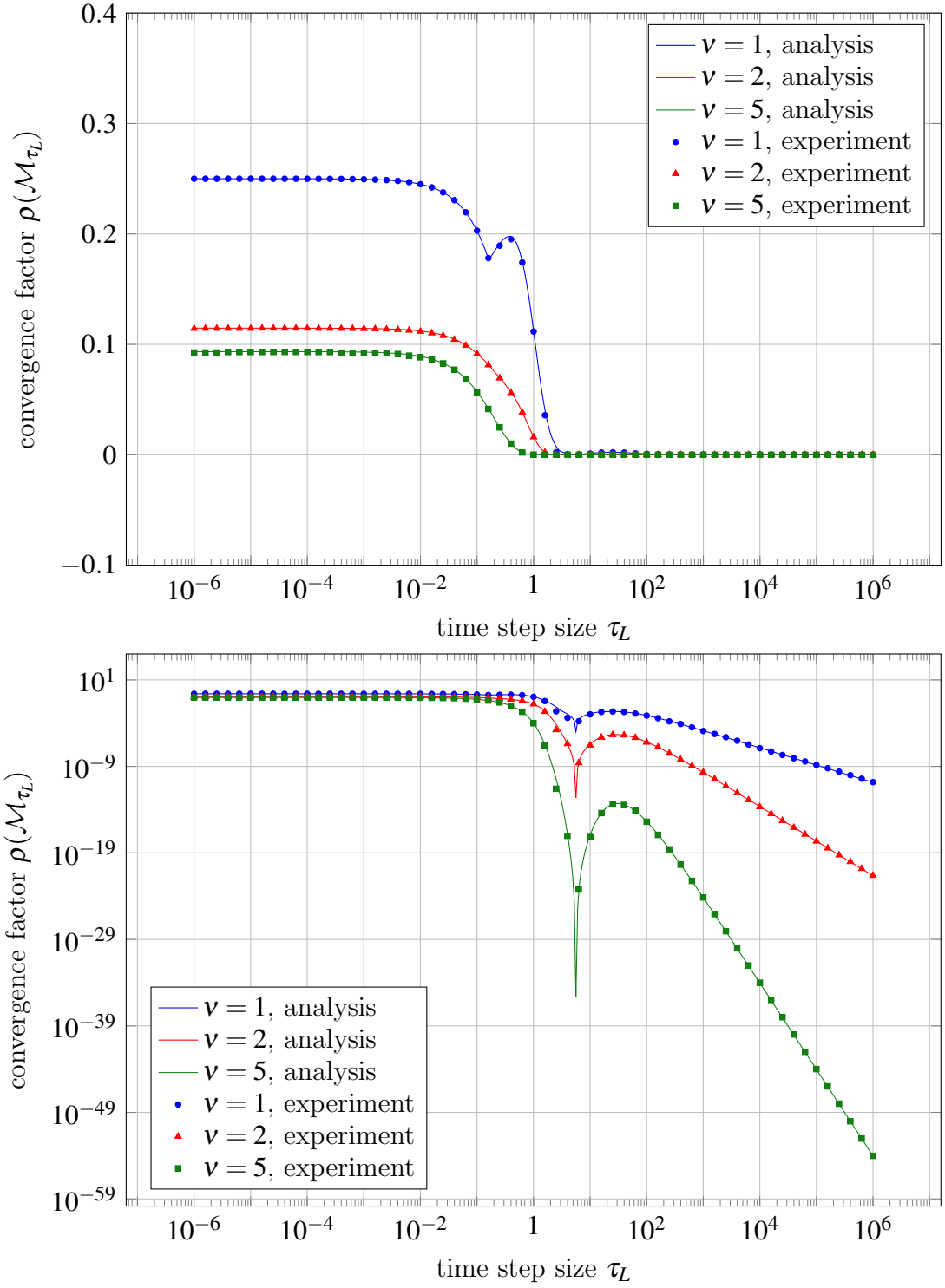

Figure 4.9: Average convergence factor $\rho(\mathcal{M}_{\tau_L})$ for different time step sizes τ_L, $p_t = 3$ and numerical convergence rates for $N_t = 1024$ time steps. Log-linear plot (top) and Log-log plot (bottom).

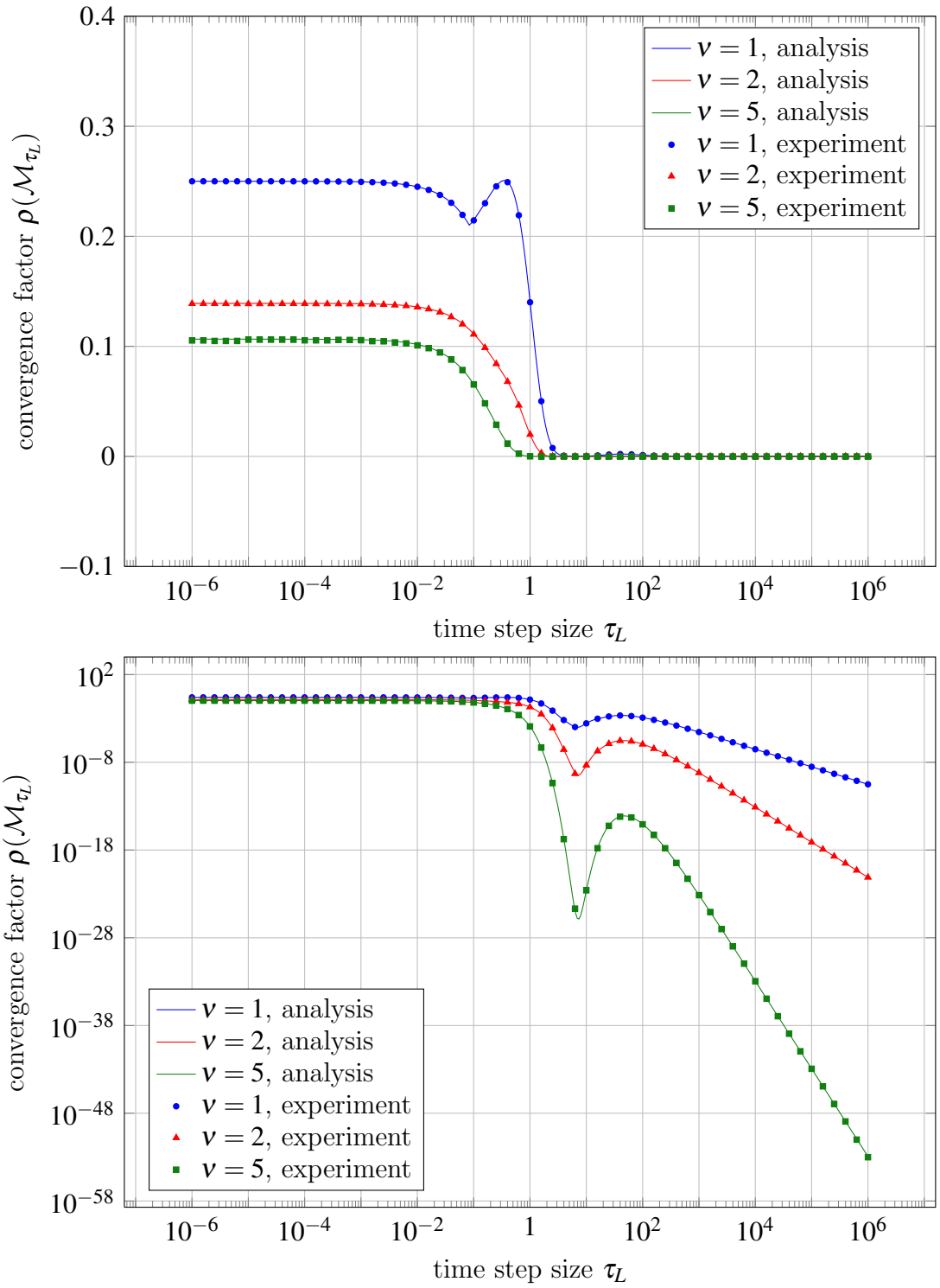

Figure 4.10: Average convergence factor $\rho(\mathcal{M}_{\tau_L})$ for different time step sizes τ_L, $p_t = 4$ and numerical convergence rates for $N_t = 1024$ time steps. Log-linear plot (top) and Log-log plot (bottom).

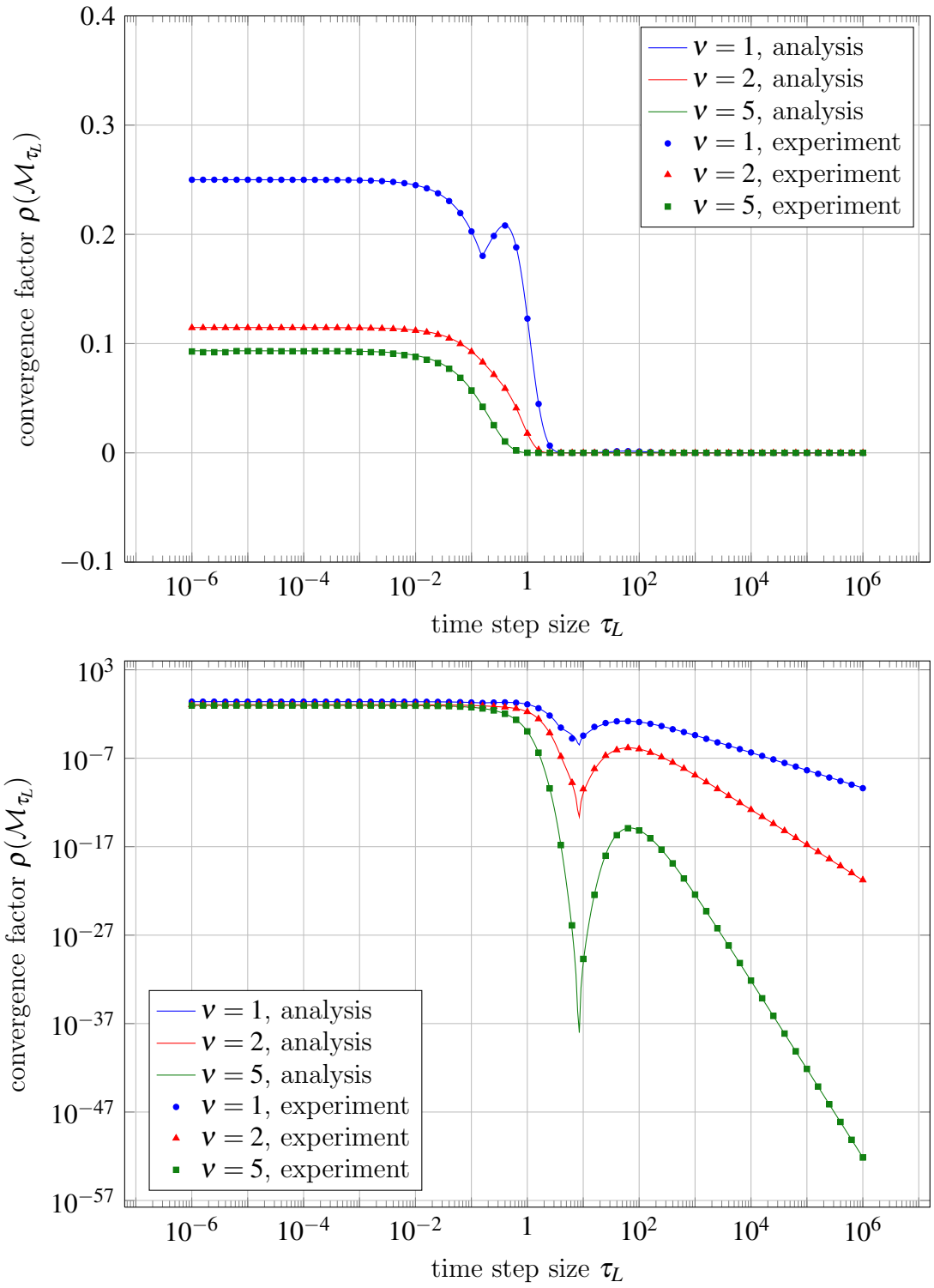

Figure 4.11: Average convergence factor $\rho(\mathcal{M}_{\tau_L})$ for different time step sizes τ_L, $p_t = 5$ and numerical convergence rates for $N_t = 1024$ time steps. Log-linear plot (top) and Log-log plot (bottom).

with the following matrices $A_{\tau,h}$ and $B_{\tau,h}$

$$A_{\tau,h} := M_h \otimes K_\tau + K_h \otimes M_\tau, \qquad B_{\tau,h} := -M_h \otimes N_\tau.$$

Here we assume, that we have a uniform decomposition of the simulation interval $[0,T]$ with time step size τ and that we also have a uniform decomposition of the one dimensional domain $\Omega = (0,1)$ with mesh size h. Furthermore we use piecewise linear continuous ansatz functions to approximate the solutions in space. Hence we have to deal with the standard one dimensional mass and stiffness matrices

$$M_h = \frac{h}{6}\begin{pmatrix} 4 & 1 & & & \\ 1 & 4 & 1 & & \\ & \ddots & \ddots & \ddots & \\ & & 1 & 4 & 1 \\ & & & 1 & 4 \end{pmatrix}, \qquad K_h = \frac{1}{h}\begin{pmatrix} 2 & -1 & & & \\ -1 & 2 & -1 & & \\ & \ddots & \ddots & \ddots & \\ & & -1 & 2 & -1 \\ & & & -1 & 2 \end{pmatrix}.$$

4.3.1 Smoothing analysis

In this subsection we study the smoothing behaviour of the damped block Jacobi smoother (4.7). The iteration matrix of the damped block Jacobi is given by

$$\mathcal{S}^{\nu}_{\tau_L,h_L} = \left[I - \omega_t (D_{\tau_L,h_L})^{-1} \mathcal{L}_{\tau_L,h_L}\right]^{\nu},$$

where D_{τ_L,h_L} is a block diagonal matrix with blocks A_{τ_L,h_L}. For the analysis we can use the results which we obtained in the last section, where we have analyzed the two-grid cycle for the simpler ODE case.

In the following we denote by $N_{L_t} \in \mathbb{N}$ the number of time steps for the level $L \in \mathbb{N}_0$, by $N_t = p_t + 1 \in \mathbb{N}$ we denote the degrees of freedom with respect to the polynomial degree p_t and with $N_{L_x} \in \mathbb{N}$ we denote the degrees of freedom with respect to the space discretization for the Level L.

We start by transforming the problem (4.31) into the frequency domain. To do so, we first have to prove the following lemma.

Lemma 4.3.1. *Let $\boldsymbol{u} = (\boldsymbol{u}_1, \boldsymbol{u}_2, \ldots, \boldsymbol{u}_{N_{L_t}})^\top \in \mathbb{R}^{N_t N_{L_x} N_{L_t}}$ for $N_t, N_{L_x}, N_{L_t} \in \mathbb{N}$ where we assume that N_{L_x} and N_{L_t} are even numbers. Furthermore we assume that*

$$\boldsymbol{u}_n \in \mathbb{R}^{N_t N_{L_x}} \qquad \text{and} \qquad \boldsymbol{u}_{n,r} \in \mathbb{R}^{N_t}$$

for $n = 1, \ldots, N_{L_t}$ and $r = 1, \ldots, N_{L_x}$. Then the vector $\boldsymbol{u}$ can be written as

$$\boldsymbol{u} = \sum_{\theta_x \in \Theta_{L_x}} \sum_{\theta_t \in \Theta_{L_t}} \psi^{L_x,L_t}(\theta_x, \theta_t)$$

with the vectors

$$\boldsymbol{\psi}_{n,r}^{L_x,L_t}(\theta_x,\theta_t) := U\boldsymbol{\Phi}_{n,r}^{L_x,L_t}(\theta_x,\theta_t), \qquad \boldsymbol{\Phi}_{n,r}^{L_x,L_t}(\theta_x,\theta_t) := \boldsymbol{\Phi}_n^{L_t}(\theta_t)\boldsymbol{\varphi}^{L_x}(\theta_x)[r]$$

for $n = 1,\ldots,N_{L_t}$, $r = 1,\ldots,N_{L_x}$ *and with the coefficient matrix*

$$U := \operatorname{diag}(\hat{u}_{x,t}[1],\ldots,\hat{u}_{x,t}[N_t]) \in \mathbb{C}^{N_t\times N_t}$$

with the coefficients for $\theta_x \in \Theta_{L_x}$ *and* $\theta_t \in \Theta_{L_t}$

$$\hat{u}_{x,t}[\ell] := \frac{1}{N_{L_x}}\frac{1}{N_{L_t}}\sum_{r=1}^{N_{L_x}}\sum_{n=1}^{N_{L_t}} \boldsymbol{u}_{n,r}[\ell]\boldsymbol{\varphi}(-\theta_x)[r]\boldsymbol{\varphi}(-\theta_t)[n].$$

Proof. For $\boldsymbol{u} = (\boldsymbol{u}_1,\boldsymbol{u}_2,\ldots,\boldsymbol{u}_{N_{L_t}})^\top \in \mathbb{R}^{N_tN_{L_x}N_{L_t}}$ we define for $s = 1,\ldots,N_{L_x}$ the vector $\boldsymbol{w}^s \in \mathbb{R}^{N_{L_t}N_t}$ as $\boldsymbol{w}_n^s[\ell] := \boldsymbol{u}_{n,s}[\ell]$. Applying Lemma 4.2.10 to the vector $\boldsymbol{w}^s$ results in

$$\boldsymbol{u}_{i,s}[\ell] = \boldsymbol{w}_i^s[\ell] = \sum_{\theta_t\in\Theta_{L_t}} \boldsymbol{\psi}^{L_t}(\theta_t) = \sum_{\theta_t\in\Theta_{L_t}} U_t[\ell,\ell]\boldsymbol{\varphi}(\boldsymbol{\theta_t})[i],$$

with

$$U_t[\ell,\ell] = \hat{w}_t^s[\ell] = \frac{1}{N_L}\sum_{n=1}^{N_{L_t}} \boldsymbol{u}_{n,s}[\ell]\boldsymbol{\varphi}(-\theta_t)[n].$$

Next we define for a fixed $n \in \{1,\ldots,N_{L_t}\}$ and a fixed $\ell \in \{1,\ldots,N_t\}$ the vector $\boldsymbol{z}^{n,\ell} \in \mathbb{R}^{N_{L_x}}$ as $\boldsymbol{z}^{n,\ell}[s] := u_{n,s}[\ell]$. By using Theorem 4.2.8 with respect to the vector $\boldsymbol{z}^{n,\ell}$ we obtain for $s = 1,\ldots,N_{L_x}$

$$u_{n,s}[\ell] = \boldsymbol{z}^{n,\ell}[s] = \sum_{\theta_x\in\Theta_{L_x}} \hat{z}_x^{n,\ell}\boldsymbol{\varphi}(\theta_x)[s],$$

with

$$\hat{z}_x^{n,\ell} = \frac{1}{N_{L_x}}\sum_{r=1}^{N_{L_x}} \boldsymbol{u}_{n,r}[\ell]\boldsymbol{\varphi}(-\theta_x)[r].$$

By combining the results from above we obtain the statement of this lemma with

$$\begin{aligned}\boldsymbol{u}_{i,s}[\ell] &= \sum_{\theta_x\in\Theta_{L_x}}\sum_{\theta_t\in\Theta_{L_t}} \boldsymbol{\varphi}(\theta_x)[s]\boldsymbol{\varphi}(\boldsymbol{\theta_t})[i]\frac{1}{N_{L_x}}\frac{1}{N_{L_t}}\sum_{r=1}^{N_{L_x}}\sum_{n=1}^{N_{L_t}} \boldsymbol{u}_{n,r}[\ell]\boldsymbol{\varphi}(-\theta_x)[r]\boldsymbol{\varphi}(-\theta_t)[n] \\ &= \sum_{\theta_x\in\Theta_{L_x}}\sum_{\theta_t\in\Theta_{L_t}} \hat{u}_{x,t}[\ell]\boldsymbol{\varphi}(\theta_x)[s]\boldsymbol{\varphi}(\boldsymbol{\theta_t})[i]\end{aligned}$$

$$= \sum_{\theta_x \in \Theta_{L_x}} \sum_{\theta_t \in \Theta_{L_t}} U[\ell,\ell] \boldsymbol{\Phi}_{i,s}^{L_x,L_t}(\theta_x,\theta_t)[\ell]$$
$$= \sum_{\theta_x \in \Theta_{L_x}} \sum_{\theta_t \in \Theta_{L_t}} \boldsymbol{\psi}_{i,s}^{L_x,L_t}(\theta_x,\theta_t)[\ell].$$

■

Lemma 4.3.1 motivates the following definition.

Definition 4.3.2 (Fourier space)**.** *For $N_t, N_{L_x}, N_{L_t} \in \mathbb{N}$ and the frequency $\theta_x \in \Theta_{L_x}$ and $\theta_t \in \Theta_{L_t}$ let the vector $\boldsymbol{\Phi}^{L_x,L_t}(\theta_x,\theta_t) \in \mathbb{C}^{N_t N_{L_x} N_{L_t}}$ be defined as in Lemma 4.3.1. Then we define the linear space of Fourier modes with frequencies (θ_x,θ_t) as*

$$\begin{aligned}\Psi_{L_x,L_t}(\theta_x,\theta_t) &:= \operatorname{span}\left\{\boldsymbol{\Phi}^{L_x,L_t}(\theta_x,\theta_t)\right\} \\ &= \Big\{\boldsymbol{\psi}^{L_x,L_t}(\theta_x,\theta_t) \in \mathbb{C}^{N_t N_{L_x} N_{L_t}} : \boldsymbol{\psi}_{n,r}^{L_x,L_t}(\theta_x,\theta_t) := U\boldsymbol{\Phi}_{n,r}^{L_x,L_t}(\theta_x,\theta_t), \\ &\qquad n = 1,\dots,N_{L_t}, r = 1,\dots,N_{L_x} \text{ and } U \in \mathbb{C}^{N_t \times N_t}\Big\}.\end{aligned}$$

To analyze the mapping properties of the occurring operators, we need the following shifting results.

Lemma 4.3.3. *For $N_t, N_{L_x}, N_{L_t} \in \mathbb{N}$ and the frequencies $\theta_x \in \Theta_{L_x}$, $\theta_t \in \Theta_{L_t}$ let $\boldsymbol{\psi}^{L_x,L_t}(\theta_x,\theta_t) \in \Psi_{L_x,L_t}(\theta_x,\theta_t)$. Then the following shifting equalities hold true*

$$\boldsymbol{\psi}_{n-1,r}^{L_x,L_t}(\theta_x,\theta_t) = e^{-\mathbb{i}\theta_t}\boldsymbol{\psi}_{n,r}^{L_x,L_t}(\theta_x,\theta_t),$$
$$\boldsymbol{\psi}_{n,r-1}^{L_x,L_t}(\theta_x,\theta_t) = e^{-\mathbb{i}\theta_x}\boldsymbol{\psi}_{n,r}^{L_x,L_t}(\theta_x,\theta_t)$$

for $n = 2,\dots,N_{L_t}$ and $r = 2,\dots,N_{L_x}$.

Proof. As in the proof of Lemma 4.2.13 the statement of this lemma follows by the fact, that

$$\boldsymbol{\varphi}(\theta)[n-1] = e^{\mathbb{i}(n-1)\theta} = e^{-\mathbb{i}\theta}e^{\mathbb{i}n\theta} = e^{-\mathbb{i}\theta}\boldsymbol{\varphi}(\theta)[n],$$

which can be applied for the frequencies in space $\theta_x \in \Theta_{L_x}$ and the frequencies in time $\theta_t \in \Theta_{L_t}$. ■

In the next lemma the Fourier symbol for the space-time operator $\mathcal{L}_{\tau_L,h_L}$ will be computed.

Lemma 4.3.4. *For the frequencies $\theta_x \in \Theta_{L_x}$ and $\theta_t \in \Theta_{L_t}$ we consider the vector $\boldsymbol{\psi}^{L_x,L_t}(\theta_x,\theta_t) \in \Psi_{L_x,L_t}(\theta_x,\theta_t)$. Then for $n = 2,\dots,N_{L-t}$ and $r = 2,\dots,N_{L_x}-1$ there holds*

$$\left(\mathcal{L}_{\tau_L,h_L}\boldsymbol{\psi}^{L_x,L_t}(\theta_x,\theta_t)\right)_{n,r} = \hat{\mathcal{L}}_{\tau_L,h_L}(\theta_x,\theta_t)\boldsymbol{\psi}_{n,r}^{L_x,L_t}(\theta_x,\theta_t),$$

where the Fourier symbol is given by

$$\hat{\mathcal{L}}_{\tau_L,h_L}(\theta_x,\theta_t) := \frac{h_L}{3}(2+\cos(\theta_x))\left[K_{\tau_L}+h_L^{-2}\beta(\theta_x)M_{\tau_L}-e^{-\mathbb{i}\theta_t}N_{\tau_L}\right] \in \mathbb{C}^{N_t\times N_t},$$

with the function

$$\beta(\theta_x) := 6\,\frac{1-\cos(\theta_x)}{2+\cos(\theta_x)} \in [0,12].$$

Proof. Let $\psi^{L_x,L_t}(\theta_x,\theta_t) \in \Psi_{L_x,L_t}(\theta_x,\theta_t)$ then we have for $n=2,\dots,N_{L_t}$

$$\left(\mathcal{L}_{\tau_L,h_L}\psi^{L_x,L_t}(\theta_x,\theta_t)\right)_n = B_{\tau_L,h_L}\psi^{L_x,L_t}_{n-1}(\theta_x,\theta_t)+A_{\tau_L,h_L}\psi^{L_x,L_t}_{n}(\theta_x,\theta_t).$$

Applying Lemma 4.3.3 results in

$$= \left(e^{-\mathbb{i}\theta_t}B_{\tau_L,h_L}+A_{\tau_L,h_L}\right)\psi^{L_x,L_t}_n(\theta_x,\theta_t).$$

Hence, we have to study the action of $A_{\tau,h}$ and $B_{\tau,h}$ onto the vector $\psi^{L_x,L_t}_n(\theta_x,\theta_t)$. By using the definition of $B_{\tau,h}$ we obtain for $r=2,\dots,N_{L_x}-1$ and $\ell=1,\dots,N_t$

$$\begin{aligned}\left(B_{\tau_L,h_L}\psi^{L_x,L_t}_n(\theta_x,\theta_t)\right)_r[\ell] &= -\sum_{s=1}^{N_{L_x}}\sum_{k=1}^{N_t} M_{h_L}[r,s]N_{\tau_L}[\ell,k]\psi^{L_x,L_t}_{n,s}(\theta_x,\theta_t)[k]\\ &= -\sum_{k=1}^{N_t}\frac{h_L}{6}\left(\psi^{L_x,L_t}_{n,r-1}(\theta_x,\theta_t)[k]+4\psi^{L_x,L_t}_{n,r}(\theta_x,\theta_t)[k]+\psi^{L_x,L_t}_{n,r+1}(\theta_x,\theta_t)[k]\right)N_{\tau_L}[\ell,k].\end{aligned}$$

Applying Lemma 4.3.3 leads to

$$\begin{aligned}&= -\frac{h_L}{6}\sum_{k=1}^{N_t}N_{\tau_L}[\ell,k]\left(e^{-\mathbb{i}\theta_x}+4+e^{\mathbb{i}\theta_x}\right)\psi^{L_x,L_t}_{n,r}(\theta_x,\theta_t)[k]\\ &= -\frac{h_L}{3}(2+\cos(\theta_x))\sum_{k=1}^{N_t}N_{\tau_L}[\ell,k]\psi^{L_x,L_t}_{n,r}(\theta_x,\theta_t)[k]\\ &= -\frac{h_L}{3}(2+\cos(\theta_x))\left(N_{\tau_L}\psi^{L_x,L_t}_{n,r}(\theta_x,\theta_t)\right)[\ell].\end{aligned}$$

Next we study the action of the matrix $A_{\tau,h}$ onto the local vector $\psi^{L_x,L_t}_n(\theta_x,\theta_t)$.

$$\begin{aligned}\left(A_{\tau_L,h_L}\psi^{L_x,L_t}_n(\theta_x,\theta_t)\right)_r[\ell] = &\sum_{s=1}^{N_{L_x}}\sum_{k=1}^{N_t}M_{h_L}[r,s]K_{\tau_L}[\ell,k]\psi^{L_x,L_t}_{n,s}(\theta_x,\theta_t)[k]\\ &+\sum_{s=1}^{N_{L_x}}\sum_{k=1}^{N_t}K_{h_L}[r,s]M_{\tau_L}[\ell,k]\psi^{L_x,L_t}_{n,s}(\theta_x,\theta_t)[k]\end{aligned}$$

$$= \frac{h_L}{3}(2+\cos(\theta_x)) \sum_{k=1}^{N_t} K_{\tau_L}[\ell,k]\psi_{n,s}^{L_x,L_t}(\theta_x,\theta_t)[k]$$
$$+ \sum_{k=1}^{N_t} \frac{1}{h_L}\left(-\psi_{n,r-1}^{L_x,L_t}(\theta_x,\theta_t)[k] + 2\psi_{n,r}^{L_x,L_t}(\theta_x,\theta_t)[k] - \psi_{n,r+1}^{L_x,L_t}(\theta_x,\theta_t)[k]\right) M_{\tau_L}[\ell,k].$$

Using Lemma 4.3.3 results in

$$= \frac{h_L}{3}(2+\cos(\theta_x)) \left(K_{\tau_L}\psi_{n,r}^{L_x,L_t}(\theta_x,\theta_t)\right)[\ell]$$
$$+ \frac{2}{h_L}(1-\cos(\theta_x)) \sum_{k=1}^{N_t} M_{\tau_L}[\ell,k]\psi_{n,r}^{L_x,L_t}(\theta_x,\theta_t)[k]$$
$$= \left(\left[\frac{h_L}{3}(2+\cos(\theta_x))K_{\tau_L} + \frac{2}{h_L}(1-\cos(\theta_x))M_{\tau_L}\right]\psi_{n,r}^{L_x,L_t}(\theta_x,\theta_t)\right)[\ell].$$

Hence we have

$$\begin{aligned}
\left(\mathcal{L}_{\tau_L,h_L}\psi^{L_x,L_t}(\theta_x,\theta_t)\right)_{n,r} &= \frac{h_L}{3}(2+\cos(\theta_x))\left(K_{\tau_L} - e^{-\mathbb{i}\theta_t}N_{\tau_L}\right)\psi_{n,r}^{L_x,L_t}(\theta_x,\theta_t) \\
&\quad + \frac{2}{h_L}(1-\cos(\theta_x))M_{\tau_L}\psi_{n,r}^{L_x,L_t}(\theta_x,\theta_t) \\
&= \frac{h_L}{3}(2+\cos(\theta_x))\left(K_{\tau_L} + 6h_L^{-2}\frac{1-\cos(\theta_x)}{2+\cos(\theta_x)}M_{\tau_L} - e^{-\mathbb{i}\theta_t}N_{\tau_L}\right)\psi_{n,r}^{L_x,L_t}(\theta_x,\theta_t) \\
&= \frac{h_L}{3}(2+\cos(\theta_x))\left(K_{\tau_L} + h_L^{-2}\beta(\theta_x)M_{\tau_L} - e^{-\mathbb{i}\theta_t}N_{\tau_L}\right)\psi_{n,r}^{L_x,L_t}(\theta_x,\theta_t),
\end{aligned}$$

which completes the proof. ∎

Remark 4.3.5. *We note, that the Fourier symbol $\hat{\mathcal{L}}_{\tau_L,h_L}(\theta_x,\theta_t)$ for the space-time operator $\mathcal{L}_{\tau_L,h_L}$ is closely related to the Fourier symbol $\hat{\mathcal{L}}_{\tau_L} = K_{\tau_L} + M_{\tau_L} - e^{-\mathbb{i}\theta_t}N_{\tau_L}$ which we obtained for the ODE case, see also Lemma 4.2.14. The major difference is the additional weight $h_L^{-2}\beta(\theta_x)$ in front of the local time mass matrix M_{τ_L}.*

If we assume periodicity in space and time, i.e.

$$\begin{aligned}
u(t,0) &= u(t,1) \qquad \text{for } t \in (0,T), \\
u(0,x) &= u(T,x) \qquad \text{for } x \in \Omega = (0,1),
\end{aligned} \tag{4.32}$$

we conclude with Lemma 4.3.4, the following mapping property

$$\begin{aligned}
\mathcal{L}_{\tau_L,h_L} : \Psi_{L_x,L_t}(\theta_x,\theta_t) &\to \Psi_{L_x,L_t}(\theta_x,\theta_t), \\
U &\mapsto \hat{\mathcal{L}}_{\tau_L,h_L}(\theta_x,\theta_t)U.
\end{aligned} \tag{4.33}$$

Next we study the mapping property of the iteration matrix $\mathcal{S}_{\tau_L,h_L}^{\nu}$.

Lemma 4.3.6. *For the frequencies $\theta_x \in \Theta_{L_x}$ and $\theta_t \in \Theta_{L_t}$ we consider the vector $\psi^{L_x,L_t}(\theta_x,\theta_t) \in \Psi_{L_x,L_t}(\theta_x,\theta_t)$. Then under the assumption of periodic solutions, see (4.32), there holds for $n = 2,\dots,N_{L_t}$ and $r = 2,\dots,N_{L_x}-1$ that*

$$\left(\mathcal{S}^1_{\tau_L,h_L}\psi^{L_x,L_t}(\theta_x,\theta_t)\right)_{n,r} = \hat{\mathcal{S}}_{\tau_L,h_L}(\theta_x,\theta_t)\psi^{L_x,L_t}_{n,r}(\theta_x,\theta_t)$$

where the Fourier symbol is given by

$$\hat{\mathcal{S}}_{\tau_L,h_L}(\theta_x,\theta_t) := (1-\omega_t)I_{N_t} + \omega_t e^{-\mathbb{i}\theta_t}\left(K_{\tau_L} + h_L^{-2}\beta(\theta_x)M_{\tau_L}\right)^{-1} N_{\tau_L} \in \mathbb{C}^{N_t\times N_t},$$

with the function $\beta(\theta_x)$ as defined in Lemma 4.3.4.

Proof. Let $\psi^{L_x,L_t}(\theta_x,\theta_t) \in \Psi_{L_x,L_t}(\theta_x,\theta_t)$, then for a fixed $n = 2,\dots,N_{L_t}$ and a fixed $r = 2,\dots,N_{L_x}-1$ we have that

$$\begin{aligned}
\left(\mathcal{S}^1_{\tau_L,h_L}\psi^{L_x,L_t}(\theta_x,\theta_t)\right)_{n,r} &= \left(\left(I_{N_tN_{L_x}N_{L_t}} - \omega_t(D_{\tau_L,h_L})^{-1}\mathcal{L}_{\tau_L,h_L}\right)\psi^{L_x,L_t}(\theta_x,\theta_t)\right)_{n,r} \\
&= \left(I_{N_t} - \omega_t\left(\hat{A}_{\tau_L,h_L}(\theta_x)\right)^{-1}\hat{\mathcal{L}}_{\tau_L,h_L}(\theta_x,\theta_t)\right)\psi^{L_x,L_t}_{n,r}(\theta_x,\theta_t) \\
&=: \hat{\mathcal{S}}_{\tau_L,h_L}(\theta_x,\theta_t)\psi^{L_x,L_t}_{n,r}(\theta_x,\theta_t)
\end{aligned}$$

with

$$\begin{aligned}
\hat{A}_{\tau_L,h_L}(\theta_x) &:= \frac{h_L}{3}(2+\cos(\theta_x))K_{\tau_L} + \frac{2}{h_L}(1-\cos(\theta_x))M_{\tau_L} \\
&= \frac{h_L}{3}(2+\cos(\theta_x))\left[K_{\tau_L} + h_L^{-2}\beta(\theta_x)M_{\tau_L}\right].
\end{aligned}$$

Further calculations give

$$\begin{aligned}
\left(\hat{A}_{\tau_L,h_L}(\theta_x)\right)^{-1}\hat{\mathcal{L}}_{\tau_L,h_L}(\theta_x,\theta_t) &= \left(\hat{A}_{\tau_L,h_L}(\theta_x)\right)^{-1}\left[K_{\tau_L} + h_L^{-2}\beta(\theta_x)M_{\tau_L} - e^{-\mathbb{i}\theta_t}N_{\tau_L}\right] \\
&= I_{N_t} - e^{-\mathbb{i}\theta_t}\left[K_{\tau_L} + h_L^{-2}\beta(\theta_x)M_{\tau_L}\right]^{-1}N_{\tau_L}.
\end{aligned}$$

Hence we have

$$\begin{aligned}
\hat{\mathcal{S}}_{\tau_L,h_L}(\theta_x,\theta_t) &= I_{N_t} - \omega_t\left(I_{N_t} - e^{-\mathbb{i}\theta_t}\left(K_{\tau_L} + h_L^{-2}\beta(\theta_x)M_{\tau_L}\right)^{-1}N_{\tau_L}\right) \\
&= (1-\omega_t)I_{N_t} + \omega_t e^{-\mathbb{i}\theta_t}\left(K_{\tau_L} + h_L^{-2}\beta(\theta_x)M_{\tau_L}\right)^{-1}N_{\tau_L},
\end{aligned}$$

which completes the proof. ∎

In view of Lemma 4.3.6 the following mapping property holds true, when periodicity in space and time assumed

$$\begin{aligned}
\mathcal{S}^\nu_{\tau_L,h_L} : \Psi_{L_x,L_t}(\theta_x,\theta_t) &\to \Psi_{L_x,L_t}(\theta_x,\theta_t), \\
U &\mapsto (\hat{\mathcal{S}}_{\tau_L,h_L}(\theta_x,\theta_t))^\nu U.
\end{aligned} \tag{4.34}$$

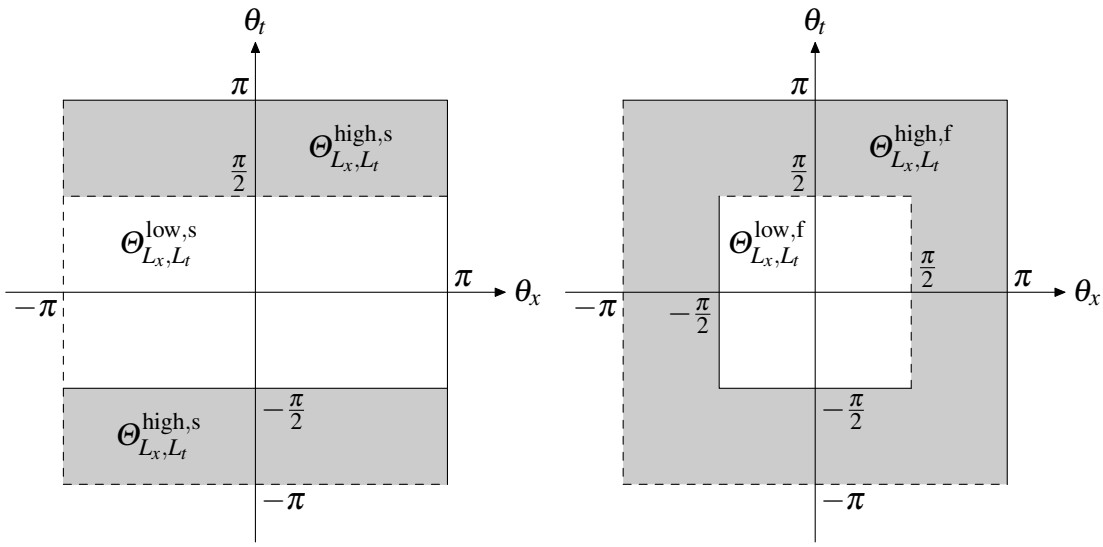

(a) Semi coarsening. (b) Full space-time coarsening.

Figure 4.12: Low and high frequencies θ_x and θ_t for semi coarsening and full space-time coarsening.

Next we will analyze the smoothing behaviour for the high frequencies. To do so, we consider two coarsening strategies. We will study the case when semi coarsening with respect to time is applied and the case when we apply full space-time coarsening. This motivates the following definition.

Definition 4.3.7. *Let $N_{L_t}, N_{L_x} \in \mathbb{N}$. Then we define the set of frequencies*

$$\Theta_{L_x,L_t} := \left\{ \left(\frac{2k\pi}{N_{L_x}}, \frac{2\ell\pi}{N_{L_t}}\right) : k = 1 - \frac{N_{L_x}}{2}, \ldots, \frac{N_{L_x}}{2} \text{ and } \ell = 1 - \frac{N_{L_t}}{2}, \ldots, \frac{N_{L_t}}{2} \right\} \subset (-\pi, \pi]^2.$$

Next we define the low and high frequencies with respect to semi coarsening in time

$$\begin{aligned} \Theta^{\text{low,s}}_{L_x,L_t} &:= \Theta_{L_x,L_t} \cap (-\pi, \pi] \times (-\frac{\pi}{2}, \frac{\pi}{2}], \\ \Theta^{\text{high,s}}_{L_x,L_t} &:= \Theta_{L_x,L_t} \setminus \Theta^{\text{low,s}}_{L_x,L_t}. \end{aligned}$$

Furthermore we define the low and high frequencies with respect to full space-time coarsening

$$\begin{aligned} \Theta^{\text{low,f}}_{L_x,L_t} &:= \Theta_{L_x,L_t} \cap (-\frac{\pi}{2}, \frac{\pi}{2}]^2, \\ \Theta^{\text{high,f}}_{L_x,L_t} &:= \Theta_{L_x,L_t} \setminus \Theta^{\text{low,f}}_{L_x,L_t}. \end{aligned}$$

In Figure 4.12 the high and low frequencies are illustrated for the two coarsening strategies. Next we define the smoothing factors with respect to these two coarsening strategies.

Definition 4.3.8 (Smoothing factors)**.** *Let $\hat{\mathcal{S}}_{\tau_L,h_L}(\theta_x,\theta_t)$ be the symbol of the block Jacobi smoother. Then we define the smoothing factor with respect to semi-coarsening in time as*

$$\mu_S^{\mathrm{s}} := \max\left\{\rho(\hat{\mathcal{S}}_{\tau_L,h_L}(\theta_x,\theta_t)) : (\theta_x,\theta_t) \in \Theta^{\mathrm{high,s}}_{L_x,L_t}\right\}.$$

Furthermore the smoothing factor with respect to full space-time coarsening is given by

$$\mu_S^{\mathrm{f}} := \max\left\{\rho(\hat{\mathcal{S}}_{\tau_L,h_L}(\theta_x,\theta_t)) : (\theta_x,\theta_t) \in \Theta^{\mathrm{high,f}}_{L_x,L_t}\right\}.$$

To analyze the smoothing behaviour we need the following lemma to compute the eigenvalues of the Fourier symbol $\hat{\mathcal{S}}_{\tau_L,h_L}(\theta_x,\theta_t)$.

Lemma 4.3.9. *The eigenvalues of the iteration matrix*

$$\left(K_{\tau_L} + h_L^{-2}\beta(\theta_x)M_{\tau_L}\right)^{-1} N_{\tau_L} \in \mathbb{R}^{N_t,N_t}$$

are given by

$$\sigma\left(\left(K_{\tau_L} + h_L^{-2}\beta(\theta_x)M_{\tau_L}\right)^{-1} N_{\tau_L}\right) = \{0, \alpha(\theta_x,\mu)\}$$

were $\mu := \tau_L h_L^{-2}$ is a discretization parameter and $\alpha(\theta_x,\mu) = R(-\mu\beta(\theta_x))$ is defined by the A-stability function $R(z)$ of the given time discretization, which is given by the (p_t, p_t+1) subdiagonal Padé approximation of the exponential function e^z.

Proof. The statement of this lemma follows simply by using $\lambda = -h_L^{-2}\beta(\theta_x)$ in the proof of Theorem 4.2.17. ∎

Now we are able to compute the spectral radius for the Fourier symbol $\hat{\mathcal{S}}_{\tau_L,h_L}(\theta_x,\theta_t)$.

Lemma 4.3.10. *The spectral radius of the Fourier symbol $\hat{\mathcal{S}}_{\tau_L,h_L}(\theta_x,\theta_t)$ is given by*

$$\rho\left(\hat{\mathcal{S}}_{\tau_L,h_L}(\theta_x,\theta_t)\right) = \max\left\{|1-\omega_t|, \hat{\mathcal{S}}(\omega_t,\alpha(\theta_x,\mu),\theta_t)\right\}$$

with

$$\left(\hat{\mathcal{S}}(\omega_t,\alpha,\theta_t)\right)^2 := (1-\omega_t)^2 + 2\omega_t(1-\omega_t)\alpha\cos(\theta_t) + \alpha^2\omega_t^2$$

where $\alpha(\theta_x,\mu) = R(-\mu\beta(\theta_x))$ and $R(z)$ is the (p_t, p_t+1) subdiagonal Padé approximation of the exponential function e^z and $\mu := \tau_L h_L^{-2}$ is a discretization parameter.

Proof. The Fourier symbol $\hat{\mathcal{S}}_{\tau_L,h_L}(\theta_x,\theta_t)$ has the same structure as the Fourier symbol which is analyzed in Lemma 4.2.19. Hence the statement of this lemma follows by applying Lemma 4.3.9 in the same way as in Lemma 4.2.19. ∎

Next we study the smoothing behaviour of the damped block Jacobi iteration for the case when semi-coarsening with respect to time is applied.

Lemma 4.3.11. *For the function*

$$\left(\hat{\mathcal{S}}(\omega_t,\alpha,\theta_t)\right)^2 := (1-\omega_t)^2 + 2\omega_t(1-\omega_t)\alpha\cos(\theta_t) + \alpha^2\omega_t^2$$

with $\alpha = \alpha(\theta_x,\mu)$ as defined in Lemma 4.3.9 and even polynomial degrees p_t the following min-max principle holds true

$$\inf_{\omega_t\in(0,1]} \sup_{\substack{\theta_t\in[\frac{\pi}{2},\pi]\\ \theta_x\in[0,\pi]}} \hat{\mathcal{S}}(\omega_t,\alpha(\theta_x,\mu),\theta_t) = \frac{1}{\sqrt{2}}$$

for any discretization parameter $\mu \geq 0$ with the optimal parameters

$$\omega_t^* = \frac{1}{2}, \qquad \theta_t^* = \frac{\pi}{2} \qquad \text{and} \qquad \theta_x^* = 0.$$

Proof. Since we consider even polynomial degrees p_t, we conclude that the (p_t, p_t+1) subdiagonal Padé approximation $R(z)$ of the exponential function e^z is positive for all $z \leq 0$. Hence we also have that $\alpha(\theta_x,\mu) = R(-\mu\beta(\theta_x))$ is positive for all $\mu \geq 0$ and $\theta_x \in [0,\pi]$. Since $\omega_t \in (0,1]$ we obtain that

$$\theta_t^* := \operatorname*{argsup}_{\theta_t\in[\frac{\pi}{2},\pi]} \hat{\mathcal{S}}(\omega_t,\alpha(\theta_x,\mu),\theta_t) = \frac{\pi}{2}.$$

Since $\alpha(0,\mu) = 1$ and $|\alpha(\theta_x,\mu)| \leq 1$ for all $\theta_x \in [0,\pi]$ and $\mu \geq 0$ we conclude that

$$\theta_x^* := \operatorname*{argsup}_{\theta_x\in[0,\pi]} \hat{\mathcal{S}}(\omega_t,\alpha(\theta_x,\mu),\theta^*) = 0.$$

Hence we have to find the infimum of

$$\left(\hat{\mathcal{S}}(\omega_t,\alpha(\theta_x^*,\mu),\theta_t^*)\right)^2 = (1-\omega_t)^2 + \omega_t^2,$$

which is obtained for $\omega_t^* = \frac{1}{2}$. This implies that

$$\left(\hat{\mathcal{S}}(\omega_t^*,\alpha(\theta_x^*,\mu),\theta_t^*)\right)^2 = \frac{1}{2},$$

which completes the proof. ∎

With the next lemma we can bound the smoothing factor μ_S^s for the case when semi coarsening with respect to time is used.

Lemma 4.3.12. *Let $\hat{\mathcal{S}}(\omega_t, \alpha(\theta_x, \mu), \theta_t)$ be defined as in Lemma 4.3.12. Then for the choice $\omega_t^* = \frac{1}{2}$ and any polynomial degree $p_t \in \mathbb{N}_0$ the following bound holds true*

$$\sup_{\substack{\theta_t \in [\frac{\pi}{2}, \pi] \\ \theta_x \in [0, \pi]}} \hat{\mathcal{S}}(\omega_t, \alpha(\theta_x, \mu), \theta_t) \leq \frac{1}{\sqrt{2}}.$$

Proof. For even polynomial degrees p_t we can apply Lemma 4.3.11 to end up with the stated bound. For odd polynomial degrees the $(p_t, p_t + 1)$ subdiagonal Padé approximation $R(z)$ of the exponential function e^z is negative for large negative values of z. If the value of $\alpha(\theta_x^*, \mu) = R(-\mu\beta(\theta_x^*))$ for the optimal parameter $\theta_x^* \in [0, \pi]$ is positive we end up with the bound of Lemma 4.3.11, otherwise if $\alpha(\theta_x^*, \mu)$ is negative we have that

$$\theta_t^* := \operatorname*{argsup}_{\theta_t \in [\frac{\pi}{2}, \pi]} \hat{\mathcal{S}}(\omega_t, \alpha(\theta_x^*, \mu), \theta_t) = \pi.$$

For a negative $\alpha(\theta_x^*, \mu)$ this implies that

$$\sup_{\substack{\theta_t \in [\frac{\pi}{2}, \pi] \\ \theta_x \in [0, \pi]}} \hat{\mathcal{S}}(\omega_t^*, \alpha(\theta_x, \mu), \theta_t) \leq \frac{1}{2}(1 + |\alpha(\theta_x^*, \mu)|).$$

Since any subdiagonal $(p_t, p_t + 1)$ Padé approximation $R(z)$ is bounded from below by $R(z) \geq \frac{1}{2}(5 - 3\sqrt{3})$ for all $z < 0$ we get the estimate

$$\leq \frac{3}{4}(\sqrt{3} - 1) < \frac{1}{\sqrt{2}}.$$

■

With Lemma 4.3.12 we conclude, that the smoothing factor with respect to semi-coarsening in time is bounded by

$$\mu_S^{\mathrm{s}} \leq \frac{1}{\sqrt{2}}.$$

Hence, by applying the damped block Jacobi smoother with the optimal damping parameter $\omega_t^* = \frac{1}{2}$, the error components with respect to the high frequencies $\Theta_{L_x, L_t}^{\mathrm{high,s}}$ are damped by a factor of at least $\frac{1}{\sqrt{2}}$. To study the smoothing behaviour when full space-time coarsening is applied, we consider the following lemma.

Lemma 4.3.13. *For the optimal choice of the damping parameter $\omega_t^* = \frac{1}{2}$ there holds*

$$\sup_{\theta_t \in [0, \pi]} \hat{\mathcal{S}}(\omega_t^*, \alpha, \theta_t) = \frac{1}{2}(1 + |\alpha|)$$

with the optimal parameter

$$\theta_t^* = \begin{cases} 0 & \alpha \geq 0, \\ \pi & \alpha > 0. \end{cases}$$

Proof. Let $\alpha \in \mathbb{R}$. For the optimal damping parameter $\omega_t^* = \frac{1}{2}$ we have

$$\left(\hat{\mathcal{S}}(\omega_t^*, \alpha, \theta_t)\right)^2 = \frac{1}{4}\left(1 + 2\alpha\cos(\theta_t) + \alpha^2\right).$$

First we will study the case $\alpha \geq 0$. Hence we have

$$\theta_t^* := \operatorname*{argsup}_{\theta_t \in [0,\pi]} \hat{\mathcal{S}}(\omega_t^*, \alpha, \theta_t) = 0.$$

For the case $\alpha < 0$ we further obtain

$$\theta_t^* := \operatorname*{argsup}_{\theta_t \in [0,\pi]} \hat{\mathcal{S}}(\omega_t^*, \alpha, \theta_t) = \pi.$$

This implies that

$$\left(\hat{\mathcal{S}}(\omega_t^*, \alpha, \theta_t*)\right)^2 = \frac{1}{4}\left(1 + 2\,|\alpha| + \alpha^2\right) = \frac{1}{4}\left(1 + |\alpha|\right)^2,$$

which completes the proof. ∎

Lemma 4.3.13 shows, that we obtain a good smoothing behaviour for the high frequencies with respect to the space discretization, i.e. $\theta_x \in \Theta_{L_x}^{\text{high}}$, if $\alpha = \alpha(\theta_x, \mu)$ is sufficiently small for any frequency $\theta_x \in [\frac{\pi}{2}, \pi]$. Hence we conclude by combining Lemma 4.3.12 with Lemma 4.3.13, that a good smoothing behaviour is obtained for all frequencies $(\theta_x, \theta_t) \in \Theta_{L_x,L_t}^{\text{high,f}}$, if the function $\alpha = \alpha(\theta_x, \mu)$ is sufficiently small. This results in a restriction on the discretization parameter μ. With the next lemma we will analyze the behaviour of the smoothing factor μ_S^{f} with respect to the discretization parameter μ for even polynomial degrees $p_t \in \mathbb{N}_0$.

Lemma 4.3.14. *Let $p_t \in \mathbb{N}_0$ be even. Then for the optimal choice of the damping parameter $\omega_t^* = \frac{1}{2}$ there holds*

$$\sup_{\substack{\theta_t \in [0,\pi] \\ \theta_x \in [\frac{\pi}{2},\pi]}} \hat{\mathcal{S}}(\omega_t^*, \alpha(\theta_x, \mu), \theta_t) = \frac{1}{2}(1 + R(-3\mu))$$

where $R(z)$ is the $(p_t, p_t + 1)$ subdiagonal Padé approximation of the exponential function e^z.

Proof. In view of Lemma 4.3.13 it remains to compute the supremum

$$\sup_{\theta_x \in [\frac{\pi}{2}, \pi]} \frac{1}{2}(1 + |\alpha(\theta_x, \mu)|).$$

Since for even polynomial degrees p_t the function $\alpha(\theta_x, \mu) = R(-\mu\beta(\theta_x))$ is monotonically decreasing with respect to $\beta(\theta_x)$, the supremum is obtained for $\beta(\theta_x) = 3$ since $\beta(\theta_x) \in [3, 12]$ for $\theta_x \in [\frac{\pi}{2}, \pi]$. This implies that $\theta_x^* = \frac{\pi}{2}$ and we obtain the statement of the lemma with

$$\begin{aligned}\sup_{\substack{\theta_t \in [0,\pi] \\ \theta_x \in [\frac{\pi}{2}, \pi]}} \hat{\mathcal{S}}(\omega_t^*, \alpha(\theta_x, \mu)), \theta_t) = \hat{\mathcal{S}}(\omega_t^*, \alpha(\theta_x^*, \mu), \theta_t^*) &= \frac{1}{2}(1 + |\alpha(\theta_x^*, \mu)|) \\ &= \frac{1}{2}(1 + R(-3\mu)).\end{aligned}$$

■

Remark 4.3.15. *Lemma 4.3.14 is only proven for even polynomial degrees, but the statement of this lemma is also true for odd polynomial degrees p_t. Only the proof gets more complicated, since the Padé approximation $R(z)$, $z \leq 0$ is not monotonically decreasing for odd polynomial degrees.*

Remark 4.3.16. *In view of Lemma 4.3.14 we obtain a good smoothing behaviour for the high frequencies in space $\theta_x \in \Theta_{L_x}^{\text{high}}$, i.e. $\mu_S^{\text{f}} \leq \frac{1}{\sqrt{2}}$, if the discretization parameter μ is large enough, i.e.*

$$\mu \geq \mu_{p_t}^* \quad \text{with} \quad R(-3\mu_{p_t}^*) = \sqrt{2} - 1. \tag{4.35}$$

Hence we are able to compute the critical discretization parameter $\mu_{p_t}^*$ with respect to the polynomial degree p_t

$$\begin{aligned}\mu_0^* &= \frac{\sqrt{2}}{3} \approx 0.4714045208, \\ \mu_1^* &= \frac{1}{3}(-3 - \sqrt{2} + \sqrt{11 + 12\sqrt{2}}) \approx 0.2915022565, \\ \mu_2^* &\approx 0.2938105446, \\ \mu_3^* &\approx 0.2937911168, \\ \mu_\infty^* &\approx 0.2937911957.\end{aligned}$$

To compute the critical discretization parameter μ_∞^* we used the fact, that the $(p_t, p_t + 1)$ subdiagonal Padé approximation $R(z)$ converges to the exponential function e^z for $z \leq 0$ as $p_t \to \infty$.

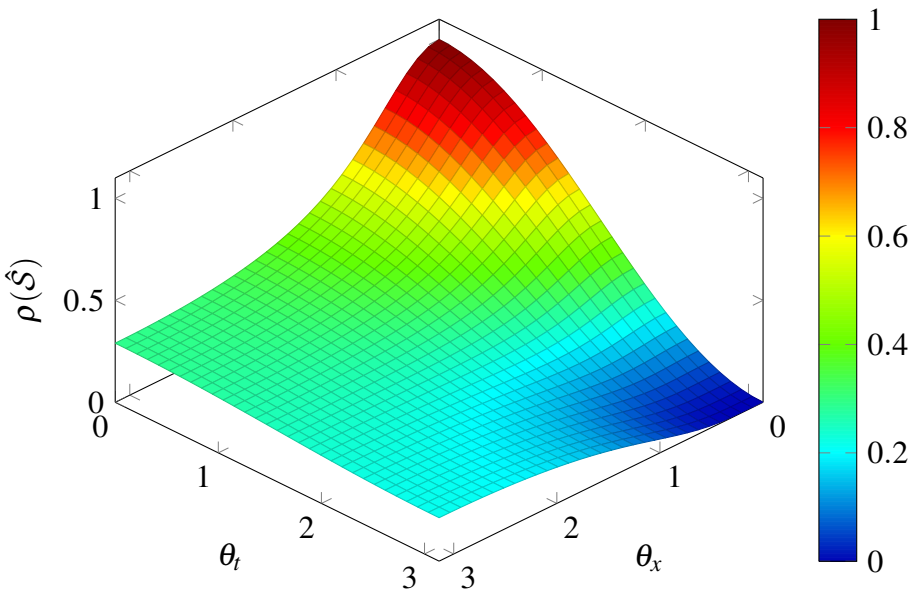

Figure 4.13: Smoothing factor $\hat{\mathcal{S}}(\omega_t^*, \alpha(\theta_x, \mu), \theta_t)^2$ for $\theta_x, \theta_t \in [0, \pi]$ with the discretization parameter $\mu = 1$ and $p_t = 0$.

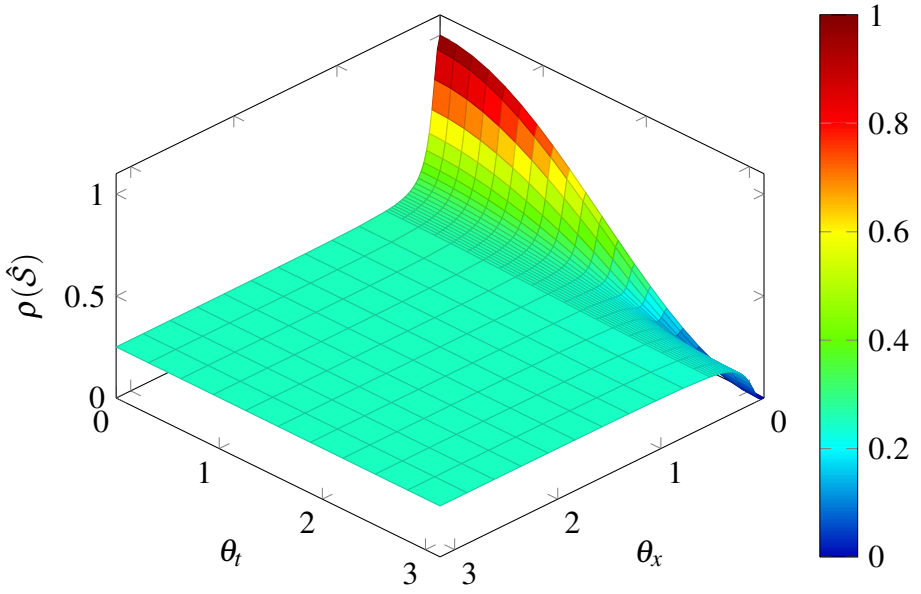

Figure 4.14: Smoothing factor $\hat{\mathcal{S}}(\omega_t^*, \alpha(\theta_x, \mu), \theta_t)^2$ for $\theta_x, \theta_t \in [0, \pi]$ with the discretization parameter $\mu = 100$ and $p_t = 0$.

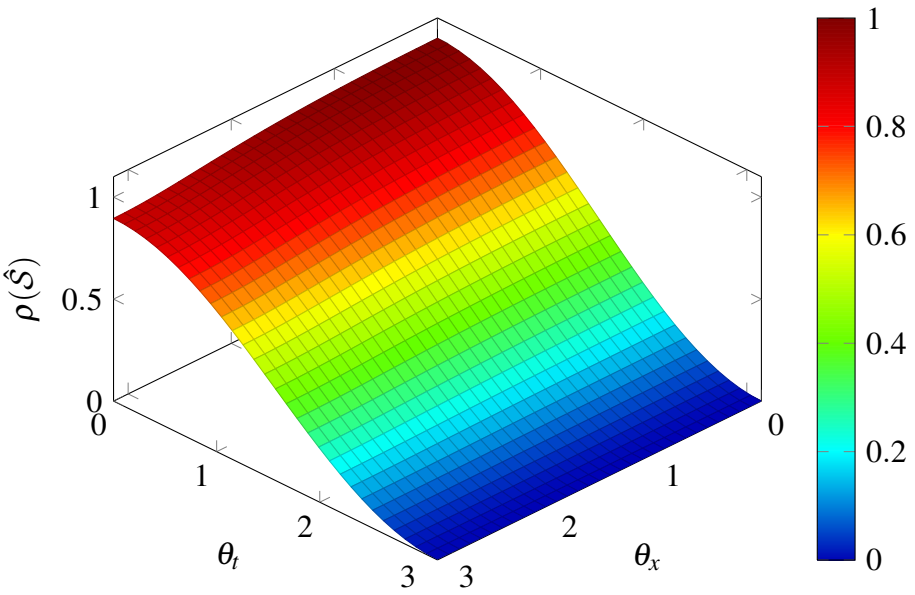

Figure 4.15: Smoothing factor $\hat{\mathcal{S}}(\omega_t^*, \alpha(\theta_x, \mu), \theta_t)^2$ for $\theta_x, \theta_t \in [0, \pi]$ with the discretization parameter $\mu = 0.01$ and $p_t = 0$.

Remark 4.3.17. *Lemma 4.3.13 shows, that for all frequencies* $(\theta_x, \theta_t) \in \Theta_{L_x, L_t}$ *the following bound holds true*

$$\hat{\mathcal{S}}(\omega_t^*, \alpha(\theta_x, \mu)), \theta_t) \leq \frac{1}{2}(1 + |R(-\beta(\theta_x)\mu)|) \leq 1.$$

Only for $\theta_x = 0$ *we have that* $\beta(\theta_x) = 0$, *which implies* $R(-\beta(\theta_x)\mu)) = 1$. *Hence if the discretization parameter* $\mu = \tau_L h_L^{-2}$ *is large enough we have that*

$$|R(-\beta(\theta_x)\mu)| \approx 0$$

for almost all frequencies $\theta_x \in \Theta_{L_x}$, *which implies a good smoothing behaviour for almost all frequencies, see also Figure 4.13–4.15. Only the frequencies* $\theta_x \in \Theta_{L_x}$ *which are close to zero imply* $\hat{\mathcal{S}}(\omega_t^*, \alpha(\theta_x, \mu)), \theta_t) \approx 1$. *Hence for a large discretization parameter* μ *the smoother itself is almost a good iterative solver, only the frequencies* $\theta_x \in \Theta_{L_x}$ *which are close to zero, i.e. very few low frequencies* $\theta_x \in \Theta_{L_x}^{\text{low}}$, *spoil this effect. To obtain also a perfect solver for a large discretization parameter* μ *we can simply apply a correction step after one damped block Jacobi iteration by restricting the defect in space several times until we arrive at a very coarse problem. For this small problem one can solve the coarse correction exactly by solving these small problems forward in time. Afterwards we correct the solution by prolongating the coarse corrections back to the fine space-grids.*

4.3.2 Two-grid analysis

In this subsection we study the convergence behaviour of the two-grid cycle. The iteration matrices for the two-grid cycles with respect to semi-coarsening and full space-time coarsening are given by

$$\mathcal{M}^{\mathrm{s}}_{\tau_L,h_L} := \mathcal{S}^{\nu_2}_{\tau_L,h_L}\left[I - \mathcal{P}^{L_x,L_t}_{\mathrm{s}}\left(\mathcal{L}_{2\tau_L,h_L}\right)^{-1}\mathcal{R}^{L_x,L_t}_{\mathrm{s}}\mathcal{L}_{\tau_L,h_L}\right]\mathcal{S}^{\nu_1}_{\tau_L,h_L},$$
$$\mathcal{M}^{\mathrm{f}}_{\tau_L,h_L} := \mathcal{S}^{\nu_2}_{\tau_L,h_L}\left[I - \mathcal{P}^{L_x,L_t}_{\mathrm{f}}\left(\mathcal{L}_{2\tau_L,2h_L}\right)^{-1}\mathcal{R}^{L_x,L_t}_{\mathrm{f}}\mathcal{L}_{\tau_L,h_L}\right]\mathcal{S}^{\nu_1}_{\tau_L,h_L},$$

with the restriction and prolongation matrices

$$\mathcal{R}^{L_x,L_t}_{\mathrm{s}} := I_{N_{L_x}} \otimes \mathcal{R}^{L_t}, \qquad \mathcal{R}^{L_x,L_t}_{\mathrm{f}} := \mathcal{R}^{L_x}_{x} \otimes \mathcal{R}^{L_t},$$
$$\mathcal{P}^{L_x,L_t}_{\mathrm{s}} := I_{N_{L_x}} \otimes \mathcal{P}^{L_t}, \qquad \mathcal{P}^{L_x,L_t}_{\mathrm{f}} := \mathcal{P}^{L_x}_{x} \otimes \mathcal{P}^{L_t}.$$

The restriction and prolongation matrices with respect to time, i.e. $\mathcal{R}^{L_t}$ and $\mathcal{P}^{L_t}$ are given by (4.27) and (4.28). Further, for the one dimensional case, the restriction and prolongation matrices with respect to space are given by

$$\mathcal{R}^{L_x}_{x} := \frac{1}{2}\begin{pmatrix} 2 & 1 & & & & & \\ & 1 & 2 & 1 & & & \\ & & \ddots & \ddots & \ddots & & \\ & & & 1 & 2 & 1 & \\ & & & & & 1 & 2 \end{pmatrix} \in \mathbb{R}^{N_{L_x}\times N_{L_x-1}}, \tag{4.36}$$

$$\mathcal{P}^{L_x}_{x} := (\mathcal{R}^{L_x}_{x})^{\top} \in \mathbb{R}^{N_{L_x-1}\times N_{L_x}}. \tag{4.37}$$

To analyze the two-grid iteration matrices $\mathcal{M}^{\mathrm{s}}_{\tau_L,h_L}$ and $\mathcal{M}^{\mathrm{f}}_{\tau_L,h_L}$ we need the following lemma.

Lemma 4.3.18. *Let $\boldsymbol{u} = (\boldsymbol{u}_1, \boldsymbol{u}_2, \ldots, \boldsymbol{u}_{N_{L_t}})^{\top} \in \mathbb{R}^{N_t N_{L_x} N_{L_t}}$ for $N_t, N_{L_x}, N_{L_t} \in \mathbb{N}$ where we assume that N_{L_x} and N_{L_t} are even numbers. Furthermore we assume that*

$$\boldsymbol{u}_n \in \mathbb{R}^{N_t N_{L_x}} \qquad \text{and} \qquad \boldsymbol{u}_{n,r} \in \mathbb{R}^{N_t}$$

for $n = 1,\ldots,N_{L_t}$ and $r = 1,\ldots,N_{L_x}$. Then the vector $\boldsymbol{u}$ can be written as

$$\boldsymbol{u} = \sum_{(\theta_x,\theta_t)\in\Theta^{\mathrm{low,f}}_{L_x,L_t}} \big[\boldsymbol{\psi}^{L_x,L_t}(\theta_x,\theta_t) + \boldsymbol{\psi}^{L_x,L_t}(\gamma(\theta_x),\theta_t) + \boldsymbol{\psi}^{L_x,L_t}(\theta_x,\gamma(\theta_t)) + \boldsymbol{\psi}^{L_x,L_t}(\gamma(\theta_x),\gamma(\theta_t))\big],$$

with the shifting operator

$$\gamma(\theta) := \theta - \mathrm{sign}(\theta)\pi$$

and the vector $\boldsymbol{\psi}^{L_x,L_t}(\theta_x,\theta_t) \in \mathbb{C}^{N_t N_{L_x} N_{L_t}}$ defined as in Lemma 4.3.1.

Proof. Using Lemma 4.3.1 and Lemma 4.2.30 results in the statement of this lemma with

$$\begin{aligned}
\boldsymbol{u} &= \sum_{\theta_x\in\Theta_{L_x}}\sum_{\theta_t\in\Theta_{L_t}} \boldsymbol{\psi}^{L_x,L_t}(\theta_x,\theta_t)\\
&= \sum_{\theta_x\in\Theta_{L_x}^{\text{low}}}\sum_{\theta_t\in\Theta_{L_t}^{\text{low}}} \boldsymbol{\psi}^{L_x,L_t}(\theta_x,\theta_t) + \sum_{\theta_x\in\Theta_{L_x}^{\text{high}}}\sum_{\theta_t\in\Theta_{L_t}^{\text{low}}} \boldsymbol{\psi}^{L_x,L_t}(\theta_x,\theta_t)\\
&\quad + \sum_{\theta_x\in\Theta_{L_x}^{\text{low}}}\sum_{\theta_t\in\Theta_{L_t}^{\text{high}}} \boldsymbol{\psi}^{L_x,L_t}(\theta_x,\theta_t) + \sum_{\theta_x\in\Theta_{L_x}^{\text{high}}}\sum_{\theta_t\in\Theta_{L_t}^{\text{high}}} \boldsymbol{\psi}^{L_x,L_t}(\theta_x,\theta_t)\\
&= \sum_{(\theta_x,\theta_t)\in\Theta_{L_x,L_t}^{\text{low,f}}} \big[\boldsymbol{\psi}^{L_x,L_t}(\theta_x,\theta_t) + \boldsymbol{\psi}^{L_x,L_t}(\gamma(\theta_x),\theta_t)\\
&\qquad\qquad + \boldsymbol{\psi}^{L_x,L_t}(\theta_x,\gamma(\theta_t)) + \boldsymbol{\psi}^{L_x,L_t}(\gamma(\theta_x),\gamma(\theta_t))\big].
\end{aligned}$$

■

Lemma 4.3.18 motivates the following definition.

Definition 4.3.19 (Space of harmonics)**.** *For $N_t, N_{L_x}, N_{L_t} \in \mathbb{N}$ and the frequencies $(\theta_x,\theta_t) \in \Theta_{L_x,L_t}^{\text{low,f}}$ let the vector $\boldsymbol{\Phi}^{L_x,L_t}(\theta_x,\theta_t) \in \mathbb{C}^{N_t N_{L_x} N_{L_t}}$ be defined as in Lemma 4.3.1. Then we define the linear space of harmonics with frequencies (θ_x,θ_t) as*

$$\begin{aligned}
\mathcal{E}_{L_x,L_t}(\theta_x,\theta_t) &:= \operatorname{span}\big\{\boldsymbol{\Phi}^{L_x,L_t}(\theta_x,\theta_t), \boldsymbol{\Phi}^{L_x,L_t}(\gamma(\theta_x),\theta_t),\\
&\qquad \boldsymbol{\Phi}^{L_x,L_t}(\theta_x,\gamma(\theta_t)), \boldsymbol{\Phi}^{L_x,L_t}(\gamma(\theta_x),\gamma(\theta_t))\big\}\\
&= \big\{\boldsymbol{\psi}^{L_x,L_t}(\theta_x,\theta_t) \in \mathbb{C}^{N_t N_{L_x} N_{L_t}} :\\
&\quad \boldsymbol{\psi}^{L_x,L_t}_{n,r}(\theta_x,\theta_t) = U_1 \boldsymbol{\Phi}^{L_x,L_t}_{n,r}(\theta_x,\theta_t) + U_2 \boldsymbol{\Phi}^{L_x,L_t}_{n,r}(\gamma(\theta_x),\theta_t)\\
&\qquad + U_3 \boldsymbol{\Phi}^{L_x,L_t}_{n,r}(\theta_x,\gamma(\theta_t)) + U_4 \boldsymbol{\Phi}^{L_x,L_t}_{n,r}(\gamma(\theta_x),\gamma(\theta_t)),\\
&\quad \text{for all } n = 1,\dots,N_{L_t}, r = 1,\dots,N_{L_x} \text{ and } U_1,U_2,U_3,U_4 \in \mathbb{C}^{N_t\times N_t}\big\}.
\end{aligned}$$

Under the assumption of periodic solutions, see (4.32), Lemma 4.3.4 implies the following mapping property for the system matrix $\mathcal{L}_{\tau_L,h_L}$ for all frequencies $(\theta_x,\theta_t) \in \Theta_{L_x,L_t}^{\text{low,f}}$

$$\begin{aligned}
&\mathcal{L}_{\tau_L,h_L} : \mathcal{E}_{L_x,L_t}(\theta_x,\theta_t) \to \mathcal{E}_{L_x,L_t}(\theta_x,\theta_t)\\
&\qquad \begin{pmatrix} U_1\\ U_2\\ U_3\\ U_4 \end{pmatrix} \mapsto \begin{pmatrix} \hat{\mathcal{L}}_{\tau_L,h_L}(\theta_x,\theta_t)U_1\\ \hat{\mathcal{L}}_{\tau_L,h_L}(\gamma(\theta_x),\theta_t)U_2\\ \hat{\mathcal{L}}_{\tau_L,h_L}(\theta_x,\gamma(\theta_t))U_3\\ \hat{\mathcal{L}}_{\tau_L,h_L}(\gamma(\theta_x),\gamma(\theta_t))U_4 \end{pmatrix} =: \widetilde{\mathcal{L}}_{\tau_L,h_L}(\theta_x,\theta_t) \begin{pmatrix} U_1\\ U_2\\ U_3\\ U_4 \end{pmatrix},
\end{aligned} \tag{4.38}$$

where $\widetilde{\mathcal{L}}_{\tau_L,h_L}(\theta_x,\theta_t) \in \mathbb{C}^{4N_t \times 4N_t}$ is a block diagonal matrix. With the same arguments we obtain with Lemma 4.3.6 the mapping property for the smoother for all frequencies $(\theta_x,\theta_t) \in \Theta^{\text{low,f}}_{L_x,L_t}$

$$\begin{aligned}
&\mathcal{S}^{\nu}_{\tau_L,h_L} : \mathcal{E}_{L_x,L_t}(\theta_x,\theta_t) \to \mathcal{E}_{L_x,L_t}(\theta_x,\theta_t) \\
&\qquad \begin{pmatrix} U_1 \\ U_2 \\ U_3 \\ U_4 \end{pmatrix} \mapsto \begin{pmatrix} (\hat{\mathcal{S}}_{\tau_L,h_L}(\theta_x,\theta_t))^{\nu} U_1 \\ (\hat{\mathcal{S}}_{\tau_L,h_L}(\gamma(\theta_x),\theta_t))^{\nu} U_2 \\ (\hat{\mathcal{S}}_{\tau_L,h_L}(\theta_x,\gamma(\theta_t)))^{\nu} U_3 \\ (\hat{\mathcal{S}}_{\tau_L,h_L}(\gamma(\theta_x),\gamma(\theta_t)))^{\nu} U_4 \end{pmatrix} =: \left(\widetilde{\mathcal{S}}_{\tau_L,h_L}(\theta_x,\theta_t)\right)^{\nu} \begin{pmatrix} U_1 \\ U_2 \\ U_3 \\ U_4 \end{pmatrix},
\end{aligned} \tag{4.39}$$

with the block diagonal matrix $\widetilde{\mathcal{S}}_{\tau_L,h_L}(\theta_x,\theta_t) \in \mathbb{C}^{4N_t \times 4N_t}$.

To analyze the two-grid cycle on the space of harmonics $\mathcal{E}_{L_x,L_t}(\theta_x,\theta_t)$ for frequencies $(\theta_x,\theta_t) \in \Theta^{\text{low,f}}_{L_x,L_t}$ we further have to investigate the mapping properties of the restriction and prolongation operators for the two different coarsening strategies $\mathcal{R}^{L_x,L_t}_{\text{s}}, \mathcal{R}^{L_x,L_t}_{\text{f}}$ and $\mathcal{P}^{L_x,L_t}_{\text{s}}, \mathcal{P}^{L_x,L_t}_{\text{f}}$. The next lemma shows the mapping properties for the restriction and prolongation operators with respect to space.

Lemma 4.3.20. *Let $\mathcal{R}^{L_x}_x$ and $\mathcal{P}^{L_x}_x$ be the restriction and prolongation matrices as defined in (4.36). For $\theta_x \in \Theta^{\text{low}}_{L_x}$ let $\boldsymbol{\varphi}^{L_x}(\theta_x) \in \mathbb{C}^{N_{L_x}}$ and $\boldsymbol{\varphi}^{L_x-1}(2\theta_x) \in \mathbb{C}^{N_{L_x-1}}$ be defined as in Theorem 4.2.8. Then there holds*

$$\left(\mathcal{R}^{L_x}_x \boldsymbol{\varphi}^{L_x}(\theta_x)\right)[r] = \hat{\mathcal{R}}_x(\theta_x)\boldsymbol{\varphi}^{L_x-1}(2\theta_x)[r],$$

for $r = 2,\dots,N_{L_x-1}-1$ with the Fourier symbol $\hat{\mathcal{R}}_x(\theta_x) := 1+\cos(\theta_x)$. For the prolongation operator we further have

$$\left(\mathcal{P}^{L_x}_x \boldsymbol{\varphi}^{L_x-1}(2\theta_x)\right)[s] = \left(\hat{\mathcal{P}}_x(\theta_x)\boldsymbol{\varphi}^{L_x}(\theta_x) + \hat{\mathcal{P}}_x(\gamma(\theta_x))\boldsymbol{\varphi}^{L_x}(\gamma(\theta_x))\right)[s],$$

for $s = 2,\dots,N_{L_x}-1$ with the Fourier symbol $\hat{\mathcal{P}}_x(\theta_x) := \frac{1}{2}\hat{\mathcal{R}}_x(\theta_x)$.

Proof. To prove this lemma one can use the same techniques as used in the proofs of Lemma 4.2.34 and Lemma 4.2.35, or see [99] for example. ∎

Definition 4.3.21. *For $N_t, N_{L_x}, N_{L_t} \in \mathbb{N}$ and the frequencies $(\theta_x,\theta_t) \in \Theta^{\text{low,f}}_{L_x,L_t}$ let the vector $\boldsymbol{\Phi}^{L_x,L_t-1}(\theta_x,\theta_t) \in \mathbb{C}^{N_t N_{L_x} N_{L_t-1}}$ be defined as in Lemma 4.3.1. Then we define the linear space with frequencies $(\theta_x,2\theta_t)$ as*

$$\begin{aligned}
\Psi_{L_x,L_t-1}(\theta_x,2\theta_t) &:= \operatorname{span}\left\{\boldsymbol{\Phi}^{L_x,L_t-1}(\theta_x,2\theta_t), \boldsymbol{\Phi}^{L_x,L_t-1}(\gamma(\theta_x),2\theta_t)\right\} \\
&= \Big\{\boldsymbol{\psi}^{L_x,L_t-1}(\theta_x,2\theta_t) \in \mathbb{C}^{N_t N_{L_x} N_{L_t-1}} : \\
&\qquad \boldsymbol{\psi}^{L_x,L_t-1}_{n,r}(\theta_x,2\theta_t) = U_1 \boldsymbol{\Phi}^{L_x,L_t-1}_{n,r}(\theta_x,2\theta_t) + U_2 \boldsymbol{\Phi}^{L_x,L_t-1}_{n,r}(\gamma(\theta_x),2\theta_t) \\
&\qquad\qquad \text{for all } n = 1,\dots,N_{L_t}, r = 1,\dots,N_{L_x} \text{ and } U_1,U_2 \in \mathbb{C}^{N_t \times N_t}\Big\}.
\end{aligned}$$

For the semi-coarsening case the next lemma shows the mapping property for the restriction operator $\mathcal{R}_{\mathrm{s}}^{L_x,L_t}$.

Lemma 4.3.22. *The restriction operator $\mathcal{R}_{\mathrm{s}}^{L_x,L_t}$ fulfils the following mapping property*

$$\mathcal{R}_{\mathrm{s}}^{L_x,L_t} : \mathcal{E}_{L_x,L_t}(\theta_x,\theta_t) \to \Psi_{L_x,L_t-1}(\theta_x,2\theta_t)$$

with the mapping

$$\begin{pmatrix} U_1 \\ U_2 \\ U_3 \\ U_4 \end{pmatrix} \mapsto \widetilde{\mathcal{R}}_{\mathrm{s}}(\theta_t) \begin{pmatrix} U_1 \\ U_2 \\ U_3 \\ U_4 \end{pmatrix}$$

and the matrix

$$\widetilde{\mathcal{R}}_{\mathrm{s}}(\theta_t) := \begin{pmatrix} \hat{\mathcal{R}}(\theta_t) & 0 & \hat{\mathcal{R}}(\gamma(\theta_t)) & 0 \\ 0 & \hat{\mathcal{R}}(\theta_t) & 0 & \hat{\mathcal{R}}(\gamma(\theta_t)) \end{pmatrix}$$

with the Fourier symbol $\hat{\mathcal{R}}(\theta_t) \in \mathbb{C}^{N_t \times N_t}$ as defined in Lemma 4.2.34.

Proof. Let $\boldsymbol{\Phi}^{L_x,L_t}(\theta_x,\theta_t) \in \Psi_{L_x,L_t}(\theta_x,\theta_t)$ and $\boldsymbol{\Phi}^{L_x,L_t-1}(\theta_x,2\theta_t) \in \Psi_{L_x,L_t-1}(\theta_x,2\theta_t)$ be defined as in Lemma 4.3.1. Then for $n = 1,\ldots,N_{L_t-1}$ and $r = 1,\ldots,N_{L_x}$ we have

$$\begin{aligned} \left(\mathcal{R}_{\mathrm{s}}^{L_x,L_t}\boldsymbol{\Phi}^{L_x,L_t}(\theta_x,\theta_t)\right)_{n,r} &= \sum_{s=1}^{N_{L_x}} \sum_{m=1}^{N_{L_t}} I_{N_{L_x}}[r,s]\mathcal{R}^{L_t}[n,m]\boldsymbol{\Phi}_{m,s}^{L_x,L_t}(\theta_x,\theta_t) \\ &= \boldsymbol{\varphi}^{L_x}(\theta_x)[r] \sum_{m=1}^{N_{L_t}} \mathcal{R}^{L_t}[n,m]\boldsymbol{\Phi}_m^{L_t}(\theta_t) \\ &= \boldsymbol{\varphi}^{L_x}(\theta_x)[r] \left(\mathcal{R}^{L_t}\boldsymbol{\Phi}^{L_t}(\theta_t)\right)_n. \end{aligned}$$

Using Lemma 4.2.34 leads to

$$\begin{aligned} &= \hat{\mathcal{R}}(\theta_t)\boldsymbol{\Phi}_n^{L_t-1}(2\theta_t)\boldsymbol{\varphi}^{L_x}(\theta_x)[r] \\ &= \hat{\mathcal{R}}(\theta_t)\boldsymbol{\Phi}_{n,r}^{L_x,L_t-1}(\theta_x,2\theta_t). \end{aligned}$$

Applying this result on the vector $\boldsymbol{\psi}^{L_x,L_t}(\theta_x,\theta_t) \in \mathcal{E}_{L_x,L_t}(\theta_x,\theta_t)$ with $(\theta_x,\theta_t) \in \Theta_{L_x,L_t}^{\mathrm{f}}$ results in

$$\begin{aligned} \left(\mathcal{R}_{\mathrm{s}}^{L_x,L_t}\boldsymbol{\psi}^{L_x,L_t}(\theta_x,\theta_t)\right)_{n,r} = {} & \hat{\mathcal{R}}(\theta_t)U_1\boldsymbol{\Phi}_{n,r}^{L_x,L_t-1}(\theta_x,2\theta_t) \\ & + \hat{\mathcal{R}}(\theta_t)U_2\boldsymbol{\Phi}_{n,r}^{L_x,L_t-1}(\gamma(\theta_x),2\theta_t) \\ & + \hat{\mathcal{R}}(\gamma(\theta_t))U_3\boldsymbol{\Phi}_{n,r}^{L_x,L_t-1}(\theta_x,2\gamma(\theta_t)) \end{aligned}$$

$$+\hat{\mathcal{R}}(\gamma(\theta_t))U_4\boldsymbol{\Phi}_{n,r}^{L_x,L_t-1}(\gamma(\theta_x),2\gamma(\theta_t)).$$

Since $\boldsymbol{\Phi}_{n,r}^{L_x,L_t-1}(\theta_x,2\gamma(\theta_t)) = \boldsymbol{\Phi}_{n,r}^{L_x,L_t-1}(\theta_x,2\theta_t)$ we further obtain

$$\begin{aligned}&= \left[\hat{\mathcal{R}}(\theta_t)U_1+\hat{\mathcal{R}}(\gamma(\theta_t))U_3\right]\boldsymbol{\Phi}_{n,r}^{L_x,L_t-1}(\theta_x,2\theta_t)\\&\quad+\left[\hat{\mathcal{R}}(\theta_t)U_2+\hat{\mathcal{R}}(\gamma(\theta_t))U_4\right]\boldsymbol{\Phi}_{n,r}^{L_x,L_t-1}(\gamma(\theta_x),2\theta_t),\end{aligned}$$

which completes the proof. ∎

Lemma 4.3.23. *Under the assumptions of periodic solutions (4.32) the following mapping property for the restriction operator holds true*

$$\mathcal{R}_{\mathrm{f}}^{L_x,L_t} : \mathcal{E}_{L_x,L_t}(\theta_x,\theta_t) \to \Psi_{L_x-1,L_t-1}(2\theta_x,2\theta_t)$$

with the mapping

$$\begin{pmatrix}U_1\\U_2\\U_3\\U_4\end{pmatrix} \mapsto \widetilde{\mathcal{R}}_{\mathrm{f}}(\theta_x,\theta_t)\begin{pmatrix}U_1\\U_2\\U_3\\U_4\end{pmatrix}$$

and the matrix

$$\widetilde{\mathcal{R}}_{\mathrm{f}}(\theta_x,\theta_t) := \begin{pmatrix}\hat{\mathcal{R}}(\theta_x,\theta_t) & \hat{\mathcal{R}}(\gamma(\theta_x),\theta_t) & \hat{\mathcal{R}}(\theta_x,\gamma(\theta_t)) & \hat{\mathcal{R}}(\gamma(\theta_x),\gamma(\theta_t))\end{pmatrix}$$

with the Fourier symbol

$$\hat{\mathcal{R}}(\theta_x,\theta_t) := \hat{\mathcal{R}}_x(\theta_x)\hat{\mathcal{R}}(\theta_t) \in \mathbb{C}^{N_t\times N_t},$$

where $\hat{\mathcal{R}}_x(\theta_x)\in\mathbb{C}$ is defined as in Lemma 4.3.20.

Proof. For the frequencies $(\theta_x,\theta_t)\in\Theta_{L_x,L_t}^{\mathrm{low}}$ let $\boldsymbol{\Phi}^{L_x,L_t}(\theta_x,\theta_t)\in\Psi_{L_x,L_t}(\theta_x,\theta_t)$ and $\boldsymbol{\Phi}^{L_x-1,L_t-1}(2\theta_x,2\theta_t)\in\Psi_{L_x-1,L_t-1}(2\theta_x,2\theta_t)$ be defined as in Lemma 4.3.1. Then for $n=1,\dots,N_{L_t-1}$ and $r=2,\dots,N_{L_x-1}-1$ we have

$$\begin{aligned}\left(\mathcal{R}_{\mathrm{f}}^{L_x,L_t}\boldsymbol{\Phi}^{L_x,L_t}(\theta_x,\theta_t)\right)_{n,r} &= \sum_{s=1}^{N_{L_x}}\sum_{m=1}^{N_{L_t}}\mathcal{R}_x^{L_x}[r,s]\mathcal{R}^{L_t}[n,m]\boldsymbol{\Phi}_{m,s}^{L_x,L_t}(\theta_x,\theta_t)\\&= \left(\sum_{s=1}^{N_{L_x}}\mathcal{R}_x^{L_x}[r,s]\boldsymbol{\varphi}^{L_x}(\theta_x)[r]\right)\left(\sum_{m=1}^{N_{L_t}}\mathcal{R}^{L_t}[n,m]\boldsymbol{\Phi}_m^{L_t}(\theta_t)\right)\\&= \left(\mathcal{R}_x^{L_x}\boldsymbol{\varphi}^{L_x}(\theta_x)\right)[r]\left(\mathcal{R}^{L_t}\boldsymbol{\Phi}^{L_t}(\theta_t)\right)_n.\end{aligned}$$

Applying Lemma 4.3.20 and Lemma 4.2.34 leads to

$$= \hat{\mathcal{R}}_x(\theta_x)\hat{\mathcal{R}}(\theta_t)\boldsymbol{\Phi}_n^{L_t-1}(2\theta_t)\boldsymbol{\varphi}^{L_x-1}(2\theta_x)[r]$$

$$= \hat{\mathcal{R}}(\theta_x,\theta_t)\boldsymbol{\Phi}_{n,r}^{L_x-1,L_t-1}(2\theta_x,2\theta_t).$$

Using this result on the vector $\boldsymbol{\psi}^{L_x,L_t}(\theta_x,\theta_t) \in \mathcal{E}_{L_x,L_t}(\theta_x,\theta_t)$ with $(\theta_x,\theta_t) \in \Theta^{\mathrm{f}}_{L_x,L_t}$ results in

$$\begin{aligned}\left(\mathcal{R}_{\mathrm{f}}^{L_x,L_t}\boldsymbol{\psi}^{L_x,L_t}(\theta_x,\theta_t)\right)_{n,r} &= \hat{\mathcal{R}}(\theta_x,\theta_t)U_1\boldsymbol{\Phi}_{n,r}^{L_x-1,L_t-1}(2\theta_x,2\theta_t)\\ &\quad+\hat{\mathcal{R}}(\gamma(\theta_x),\theta_t)U_2\boldsymbol{\Phi}_{n,r}^{L_x-1,L_t-1}(2\gamma(\theta_x),2\theta_t)\\ &\quad+\hat{\mathcal{R}}(\theta_x,\gamma(\theta_t))U_3\boldsymbol{\Phi}_{n,r}^{L_x-1,L_t-1}(2\theta_x,2\gamma(\theta_t))\\ &\quad+\hat{\mathcal{R}}(\gamma(\theta_x),\gamma(\theta_t))U_4\boldsymbol{\Phi}_{n,r}^{L_x-1,L_t-1}(2\gamma(\theta_x),2\gamma(\theta_t)).\end{aligned}$$

With the relations

$$\begin{aligned}\boldsymbol{\Phi}^{L_x-1,L_t-1}(2\theta_x,2\theta_t) &= \boldsymbol{\Phi}^{L_x-1,L_t-1}(2\gamma(\theta_x),2\theta_t)\\ &= \boldsymbol{\Phi}_{n,r}^{L_x-1,L_t-1}(2\theta_x,2\gamma(\theta_t))\\ &= \boldsymbol{\Phi}_{n,r}^{L_x-1,L_t-1}(2\gamma(\theta_x),2\gamma(\theta_t))\end{aligned}$$

we obtain the statement of this lemma with

$$\begin{aligned}\left(\mathcal{R}_{\mathrm{f}}^{L_x,L_t}\boldsymbol{\psi}^{L_x,L_t}(\theta_x,\theta_t)\right)_{n,r} &= \big[\hat{\mathcal{R}}(\theta_x,\theta_t)U_1\\ &\quad+\hat{\mathcal{R}}(\gamma(\theta_x),\theta_t)U_2\\ &\quad+\hat{\mathcal{R}}(\theta_x,\gamma(\theta_t))U_3\\ &\quad+\hat{\mathcal{R}}(\gamma(\theta_x),\gamma(\theta_t))U_4\big]\boldsymbol{\Phi}_{n,r}^{L_x-1,L_t-1}(2\theta_x,2\theta_t).\end{aligned}$$

■

With the next lemmata we will analyze the mapping properties of the prolongation operators $\mathcal{P}_{\mathrm{s}}^{L_x,L_t}$ and $\mathcal{P}_{\mathrm{f}}^{L_x,L_t}$.

Lemma 4.3.24. *For $(\theta_x,\theta_t) \in \Theta^{\mathrm{f}}_{L_x,L_t}$ the prolongation operator $\mathcal{P}_{\mathrm{s}}^{L_x,L_t}$ fulfils the following mapping property*

$$\mathcal{P}_{\mathrm{s}}^{L_x,L_t} : \Psi_{L_x,L_t-1}(\theta_x,2\theta_t) \to \mathcal{E}_{L_x,L_t}(\theta_x,\theta_t)$$

with the mapping

$$\begin{pmatrix}U_1\\U_2\end{pmatrix} \mapsto \begin{pmatrix}\hat{\mathcal{P}}(\theta_t) & 0\\ 0 & \hat{\mathcal{P}}(\theta_t)\\ \hat{\mathcal{P}}(\gamma(\theta_t)) & 0\\ 0 & \hat{\mathcal{P}}(\gamma(\theta_t))\end{pmatrix}\begin{pmatrix}U_1\\U_2\end{pmatrix} =: \widetilde{\mathcal{P}}_{\mathrm{s}}(\theta_t)\begin{pmatrix}U_1\\U_2\end{pmatrix}$$

and the Fourier symbol $\hat{\mathcal{P}}(\theta_t) \in \mathbb{C}^{N_t\times N_t}$ defined as in Lemma 4.2.35.

Proof. Let $\boldsymbol{\psi}^{L_x,L_t-1}(\theta_x,2\theta_t) \in \boldsymbol{\Psi}_{L_x,L_t-1}(\theta_x,2\theta_t)$ for $(\theta_x,\theta_t) \in \Theta^{\mathrm{f}}_{L_x,L_t}$. Then we have for $n=1,\dots,N_{L_t}$ and $r=1,\dots,N_{L_x}$ that

$$\begin{aligned}
\left(\mathcal{P}^{L_x,L_t}_{\mathrm{s}}\boldsymbol{\psi}^{L_x,L_t-1}(\theta_x,2\theta_t)\right)_{n,r} &= \sum_{s=1}^{N_{L_x}}\sum_{m=1}^{N_{L_t}} I_{N_{L_x}}[r,s]\mathcal{P}^{L_t}[n,m]\boldsymbol{\psi}^{L_x,L_t-1}_{m,s}(\theta_x,2\theta_t)\\
&= \sum_{m=1}^{N_{L_t}} \mathcal{P}^{L_t}[n,m]\boldsymbol{\psi}^{L_x,L_t-1}_{m,r}(\theta_x,2\theta_t)\\
&= \sum_{m=1}^{N_{L_t}} \mathcal{P}^{L_t}[n,m]\Big[(\boldsymbol{\varphi}^{L_x}(\theta_x)[r]U_1)\boldsymbol{\Phi}^{L_t-1}_m(2\theta_t)\\
&\qquad + (\boldsymbol{\varphi}^{L_x}(\gamma(\theta_x))[r]U_2)\boldsymbol{\Phi}^{L_t-1}_m(2\theta_t)\Big].
\end{aligned}$$

Since $\boldsymbol{\varphi}^{L_x}(\theta_x)[r]U_1 \in \mathbb{C}^{N_t\times N_t}$ and $\boldsymbol{\varphi}^{L_x}(\gamma(\theta_x))[r]U_2 \in \mathbb{C}^{N_t\times N_t}$ we further obtain by applying Lemma 4.2.35 that

$$\begin{aligned}
&= \hat{\mathcal{P}}(\theta_t)(\boldsymbol{\varphi}^{L_x}(\theta_x)[r]U_1)\boldsymbol{\Phi}^{L_t}_n(\theta_t)\\
&\quad + \hat{\mathcal{P}}(\gamma(\theta_t))(\boldsymbol{\varphi}^{L_x}(\theta_x)[r]U_1)\boldsymbol{\Phi}^{L_t}_n(\gamma(\theta_t))\\
&\quad + \hat{\mathcal{P}}(\theta_t)(\boldsymbol{\varphi}^{L_x}(\gamma(\theta_x))[r]U_2)\boldsymbol{\Phi}^{L_t}_n(\theta_t)\\
&\quad + \hat{\mathcal{P}}(\gamma(\theta_t))(\boldsymbol{\varphi}^{L_x}(\gamma(\theta_x))[r]U_2)\boldsymbol{\Phi}^{L_t}_n(\gamma(\theta_t)).
\end{aligned}$$

With the definition of the Fourier mode $\boldsymbol{\Phi}^{L_x,L_t}_{n,r}(\theta_x,\theta_t)$ we get

$$\begin{aligned}
&= \hat{\mathcal{P}}(\theta_t)U_1\boldsymbol{\Phi}^{L_x,L_t}_{n,r}(\theta_x,\theta_t)\\
&\quad + \hat{\mathcal{P}}(\gamma(\theta_t))U_1\boldsymbol{\Phi}^{L_x,L_t}_{n,r}(\theta_x,\gamma(\theta_t))\\
&\quad + \hat{\mathcal{P}}(\theta_t)U_2\boldsymbol{\Phi}^{L_x,L_t}_{n,r}(\gamma(\theta_x),\theta_t)\\
&\quad + \hat{\mathcal{P}}(\gamma(\theta_t))U_2\boldsymbol{\Phi}^{L_x,L_t}_{n,r}(\gamma(\theta_x),\gamma(\theta_t)),
\end{aligned}$$

which completes the proof. ∎

Lemma 4.3.25. *Under the assumptions of periodic solutions (4.32) the following mapping property for the prolongation operator holds true*

$$\mathcal{P}^{L_x,L_t}_{\mathrm{f}} : \Psi_{L_x-1,L_t-1}(2\theta_x,2\theta_t) \to \mathcal{E}_{L_x,L_t}(\theta_x,\theta_t)$$

with the mapping

$$U \mapsto \begin{pmatrix} \hat{\mathcal{P}}(\theta_x,\theta_t)\\ \hat{\mathcal{P}}(\gamma(\theta_x),\theta_t)\\ \hat{\mathcal{P}}(\theta_x,\gamma(\theta_t))\\ \hat{\mathcal{P}}(\gamma(\theta_x),\gamma(\theta_t)) \end{pmatrix} U =: \widetilde{\mathcal{P}}_{\mathrm{f}}(\theta_x,\theta_t)U$$

and the Fourier symbol

$$\hat{\mathcal{P}}(\theta_x,\theta_t) := \hat{\mathcal{P}}_x(\theta_x)\hat{\mathcal{P}}(\theta_t),$$

where $\hat{\mathcal{P}}(\theta_t)$ is defined as in Lemma 4.2.35.

Proof. Let $\psi^{L_x-1,L_t-1}(2\theta_x,2\theta_t) \in \Psi_{L_x-1,L_t-1}(2\theta_x,2\theta_t)$ for $(\theta_x,\theta_t) \in \Theta^{\mathrm{f}}_{L_x,L_t}$. Then we have for $n = 1,\dots,N_{L_t}$ and $r = 2,\dots,N_{L_x}-1$ that

$$\begin{aligned}\left(\mathcal{P}^{L_x,L_t}_{\mathrm{f}}\psi^{L_x-1,L_t-1}(2\theta_x,2\theta_t)\right)_{n,r} &= \sum_{s=1}^{N_{L_x}}\sum_{m=1}^{N_{L_t}} \mathcal{P}^{L_x}_x[r,s]\mathcal{P}^{L_t}[n,m]\psi^{L_x-1,L_t-1}_{m,s}(2\theta_x,2\theta_t)\\ &= \left(\sum_{s=1}^{N_{L_x}} \mathcal{P}^{L_x}_x[r,s]\varphi^{L_x-1}(2\theta_x)[s]\right)\left(\sum_{m=1}^{N_{L_t}} \mathcal{P}^{L_t}[n,m]\Phi^{L_t-1}_m(2\theta_t)\right).\end{aligned}$$

Using Lemma 4.2.35 gives

$$\begin{aligned}&= \left(\hat{\mathcal{P}}_x(\theta_x)\varphi^{L_x}(\theta_x)[r] + \hat{\mathcal{P}}_x(\gamma(\theta_x))\varphi^{L_x}(\gamma(\theta_x))[r]\right)\\ &\qquad\times\left(\hat{\mathcal{P}}(\theta_t)U\Phi^{L_t}_n(\theta_t) + \hat{\mathcal{P}}(\gamma(\theta_t))U\Phi^{L_t}_n(\gamma(\theta_t))\right)\end{aligned}$$

Using the definition of the Fourier mode $\Phi^{L_x,L_t}_{n,r}(\theta_x,\theta_t)$ leads to

$$\begin{aligned}&= \hat{\mathcal{P}}(\theta_x,\theta_t)U\Phi^{L_x,L_t}_{n,r}(\theta_x,\theta_t) + \hat{\mathcal{P}}(\gamma(\theta_x),\theta_t)U\Phi^{L_x,L_t}_{n,r}(\gamma(\theta_x),\theta_t)\\ &\quad + \hat{\mathcal{P}}(\theta_x,\gamma(\theta_t))U\Phi^{L_x,L_t}_{n,r}(\theta_x,\gamma(\theta_t)) + \hat{\mathcal{P}}(\gamma(\theta_x),\gamma(\theta_t))U\Phi^{L_x,L_t}_{n,r}(\gamma(\theta_x),\gamma(\theta_t)),\end{aligned}$$

which completes the proof. ∎

Assuming periodicity in space and time (4.32) we further obtain with Lemma 4.2.37 the mapping property for the coarse grid operator, when semi coarsening with respect to time is applied

$$\begin{aligned}\left(\mathcal{L}_{2\tau_L,h_L}\right)^{-1} : \Psi_{L_x,L_t-1}(\theta_x,2\theta_t) &\to \Psi_{L_x,L_t-1}(\theta_x,2\theta_t)\\ \begin{pmatrix}U_1\\U_2\end{pmatrix} &\mapsto \left(\widetilde{\mathcal{L}}^{\mathrm{s}}_{2\tau_L,h_L}(\theta_x,2\theta_t)\right)^{-1}\begin{pmatrix}U_1\\U_2\end{pmatrix} \in \mathbb{C}^{2N_t\times N_t}\end{aligned} \tag{4.40}$$

with the matrix

$$\left(\widetilde{\mathcal{L}}^{\mathrm{s}}_{2\tau_L,h_L}(\theta_x,2\theta_t)\right)^{-1} := \begin{pmatrix}\left(\hat{\mathcal{L}}_{2\tau_L,h_L}(\theta_x,2\theta_t)\right)^{-1} & 0\\ 0 & \left(\hat{\mathcal{L}}_{2\tau_L,h_L}(\gamma(\theta_x),\theta_t)\right)^{-1}\end{pmatrix} \in \mathbb{C}^{2N_t\times 2N_t}.$$

With respect to full space-time coarsening we further conclude the following mapping property

$$\begin{aligned}\left(\mathcal{L}_{2\tau_L,2h_L}\right)^{-1} : \Psi_{L_x-1,L_t-1}(2\theta_x,2\theta_t) &\to \Psi_{L_x-1,L_t-1}(2\theta_x,2\theta_t)\\ U &\mapsto \left(\widetilde{\mathcal{L}}^{\mathrm{f}}_{2\tau_L,2h_L}(2\theta_x,2\theta_t)\right)^{-1}U \in \mathbb{C}^{N_t\times N_t},\end{aligned} \tag{4.41}$$

with

$$\left(\widetilde{\mathcal{L}}^{\mathrm{f}}_{2\tau_L,2h_L}(2\theta_x,2\theta_t)\right)^{-1} := \left(\hat{\mathcal{L}}_{2\tau_L,2h_L}(2\theta_x,2\theta_t)\right)^{-1} \in \mathbb{C}^{N_t\times N_t}.$$

Now we are able to prove the following theorems.

Theorem 4.3.26. *Let $(\theta_x,\theta_t) \in \Theta^{\mathrm{low,f}}_{L_x,L_t}$. Under the assumptions of periodic solutions (4.32) the following mapping property for the two-grid operator $\mathcal{M}^{\mathrm{s}}_{\tau_L,h_L}$ with respect to semi coarsening in time holds true*

$$\mathcal{M}^{\mathrm{s}}_{\tau_L,h_L} : \mathcal{E}_{L_x,L_t}(\theta_x,\theta_t) \to \mathcal{E}_{L_x,L_t}(\theta_x,\theta_t),$$

with the mapping

$$\begin{pmatrix} U_1 \\ U_2 \\ U_3 \\ U_4 \end{pmatrix} \mapsto \widetilde{\mathcal{M}}^{\mathrm{s}}_{\mu}(\theta_k,\theta_t) \begin{pmatrix} U_1 \\ U_2 \\ U_3 \\ U_4 \end{pmatrix}$$

and the iteration matrix

$$\widetilde{\mathcal{M}}^{\mathrm{s}}_{\mu}(\theta_k,\theta_t) := \left(\widetilde{\mathcal{S}}_{\tau_L,h_L}(\theta_x,\theta_t)\right)^{\nu_2} \widetilde{\mathcal{K}}_{\mathrm{s}}(\theta_x,\theta_t) \left(\widetilde{\mathcal{S}}_{\tau_L,h_L}(\theta_x,\theta_t)\right)^{\nu_1} \in \mathbb{C}^{4N_t\times 4N_t}$$

with

$$\widetilde{\mathcal{K}}_{\mathrm{s}}(\theta_x,\theta_t) := I_{4N_t} - \widetilde{\mathcal{P}}_{\mathrm{s}}(\theta_t) \left(\widetilde{\mathcal{L}}^{\mathrm{s}}_{2\tau_L,h_L}(\theta_x,2\theta_t)\right)^{-1} \widetilde{\mathcal{R}}_{\mathrm{s}}(\theta_t) \widetilde{\mathcal{L}}_{\tau_L,h_L}(\theta_x,\theta_t).$$

Proof. The statement of this theorem follows by using Lemma 4.3.22, Lemma 4.3.24 and the mapping properties (4.38), (4.39) and (4.40). ∎

Theorem 4.3.27. *Let $(\theta_x,\theta_t) \in \Theta^{\mathrm{low,f}}_{L_x,L_t}$. Under the assumptions of periodic solutions (4.32) the following mapping property for the two-grid operator $\mathcal{M}^{\mathrm{f}}_{\tau_L,h_L}$ with respect to full space-time coarsening holds true*

$$\mathcal{M}^{\mathrm{f}}_{\tau_L,h_L} : \mathcal{E}_{L_x,L_t}(\theta_x,\theta_t) \to \mathcal{E}_{L_x,L_t}(\theta_x,\theta_t),$$

with the mapping

$$\begin{pmatrix} U_1 \\ U_2 \\ U_3 \\ U_4 \end{pmatrix} \mapsto \widetilde{\mathcal{M}}^{\mathrm{f}}_{\mu}(\theta_k,\theta_t) \begin{pmatrix} U_1 \\ U_2 \\ U_3 \\ U_4 \end{pmatrix}$$

and the iteration matrix

$$\widetilde{\mathcal{M}}^{\mathrm{f}}_{\mu}(\theta_k,\theta_t) := \left(\widetilde{\mathcal{S}}_{\tau_L,h_L}(\theta_x,\theta_t)\right)^{\nu_2} \widetilde{\mathcal{K}}_{\mathrm{f}}(\theta_x,\theta_t) \left(\widetilde{\mathcal{S}}_{\tau_L,h_L}(\theta_x,\theta_t)\right)^{\nu_1} \in \mathbb{C}^{4N_t\times 4N_t}$$

with

$$\widetilde{\mathcal{K}}_{\mathrm{f}}(\theta_x,\theta_t) := I_{4N_t} - \widetilde{\mathcal{P}}_{\mathrm{f}}(\theta_x,\theta_t) \left(\widetilde{\mathcal{L}}^{\mathrm{f}}_{2\tau_L,2h_L}(2\theta_x,2\theta_t)\right)^{-1} \widetilde{\mathcal{R}}_{\mathrm{f}}(\theta_x,\theta_t) \widetilde{\mathcal{L}}_{\tau_L,h_L}(\theta_x,\theta_t).$$

Proof. The statement of this theorem is a direct consequence of Lemma 4.3.23, Lemma 4.3.25 and the mapping properties (4.38), (4.39) and (4.41). ∎

In view of Lemma 4.3.18 we can now represent the initial error $\boldsymbol{e}^0 = \boldsymbol{x} - \boldsymbol{x}^0$ as

$$\begin{aligned}\boldsymbol{e}^0 &= \sum_{(\theta_x,\theta_t)\in\Theta^{\mathrm{low,f}}_{L_x,L_t}} \big[\psi^{L_x,L_t}(\theta_x,\theta_t) + \psi^{L_x,L_t}(\gamma(\theta_x),\theta_t) \\ &\qquad\qquad + \psi^{L_x,L_t}(\theta_x,\gamma(\theta_t)) + \psi^{L_x,L_t}(\gamma(\theta_x),\gamma(\theta_t))\big] \\ &=: \sum_{(\theta_x,\theta_t)\in\Theta^{\mathrm{low,f}}_{L_x,L_t}} \tilde{\psi}(\theta_x,\theta_t),\end{aligned}$$

with $\tilde{\psi}(\theta_x,\theta_t) \in \mathcal{E}_{L_x,L_t}(\theta_x,\theta_t)$ for all $(\theta_x,\theta_t) \in \Theta^{\mathrm{low,f}}_{L_x,L_t}$. Using Theorem 4.3.26 and Theorem 4.3.27 we now can analyze the convergence behaviour of the two-grid cycles by simply computing the largest spectral radius of $\widetilde{\mathcal{M}}^{\mathrm{s}}_{\mu}(\theta_k,\theta_t)$ or $\widetilde{\mathcal{M}}^{\mathrm{f}}_{\mu}(\theta_k,\theta_t)$ with respect to the frequencies $(\theta_x,\theta_t) \in \Theta^{\mathrm{low,f}}_{L_x,L_t}$. This motivates the following definition.

Definition 4.3.28 (Two-grid convergence factors)**.** *For the two-grid iterations matrices $\mathcal{M}^{\mathrm{s}}_{\tau_L,h_L}$ and $\mathcal{M}^{\mathrm{f}}_{\tau_L,h_L}$ we define the asymptotic convergence factors as*

$$\begin{aligned}\rho(\hat{\mathcal{M}}^{\mathrm{s}}_{\mu}) &:= \max\Big\{\rho(\widetilde{\mathcal{M}}^{\mathrm{s}}_{\mu}(\theta_k,\theta_t)) : (\theta_x,\theta_t) \in \Theta^{\mathrm{low,f}}_{L_x,L_t} \text{ with } \theta_x \neq 0\Big\}, \\ \rho(\hat{\mathcal{M}}^{\mathrm{f}}_{\mu}) &:= \max\Big\{\rho(\widetilde{\mathcal{M}}^{\mathrm{f}}_{\mu}(\theta_k,\theta_t)) : (\theta_x,\theta_t) \in \Theta^{\mathrm{low,f}}_{L_x,L_t} \text{ with } \theta_x \neq 0\Big\}.\end{aligned}$$

Remark 4.3.29. *In the definition of the two-grid convergence factors we have neglected all frequencies $(0,\theta_t) \in \Theta^{\mathrm{low,f}}_{L_x,L_t}$ since the Fourier symbol with respect to the Laplacian is zero for $\theta_x = 0$, see also the remarks in [99, chapter 4].*

To derive the average convergence factors $\rho(\hat{\mathcal{M}}^{\mathrm{s}}_{\mu})$ and $\rho(\hat{\mathcal{M}}^{\mathrm{f}}_{\mu})$ for a given discretization parameter $\mu \in \mathbb{R}_+$ and a given polynomial degree $p_t \in \mathbb{N}_0$ we have to compute the eigenvalues of

$$\widetilde{\mathcal{M}}^{\mathrm{s}}_{\mu}(\theta_k,\theta_t) \in \mathbb{C}^{4N_t\times 4N_t} \quad \text{and} \quad \widetilde{\mathcal{M}}^{\mathrm{f}}_{\mu}(\theta_k,\theta_t) \in \mathbb{C}^{4N_t\times 4N_t}, \tag{4.42}$$

with $N_t = p_t + 1$ for each low frequency $(\theta_x,\theta_t) \in \Theta^{\mathrm{low,f}}_{L_x,L_t}$. Since it is very difficult to find an algebraic exact expression for the eigenvalues of the iteration matrices (4.42), we will compute the eigenvalues numerically. In particular we will compute the average convergence factors for the domain $\Omega = (0,1)$ with a decomposition into 1024 uniform sub intervals, i.e. $N_{L_x} = 1023$. Furthermore we will analyze the two-grid cycles for $N_{L_t} = 256$ time steps.

With respect to the discretization parameter $\mu = \tau_L h_L^{-2} \in [10^{-6}, 10^{6}]$ and for different polynomial degrees $p_t \in \{0,1,2\}$ the theoretical convergence factors $\rho(\hat{\mathcal{M}}^{\mathrm{s}}_{\mu})$

are plotted as solid lines in Figure 4.16–4.18. In each plot the theoretical convergence factors are compared with respect to a different number of smoothing steps $\nu_1 = \nu_2 = \nu \in \{1,2,5\}$. We observe, that the theoretical convergence rates are always bounded by $\rho(\hat{\mathcal{M}}^{\mathrm{s}}_{\mu}) \leq \frac{1}{2}$. For the case when semi coarsening with respect to time is applied we conclude, that the two-grid cycle converges for any discretization parameter μ. Furthermore for polynomial degrees $p_t \geq 1$ we see, that the theoretical convergence rates are much smaller than the convergence rates for the lowest order case $p_t = 0$.

Furthermore we have compared the theoretical results with the numerical results for solving the equation

$$\mathcal{L}_{\tau_L,h_L}\boldsymbol{x} = \boldsymbol{f}$$

with the two-grid cycle when semi coarsening with respect to time is applied. For the numerical test we use a zero right hand side, i.e. $\boldsymbol{f} = \boldsymbol{0}$ and as an initial vector $\boldsymbol{x}^0$ we use a random vector with values between zero and one. The convergence of the two-grid cycle is measured with

$$\max_{k=1,\ldots,N_{\mathrm{iter}}} \frac{\left\|\boldsymbol{r}^{k+1}\right\|_2}{\left\|\boldsymbol{r}^{k}\right\|_2}, \quad \text{with } \boldsymbol{r}^k := \boldsymbol{f} - \mathcal{L}_{\tau_L,h_L}\boldsymbol{x}^k,$$

where $N_{\mathrm{iter}} \in \mathbb{N}$, $N_{\mathrm{iter}} \leq 250$ is the number of used two-grid iterations until we have reached a given relative error reduction of $\varepsilon_{\mathrm{MG}} = 10^{-140}$. The measured numerical convergence rates are plotted in Figures 4.16–4.18 as dots, triangles and squares. We observe, that the numerical results completely agree with the theoretical results, even if the applied Fourier mode analysis is only a rigorous analysis when periodicity in space and time is assumed.

In Figures 4.19–4.21 the theoretical convergence factors $\rho(\hat{\mathcal{M}}^{\mathrm{s}}_{\mu})$ for the two-grid cycle $\mathcal{M}^{\mathrm{f}}_{\tau_L,h_L}$ with respect to full space-time coarsening are plotted with respect to the discretization parameter $\mu \in [10^{-6}, 10^{6}]$ for different polynomial degrees $p_t \in \{0,1,2\}$. We observe, that the theoretical convergence factors are bounded by $\rho(\hat{\mathcal{M}}^{\mathrm{f}}_{\mu}) \leq \frac{1}{2}$ if the discretization parameter μ is large enough, i.e. for $\mu \geq \mu^*$. In Remark 4.3.16 we already computed these critical values μ^* for several polynomial degrees p_t. As before we compared the theoretical results with the numerical results when full space-time coarsening is applied. In Figures 4.19–4.21 the measured numerical convergence rates are plotted as dots, triangles and squares. We observe, that the theoretical results agree with the numerical results.

Overall we conclude, that the two-grid cycle always converges to the exact solution of the linear system (4.31) when semi coarsening with respect to time is applied. Furthermore, if the discretization parameter μ is large enough, we also can apply full space-time coarsening, which leads to a smaller coarse problem compared to the semi coarsening case.

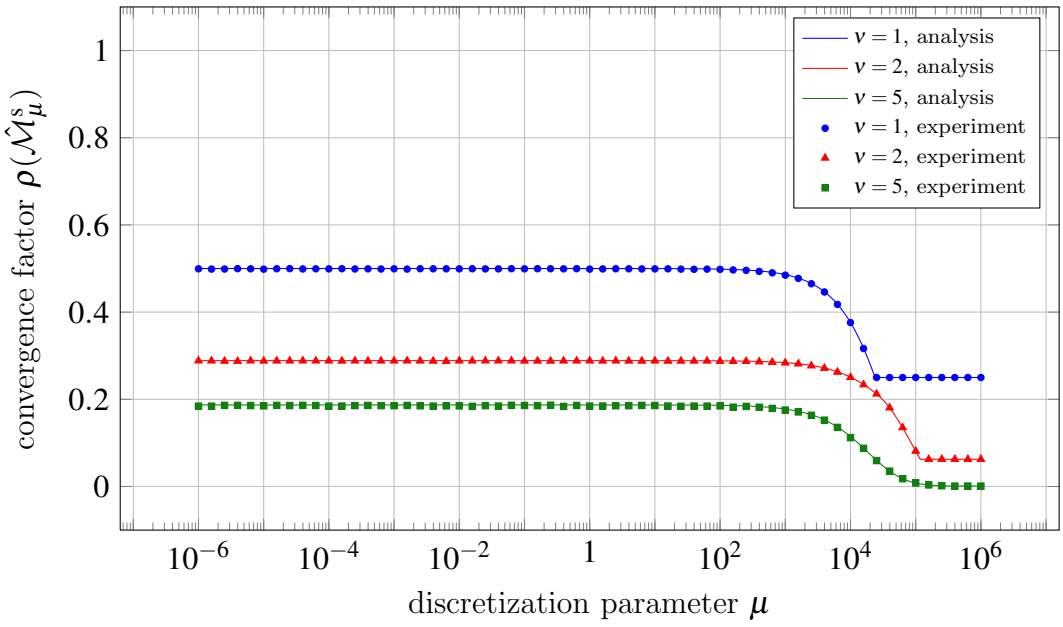

Figure 4.16: Average convergence factor $\rho(\hat{\mathcal{M}}_\mu^s)$ for different discretization parameter μ, $p_t = 0$ and numerical convergence rates for $N_t = 256$ time steps and $N_x = 1023$.

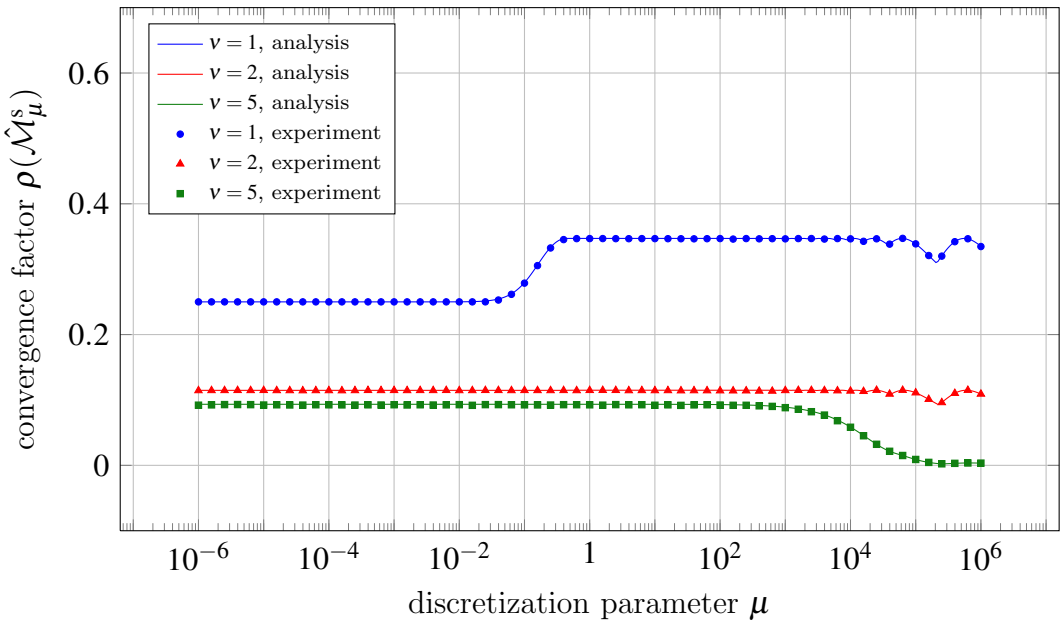

Figure 4.17: Average convergence factor $\rho(\hat{\mathcal{M}}_\mu^s)$ for different discretization parameter μ, $p_t = 1$ and numerical convergence rates for $N_t = 256$ time steps and $N_x = 1023$.

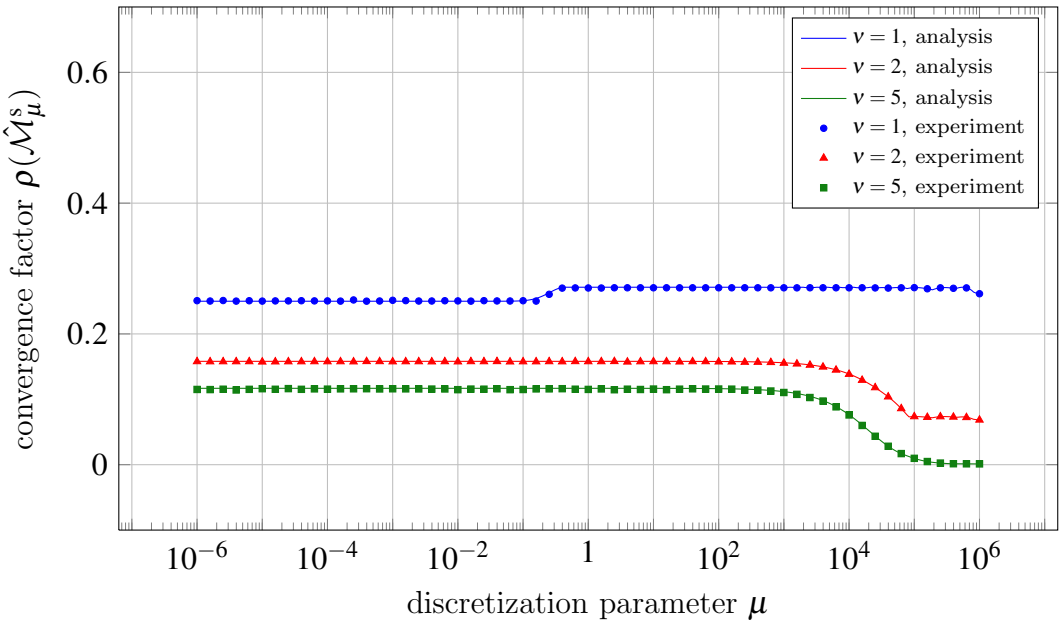

Figure 4.18: Average convergence factor $\rho(\hat{\mathcal{M}}_\mu^{\mathrm{s}})$ for different discretization parameter μ, $p_t = 2$ and numerical convergence rates for $N_t = 256$ time steps and $N_x = 1023$.

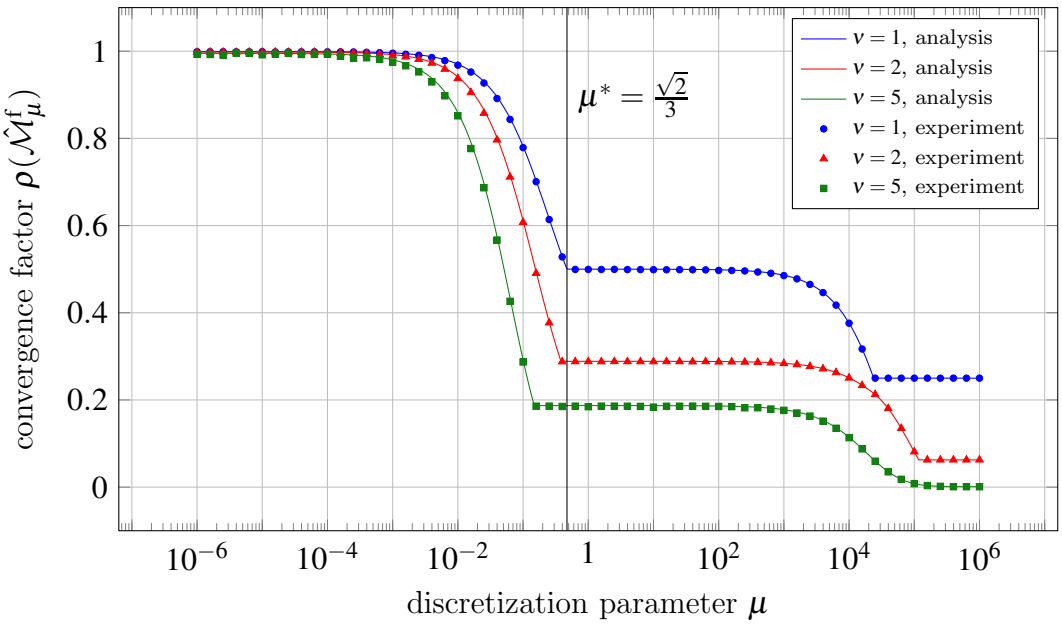

Figure 4.19: Average convergence factor $\rho(\hat{\mathcal{M}}_\mu^{\mathrm{f}})$ for different discretization parameter μ, $p_t = 0$ and numerical convergence rates for $N_t = 256$ time steps and $N_x = 1023$.

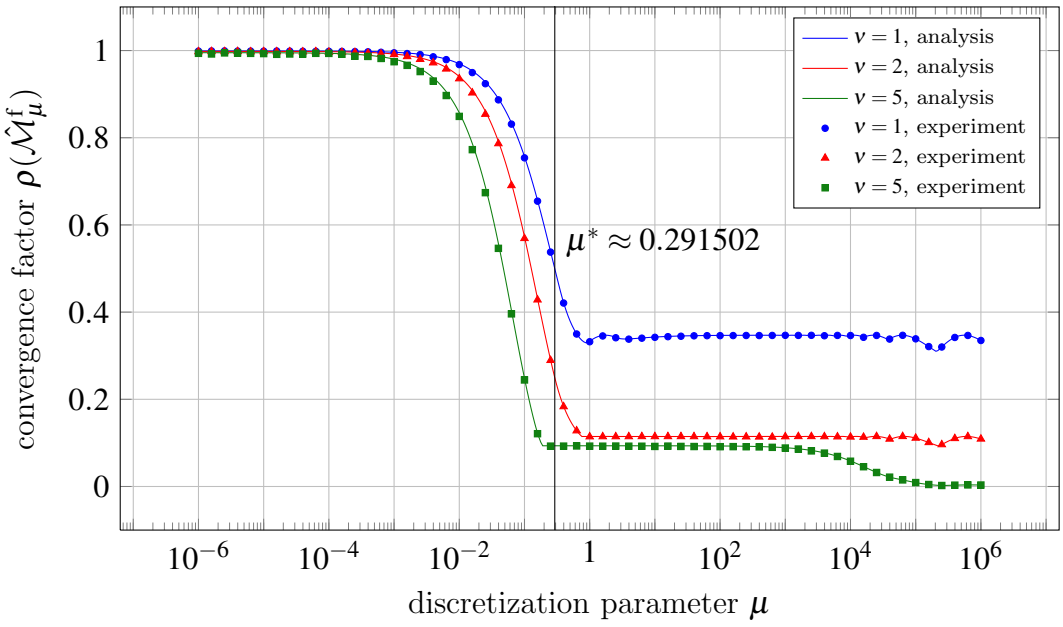

Figure 4.20: Average convergence factor $\rho(\hat{\mathcal{M}}_\mu^{\mathrm{f}})$ for different discretization parameter μ, $p_t = 1$ and numerical convergence rates for $N_t = 256$ time steps and $N_x = 1023$.

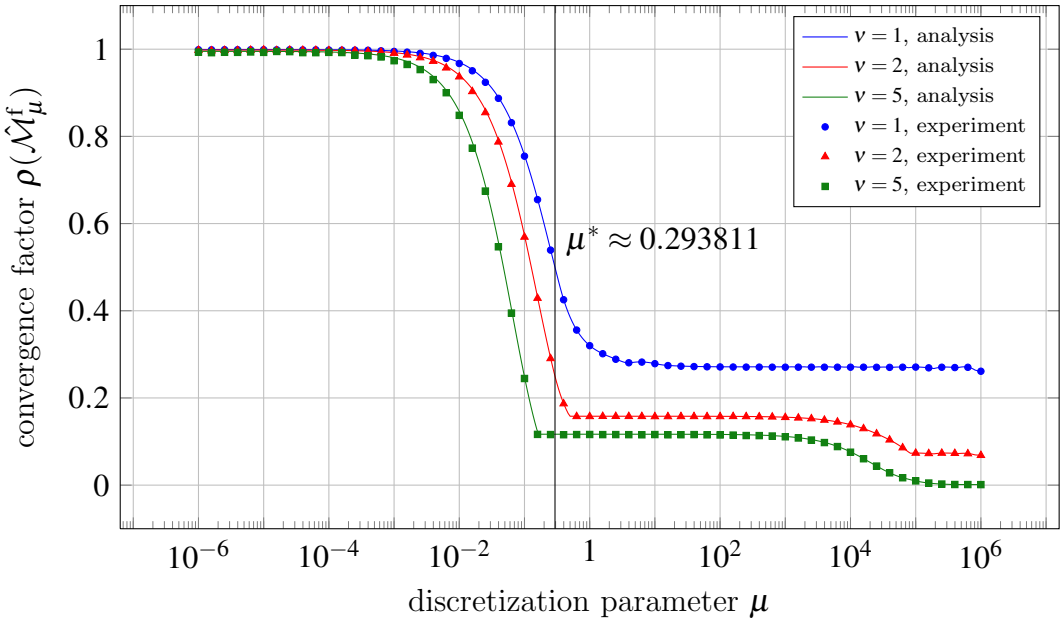

Figure 4.21: Average convergence factor $\rho(\hat{\mathcal{M}}_\mu^{\mathrm{f}})$ for different discretization parameter μ, $p_t = 2$ and numerical convergence rates for $N_t = 256$ time steps and $N_x = 1023$.

Remark 4.3.30. *For the two-grid analysis above we used for the applied block Jacobi smoother*

$$\mathcal{S}^{\nu}_{\tau_L,h_L} = \left[I - \omega_t (D_{\tau_L,h_L})^{-1} \mathcal{L}_{\tau_L,h_L}\right]^{\nu} \tag{4.43}$$

the exact inverse of the diagonal matrix $D_{\tau_L,h_L} = \operatorname{diag}\left\{A_{\tau_L,h_L}\right\}_{n=1}^{N_{L_t}}$. *For practical reasons we will use an approximation* $\widetilde{D}^{-1}_{\tau_L,h_L}$ *for the inverse of the diagonal matrix* D_{τ_L,h_L} *by applying one multigrid iteration with respect to the blocks* A_{τ_L,h_L}. *Hence the smoother (4.43) changes to*

$$\overline{\mathcal{S}}^{\nu}_{\tau_L,h_L} := \left[I - \omega_t \left(I - \mathcal{M}_{\tau_L,h_L}\right) (D_{\tau_L,h_L})^{-1} \mathcal{L}_{\tau_L,h_L}\right]^{\nu}, \tag{4.44}$$

with the matrix $\mathcal{M}_{\tau_L,h_L} := \operatorname{diag}\left\{\mathcal{M}^x_{\tau_L,h_L}\right\}_{n=1}^{N_{L_t}}$ *where* $\mathcal{M}^x_{\tau_L,h_L}$ *is the iteration matrix of the applied multigrid scheme with respect to the matrix* A_{τ_L,h_L}. *In the case that the iteration matrix* $\mathcal{M}^x_{\tau_L,h_L}$ *is given by a two-grid cycle, we further obtain the following representation*

$$\mathcal{M}^x_{\tau_L,h_L} = \mathcal{S}^{x,\nu_2^x}_{\tau_L,h_L} \left[I - \overline{\mathcal{P}}^{L_x}_x A^{-1}_{\tau_L,2h_L} \overline{\mathcal{R}}^{L_x}_x A_{\tau_L,h_L}\right] \mathcal{S}^{x,\nu_1^x}_{\tau_L,h_L},$$

with a damped Jacobi smoother with respect to space

$$\mathcal{S}^{x,\nu^x}_{\tau_L,h_L} := \left[I - \omega_x \left(D^x_{\tau_L,h_L}\right)^{-1} A_{\tau_L,h_L}\right]^{\nu^x}, \quad D^x_{\tau_L,h_L} := \operatorname{diag}\Big\{\frac{2h}{3} K_{\tau_L} + \frac{2}{h} M_{\tau_L}\Big\}_{r=1}^{N_{L_x}}$$

and the restriction and prolongation operators

$$\overline{\mathcal{R}}^{L_x}_x := \mathcal{R}^{L_x}_x \otimes I_{N_t} \quad \text{and} \quad \overline{\mathcal{P}}^{L_x}_x := \mathcal{P}^{L_x}_x \otimes I_{N_t}.$$

With the different smoother (4.44) we also have to analyze the two different two-grid iteration matrices

$$\overline{\mathcal{M}}^{\mathrm{s}}_{\tau_L,h_L} := \overline{\mathcal{S}}^{\nu_2}_{\tau_L,h_L} \left[I - \mathcal{P}^{L_x,L_t}_{\mathrm{s}} \left(\mathcal{L}_{2\tau_L,h_L}\right)^{-1} \mathcal{R}^{L_x,L_t}_{\mathrm{s}} \mathcal{L}_{\tau_L,h_L}\right] \overline{\mathcal{S}}^{\nu_1}_{\tau_L,h_L}, \tag{4.45}$$

$$\overline{\mathcal{M}}^{\mathrm{f}}_{\tau_L,h_L} := \overline{\mathcal{S}}^{\nu_2}_{\tau_L,h_L} \left[I - \mathcal{P}^{L_x,L_t}_{\mathrm{f}} \left(\mathcal{L}_{2\tau_L,2h_L}\right)^{-1} \mathcal{R}^{L_x,L_t}_{\mathrm{f}} \mathcal{L}_{\tau_L,h_L}\right] \overline{\mathcal{S}}^{\nu_1}_{\tau_L,h_L}. \tag{4.46}$$

Hence it remains to analyze the mapping property of the operator $\mathcal{M}_{\tau_L,h_L}$ *on the space of harmonics* $\mathcal{E}_{L_x,L_t}(\theta_x,\theta_t)$. *By several computations we find under the assumptions of periodic solutions (4.32) that*

$$\mathcal{M}_{\tau_L,h_L} : \mathcal{E}_{L_x,L_t}(\theta_x,\theta_t) \to \mathcal{E}_{L_x,L_t}(\theta_x,\theta_t)$$

with the mapping

$$\begin{pmatrix} U_1 \\ U_2 \\ U_3 \\ U_4 \end{pmatrix} \mapsto \begin{pmatrix} \widetilde{M}_{\tau_L,h_L}(\theta_x) & 0 \\ 0 & \widetilde{M}_{\tau_L,h_L}(\theta_x) \end{pmatrix} \begin{pmatrix} U_1 \\ U_2 \\ U_3 \\ U_4 \end{pmatrix}, \tag{4.47}$$

and the iteration matrix

$$\widetilde{M}_{\tau_L,h_L}(\theta_x) := \widetilde{\mathcal{S}}^{x,\nu_1^x}_{\tau_L,h_L}(\theta_x)\mathcal{K}^x_{\tau_L,h_L}(\theta_x)\widetilde{\mathcal{S}}^{x,\nu_2^x}_{\tau_L,h_L}(\theta_x) \in \mathbb{C}^{2N_t\times 2N_t},$$
$$\mathcal{K}^x_{\tau_L,h_L}(\theta_x,\theta_t) := I_{2N_t} - \widetilde{\mathcal{P}}_x(\theta_x)\widetilde{A}^{-1}_{\tau_L,2h_L}(2\theta_x)\widetilde{\mathcal{R}}_x(\theta_x)\widetilde{A}_{\tau_L,h_L}(\theta_x) \in \mathbb{C}^{2N_t\times 2N_t},$$

with the matrices

$$\widetilde{A}_{\tau_L,h_L}(\theta_x) := \begin{pmatrix} \hat{A}_{\tau_L,h_L}(\theta_x) & 0 \\ 0 & \hat{A}_{\tau_L,h_L}(\gamma(\theta_x)) \end{pmatrix} \in \mathbb{C}^{2N_t\times 2N_t},$$
$$\widetilde{A}^{-1}_{\tau_L,2h_L}(2\theta_x) := \left(\hat{A}_{\tau_L,2h_L}(2\theta_x)\right)^{-1} \in \mathbb{C}^{N_t\times N_t}$$
$$\widetilde{\mathcal{S}}^{x,\nu^x}_{\tau_L,h_L}(\theta_x) := \begin{pmatrix} \left(\hat{\mathcal{S}}_{\tau_L,h_L}(\omega_x,\theta_x)\right)^{\nu^x} & 0 \\ 0 & \left(\hat{\mathcal{S}}_{\tau_L,h_L}(\omega_x,\gamma(\theta_x))\right)^{\nu^x} \end{pmatrix} \in \mathbb{C}^{2N_t\times 2N_t},$$
$$\widetilde{\mathcal{R}}_x(\theta_x) := \begin{pmatrix} \hat{\mathcal{R}}_x(\theta_x)I_{N_t} & \hat{\mathcal{R}}_x(\gamma(\theta_x))I_{N_t} \end{pmatrix} \in \mathbb{C}^{2N_t\times N_t},$$
$$\widetilde{\mathcal{P}}_x(\theta_x) := \begin{pmatrix} \hat{\mathcal{P}}_x(\theta_x)I_{N_t} \\ \hat{\mathcal{P}}_x(\gamma(\theta_x))I_{N_t} \end{pmatrix} \in \mathbb{C}^{N_t\times 2N_t}$$

and the Fourier symbols

$$\hat{A}_{\tau_L,h_L}(\theta_x) := \frac{h_L}{3}\left(2+\cos(\theta_x)\right)K_{\tau_L} + \frac{2}{h_L}\left(1-\cos(\theta_x)\right)M_{\tau_L} \in \mathbb{C}^{N_t\times N_t},$$
$$\hat{\mathcal{S}}_{\tau_L,h_L}(\omega_x,\theta_x) := I_{N_t} - \omega_x\left(\frac{2h_L}{3}K_{\tau_L} + \frac{2}{h_L}M_{\tau_L}\right)^{-1}\hat{A}_{\tau_L,h_L}(\theta_x) \in \mathbb{C}^{N_t\times N_t}.$$

Hence we can analyze the modified two-grid iteration matrices (4.45) by taking the additional approximation with the mapping (4.47) into account. For the smoothing steps $\nu_1^x = \nu_2^x = 2$ and the damping parameter $\omega_x = \frac{2}{3}$ the theoretical convergence rates with respect to semi coarsening in time are plotted in Figures 4.22–4.24 for the discretization parameter $\mu \in [10^{-6}, 10^6]$ with respect to the polynomial degrees $p_t \in \{0,1,2\}$. We observe, that the theoretical convergence rates are always bounded by $\rho(\overline{\mathcal{M}}^{\mathrm{s}}_{\mu}) \leq \frac{1}{2}$. Further we notice that the derived theoretical convergence rates are a little bit higher for small discretization parameters μ, compared to the case when the exact inverse of the diagonal matrix D_{τ_L,h_L} is used. The measured numerical rates are plotted as dots, triangles and squares in Figures 4.22–4.24. We observe, that the theoretical convergence rates coincide with the numerical results.

In Figures 4.25–4.27 the convergence of the two-grid cycle for the full space-time coarsening case is studied. Here we see, that the computed convergence rates are very close to the results which we obtained for the case when the exact inverse of the diagonal matrix D_{τ_L,h_L} is used.

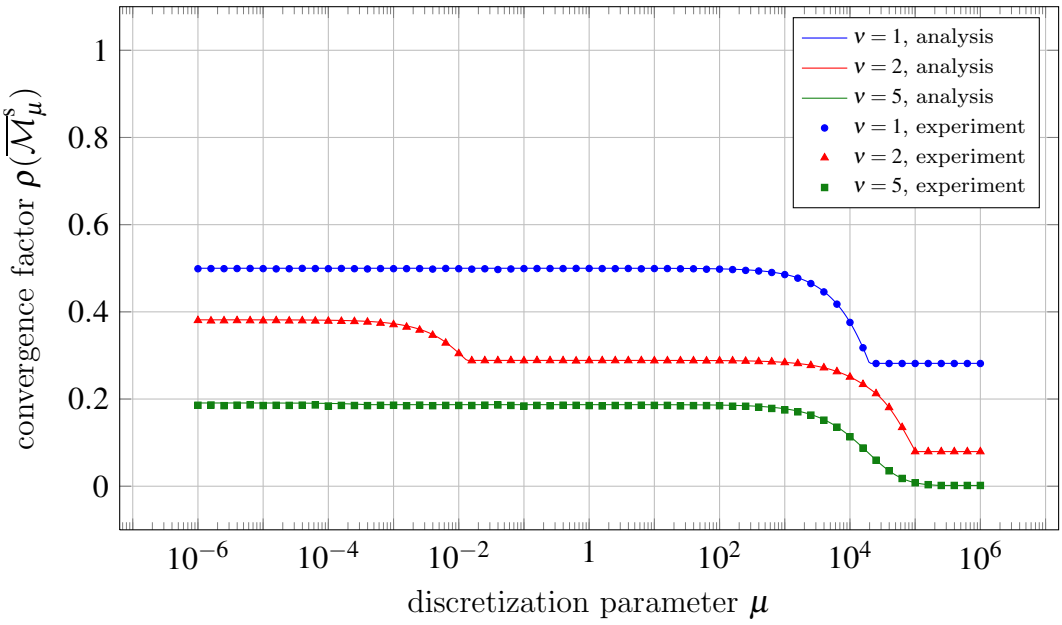

Figure 4.22: Average convergence factor $\rho(\overline{\mathcal{M}}_\mu^s)$ for different discretization parameter μ, $p_t = 0$ and numerical convergence rates for $N_t = 256$ time steps and $N_x = 1023$.

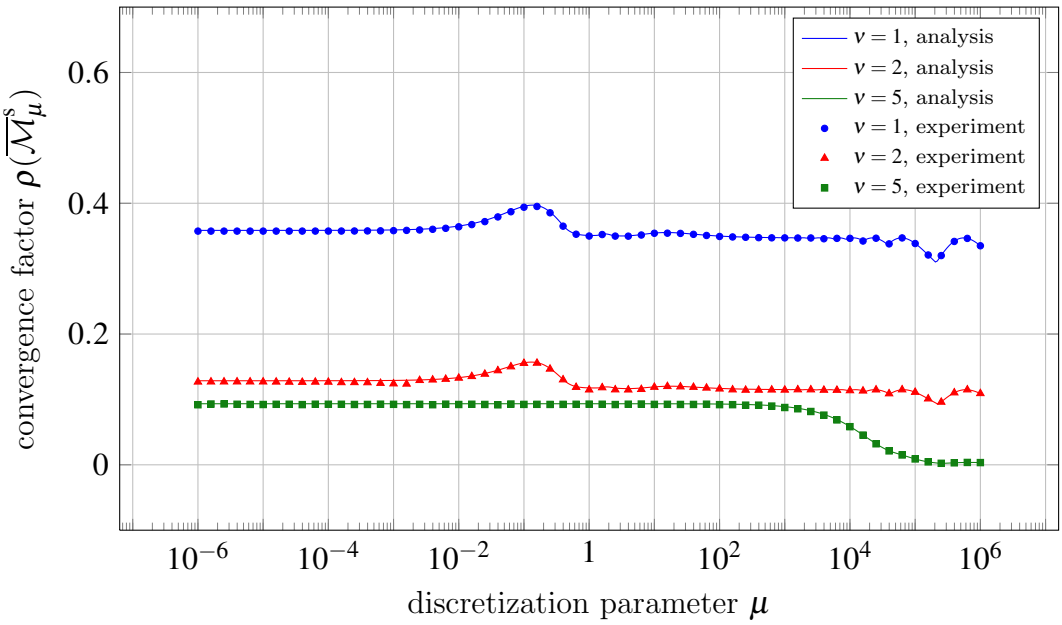

Figure 4.23: Average convergence factor $\rho(\overline{\mathcal{M}}_\mu^s)$ for different discretization parameter μ, $p_t = 1$ and numerical convergence rates for $N_t = 256$ time steps and $N_x = 1023$.

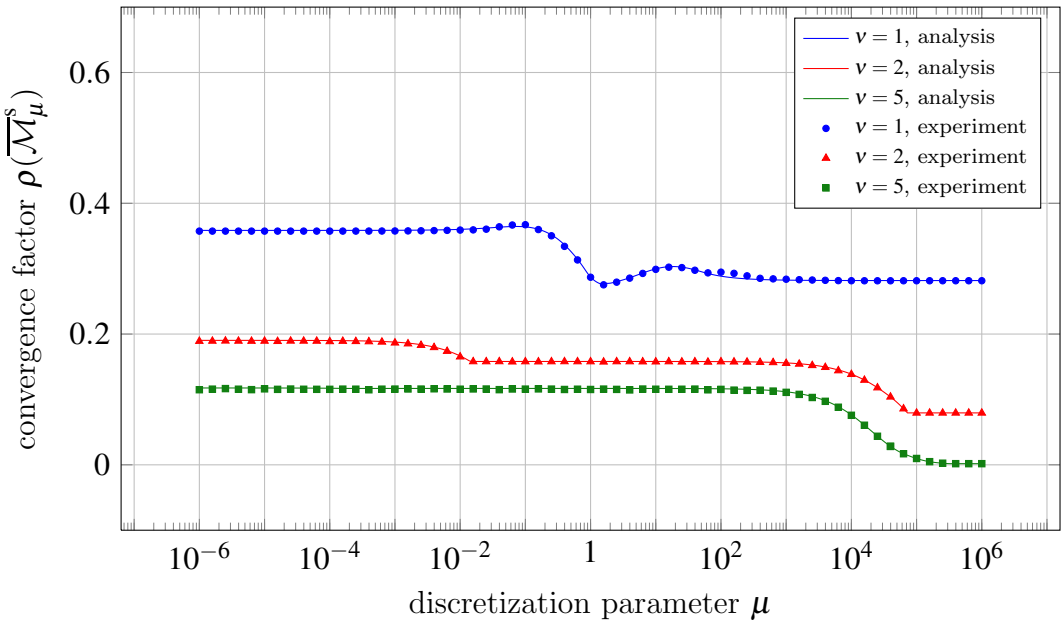

Figure 4.24: Average convergence factor $\rho(\overline{\mathcal{M}}_\mu^{\mathrm{s}})$ for different discretization parameter μ, $p_t = 2$ and numerical convergence rates for $N_t = 256$ time steps and $N_x = 1023$.

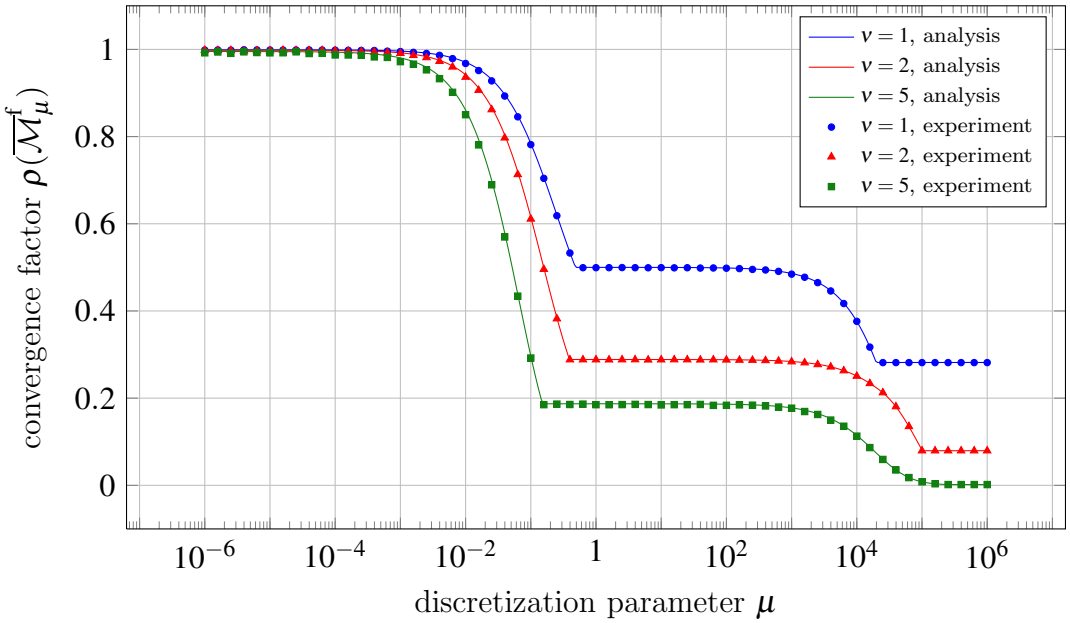

Figure 4.25: Average convergence factor $\rho(\overline{\mathcal{M}}_\mu^{\mathrm{f}})$ for different discretization parameter μ, $p_t = 0$ and numerical convergence rates for $N_t = 256$ time steps and $N_x = 1023$.

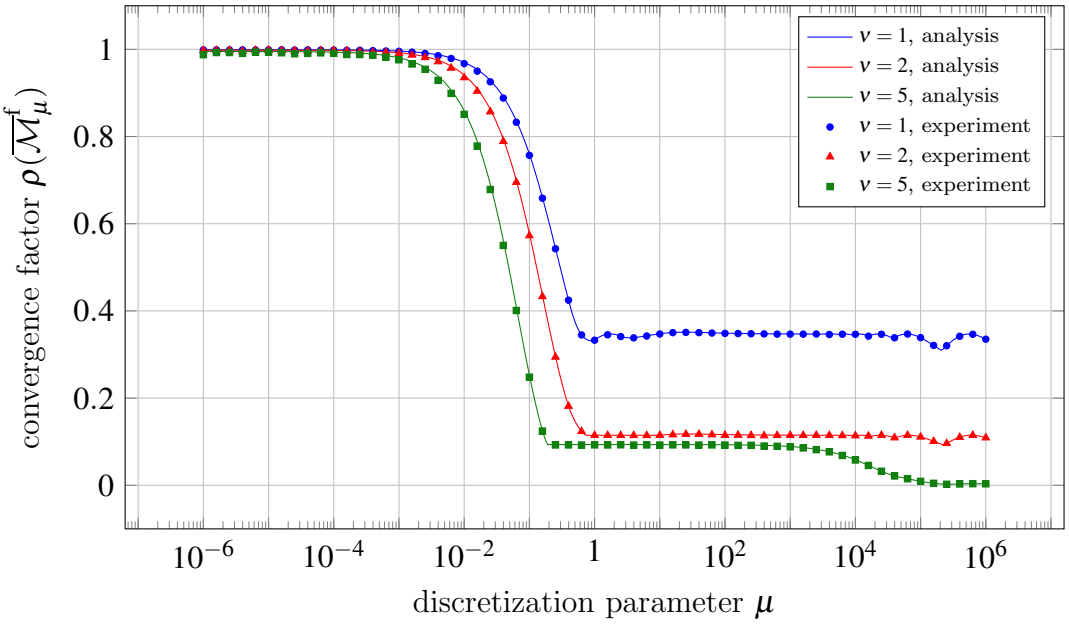

Figure 4.26: Average convergence factor $\rho(\overline{\mathcal{M}}_\mu^{\mathrm{f}})$ for different discretization parameter μ, $p_t = 1$ and numerical convergence rates for $N_t = 256$ time steps and $N_x = 1023$.

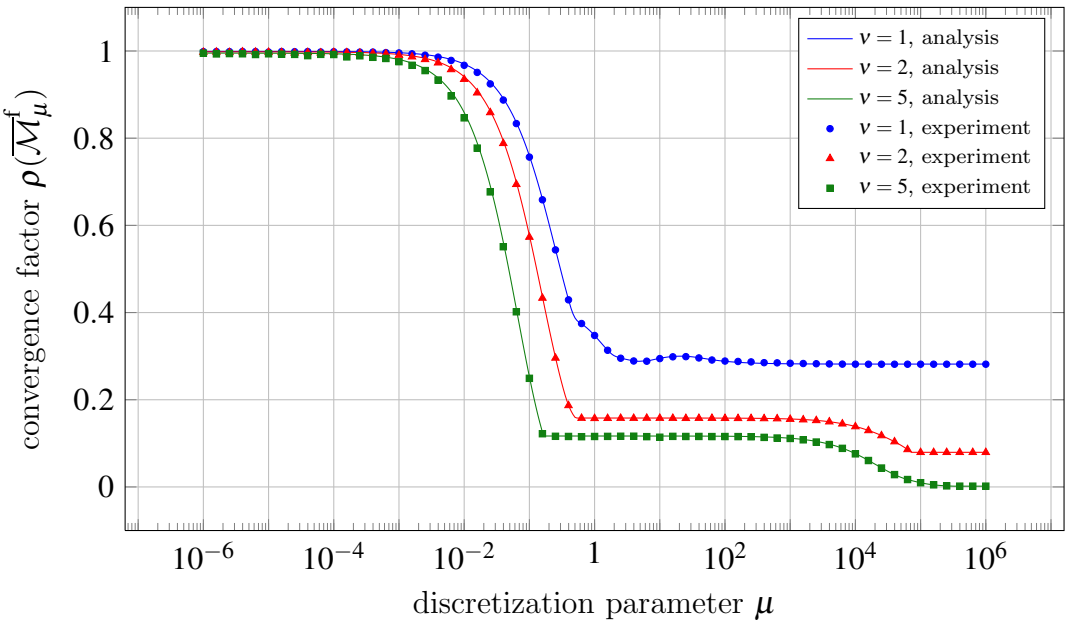

Figure 4.27: Average convergence factor $\rho(\overline{\mathcal{M}}_\mu^{\mathrm{f}})$ for different discretization parameter μ, $p_t = 2$ and numerical convergence rates for $N_t = 256$ time steps and $N_x = 1023$.

4.4 Numerical examples

In this section applications of the space-time multigrid approach, introduced in Section 4.1 will be presented. In the last Section 4.3 the two-grid cycles with respect to semi coarsening in time and full space-time coarsening have been analyzed. There we concluded, that semi coarsening with respect to time is always possible and that full space-time coarsening can be applied, if the discretization parameter $\mu_L = \tau_L h_L^{-2}$ is large enough, i.e. $\mu_L \geq \mu^*$. Hence, also for the multigrid cycle we are able to apply full space-time coarsening only, if $\mu_L \geq \mu^*$. Whereas for $\mu_L < \mu^*$ we have to apply semi coarsening with respect to time. When semi coarsening is applied, we have for the next coarser level

$$\mu_{L-1} = 2\tau_L h_L^{-2} = 2\mu_L.$$

This implies that the discretization parameter μ_{L-1} gets larger when semi coarsening with respect to time is used. Hence, if $\mu_{L-k} \geq \mu^*$ for $k < L$ we can apply full space-time coarsening to reduce the computational costs. If full space-time coarsening is applied, we have

$$\mu_{L-1} = 2\tau_L (2h_L)^{-2} = \frac{1}{2}\mu_L,$$

which results in a smaller discretization parameter μ_{L-1}. We therefore will combine semi coarsening in time or full space-time coarsening in the right way, to get to the next coarser space-time level. For different discretization parameters $\mu = c\mu^*$, $c \in \{\frac{1}{10}, 1, 10\}$ this coarsening strategy is shown in Figure 4.28 for 8 time and 4 space levels. The restriction and prolongation operators for the space-time multigrid scheme are then defined by the given coarsening strategy.

Next we will study some examples to show the performance of this space-time multigrid approach.

Example 4.4.1 (Tensor product space-time elements)**.** In this example we consider the spatial domain $\Omega = (0,1)^3$ and the simulation interval $(0,T)$ with $T = 1$. The initial decomposition for the spatial domain Ω is given by 12 tetrahedra. We will use several uniform refinement levels to study the convergence behaviour of the space-time multigrid solver with respect to the space-discretization. For the coarsest time level we will use one time step, i.e. $\tau_0 = 1$. The ansatz functions in space are given by piecewise linear continuous functions and for the time discretization we will use piecewise linear discontinuous ansatz functions, i.e. $p_t = 1$. Hence we have to solve the linear system (4.6) for the given ansatz functions. To test the performance of the space-time multigrid method we will use a zero right hand side, i.e. $\boldsymbol{f} = \boldsymbol{0}$ and as an initial guess $\boldsymbol{x}^0$ we will use a random vector with

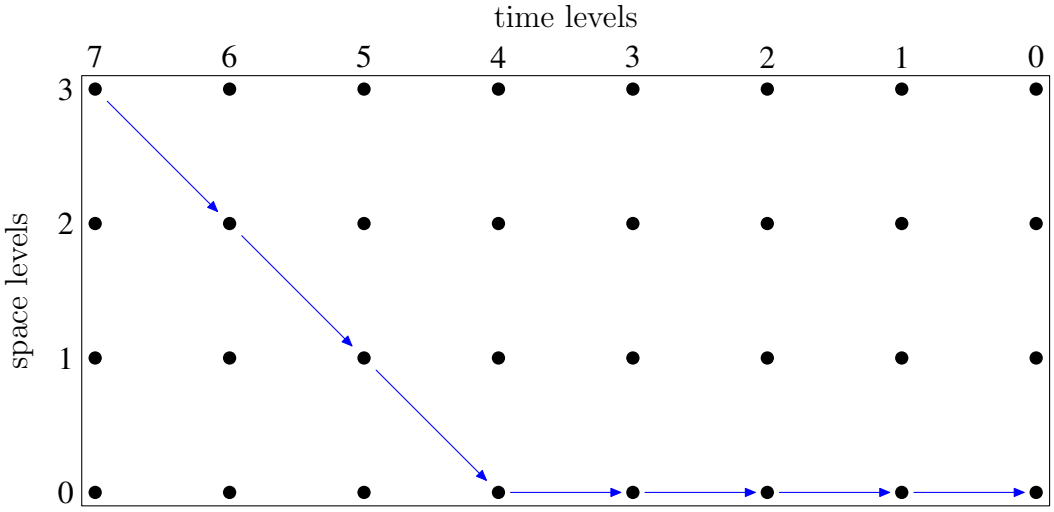

(a) Discretization parameter on the finest space-time level: $\mu_7 = 10\mu^*$.

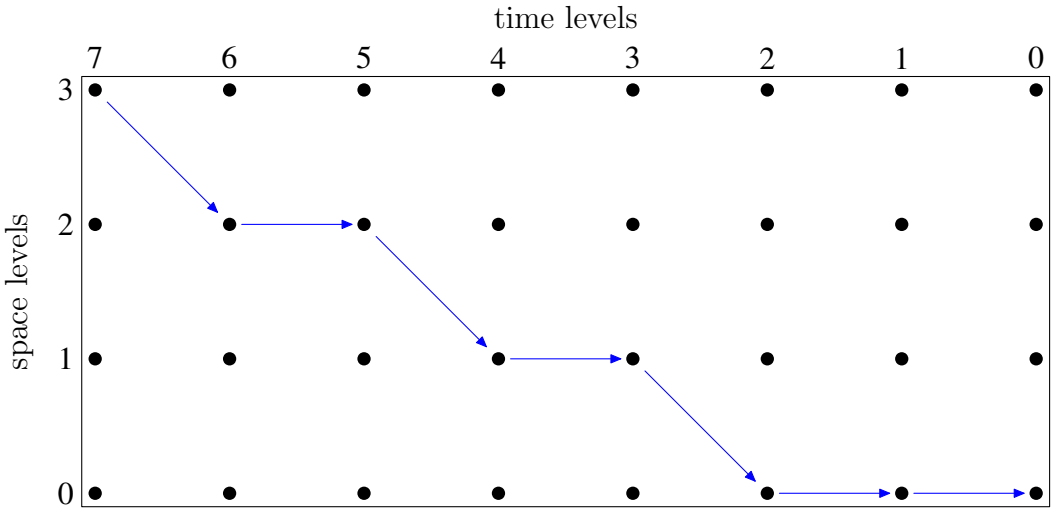

(b) Discretization parameter on the finest space-time level: $\mu_7 = \mu^*$.

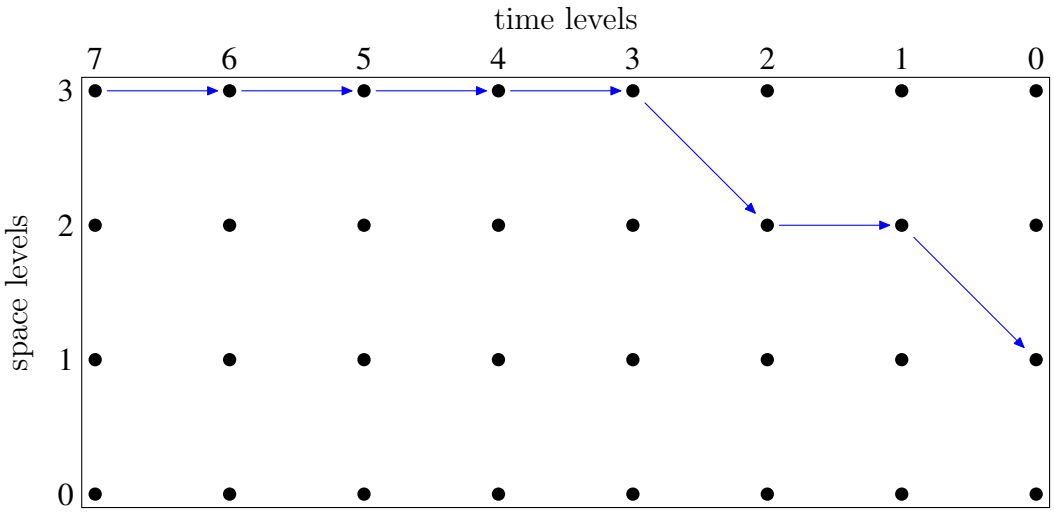

(c) Discretization parameter on the finest space-time level: $\mu_7 = 0.1\mu^*$.

Figure 4.28: Space-time coarsening for different discretization parameter μ_L.

		time levels														
		0	1	2	3	4	5	6	7	8	9	10	11	12	13	14
space levels	0	1	7	7	7	7	7	7	7	8	8	9	9	9	9	9
	1	1	7	7	7	7	7	7	7	8	8	9	9	9	9	9
	2	1	7	7	7	7	7	8	7	8	8	9	9	9	9	9
	3	1	7	7	7	7	8	8	8	8	8	9	9	9	9	9
	4	1	7	7	7	8	8	8	8	8	8	8	9	9	9	9
	5	1	7	7	7	7	7	8	8	8	8	8	9	9	9	9

Table 4.1: Multigrid iterations for Example 4.4.1.

values between zero and one. For the space-time multigrid solver we will use the following settings with respect to time

$$\nu_1 = \nu_2 = 2, \qquad \omega_t = \frac{1}{2}, \qquad \gamma = 1.$$

We will apply for each block A_{τ_L,h_L} one geometric multigrid iteration to approximate the inverse of the diagonal matrix D_{τ_L,h_L}. For this multigrid cycle we will use the the following settings

$$\nu_1^x = \nu_2^x = 2, \qquad \omega_x = \frac{2}{3}, \qquad \gamma_x = 1.$$

For the smoother we use a damped block Jacobi smoother. We will apply the described space-time multigrid solver until we have reached a given relative error reduction of $\varepsilon_{\text{MG}} = 10^{-8}$. In Table 4.1 the iteration numbers for several space and time levels are given. We observe, that the iteration numbers stay bounded independent of the mesh size h_{L_x}, the time step size τ_{L_t} and the number of used time steps $N_{L_t} = 2^{L_t}$.

Example 4.4.2 (High order time discretizations)**.** In this example we will study the convergence of the space-time multigrid method with respect to different polynomial degrees p_t, which are used for the underlying time discretization. To do so, we will consider the spatial domain $\Omega = (0,1)^2$ and the simulation interval $(0,T)$ with $T = 1024$. For the space-time discretization we will use tensor product space-time elements with piecewise linear continuous ansatz functions in space. For the discretization in time we will use a fixed time step size $\tau = 1$. For the initial triangulation of the spatial domain Ω we will consider 4 triangles, which will be refined uniformly several times. For the space-time multigrid approach we will use the same settings as in Example 4.4.1. We solve the linear system (4.6) with a zero right hand side, i.e. $\boldsymbol{f} = \boldsymbol{0}$ and for the initial vector $\boldsymbol{x}^0$ we will use a random vector with values between zero and one. We apply the space-time multigrid solver until we have reached a relative error reduction of $\varepsilon_{\text{MG}} = 10^{-8}$. In

space levels	polynomial degree p_t													
	0	1	2	3	4	5	10	15	20	25	30	35	40	45
0	7	7	6	6	6	6	5	5	4	4	4	4	5	5
1	7	7	7	7	7	7	7	7	7	7	7	7	7	7
2	7	7	7	7	7	7	7	7	7	7	7	7	7	7
3	7	7	7	7	7	7	7	7	7	7	7	7	7	7
4	7	7	7	7	7	7	7	7	7	7	7	7	7	7
5	7	7	7	7	7	7	7	7	7	7	7	7	7	7
6	7	7	7	7	7	7	7	7	7	7	7	7	7	7
7	7	7	7	7	7	7	7	7	7	7	7	7	7	7

Table 4.2: Multigrid iterations with respect to the polynomial degree p_t.

Table 4.2 the iteration numbers for different polynomial degrees p_t and different space levels are given. We observe, that the iteration numbers are bounded, independent of the ansatz functions which are used for the time discretization.

Example 4.4.3 (Simplex space-time elements)**.** In this example we study the space-time multigrid approach when simplex space-time elements are used for discretizing the model problem (2.1) by the discontinuous Galerkin scheme (2.2). We consider the spatial domains $\Omega = (0,1)^d$ for $d = 1,2,3$ and the simulation end time $T = 1$. Hence, the space-time domains are given by the unit cubes $Q = (0,1)^{d+1}$. We decompose the space-time domains Q with $(d+1)$ dimensional simplices. For $d = 1$ we will use 2 triangles, for $d = 2$ we will use 6 tetrahedra and for $d = 3$ we will use 24 pentatopes for the initial decompositions. We further apply several uniform refinement steps to analyze the performance of the presented solver. To solve the linear system (4.6) for this example, we will apply the preconditioned GMRES method, where the preconditioner is given by one cycle of the space-time multigrid method. For the penalty parameter we use $\sigma = 15$ and as a polynomial degree we choose $p = 1$. To approximate the inverse of the diagonal matrix D_{τ_L,h_L} we will use an algebraic multigrid solver as implemented in the package *hypre*, see [28,29]. As in the previous examples we use a zero right hand side and a random initial vector $\boldsymbol{x}^0$ with values between zero and one. Since we are using uniform decompositions for the space-time domains Q, we obtain for the discretization parameter μ for any level that

$$\mu = \tau h^{-2} \approx h^{-1} \geq 1.$$

Hence we can apply for all space-time levels full space-time coarsening, i.e. the standard geometric coarsening for simplicial meshes. In the Tables 4.3–4.5 the iteration numbers for the preconditioned GMRES method are given for a relative error reduction of $\varepsilon_{\text{GMRES}} = 10^{-8}$. We observe, that the iteration numbers stay bounded independent of how many refinement steps are used.

level	elements	dof	iter
0	2	2	1
1	8	16	4
2	32	80	5
3	128	352	6
4	512	1 472	6
5	2 048	6 016	6
6	8 192	24 320	6
7	32 768	97 792	6
8	131 072	392 192	6
9	524 288	1570 816	6
10	2 097 152	6 287 360	6

Table 4.3: Multigrid iterations for $d = 1$.

level	elements	dof	iter
0	6	4	1
1	48	104	4
2	384	1 168	5
3	3072	10 784	6
4	24 576	92 224	6
5	196 608	761 984	6
6	1 572 864	6 193 408	6
7	12 582 912	49 938 944	6

Table 4.4: Multigrid iterations for $d = 2$.

level	elements	dof	iter
0	24	25	1
1	384	968	6
2	6 144	22 312	9
3	98 304	421 040	9
4	1 572 864	7 287 520	9

Table 4.5: Multigrid iterations for $d = 3$.

4.5 Parallelization

One big advantage of the presented space-time multigrid approach is, that it can be parallelized with respect to time. The idea of solving time dependent problems parallel in time is not new. For example the parareal algorithm has become popular in the last years. This algorithm has been introduced in [55] and has been analyzed in [7, 33, 58, 59, 87]. A lot of applications can be found, for example, in [30,31,34,35,80]. Other methods to solve evolution equations parallel in time are multiple shooting methods, which have been introduced in [51, 71]. Multigrid methods for parabolic problems have been introduced in [38] and have been further developed in [44, 45, 47, 57, 101, 102, 107]. The main difference with the approach in this work is the line wise smoother which is used, i.e. the damped block Jacobi smoother (4.7).

The application of this damped block Jacobi smoother can be done in parallel with respect to time. For each space-time slab we have to apply one multigrid

cycle in space to approximate the inverse of the diagonal matrix D_{τ_L,h_L}. The application of this space multigrid cycle can be done also in parallel, where one may use parallel packages like in [28,29,43]. Hence the problem (4.6) can be fully parallelized with respect to space and time, see also Figures 4.29.

The next example will show the parallel performance of this space-time multigrid approach.

Example 4.5.1 (Parallel computations)**.** In this example we consider the spatial domain $\Omega = (0,1)^3$, which is decomposed into 49 152 tetrahedra. For the discretization in space we will use piecewise linear continuous ansatz functions and for the time discretization we will use piecewise linear discontinuous functions with a fixed time step size $\tau = 10^{-1}$. For the space-time multigrid settings we apply the same configuration as in Example 4.4.1.

To show the parallel performance with respect to time, we first study the weak scaling behaviour of the presented multigrid approach. To do so, we use a fixed number of time steps per core, i.e. 4 time steps for each core. Furthermore we increase the number of cores when we increase the number of time steps. Hence the computational costs for one space-time multigrid cycle stay almost the same for each core. Only the costs for the communication grows, since the space-time hierarchy gets bigger, when we increase the number of time steps. In Table 4.6 the measured times for solving the linear system (4.6) for a different number of time steps are given. We obtain, that the multigrid iterations stay bounded, if we increase the problem size. Further we see, that the computational costs stay almost bounded if we increase the number of cores, see also Figure 4.30. Only for one and two cores we obtain better results for the measured solving times, because in these cases almost no communication is needed.

To test the strong scaling behaviour, we fix the problem size. In particular we will use 4 096 time steps, which results in a linear system with 61 202 432 unknowns. Then we increase the number of cores, which then results in smaller problems per computing core. In Table 4.6 the measured times are given for a different number of cores. We see, that the computational costs are almost divided by two, if we double the number of cores, see also the Figure 4.31. For one core we obtain a better performance, because no communication is involved. The computational costs when using $P = 2\,048$ cores are a little bit higher, since the problem size per core gets to small.

All the parallel computations of this example were performed on the *Vienna Scientific Cluster VSC-2*.

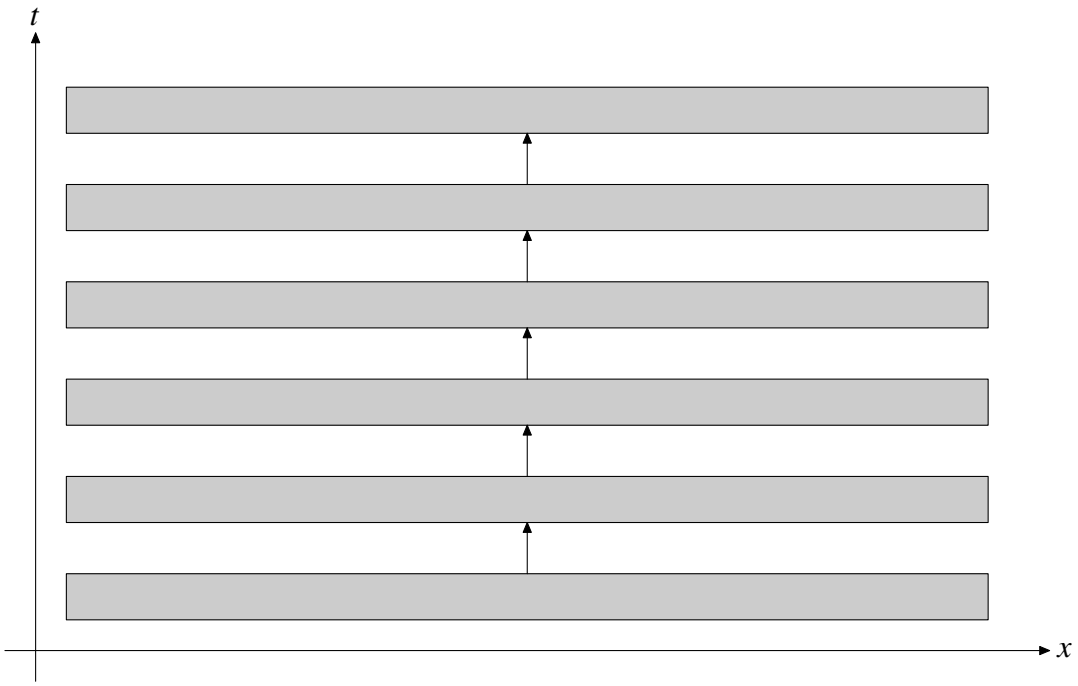

(a) Parallelization only in time direction.

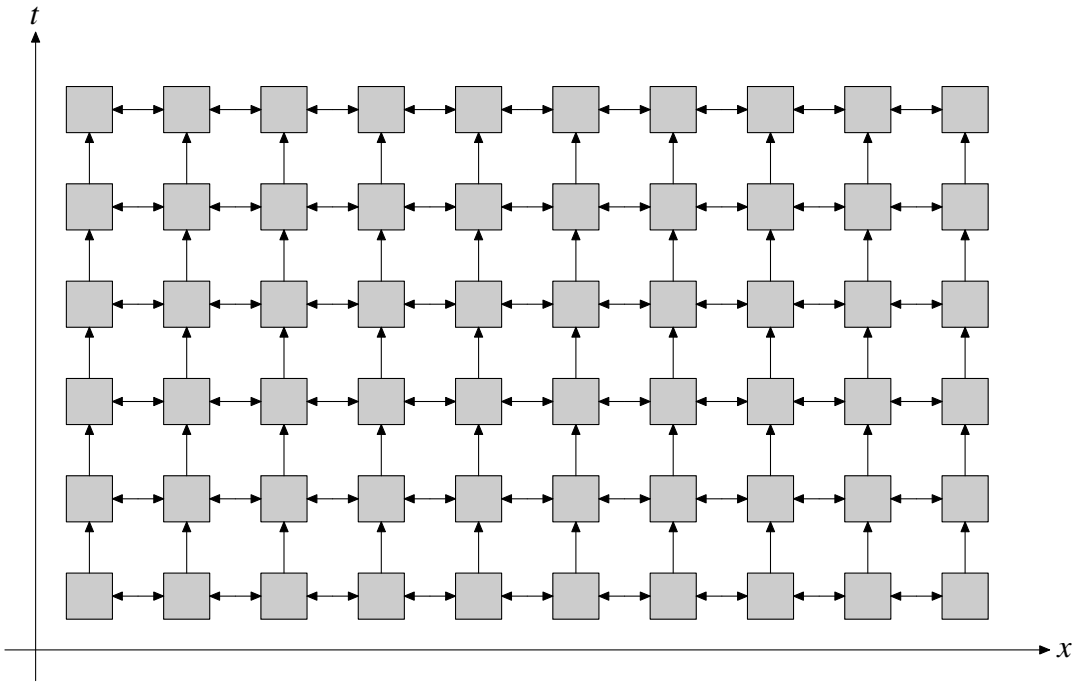

(b) Full space-time parallelization.

Figure 4.29: Communication pattern on a fixed level.

cores	time steps	dof	iter	time
1	4	59 768	9	6.8
2	8	119 536	9	8.1
4	16	239 072	9	9.2
8	32	478 144	9	9.2
16	64	956 288	9	9.2
32	128	1 912 576	9	9.3
64	256	3 825 152	9	9.1
128	512	7 650 304	9	9.4
256	1 024	15 300 608	9	9.4
512	2 048	30 601 216	9	9.4
1 024	4 096	61 202 432	9	9.4
2 048	8 192	122 404 864	9	9.5

Table 4.6: Weak scaling results with solving times in [s].

cores	time steps	dof	iter	time
1	4 096	61 202 432	9	6 960.7
2	4 096	61 202 432	9	3 964.8
4	4 096	61 202 432	9	2 106.2
8	4 096	61 202 432	9	1 056.0
16	4 096	61 202 432	9	530.4
32	4 096	61 202 432	9	269.5
64	4 096	61 202 432	9	135.2
128	4 096	61 202 432	9	68.2
256	4 096	61 202 432	9	34.7
512	4 096	61 202 432	9	17.9
1 024	4 096	61 202 432	9	9.4
2 048	4 096	61 202 432	9	5.4

Table 4.7: Strong scaling results with solving times in [s].

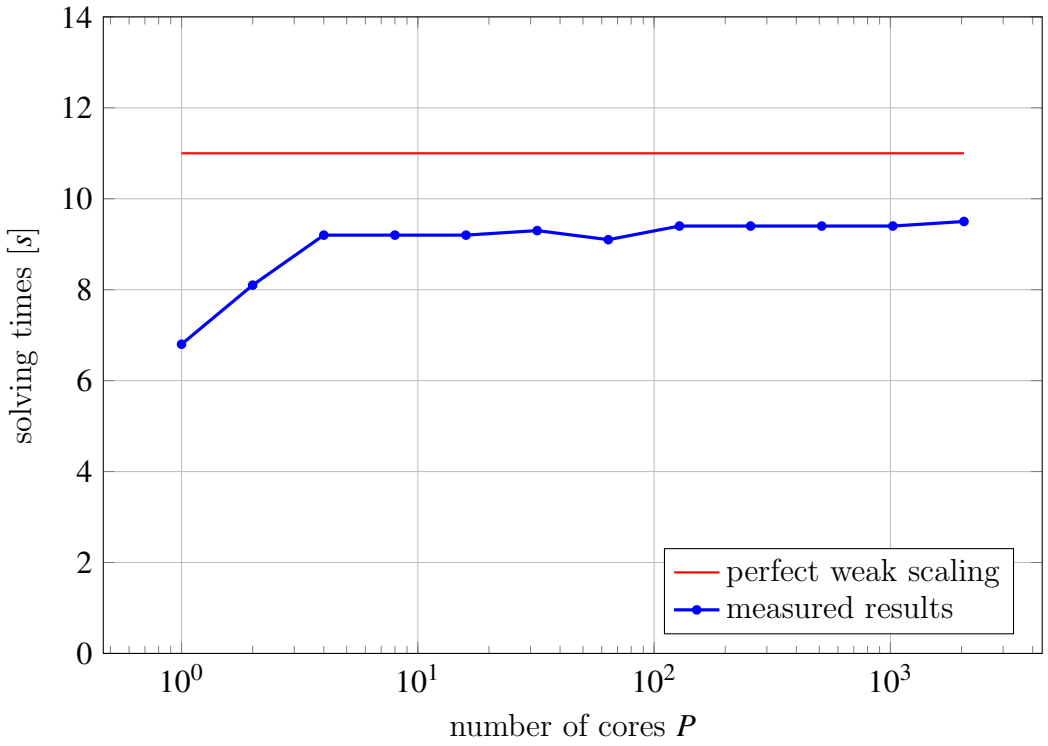

Figure 4.30: Weak scaling results.

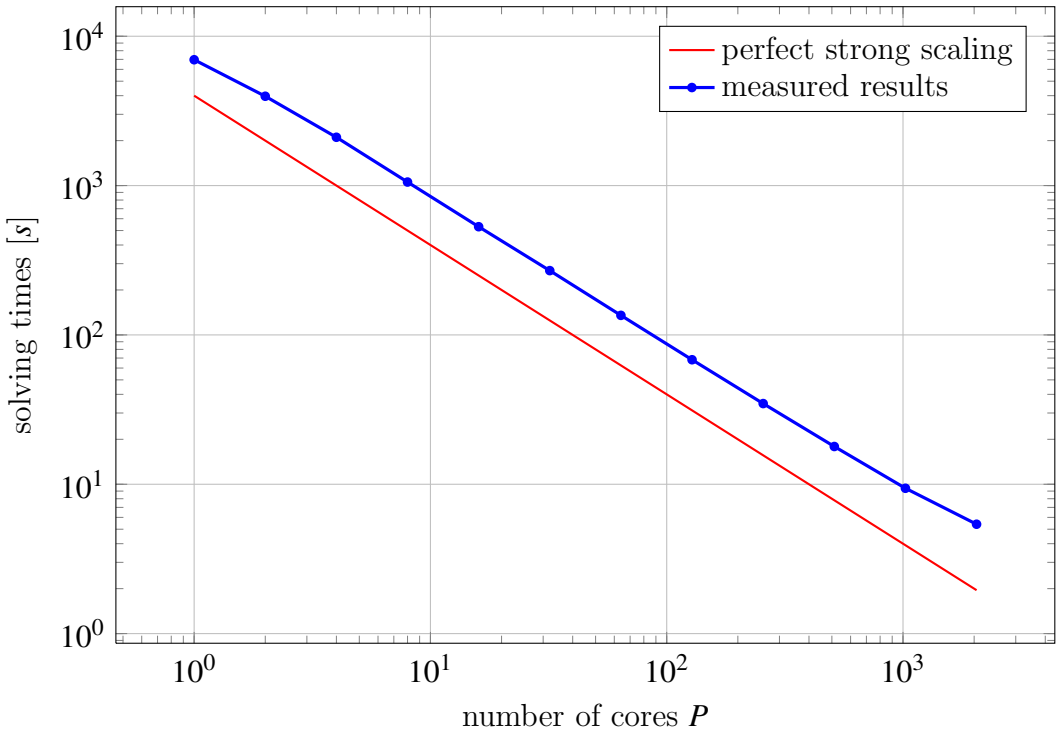

Figure 4.31: Strong scaling results.

5 APPLICATIONS

In this chapter we will apply the space-time discretization scheme (2.2) introduced in Chapter 2 and the hybrid space-time formulation (3.7) as given in Chapter 3 to the Navier-Stokes equations, i.e. for $\nu > 0$ we consider the following problem

$$\begin{aligned} \partial_t \boldsymbol{u} - \nu \Delta \boldsymbol{u} + (\boldsymbol{u} \cdot \nabla_{\boldsymbol{x}})\, \boldsymbol{u} + \nabla_{\boldsymbol{x}} p &= \boldsymbol{f} && \text{in } Q, \\ \operatorname{div}(\boldsymbol{u}) &= 0 && \text{in } Q, \\ \boldsymbol{u} &= \boldsymbol{g}_D && \text{on } \Sigma_D, \\ \nu\, (\nabla_{\boldsymbol{x}} \boldsymbol{u})\, \boldsymbol{n}_{\boldsymbol{x}} - p \boldsymbol{n}_{\boldsymbol{x}} &= \boldsymbol{0} && \text{on } \Sigma_N, \\ \boldsymbol{u} &= \boldsymbol{u}_0 && \text{on } \Sigma_0. \end{aligned} \tag{5.1}$$

Space-time methods for flow problems have been studied for example in [52, 92–94, 100]. In the first section we will introduce the space-time discretization for the Navier-Stokes problem (5.1). A hybrid discretization scheme will be derived in Section 5.2 and in the last section we will apply this method to simulate the flow in a pump.

5.1 Space-time discretizations

In this section we derive a space-time discretization scheme for the problem (5.1). This scheme is based on the space-time formulation (2.2) as introduced in Chapter 2. First we will define the discrete function spaces which we use to approximate the model problem (5.1). Let $p \in \mathbb{N}_0$, then we define the spaces of piecewise polynomials

$$\begin{aligned} V_h^{p+1}(\mathcal{T}_N) &:= \left[S_h^{p+1}(\mathcal{T}_N) \right]^d \\ &= \left\{ \boldsymbol{v}_h \in [L_2(Q)]^d : \boldsymbol{v}_{h|\tau_\ell} \in \left[\mathbb{P}_{p+1}(\tau_\ell) \right]^d \text{ for all } \tau_\ell \in \mathcal{T}_N, \boldsymbol{v}_h = \boldsymbol{0} \text{ on } \Sigma_D \right\} \\ Q_h^p(\mathcal{T}_N) &:= \left\{ q_h \in L_2(Q) : q_{h|\tau_\ell} \in \mathbb{P}_p(\tau_\ell) \text{ for all } \tau_\ell \in \mathcal{T}_N \right\}. \end{aligned}$$

In the first equation of the model problem (5.1) the vector valued heat equation is contained. This part will be discretized by the space-time formulation (2.2). This motivates to define the following bilinear form.

$$A(\boldsymbol{u}_h, \boldsymbol{v}_h) := \sum_{i=1}^{d} \left[b(\boldsymbol{u}_h[i], \boldsymbol{v}_h[i]) + \nu a(\boldsymbol{u}_h[i], \boldsymbol{v}_h[i]) \right] \tag{5.2}$$

Next we will derive a discretization scheme for the gradient of the pressure, i.e. $\nabla_{\boldsymbol{x}} p$. To do so, we multiply the gradient of the pressure with a test function $\boldsymbol{v}_h \in V_h^{p+1}(\mathcal{T}_N)$ and integrate over the space-time domain Q. Hence we have

$$-\int_Q \nabla_{\boldsymbol{x}} p(\boldsymbol{x},t)\cdot \boldsymbol{v}_h(\boldsymbol{x},t)\mathrm{d}(\boldsymbol{x},t) = -\sum_{\ell=1}^{N}\int_{\tau_\ell} \nabla_{\boldsymbol{x}} p(\boldsymbol{x},t)\cdot \boldsymbol{v}_h(\boldsymbol{x},t)\mathrm{d}(\boldsymbol{x},t).$$

Integration by parts yields

$$\begin{aligned}
&= \sum_{\ell=1}^{N}\int_{\tau_\ell} p(\boldsymbol{x},t)\mathrm{div}(\boldsymbol{v}_h(\boldsymbol{x},t))\mathrm{d}(\boldsymbol{x},t) - \sum_{\ell=1}^{N}\int_{\partial\tau_\ell} p(\boldsymbol{x},t)\boldsymbol{v}_h(\boldsymbol{x},t)\cdot \boldsymbol{n}_{\boldsymbol{x}}\mathrm{d}s_{(\boldsymbol{x},t)}\\
&= \sum_{\ell=1}^{N}\int_{\tau_\ell} p(\boldsymbol{x},t)\mathrm{div}(\boldsymbol{v}_h(\boldsymbol{x},t))\mathrm{d}(\boldsymbol{x},t) - \int_{\Sigma_N} p(\boldsymbol{x},t)\boldsymbol{v}_h(\boldsymbol{x},t)\cdot \boldsymbol{n}_{\boldsymbol{x}}\mathrm{d}s_{(\boldsymbol{x},t)}\\
&\quad - \sum_{\Gamma_{k\ell}\in\mathcal{I}_N}\int_{\Gamma_{k\ell}} [p\,\boldsymbol{v}_h]_{\Gamma_{k\ell},\boldsymbol{x}}(\boldsymbol{x},t)\mathrm{d}s_{(\boldsymbol{x},t)}.
\end{aligned}$$

By rewriting the jump terms we have

$$\begin{aligned}
&= \sum_{\ell=1}^{N}\int_{\tau_\ell} p(\boldsymbol{x},t)\mathrm{div}(\boldsymbol{v}_h(\boldsymbol{x},t))\mathrm{d}(\boldsymbol{x},t) - \int_{\Sigma_N} p(\boldsymbol{x},t)\boldsymbol{v}_h(\boldsymbol{x},t)\cdot \boldsymbol{n}_{\boldsymbol{x}}\mathrm{d}s_{(\boldsymbol{x},t)}\\
&\quad - \sum_{\Gamma_{k\ell}\in\mathcal{I}_N}\int_{\Gamma_{k\ell}} \Big[[p]_{\Gamma_{k\ell},\boldsymbol{x}}(\boldsymbol{x},t)\cdot\langle \boldsymbol{v}_h\rangle_{\Gamma_{k\ell}}(\boldsymbol{x},t) + \langle p\rangle_{\Gamma_{k\ell}}(\boldsymbol{x},t)\,[\boldsymbol{v}_h]_{\Gamma_{k\ell},\boldsymbol{x}}(\boldsymbol{x},t)\Big]\mathrm{d}s_{(\boldsymbol{x},t)}.
\end{aligned}$$

If we assume that the pressure p is continuous we obtain

$$\begin{aligned}
&= \sum_{\ell=1}^{N}\int_{\tau_\ell} p(\boldsymbol{x},t)\mathrm{div}(\boldsymbol{v}_h(\boldsymbol{x},t))\mathrm{d}(\boldsymbol{x},t) - \sum_{\Gamma_{k\ell}\in\mathcal{I}_N}\int_{\Gamma_{k\ell}} \langle p\rangle_{\Gamma_{k\ell}}(\boldsymbol{x},t)\,[\boldsymbol{v}_h]_{\Gamma_{k\ell},\boldsymbol{x}}(\boldsymbol{x},t)\mathrm{d}s_{(\boldsymbol{x},t)}\\
&\quad - \int_{\Sigma_N} p(\boldsymbol{x},t)\boldsymbol{v}_h(\boldsymbol{x},t)\cdot \boldsymbol{n}_{\boldsymbol{x}}\mathrm{d}s_{(\boldsymbol{x},t)}.
\end{aligned}$$

This motivates to define the bilinear form

$$\begin{aligned}
B(\boldsymbol{v}_h,p_h) := &\sum_{\ell=1}^{N}\int_{\tau_\ell} p_h(\boldsymbol{x},t)\,\mathrm{div}(\boldsymbol{v}_h(\boldsymbol{x},t))\mathrm{d}(\boldsymbol{x},t)\\
&- \sum_{\Gamma_{k\ell}\in\mathcal{I}_N}\int_{\Gamma_{k\ell}} \langle p_h\rangle_{\Gamma_{k\ell}}(\boldsymbol{x},t)\,[\boldsymbol{v}_h]_{\Gamma_{k\ell},\boldsymbol{x}}(\boldsymbol{x},t)\mathrm{d}s_{(\boldsymbol{x},t)}.
\end{aligned} \tag{5.3}$$

If we assume, that $\boldsymbol{u}$ is a classical solution of the model problem (5.1) we have for $q_h \in Q_h^p(\mathcal{T}_N)$

$$\begin{aligned} B(\boldsymbol{u}, q_h) = \sum_{\ell=1}^{N} \int_{\tau_\ell} q_h(\boldsymbol{x},t)\,\mathrm{div}(\boldsymbol{u}(\boldsymbol{x},t))\mathrm{d}(\boldsymbol{x},t) \\ - \sum_{\Gamma_{k\ell}\in\mathcal{I}_N} \int_{\Gamma_{k\ell}} \langle q_h\rangle_{\Gamma_{k\ell}}(\boldsymbol{x},t)\,[\boldsymbol{u}]_{\Gamma_{k\ell},\boldsymbol{x}}(\boldsymbol{x},t)\mathrm{d}s_{(\boldsymbol{x},t)} = 0. \end{aligned} \tag{5.4}$$

Hence we will use the formulation (5.4) to discretize the second equation of the model problem (5.1). Finally we define a stabilization term for the pressure

$$D(p_h, q_h) := \sigma_p \sum_{\Gamma_{k\ell}\in\mathcal{I}_N} \overline{h}_{k\ell} \int_{\Gamma_{k\ell}} [p_h]_{\Gamma_{k\ell}}(\boldsymbol{x},t)\cdot[q_h]_{\Gamma_{k\ell}}(\boldsymbol{x},t)\mathrm{d}s_{(\boldsymbol{x},t)}. \tag{5.5}$$

Now we are able to formulate the discretization scheme for the model problem (5.1).

Find $\boldsymbol{u}_h = \boldsymbol{u}_{h,0} + \mathcal{E}\boldsymbol{g}_D$ with $\boldsymbol{u}_{h,0} \in V_h^{p+1}(\mathcal{T}_N)$ and $p_h \in Q_h^p(\mathcal{T}_N)$, such that

$$\begin{aligned} A(\boldsymbol{u}_h, \boldsymbol{v}_h) + \langle(\boldsymbol{u}_h\cdot\nabla_{\boldsymbol{x}})\boldsymbol{u}_h, \boldsymbol{v}_h\rangle_Q - B(\boldsymbol{v}_h, p_h) = \langle \boldsymbol{f}, \boldsymbol{v}_h\rangle_Q + \langle \boldsymbol{u}_0, \boldsymbol{v}_h\rangle_{\Sigma_0}, \\ B(\boldsymbol{u}_h, q_h) + D(p_h, q_h) = 0 \end{aligned} \tag{5.6}$$

for all $\boldsymbol{v}_h \in V_h^{p+1}(\mathcal{T}_N)$ and $q_h \in Q_h^p(\mathcal{T}_N)$.

Remark 5.1.1. *In the discrete formulation (5.6) the nonlinearity is treated in the simplest way. For discontinuous Galerkin schemes it is possible to apply an upwind technique for the nonlinear convective term, see [79].*

Lemma 5.1.2 (Stability condition)**.** *For the decomposition $\mathcal{T}_N$ and the discrete subspace*

$$\widetilde{V}_h^{p+1}(\mathcal{T}_N) := \left\{ \boldsymbol{v}_h \in V_h^{p+1}(\mathcal{T}_N)\cap\mathcal{C}(\mathcal{T}_N) : \boldsymbol{v}_h = \boldsymbol{0} \text{ on } \Sigma_D\cup\Sigma_0\cup\Sigma_T \right\} \subset V_h^{p+1}(\mathcal{T}_N),$$

let the stability estimate

$$\sup_{\boldsymbol{0}\neq\boldsymbol{v}_h\in\widetilde{V}_h^{p+1}(\mathcal{T}_N)} \frac{\int_Q \nabla_{\boldsymbol{x}} p_h(\boldsymbol{x},t)\cdot\boldsymbol{v}_h(\boldsymbol{x},t)\mathrm{d}(\boldsymbol{x},t)}{\|\boldsymbol{v}_h\|_{[H^1(Q)]^d}} \geq c_S\|p_h\|_{L_2(Q)} \tag{5.7}$$

be fulfilled for all $p_h \in Q_h^p(\mathcal{T}_N)\cap\mathcal{C}(\mathcal{T}_N)$, then the following stability estimate

$$\sup_{\boldsymbol{0}\neq\boldsymbol{v}_h\in V_h^{p+1}(\mathcal{T}_N)} \frac{B(\boldsymbol{v}_h, p_h)}{\|\boldsymbol{v}_h\|_{\mathbf{DG}}} \geq \tilde{c}_S\|p_h\|_{L_2(Q)} \tag{5.8}$$

holds for all $p_h \in \ker(D) = Q_h^p(\mathcal{T}_N)\cap\mathcal{C}(\mathcal{T}_N)$, with the vector valued energy norm

$$\|\boldsymbol{v}_h\|_{\mathbf{DG}}^2 := \sum_{i=1}^{d} \|\boldsymbol{v}_h[i]\|_{\mathrm{DG}}^2.$$

Proof. For $\boldsymbol{v}_h \in \widetilde{V}_h^{p+1}(\mathcal{T}_N)$ and $i = 1,\dots,d$ we observe that

$$\begin{aligned}
\|\boldsymbol{v}_h[i]\|_{\mathrm{DG}}^2 &= \|\boldsymbol{v}_h[i]\|_A^2 + \|\boldsymbol{v}_h[i]\|_B^2 \\
&= \sum_{\ell=1}^{N} \|\nabla_{\boldsymbol{x}} \boldsymbol{v}_h[i]\|_{[L_2(\tau_\ell)]^d}^2 + \sum_{\ell=1}^{N} h_\ell \|\partial_t \boldsymbol{v}_h[i]\|_{L_2(\tau_\ell)}^2 \\
&\le (1+h_{\max}) \sum_{\ell=1}^{N} \left[\|\nabla_{\boldsymbol{x}} \boldsymbol{v}_h[i]\|_{[L_2(\tau_\ell)]^d}^2 + \|\partial_t \boldsymbol{v}_h[i]\|_{L_2(\tau_\ell)}^2 \right] \\
&= (1+h_{\max}) \sum_{\ell=1}^{N} \|\nabla \boldsymbol{v}_h[i]\|_{[L_2(\tau_\ell)]^{d+1}}^2 \le (1+h_{\max}) \|\boldsymbol{v}_h[i]\|_{H^1(Q)}^2,
\end{aligned}$$

with $h_{\max} := \max\{h_\ell : \ell = 1,\dots,N\}$. Hence we have

$$\|\boldsymbol{v}_h\|_{\mathrm{DG}} \le \sqrt{1+h_{\max}}\, \|\boldsymbol{v}_h\|_{[H^1(Q)]^d}.$$

Further, for $p_h \in Q_h^p(\mathcal{T}_N) \cap \mathcal{C}(\mathcal{T}_N)$ and $\boldsymbol{v}_h \in \widetilde{V}_h^{p+1}(\mathcal{T}_N)$ we obtain

$$\begin{aligned}
B(\boldsymbol{v}_h, p_h) &= \sum_{\ell=1}^{N} \int_{\tau_\ell} p_h(\boldsymbol{x},t) \mathrm{div}(\boldsymbol{v}_h(\boldsymbol{x},t)) \mathrm{d}(\boldsymbol{x},t) \\
&\qquad - \sum_{\Gamma_{k\ell} \in \mathcal{I}_N} \int_{\Gamma_{k\ell}} \langle p_h \rangle_{\Gamma_{k\ell}}(\boldsymbol{x},t)\, [\boldsymbol{v}_h]_{\Gamma_{k\ell},\boldsymbol{x}}(\boldsymbol{x},t) \mathrm{d}s_{(\boldsymbol{x},t)} \\
&= \sum_{\ell=1}^{N} \int_{\tau_\ell} p_h(\boldsymbol{x},t) \mathrm{div}(\boldsymbol{v}_h(\boldsymbol{x},t)) \mathrm{d}(\boldsymbol{x},t) \\
&= \int_{Q} p_h(\boldsymbol{x},t) \mathrm{div}(\boldsymbol{v}_h(\boldsymbol{x},t)) \mathrm{d}(\boldsymbol{x},t) = - \int_{Q} \nabla_{\boldsymbol{x}} p_h(\boldsymbol{x},t) \cdot \boldsymbol{v}_h(\boldsymbol{x},t) \mathrm{d}(\boldsymbol{x},t).
\end{aligned}$$

Hence we have

$$\begin{aligned}
\sup_{\mathbf{0} \neq \boldsymbol{v}_h \in V_h^{p+1}(\mathcal{T}_N)} \frac{B(\boldsymbol{v}_h, p_h)}{\|\boldsymbol{v}_h\|_{\mathbf{DG}}} &\ge \sup_{\mathbf{0} \neq \boldsymbol{v}_h \in \widetilde{V}_h^{p+1}(\mathcal{T}_N)} \frac{B(\boldsymbol{v}_h, p_h)}{\|\boldsymbol{v}_h\|_{\mathbf{DG}}} \\
&= \sup_{\mathbf{0} \neq \boldsymbol{v}_h \in \widetilde{V}_h^{p+1}(\mathcal{T}_N)} \frac{-\int_Q \nabla_{\boldsymbol{x}} p_h(\boldsymbol{x},t) \cdot \boldsymbol{v}_h(\boldsymbol{x},t) \mathrm{d}(\boldsymbol{x},t)}{\|\boldsymbol{v}_h\|_{\mathbf{DG}}} \\
&\ge \frac{1}{\sqrt{1+h_{\max}}} \sup_{\mathbf{0} \neq \boldsymbol{v}_h \in \widetilde{V}_h^{p+1}} \frac{-\int_Q \nabla_{\boldsymbol{x}} p_h(\boldsymbol{x},t) \cdot \boldsymbol{v}_h(\boldsymbol{x},t) \mathrm{d}(\boldsymbol{x},t)}{\|\boldsymbol{v}_h\|_{[H^1(Q)]^d}} \\
&\ge \frac{c_S}{\sqrt{1+h_{\max}}} \|p_h\|_{L_2(Q)}.
\end{aligned}$$

■

Remark 5.1.3. *If we compare the stability estimate (5.7) with the standard stability estimate for the stationary case, i.e.*

$$\sup_{\mathbf{0}\neq \boldsymbol{v}_h\in\left[S_h^{p+1}(\mathcal{T}_N)\right]^{d+1}} \frac{\int_Q \nabla p_h(\boldsymbol{x},t)\cdot \boldsymbol{v}_h(\boldsymbol{x},t)\mathrm{d}(\boldsymbol{x},t)}{\|\boldsymbol{v}_h\|_{\left[H^1(Q)\right]^{d+1}}} \geq c_S \|p_h\|_{L_2(Q)},$$

we observe, that in the stability estimate (5.7) only the spatial gradient $\nabla_{\boldsymbol{x}}$ appears instead of the full gradient ∇. Hence, to prove the stability estimate (5.7) for the finite element pairing $(V_h^{p+1}(\mathcal{T}_N), Q_h^p(\mathcal{T}_N))$, one has to modify the standard proof for the stability estimate of the standard Taylor-Hood elements.

Remark 5.1.4. *For the linearized Navier-Stokes equations the stability result of Lemma 5.1.2 implies with the stability estimate for the bilinear form $A(\cdot,\cdot)$, see Theorem 2.2.21, the unique solvability of the discrete variational problem*

Find $\boldsymbol{u}_{h,0}\in V_h^{p+1}(\mathcal{T}_N)$ and $p_h\in Q_h^p(\mathcal{T}_N)$, such that

$$\begin{aligned} A(\boldsymbol{u}_{h,0},\boldsymbol{v}_h) - B(\boldsymbol{v}_h,p_h) &= \langle \boldsymbol{f},\boldsymbol{v}_h\rangle_Q + \langle \boldsymbol{u}_0,\boldsymbol{v}_h\rangle_{\Sigma_0} - A(\mathcal{E}\boldsymbol{g}_D,\boldsymbol{v}_h),\\ B(\boldsymbol{u}_{h,0},q_h) + D(p_h,q_h) &= -B(\mathcal{E}\boldsymbol{g}_D,q_h) \end{aligned}$$

for all $\boldsymbol{v}_h\in V_h^{p+1}(\mathcal{T}_N)$ and $q_h\in Q_h^p(\mathcal{T}_N)$.

Furthermore, by assuming quasi uniform decompositions $\mathcal{T}_N$ and by using standard arguments we observe the following error estimate in the energy norms

$$\|\boldsymbol{u}-\boldsymbol{u}_h\|_{\mathbf{DG}} + \|p-p_h\|_{L_2(Q)} \leq c h^{\min\{s,p+2\}-1}\left[|\boldsymbol{u}|_{[H^s(\mathcal{T}_N)]^{d+1}} + |\boldsymbol{p}|_{H^{s-1}(\mathcal{T}_N)}\right], \quad (5.9)$$

with $u_h = \boldsymbol{u}_{h,0} + \mathcal{E}\boldsymbol{g}_D$ and $s\geq 2$.

In what follows, we will introduce the equivalent system of algebraic equations for the discrete problem (5.6). For the discrete function spaces $V_h^{p+1}(\mathcal{T}_N)$ and $Q_h^p(\mathcal{T}_N)$ we define the basis functions

$$V_h^{p+1}(\mathcal{T}_N) = \operatorname{span}\{\boldsymbol{\varphi}_{\ell=1}\}_{\ell}^{M_u}, \quad \boldsymbol{u}_{h,0}(\boldsymbol{x},t) = \sum_{\ell=1}^{M_u} \boldsymbol{u}[\ell]\boldsymbol{\varphi}_\ell(\boldsymbol{x},t) \quad \text{for } \boldsymbol{u}_{h,0}\in V_h^{p+1}(\mathcal{T}_N),$$

$$Q_h^p(\mathcal{T}_N) = \operatorname{span}\{\psi_n\}_{n=1}^{M_p}, \qquad p_h(\boldsymbol{x},t) = \sum_{n=1}^{M_p} \boldsymbol{p}[n]\psi_n(\boldsymbol{x},t) \qquad \text{for } p_h\in Q_h^p(\mathcal{T}_N).$$

We define the nonlinear operator

$$(K_h\boldsymbol{u})[k] := A(\boldsymbol{u}_h,\boldsymbol{\varphi}_k) + \langle (\boldsymbol{u}_h\cdot\nabla_{\boldsymbol{x}})\boldsymbol{u}_h,\boldsymbol{\varphi}_k\rangle_Q$$

for $\boldsymbol{u}_h = \mathcal{E}\boldsymbol{g}_D + \sum_{\ell=1}^{M_u} \boldsymbol{u}[\ell]\boldsymbol{\varphi}_\ell$ and the matrices

$$B_h[m,\ell] := B(\boldsymbol{\varphi}_\ell, \psi_m), \qquad D_h[m,n] := D(\psi_n, \psi_m),$$

for $k,\ell = 1,\dots,M_u$ and $m,n = 1,\dots,M_p$. Then the discrete variational problem (5.6) is equivalent to the system of algebraic equations

$$\begin{pmatrix} K_h & -B_h{}^\top \\ B_h & D_h \end{pmatrix} \begin{pmatrix} \boldsymbol{u} \\ \boldsymbol{p} \end{pmatrix} = \begin{pmatrix} \boldsymbol{f}_u \\ \boldsymbol{f}_p \end{pmatrix}, \tag{5.10}$$

with the vectors

$$\begin{aligned} \boldsymbol{f}_u[k] &:= \langle \boldsymbol{f}, \boldsymbol{\varphi}_k \rangle_Q + \langle \boldsymbol{u}_0, \boldsymbol{\varphi}_k \rangle_{\Sigma_0}, \\ \boldsymbol{f}_p[m] &:= -B(\mathcal{E}\boldsymbol{g}_D, \psi_m) \end{aligned}$$

for $k = 1,\dots,M_u$ and $m = 1,\dots,M_p$. To solve the nonlinear problem (5.10) we apply a fixed point scheme or Newton's method.

Example 5.1.5. In this example we consider the spatial domain $\Omega = (0,1)^2$ and the simulation time $T = 1$. The Neumann and Dirichlet space-time boundaries are given by

$$\begin{aligned} \Sigma_N &:= \{(1,x_2) \in \mathbb{R}^2 : 0 \le x_2 \le 1\} \times [0,T], \\ \Sigma_D &:= \overline{(\partial\Omega \times [0,T]) \setminus \Sigma_N}. \end{aligned}$$

The given data $\boldsymbol{f}$, $\boldsymbol{g}_D$ and $\boldsymbol{u}_0$ are chosen, such that the solutions $\boldsymbol{u}$ and p of (5.1) are given by the regular functions

$$\boldsymbol{u}(x_1,x_2,t) = \begin{pmatrix} t(1-x_1)\cos(x_2) \\ t\sin(x_2) \end{pmatrix}, \qquad p(x_1,x_2,t) = -\nu t \cos(x_2)$$

with $\nu = 1$. For the initial decomposition of the space-time domain $Q = (0,1)^3$ we use $N = 6$ tetrahedra, as given in Figure 2.4a. To study the convergence behaviour of the numerical approach (5.6) we apply several uniform refinement steps. Further we use the element pairings $(V_h^1(\mathcal{T}_N), Q_h^0(\mathcal{T}_N))$ and $(V_h^2(\mathcal{T}_N), Q_h^1(\mathcal{T}_N))$, i.e. $p = 0$ and $p = 1$, to compute approximations for the given exact solution. As a stabilization parameter we use $\sigma = 10(p+1)$ and $\sigma_p = 10$. To solve the nonlinear system (5.10) we apply Newton's method, where each linear problem is solved with the solver package PARDISO [82, 83]. In the Tables 5.1–5.2 the numerical errors are given in the energy norms $\|\boldsymbol{u} - \boldsymbol{u}_h\|_{\mathbf{DG}}$ and $\|p - p_h\|_{L_2(Q)}$. We observe, that the convergence rates behave as expected.

level	elements	dof $\boldsymbol{u}_h$	dof p_h	$\|\boldsymbol{u}-\boldsymbol{u}_h\|_{\mathbf{DG}}$	eoc	$\|p-p_h\|_{L_2(Q)}$	eoc
0	6	16	6	$5.9776-1$	–	$3.1450-1$	–
1	48	248	48	$2.9742-1$	1.01	$2.4636-1$	0.35
2	384	2 512	384	$1.6879-1$	0.82	$2.1774-1$	0.18
3	3 072	22 304	3 072	$9.7794-2$	0.79	$1.6074-1$	0.44
4	24 576	187 456	24 576	$4.9947-2$	0.97	$9.1229-2$	0.82
5	196 608	1 536 128	196 608	$2.2355-2$	1.16	$4.0581-2$	1.17
Theory:					1.00		1.00

Table 5.1: Numerical results for the finite element pairing $(V_h^1(\mathcal{T}_N), Q_h^0(\mathcal{T}_N))$.

level	elements	dof $\boldsymbol{u}_h$	dof p_h	$\|\boldsymbol{u}-\boldsymbol{u}_h\|_{\mathbf{DG}}$	eoc	$\|p-p_h\|_{L_2(Q)}$	eoc
0	6	54	24	$1.0881-1$	–	$1.7006-1$	–
1	48	684	192	$3.1840-2$	1.77	$1.9859-2$	3.10
2	384	6 552	1 536	$7.9904-3$	1.99	$4.0378-3$	2.30
3	3 072	56 880	12 288	$1.9818-3$	2.01	$9.6060-4$	2.07
4	24 576	473 184	98 304	$4.9134-4$	2.01	$2.3394-4$	2.04
Theory:					2.00		2.00

Table 5.2: Numerical results for the finite element pairing $(V_h^2(\mathcal{T}_N), Q_h^1(\mathcal{T}_N))$.

5.2 Hybrid space-time discretizations

In this section a hybrid discretization scheme with respect to the problem (5.1) will be derived. As in Chapter 3 we introduce a decomposition of the space-time domain $Q \subset \mathbb{R}^{d+1}$ into non-overlapping subdomains Q_i for $i = 1, \ldots, P$. We will use the same notations as in Chapter 3 for the interface Σ, the interior facets on the interface Σ_h and the decompositions $\mathcal{T}_{N_i}$ for the subdomains Q_i with interior facets $\mathcal{I}_{N_i}$. On the interface Σ we define for $p \in \mathbb{N}_0$ the following discrete functions spaces of piecewise polynomials

$$V_h^{p+1}(\Sigma_h) := \left\{ \boldsymbol{\mu}_h \in [L_2(\Sigma)]^d : \boldsymbol{\mu}_{h|\Gamma_{k\ell}} \in \left[\mathbb{P}_{p+1}(\Gamma_{k\ell})\right]^d \text{ for all } \Gamma_{k\ell} \in \Sigma_h \right\},$$
$$Q_h^p(\Sigma_h) := \left\{ \eta_h \in L_2(\Sigma) : \eta_{h|\Gamma_{k\ell}} \in \mathbb{P}_p(\Gamma_{k\ell}) \text{ for all } \Gamma_{k\ell} \in \Sigma_h \right\}.$$

Summing up all local decompositions $\mathcal{T}_{N_i}$ for $i = 1, \ldots, P$ results in a decomposition of the space-time domain Q, i.e.

$$\overline{Q} = \overline{\mathcal{T}}_N := \bigcup_{i=1}^{P} \bigcup_{\tau_\ell^i \in \mathcal{T}_{N_i}} \overline{\tau}_\ell^i.$$

With respect to the decomposition $\mathcal{T}_N$ we can use the space-time formulation (5.6) to get an approximation for the problem (5.1). On each subdomain Q_i we will

apply the space-time formulation (5.6). To do so, we define for $\boldsymbol{u}_h, \boldsymbol{v}_h \in V_h^{p+1}(\mathcal{T}_N)$ and $p_h, q_h \in Q_h^p(\mathcal{T}_N)$ the following local bilinear forms

$$\begin{aligned}
A^{(i)}(\boldsymbol{u}_h, \boldsymbol{v}_h) &:= \sum_{i=1}^{d} \left[b^{(i)}(\boldsymbol{u}_h[i], \boldsymbol{v}_h[i]) + \nu a^{(i)}(\boldsymbol{u}_h[i], \boldsymbol{v}_h[i]) \right], \\
B^{(i)}(\boldsymbol{v}_h, p_h) &:= \sum_{\ell=1}^{N_i} \int_{\tau_\ell^i} p_h(\boldsymbol{x},t) \mathrm{div}(\boldsymbol{v}_h(\boldsymbol{x},t)) \mathrm{d}(\boldsymbol{x},t) \\
&\quad - \sum_{\Gamma_{k\ell} \in \mathcal{I}_{N_i}} \int_{\Gamma_{k\ell}} \langle p_h \rangle_{\Gamma_{k\ell}}(\boldsymbol{x},t) \, [\boldsymbol{v}_h]_{\Gamma_{k\ell},\boldsymbol{x}}(\boldsymbol{x},t) \mathrm{d}s_{(\boldsymbol{x},t)}, \\
D^{(i)}(p_h, q_h) &:= \sigma_p \sum_{\Gamma_{k\ell} \in \mathcal{I}_{N_i}} \overline{h}_{k\ell} \int_{\Gamma_{k\ell}} [p_h]_{\Gamma_{k\ell}}(\boldsymbol{x},t) \cdot [q_h]_{\Gamma_{k\ell}}(\boldsymbol{x},t) \mathrm{d}s_{(\boldsymbol{x},t)}
\end{aligned}$$

for $i = 1, \ldots, P$. Further we define the local right hand sides

$$F^{(i)}(\boldsymbol{v}_h) := \langle \boldsymbol{f}, \boldsymbol{v}_h \rangle_{Q_i} + \langle \boldsymbol{u}_0, \boldsymbol{v}_h \rangle_{\Sigma_0 \cap \partial Q_i},$$

for all $i = 1, \ldots, P$. With these local bilinear forms we obtain

$$\begin{aligned}
\langle (\boldsymbol{u}_h \cdot \nabla_{\boldsymbol{x}}) \boldsymbol{u}_h, \boldsymbol{v}_h \rangle_Q - B(\boldsymbol{v}_h, p_h) &= \sum_{i=1}^{P} \left[\langle (\boldsymbol{u}_h \cdot \nabla_{\boldsymbol{x}}) \boldsymbol{u}_h, \boldsymbol{v}_h \rangle_{Q_i} - B^{(i)}(\boldsymbol{v}_h, p_h) \right] \\
&\quad + \sum_{\Gamma_{k\ell} \in \Sigma_h} \int_{\Gamma_{k\ell}} \langle p_h \rangle_{\Gamma_{k\ell}}(\boldsymbol{x},t) \, [\boldsymbol{v}_h]_{\Gamma_{k\ell},\boldsymbol{x}}(\boldsymbol{x},t) \mathrm{d}s_{(\boldsymbol{x},t)}.
\end{aligned} \tag{5.11}$$

Furthermore we have

$$\begin{aligned}
B(\boldsymbol{u}_h, q_h) + D(p_h, q_h) &= \sum_{i=1}^{P} \left[B^{(i)}(\boldsymbol{u}_h, q_h) + D^{(i)}(p_h, q_h) \right] \\
&\quad - \sum_{\Gamma_{k\ell} \in \Sigma_h} \int_{\Gamma_{k\ell}} \langle q_h \rangle_{\Gamma_{k\ell}}(\boldsymbol{x},t) \, [\boldsymbol{u}_h]_{\Gamma_{k\ell},\boldsymbol{x}}(\boldsymbol{x},t) \mathrm{d}s_{(\boldsymbol{x},t)} \\
&\quad + \sigma_p \sum_{\Gamma_{k\ell} \in \Sigma_h} \overline{h}_{k\ell} \int_{\Gamma_{k\ell}} [p_h]_{\Gamma_{k\ell}}(\boldsymbol{x},t) \cdot [q_h]_{\Gamma_{k\ell}}(\boldsymbol{x},t) \mathrm{d}s_{(\boldsymbol{x},t)}.
\end{aligned} \tag{5.12}$$

To reduce the coupling on the interface Σ, we will rewrite the coupling terms of (5.11) and (5.12) by introduce the new variables

$$\begin{aligned}
\boldsymbol{\lambda}_{h|\Gamma_{k\ell}}(\boldsymbol{x},t) &:= \langle \boldsymbol{u}_h \rangle_{\Gamma_{k\ell}}(\boldsymbol{x},t), & \boldsymbol{\mu}_{h|\Gamma_{k\ell}}(\boldsymbol{x},t) &:= \langle \boldsymbol{v}_h \rangle_{\Gamma_{k\ell}}(\boldsymbol{x},t), \\
\rho_{h|\Gamma_{k\ell}}(\boldsymbol{x},t) &:= \langle p_h \rangle_{\Gamma_{k\ell}}(\boldsymbol{x},t), & \eta_{h|\Gamma_{k\ell}}(\boldsymbol{x},t) &:= \langle q_h \rangle_{\Gamma_{k\ell}}(\boldsymbol{x},t),
\end{aligned}$$

for $(\boldsymbol{x},t) \in \Gamma_{k\ell}$ and $\Gamma_{k\ell} \in \Sigma_h$. With these new variables we obtain

$$\sum_{\Gamma_{k\ell} \in \Sigma_h} \int_{\Gamma_{k\ell}} \langle p_h \rangle_{\Gamma_{k\ell}}(\boldsymbol{x},t) \, [\boldsymbol{v}_h]_{\Gamma_{k\ell},\boldsymbol{x}}(\boldsymbol{x},t) \mathrm{d}s_{(\boldsymbol{x},t)} = \sum_{\Gamma_{k\ell} \in \Sigma_h} \int_{\Gamma_{k\ell}} \rho_h(\boldsymbol{x},t) \, [\boldsymbol{v}_h]_{\Gamma_{k\ell},\boldsymbol{x}}(\boldsymbol{x},t) \mathrm{d}s_{(\boldsymbol{x},t)}$$

$$= \sum_{\Gamma_{k\ell}\in\Sigma_h} \int_{\Gamma_{k\ell}} \rho_h(\boldsymbol{x},t)\left(\boldsymbol{v}_{h|\tau_k}\cdot\boldsymbol{n}_{k,\boldsymbol{x}} + \boldsymbol{v}_{h|\tau_\ell}\cdot\boldsymbol{n}_{\ell,\boldsymbol{x}}(\boldsymbol{x},t)\right)\mathrm{d}s_{(\boldsymbol{x},t)}$$

$$= \sum_{i=1}^{P}\sum_{\ell=1}^{N_i} \sum_{\substack{\Gamma_{k\ell}\in\Sigma_h \\ \Gamma_{k\ell}\subset\partial\tau_\ell^i}} \int_{\Gamma_{k\ell}} \rho_h(\boldsymbol{x},t)\left(\boldsymbol{v}_{h|\tau_\ell}\cdot\boldsymbol{n}_{\ell,\boldsymbol{x}}(\boldsymbol{x},t)\right)\mathrm{d}s_{(\boldsymbol{x},t)}.$$

Further we have

$$\sum_{\Gamma_{k\ell}\in\Sigma_h} \int_{\Gamma_{k\ell}} \langle q_h\rangle_{\Gamma_{k\ell}}(\boldsymbol{x},t)\,[\boldsymbol{u}_h]_{\Gamma_{k\ell},\boldsymbol{x}}(\boldsymbol{x},t)\mathrm{d}s_{(\boldsymbol{x},t)} = \sum_{\Gamma_{k\ell}\in\Sigma_h} \int_{\Gamma_{k\ell}} \eta_h(\boldsymbol{x},t)\,[\boldsymbol{u}_h]_{\Gamma_{k\ell},\boldsymbol{x}}(\boldsymbol{x},t)\mathrm{d}s_{(\boldsymbol{x},t)}$$

$$= \sum_{i=1}^{P}\sum_{\ell=1}^{N_i} \sum_{\substack{\Gamma_{k\ell}\in\Sigma_h \\ \Gamma_{k\ell}\subset\partial\tau_\ell^i}} \int_{\Gamma_{k\ell}} \eta_h(\boldsymbol{x},t)\left(\boldsymbol{u}_{h|\tau_\ell}\cdot\boldsymbol{n}_{\ell,\boldsymbol{x}}(\boldsymbol{x},t)\right)\mathrm{d}s_{(\boldsymbol{x},t)}.$$

For the remaining coupling term in (5.12) we need the following definition.

Definition 5.2.1 (Hybrid jump)**.** *Let $\Gamma_{k\ell}\in\Sigma_h$ be a facet on the interface Σ with the outer unit normal vector $\boldsymbol{n}_k = (\boldsymbol{n}_{k,\boldsymbol{x}}, n_{k,t})^\top$ with respect to the element τ_k. For a discrete function $p_h\in Q_h^p(\mathcal{T}_N)$ and a function $\rho_h\in Q_h^p(\Sigma_h)$ the hybrid jump for the element τ_k is given by*

$$[p_h/\rho_h]_{\partial\tau_k}(\boldsymbol{x},t) := \Big[p_{h|\tau_k}(\boldsymbol{x},t) - \rho_h(\boldsymbol{x},t)\Big]\boldsymbol{n}_k \quad \text{for } (\boldsymbol{x},t)\in\Gamma_{k\ell} \quad a.e.$$

With this definition of the hybrid jump we obtain

$$[p_h]_{\Gamma_{k\ell}}(\boldsymbol{x},t)\cdot[q_h]_{\Gamma_{k\ell}}(\boldsymbol{x},t) = 2\,[p_h/\rho_h]_{\partial\tau_k}(\boldsymbol{x},t)\cdot[q_h/\eta_h]_{\partial\tau_k}(\boldsymbol{x},t) + 2\,[p_h/\rho_h]_{\partial\tau_\ell}(\boldsymbol{x},t)\cdot[q_h/\eta_h]_{\partial\tau_\ell}(\boldsymbol{x},t).$$

Hence we have

$$\sum_{\Gamma_{k\ell}\in\Sigma_h} \overline{h}_{k\ell}\int_{\Gamma_{k\ell}} [p_h]_{\Gamma_{k\ell}}(\boldsymbol{x},t)\cdot[q_h]_{\Gamma_{k\ell}}(\boldsymbol{x},t)\mathrm{d}s_{(\boldsymbol{x},t)}$$

$$= 2\sum_{i=1}^{P}\sum_{\ell=1}^{N_i} \sum_{\substack{\Gamma_{k\ell}\in\Sigma_h \\ \Gamma_{k\ell}\subset\partial\tau_\ell^i}} \overline{h}_{k\ell}\int_{\Gamma_{k\ell}} [p_h/\rho_h]_{\partial\tau_\ell}(\boldsymbol{x},t)\cdot[q_h/\eta_h]_{\partial\tau_\ell}(\boldsymbol{x},t)\mathrm{d}s_{(\boldsymbol{x},t)}.$$

For each subdomain Q_i, $i = 1,\ldots,P$ this motivates to define the local bilinear

forms

$$
\begin{aligned}
c_A^{(i)}(\boldsymbol{u}_h,\boldsymbol{\lambda}_h;\boldsymbol{v}_h,\boldsymbol{\mu}_h) &:= \sum_{j=1}^{d} c^{(i)}(\boldsymbol{u}_h[j],\boldsymbol{\lambda}_h[j];\boldsymbol{v}_h[j],\boldsymbol{\mu}_h[j]),\\
c_B^{(i)}(\boldsymbol{v}_h,\boldsymbol{\mu}_h;p_h,\rho_h) &:= -\sum_{\ell=1}^{N_i}\sum_{\substack{\Gamma_{k\ell}\in\Sigma_h\\ \Gamma_{k\ell}\subset\partial\tau_\ell^i}}\int_{\Gamma_{k\ell}} \rho_h(\boldsymbol{x},t)\left(\boldsymbol{v}_{h|\tau_\ell}\cdot\boldsymbol{n}_{\ell,\boldsymbol{x}}(\boldsymbol{x},t)\right)\mathrm{d}s_{(\boldsymbol{x},t)},\\
c_D^{(i)}(p_h,\rho_h;q_h,\eta_h) &:= 2\sigma_p\sum_{\ell=1}^{N_i}\sum_{\substack{\Gamma_{k\ell}\in\Sigma_h\\ \Gamma_{k\ell}\subset\partial\tau_\ell^i}}\overline{h}_{k\ell}\int_{\Gamma_{k\ell}}[p_h/\rho_h]_{\partial\tau_\ell}(\boldsymbol{x},t)\cdot[q_h/\eta_h]_{\partial\tau_\ell}(\boldsymbol{x},t)\mathrm{d}s_{(\boldsymbol{x},t)}.
\end{aligned}
\tag{5.13}
$$

With the local bilinear forms (5.13), we are now able to formulate the hybrid space-time discretization scheme.

Find $\boldsymbol{u}_h = \boldsymbol{u}_{h,0} + \mathcal{E}\boldsymbol{g}_D$ with $\boldsymbol{u}_{h,0}\in V_h^{p+1}(\mathcal{T}_N)$, $\boldsymbol{\lambda}_h\in V_h^{p+1}(\Sigma_h)$, $p_h\in Q_h^p(\mathcal{T}_N)$ and $\rho_h\in Q_h^p(\Sigma_h)$, such that

$$
\begin{aligned}
&\sum_{i=1}^{P}\Big[A^{(i)}(\boldsymbol{u}_h,\boldsymbol{v}_h)+c_A^{(i)}(\boldsymbol{u}_h,\boldsymbol{\lambda}_h;\boldsymbol{v}_h,\boldsymbol{\mu}_h)+\langle(\boldsymbol{u}_h\cdot\nabla_{\boldsymbol{x}})\boldsymbol{u}_h,\boldsymbol{v}_h\rangle_{Q_i}\\
&\qquad\qquad -B^{(i)}(\boldsymbol{v}_h,p_h)-c_B^{(i)}(\boldsymbol{v}_h,\boldsymbol{\mu}_h;p_h,\rho_h)\Big]=\sum_{i=1}^{P}F^{(i)}(\boldsymbol{v}_h),\\
&\sum_{i=1}^{P}\Big[B^{(i)}(\boldsymbol{u}_h,q_h)+c_B^{(i)}(\boldsymbol{u}_h,\boldsymbol{\lambda}_h;q_h,\eta_h)\\
&\qquad\qquad +D^{(i)}(p_h,q_h)+c_D^{(i)}(p_h,\rho_h;q_h,\eta_h)\Big]=0
\end{aligned}
\tag{5.14}
$$

holds for all $\boldsymbol{v}_h\in V_h^{p+1}(\mathcal{T}_N)$, $\boldsymbol{\mu}_h\in V_h^{p+1}(\Sigma_h)$, $q_h\in Q_h^p(\mathcal{T}_N)$ and $\eta_h\in Q_h^p(\Sigma_h)$.

Next we will introduce the equivalent system of algebraic equations for the discrete variational problem (5.14). To do so, we define for each space-time decompositions $\mathcal{T}_{N_i}$, $i=1,\dots,P$ the following basis functions

$$
\begin{aligned}
V_h^{p+1}(\mathcal{T}_{N_i}) &= \operatorname{span}\left\{\boldsymbol{\varphi}_\ell^i\right\}_{\ell=1}^{M_u^i},\quad \boldsymbol{u}_{h,0}^i(\boldsymbol{x},t)=\sum_{\ell=1}^{M_u^i}\boldsymbol{u}_I^{(i)}[\ell]\boldsymbol{\varphi}_\ell^i(\boldsymbol{x},t)\quad\text{for } \boldsymbol{u}_{h,0}^i\in V_h^{p+1}(\mathcal{T}_{N_i}),\\
Q_h^p(\mathcal{T}_{N_i}) &= \operatorname{span}\left\{\psi_n^i\right\}_{n=1}^{M_p^i},\qquad p_h^i(\boldsymbol{x},t)=\sum_{n=1}^{M_p^i}\boldsymbol{p}_I^{(i)}[n]\psi_n^i(\boldsymbol{x},t)\qquad\text{for } p_h^i\in Q_h^p(\mathcal{T}_{N_i}).
\end{aligned}
$$

Furthermore, on the interface Σ we introduce the following basis functions

$$
V_h^{p+1}(\Sigma_h)=\operatorname{span}\left\{\boldsymbol{\varphi}_s^\Sigma\right\}_{s=1}^{M_u^\Sigma},\quad \boldsymbol{\lambda}_h(\boldsymbol{x},t)=\sum_{s=1}^{M_u^\Sigma}\boldsymbol{\lambda}_\Sigma[s]\boldsymbol{\varphi}_s^\Sigma(\boldsymbol{x},t)\quad\text{for } \boldsymbol{\lambda}_h\in V_h^{p+1}(\Sigma_h),
$$

$$Q_h^p(\Sigma_h) = \operatorname{span}\left\{\psi_t^\Sigma\right\}_{t=1}^{M_p^\Sigma}, \quad \rho_h(\boldsymbol{x},t) = \sum_{t=1}^{M_p^\Sigma} \rho_\Sigma[t]\psi_t^\Sigma(\boldsymbol{x},t) \quad \text{for } \rho_h \in Q_h^p(\Sigma_h).$$

Then the discrete variational problem (5.14) is equivalent to the system of algebraic equations

$$\begin{pmatrix} \begin{pmatrix} K_{II}^{(1)} & -B_{II}^{(1)\top} \\ B_{II}^{(1)} & D_{II}^{(1)} \end{pmatrix} & & & \begin{pmatrix} A_{I\Sigma}^{(1)} & -B_{I\Sigma}^{(1)} \\ & D_{I\Sigma}^{(1)} \end{pmatrix} \\ & \ddots & & \vdots \\ & & \begin{pmatrix} K_{II}^{(p)} & -B_{II}^{(p)\top} \\ B_{II}^{(p)} & D_{II}^{(p)} \end{pmatrix} & \begin{pmatrix} A_{I\Sigma}^{(p)} & -B_{I\Sigma}^{(p)} \\ & D_{I\Sigma}^{(p)} \end{pmatrix} \\ \begin{pmatrix} A_{\Sigma I}^{(1)} & \\ B_{\Sigma I}^{(1)} & D_{\Sigma I}^{(1)} \end{pmatrix} & \cdots & \begin{pmatrix} A_{\Sigma I}^{(p)} & \\ B_{\Sigma I}^{(p)} & D_{\Sigma I}^{(p)} \end{pmatrix} & \begin{pmatrix} A_{\Sigma\Sigma} & \\ & D_{\Sigma\Sigma} \end{pmatrix} \end{pmatrix} \begin{pmatrix} \begin{pmatrix} \boldsymbol{u}_I^{(1)} \\ \boldsymbol{p}_I^{(1)} \end{pmatrix} \\ \vdots \\ \begin{pmatrix} \boldsymbol{u}_I^{(p)} \\ \boldsymbol{p}_I^{(p)} \end{pmatrix} \\ \begin{pmatrix} \boldsymbol{\lambda}_\Sigma \\ \boldsymbol{\varrho}_\Sigma \end{pmatrix} \end{pmatrix} = \begin{pmatrix} \begin{pmatrix} \boldsymbol{f}_{u,I}^{(1)} \\ \boldsymbol{f}_{p,I}^{(1)} \end{pmatrix} \\ \vdots \\ \begin{pmatrix} \boldsymbol{f}_{u,I}^{(p)} \\ \boldsymbol{f}_{p,I}^{(p)} \end{pmatrix} \\ \begin{pmatrix} \boldsymbol{f}_{\lambda,\Sigma} \\ \boldsymbol{f}_{\rho,\Sigma} \end{pmatrix} \end{pmatrix}, \tag{5.15}$$

with the nonlinear operator

$$\left(K_{II}^{(i)}\boldsymbol{u}_I^{(i)}\right)[k] := A^{(i)}(\boldsymbol{u}_h, \boldsymbol{\varphi}_k^i) + c_A^{(i)}(\boldsymbol{u}_h, \boldsymbol{0}; \boldsymbol{\varphi}_k^i, \boldsymbol{0}) + \left\langle (\boldsymbol{u}_h \cdot \nabla_{\boldsymbol{x}})\boldsymbol{u}_h, \boldsymbol{\varphi}_k^i \right\rangle_{Q_i}$$

for $\boldsymbol{u}_h = \mathcal{E}\boldsymbol{g}_D + \sum_{\ell=1}^{M_u^i} \boldsymbol{u}_I^{(i)}[\ell]\boldsymbol{\varphi}_\ell^i$ and the local matrices

$$\begin{aligned} B_{II}^{(i)}[m,\ell] &:= B^{(i)}(\boldsymbol{\varphi}_\ell^i, \psi_m^i), \\ D_{II}^{(i)}[m,n] &:= D^{(i)}(\psi_n^i, \psi_m^i) + c_D^{(i)}(\psi_n^i, 0; \psi_m^i, 0), \end{aligned}$$

for $k,\ell = 1,\ldots,M_u^i$ and $m,n = 1,\ldots,M_p^i$. Furthermore the coupling matrices are given by

$$\begin{aligned} A_{I\Sigma}^{(i)}[k,s] &:= c_A^{(i)}(\boldsymbol{0}, \boldsymbol{\varphi}_s^\Sigma; \boldsymbol{\varphi}_k^i, \boldsymbol{0}), & A_{\Sigma I}^{(i)}[r,\ell] &:= c_A^{(i)}(\boldsymbol{\varphi}_\ell^i, \boldsymbol{0}; \boldsymbol{0}, \boldsymbol{\varphi}_r^\Sigma), \\ B_{I\Sigma}^{(i)}[k,t] &:= c_B^{(i)}(\boldsymbol{\varphi}_k^i, \boldsymbol{0}; 0, \psi_t^\Sigma), & B_{\Sigma I}^{(i)}[o,\ell] &:= c_B^{(i)}(\boldsymbol{\varphi}_\ell^i, \boldsymbol{0}; 0, \psi_o^\Sigma), \\ D_{I\Sigma}^{(i)}[m,t] &:= c_D^{(i)}(0, \psi_t^\Sigma; \psi_m^i, 0), & D_{\Sigma I}^{(i)}[o,n] &:= c_D^{(i)}(\psi_n^i, 0; 0, \psi_o^\Sigma) \end{aligned}$$

and the matrices with respect to the interface Σ are defined as

$$A_{\Sigma\Sigma}^{(i)}[r,s] := c_A^{(i)}(\boldsymbol{0}, \boldsymbol{\varphi}_s^\Sigma; \boldsymbol{0}, \boldsymbol{\varphi}_r^\Sigma), \qquad D_{\Sigma\Sigma}^{(i)}[o,t] := c_D^{(i)}(0, \psi_t^\Sigma; 0, \psi_o^\Sigma),$$

for

$$k,l = 1,\ldots,M_u^i \quad m,n = 1,\ldots,M_p^i \quad r,s = 1,\ldots,M_u^\Sigma \quad o,t = 1,\ldots,M_p^\Sigma.$$

Further, the right hand sides are given by

$$\begin{aligned}
\boldsymbol{f}_{u,I}^{(i)}[k] &:= F^{(i)}(\boldsymbol{\varphi}_k^i) = \langle \boldsymbol{f}, \boldsymbol{\varphi}_k^i \rangle_{Q_i} + \langle \boldsymbol{u}_0, \boldsymbol{\varphi}_k^i \rangle_{\Sigma_0 \cap \partial Q_i}, \\
\boldsymbol{f}_{p,I}^{(i)}[m] &:= -B^{(i)}(\mathcal{E}\boldsymbol{g}_D, \psi_m^i), \\
\boldsymbol{f}_{\lambda,\Sigma}[r] &:= -\sum_{i=1}^{P} c_A^{(i)}(\mathcal{E}\boldsymbol{g}_D, \boldsymbol{0}; \boldsymbol{0}, \boldsymbol{\varphi}_r^\Sigma), \\
\boldsymbol{f}_{\rho,\Sigma}[o] &:= -\sum_{i=1}^{P} c_B^{(i)}(\mathcal{E}\boldsymbol{g}_D, \boldsymbol{0}; 0, \psi_o^\Sigma).
\end{aligned}$$

Remark 5.2.2. *The nonlinearity in the system of algebraic equations (5.15) is only contained in the operators $K_{II}^{(i)}$, $i = 1, \ldots, P$. To solve this nonlinear problem, one can apply a fixed point method or Newton's method, where in each iteration a linear problem has to be solved. Since the nonlinearity is only contained in the operators $K_{II}^{(i)}$, we only have to linearize the operators $K_{II}^{(i)}$ by a linear operator $\widetilde{K}_{II}^{(i)}$. Hence the linear system, which has to be solved in each fixed point iteration or Newton step has the same structure as the system (5.15). In particular, if the assumption of Lemma 5.1.2 is fulfilled and if further the linear operators $\widetilde{K}_{II}^{(i)}$, $i = 1, \ldots, P$ are invertible we can invert each block*

$$\begin{pmatrix} \widetilde{K}_{II}^{(i)} & -B_{II}^{(i)^\top} \\ B_{II}^{(i)} & D_{II}^{(i)} \end{pmatrix}.$$

Hence we can compute the Schur complement system

$$\left[\begin{pmatrix} A_{\Sigma\Sigma} & \\ & D_{\Sigma\Sigma} \end{pmatrix} - \sum_{i=1}^{P} \begin{pmatrix} A_{\Sigma I}^{(i)} & \\ B_{\Sigma I}^{(i)} & D_{\Sigma I}^{(i)} \end{pmatrix} \begin{pmatrix} \widetilde{K}_{II}^{(i)} & -B_{II}^{(i)^\top} \\ B_{II}^{(i)} & D_{II}^{(i)} \end{pmatrix}^{-1} \begin{pmatrix} A_{I\Sigma}^{(1)} & -B_{I\Sigma}^{(i)} \\ & D_{I\Sigma}^{(i)} \end{pmatrix} \right] \begin{pmatrix} \boldsymbol{\lambda}_\Sigma \\ \boldsymbol{\varrho}_\Sigma \end{pmatrix} = \begin{pmatrix} \tilde{\boldsymbol{f}}_{\lambda,\Sigma} \\ \tilde{\boldsymbol{f}}_{\rho,\Sigma} \end{pmatrix}, \tag{5.16}$$

with the right hand side

$$\begin{pmatrix} \tilde{\boldsymbol{f}}_{\lambda,\Sigma} \\ \tilde{\boldsymbol{f}}_{\rho,\Sigma} \end{pmatrix} := \begin{pmatrix} \boldsymbol{\lambda}_\Sigma \\ \boldsymbol{\varrho}_\Sigma \end{pmatrix} - \sum_{i=1}^{P} \begin{pmatrix} A_{\Sigma I}^{(i)} & \\ B_{\Sigma I}^{(i)} & D_{\Sigma I}^{(i)} \end{pmatrix} \begin{pmatrix} \widetilde{K}_{II}^{(i)} & -B_{II}^{(i)^\top} \\ B_{II}^{(i)} & D_{II}^{(i)} \end{pmatrix}^{-1} \begin{pmatrix} \boldsymbol{f}_{u,I}^{(i)} \\ \boldsymbol{f}_{p,I}^{(i)} \end{pmatrix}.$$

Further, the local solutions are given by

$$\begin{pmatrix} \boldsymbol{u}_I^{(i)} \\ \boldsymbol{p}_I^{(i)} \end{pmatrix} = \begin{pmatrix} \widetilde{K}_{II}^{(i)} & -B_{II}^{(i)^\top} \\ B_{II}^{(i)} & D_{II}^{(i)} \end{pmatrix}^{-1} \left[\begin{pmatrix} \boldsymbol{f}_{u,I}^{(i)} \\ \boldsymbol{f}_{p,I}^{(i)} \end{pmatrix} - \begin{pmatrix} A_{I\Sigma}^{(1)} & -B_{I\Sigma}^{(i)} \\ & D_{I\Sigma}^{(i)} \end{pmatrix} \begin{pmatrix} \boldsymbol{\lambda}_\Sigma \\ \boldsymbol{\varrho}_\Sigma \end{pmatrix} \right]$$

for $i = 1, \ldots, P$. For the solution of the Schur complement system (5.16) we can use for example the GMRES method, where the inversion of the local problems can be done in parallel, either by using a direct approach, or by a suitable iterative scheme.

level	dof $\boldsymbol{u}_h$	dof p_h	dof $\boldsymbol{\lambda}_h$	dof ρ_h	$\|(\boldsymbol{u}-\boldsymbol{u}_h,\boldsymbol{u}-\boldsymbol{\lambda}_h)\|_{\mathbf{HDG}}$	eoc	$\|p-p_h\|_{L_2(Q)}$	eoc
0	120	24	216	36	$3.0715-1$	–	$2.5234-1$	–
1	1 248	192	864	144	$1.9538-1$	0.65	$2.3727-1$	0.09
2	11 136	1 536	3 456	576	$1.2347-1$	0.66	$1.9567-1$	0.28
3	93 696	12 288	13 824	2 304	$6.8429-2$	0.85	$1.2649-1$	0.63
4	768 000	98 304	55 296	9 216	$3.1597-2$	1.11	$6.0021-2$	1.08
5	6 217 728	786 432	221 184	36 864	$1.3373-2$	1.24	$2.3086-2$	1.38
Theory:						1.00		1.00

Table 5.3: Numerical results for the finite element pairing $(V_h^1(\mathcal{T}_N), Q_h^0(\mathcal{T}_N))$ and $(V_h^1(\Sigma_h), Q_h^0(\Sigma_h))$.

level	dof $\boldsymbol{u}_h$	dof p_h	dof $\boldsymbol{\lambda}_h$	dof ρ_h	$\|(\boldsymbol{u}-\boldsymbol{u}_h,\boldsymbol{u}-\boldsymbol{\lambda}_h)\|_{\mathbf{HDG}}$	eoc	$\|p-p_h\|_{L_2(Q)}$	eoc
0	336	96	432	108	$2.6865-2$	–	$1.6555-2$	–
1	3264	768	1728	432	$7.5822-3$	1.83	$4.7767-3$	1.79
2	28416	6144	6912	1728	$1.8787-3$	2.01	$1.1237-3$	2.09
3	236544	49152	27648	6912	$4.6254-4$	2.02	$2.7143-4$	2.05
4	1929216	393216	110592	27648	$1.1443-4$	2.02	$6.6604-5$	2.03
Theory:						2.00		2.00

Table 5.4: Numerical results for the finite element pairing $(V_h^2(\mathcal{T}_N), Q_h^1(\mathcal{T}_N))$ and $(V_h^2(\Sigma_h), Q_h^1(\Sigma_h))$.

Example 5.2.3. In this example we consider the spatial domain $\Omega = (0,1)^2$ with the simulation interval $[0,T]$ with $T=1$. For the boundary conditions we use the same setting as in Example 5.1.5. We also use the same data $\boldsymbol{f}$, $\boldsymbol{g}_D$ and $\boldsymbol{u}_0$ as in Example 5.1.5, i.e. we study the hybrid formulation (5.14) for approximating the exact solution

$$\boldsymbol{u}(x_1,x_2,t) = \begin{pmatrix} t(1-x_1)\cos(x_2) \\ t\sin(x_2) \end{pmatrix}, \qquad p(x_1,x_2,t) = -\nu t\cos(x_2)$$

with $\nu = 1$. Further we decompose the space-time domain Q into $P = 24$ space-time subdomains Q_i, $i = 1,\dots,P$ and the space-time subdomains itself are considered as the initial decompositions for each subdomain, see also Figure 3.2(b). As in Example 5.1.5 we apply several uniform refinement steps to analyze the convergence behaviour of the presented hybrid space-time formulation (5.14). We use the finite element pairings for $p=0$ and $p=1$ with the stabilization parameters $\sigma = 10(p+1)$ and $\sigma_p = 10$. The nonlinear equations (5.15) are solved by applying Newton's method. For the solution of the arising linear system of each Newton step we solve the Schur complement system (5.16) with the GMRES method without any preconditioning. The local problems are solved in parallel by using the solver package PARDISO. In the Tables 5.3–5.4 the errors in the energy norms $\|(\boldsymbol{u}-\boldsymbol{u}_h,\boldsymbol{u}-\boldsymbol{\lambda}_h)\|_{\mathbf{HDG}}$ and $\|p-p_h\|_{L_2(Q)}$ are given. We observe, that the convergence rate for the energy errors behave as expected.

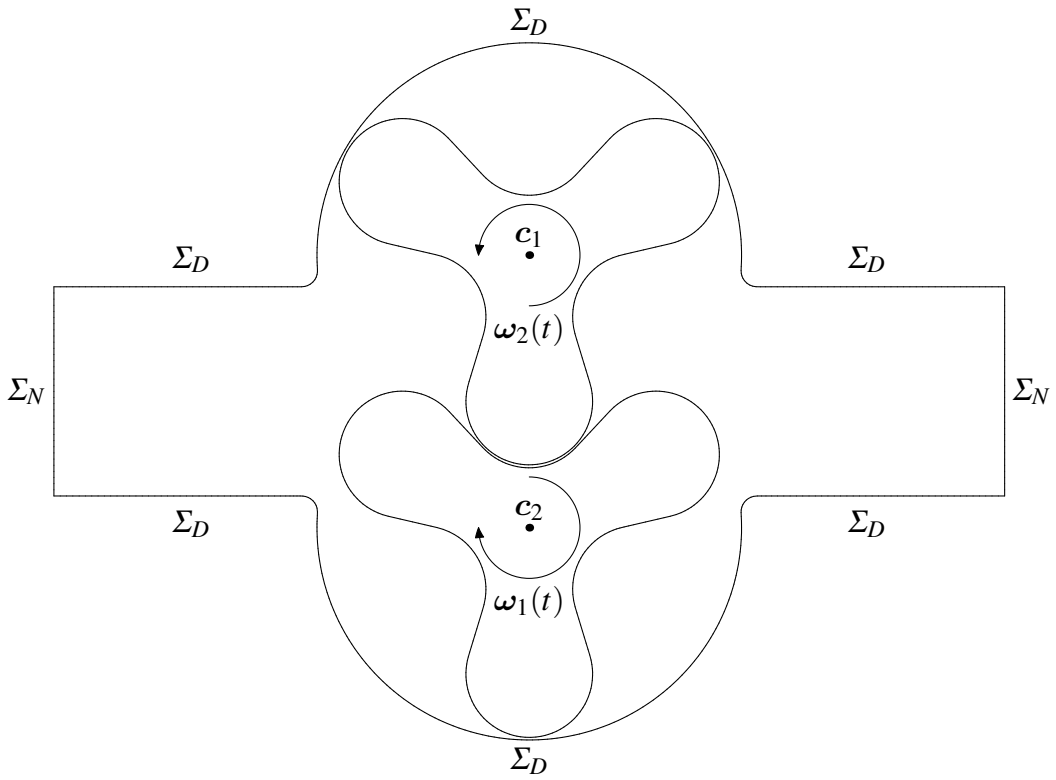

Figure 5.1: Lobe pump - spatial domain $\Omega(t)$.

5.3 Applications

In this section we apply the hybrid discretization scheme (5.14) to simulate the flow in a pump. The initial spatial domain $\Omega \subset \mathbb{R}^2$ of the pump is given in Figure 5.1. The pump consists of two rotating parts, which are called lobes. The magnitudes of the angular velocities for the two lobes are the same, only the sign is different, see also Figure 5.1. In particular, for $0 < T_a < T$ the magnitudes of the angular velocities are given by

$$\omega(t) := \frac{4\pi}{2T - T_a} \begin{cases} \frac{t^2(3T_a - 2t)}{T_a^3} & t \le T_a, \\ 1 & t > T_a \end{cases} \in \mathcal{C}^1(\mathbb{R}).$$

Hence we have

$$\omega(0) = 0 \quad \text{and} \quad \frac{\mathrm{d}}{\mathrm{d}t}\omega(t)_{|t=0} = 0.$$

The angular velocities for the two lobes are then defined as

$$\omega_1(t) := \begin{pmatrix} 0 \\ 0 \\ -\omega(t) \end{pmatrix} \quad \text{and} \quad \omega_2(t) := \begin{pmatrix} 0 \\ 0 \\ \omega(t) \end{pmatrix}.$$

With these angular velocities we define the angle for the lobes as

$$\varphi(t) := \int_0^t \omega(s)\mathrm{d}s.$$

Hence we have

$$\varphi(T) = 2\pi,$$

which implies, that at the time $t = T$ exactly one rotation is performed. Further the velocities on the lobes are defined as

$$g_{D,1}(x,t) := \omega_1(t) \times r_1(x,t) \quad \text{and} \quad g_{D,2}(x,t) := \omega_2(t) \times r_2(x,t),$$

where $r_1, r_2 \in \mathbb{R}^3$ are the vectors from the centers of the lobes to the boundary points x, i.e. $r_1(x,t) := (x,t) - (c_1,t)$ and $r_2(x,t) := (x,t) - (c_2,t)$. On the boundary Σ_D the velocity is zero, i.e. $g_D(x,t) = \mathbf{0}$ for $(x,t) \in \Sigma_D$. On the boundary Σ_N we apply homogeneous Neumann boundary conditions, as defined in (5.1).

Since the spatial domain Ω is a two dimensional domain, we have

$$Q = \Omega \times [0,T] \subset \mathbb{R}^3.$$

For $T = 100$ and $T_a = 50$ the space-time domain Q is shown in Figure 5.2. Because the space-time domain Q is a bounded subset in $\mathbb{R}^3$ we can use a standard meshing tool, like [85], to generate a space-time decomposition into tetrahedra. The space-time mesh which we are using for the simulation consists of $N = 766\,105$ elements, see also Figure 5.2. To apply the hybrid space-time discretization scheme (5.14), we subdivide the space-time decomposition into $P = 64$ subdomains, see also Figure 5.3. For the space-time discretization scheme (5.14) we use for the viscosity constant $\nu = \frac{1}{2}$ the stabilization parameters , $\sigma = 20$ and $\sigma_p = 10$ for $p = 1$. For the solution of the nonlinear equations (5.15) we apply Newton's method, where the linear system in each Newton step is solved via the Schur complement system (5.16). We apply the Newton's method until we have reached a relative error reduction of $\varepsilon_N = 10^{-10}$, which results in 6 Newton steps which have to be used to solve the nonlinear problem (5.15).

The resulting velocity field is plotted for different time steps in the Figures 5.4–5.11. We observe, that the flow is transported from the right side of the pump to the left side via the cavities of the rotating lobes. Between the two lobes we see, that the magnitude of the velocity has its maximum, where additional local refinement in the space-time domain Q would be needed, to resolve these local phenomena.

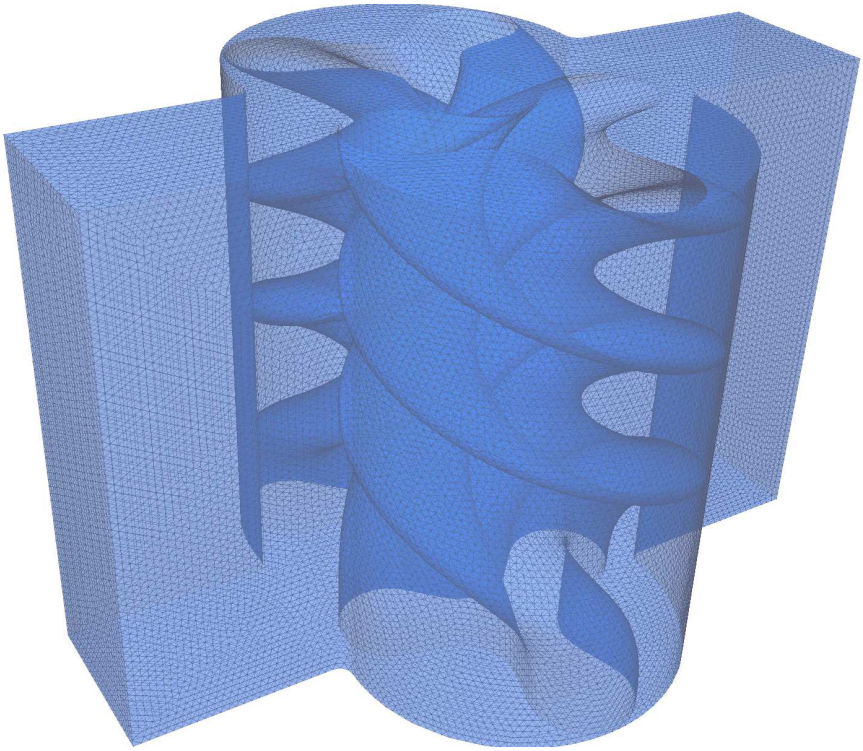

Figure 5.2: Space-time domain Q for the lobe pump.

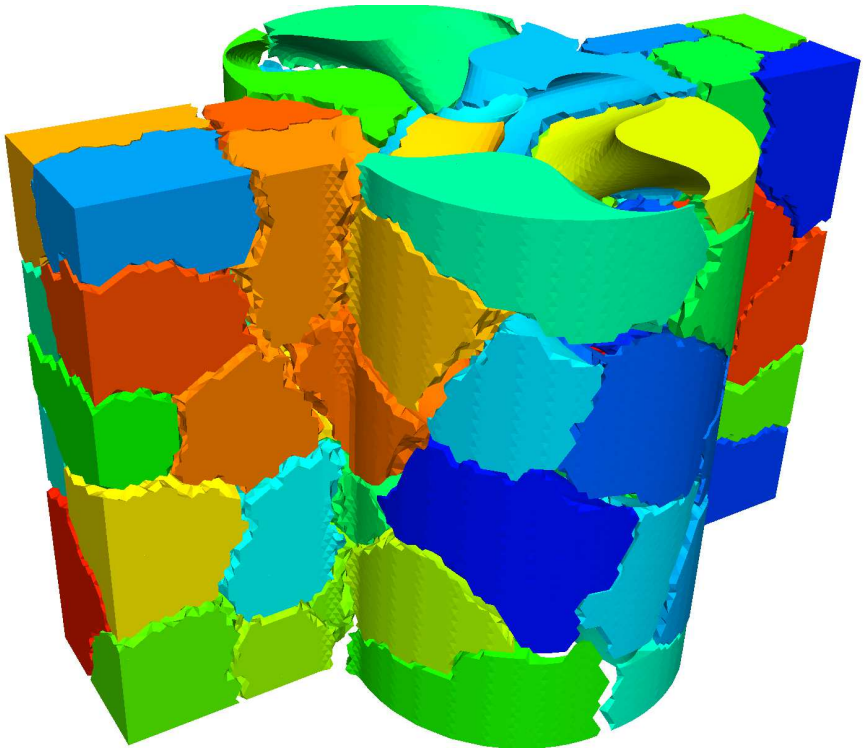

Figure 5.3: Space-time decomposition into $P = 64$ subdomains.

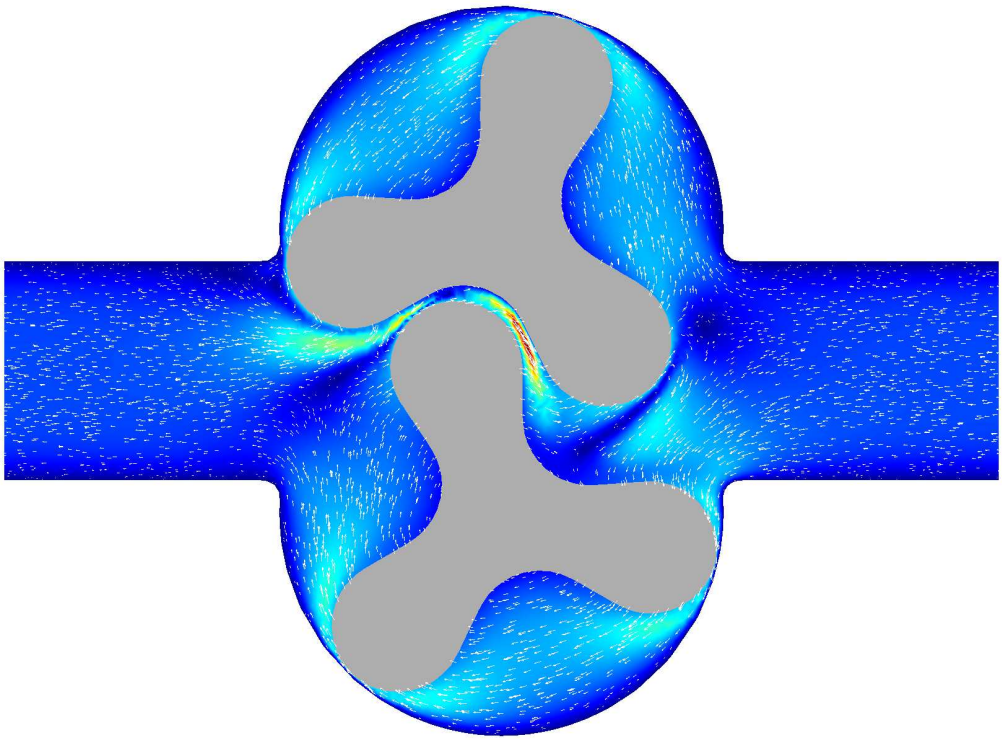

Figure 5.4: Lobe pump - velocity field for $t = 32$.

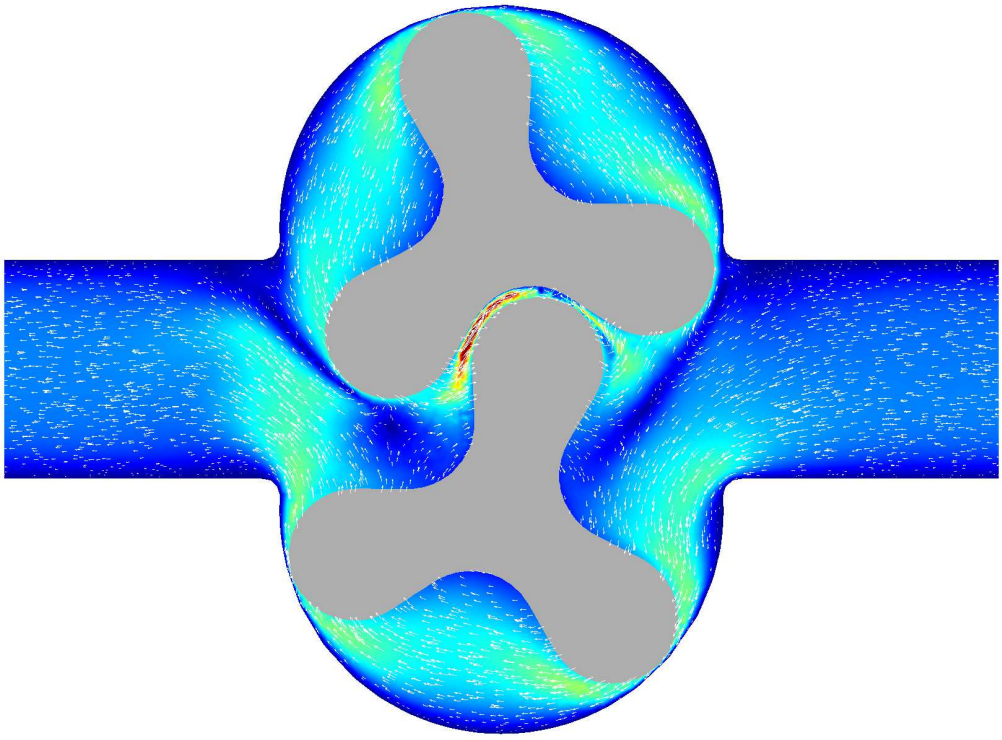

Figure 5.5: Lobe pump - velocity field for $t = 40$.

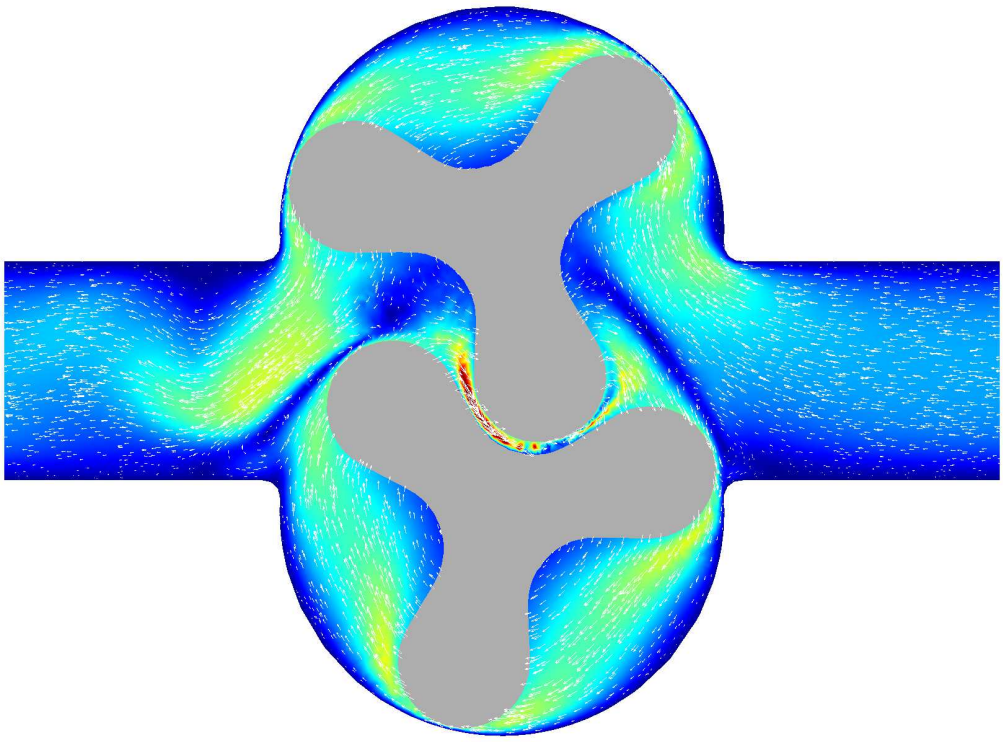

Figure 5.6: Lobe pump - velocity field for $t = 53$.

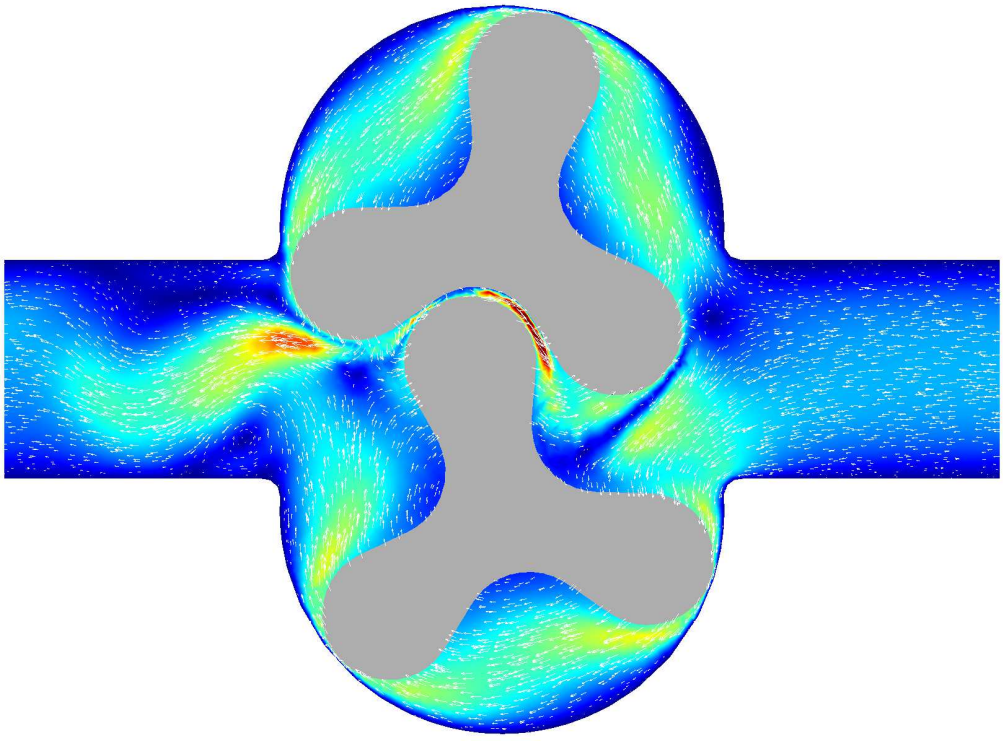

Figure 5.7: Lobe pump - velocity field for $t = 60$.

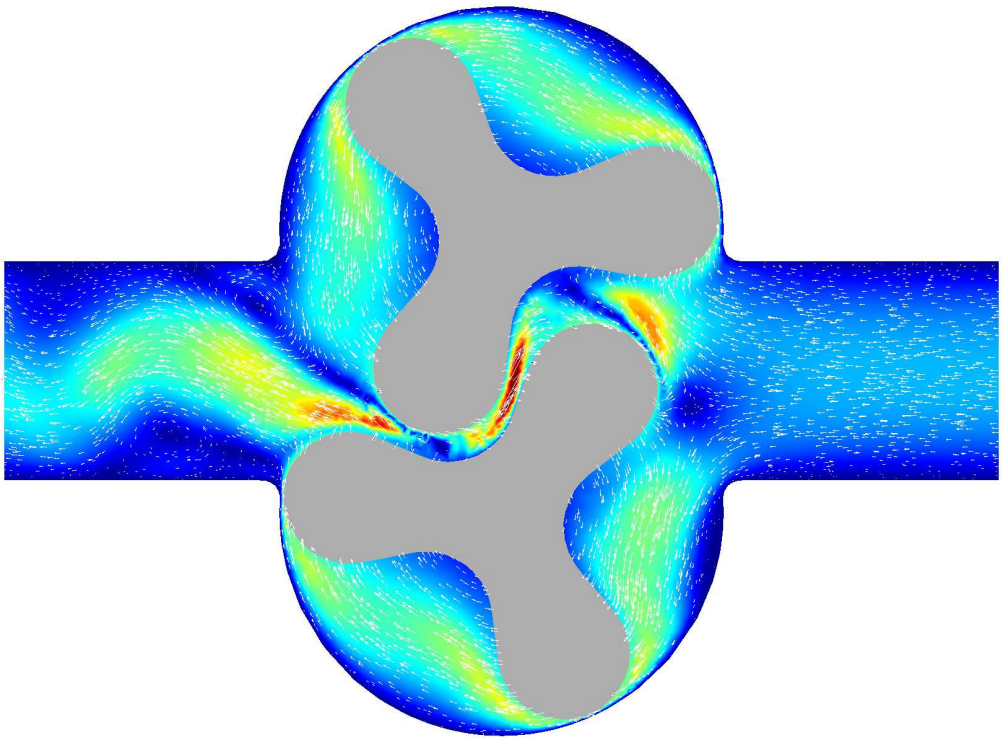

Figure 5.8: Lobe pump - velocity field for $t = 70$.

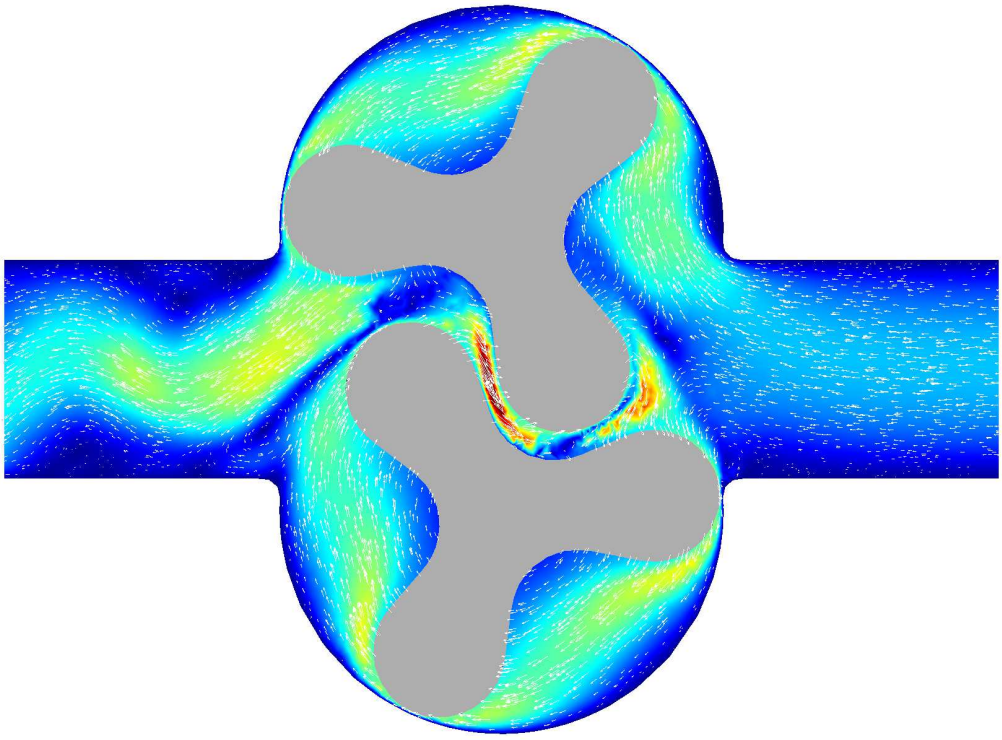

Figure 5.9: Lobe pump - velocity field for $t = 80$.

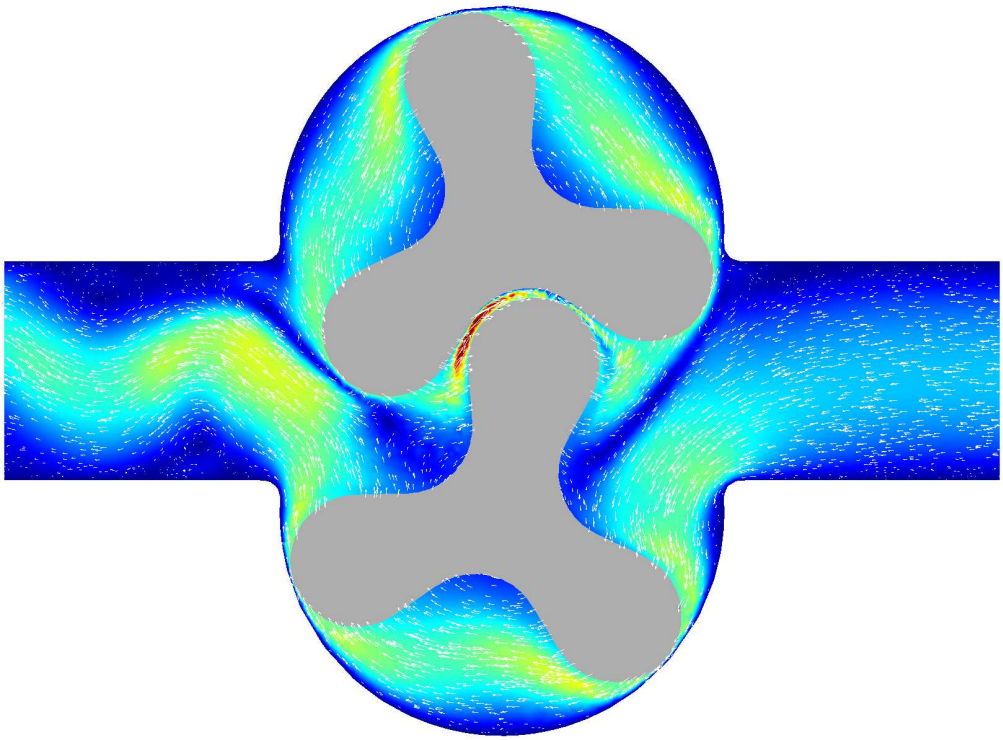

Figure 5.10: Lobe pump - velocity field for $t = 90$.

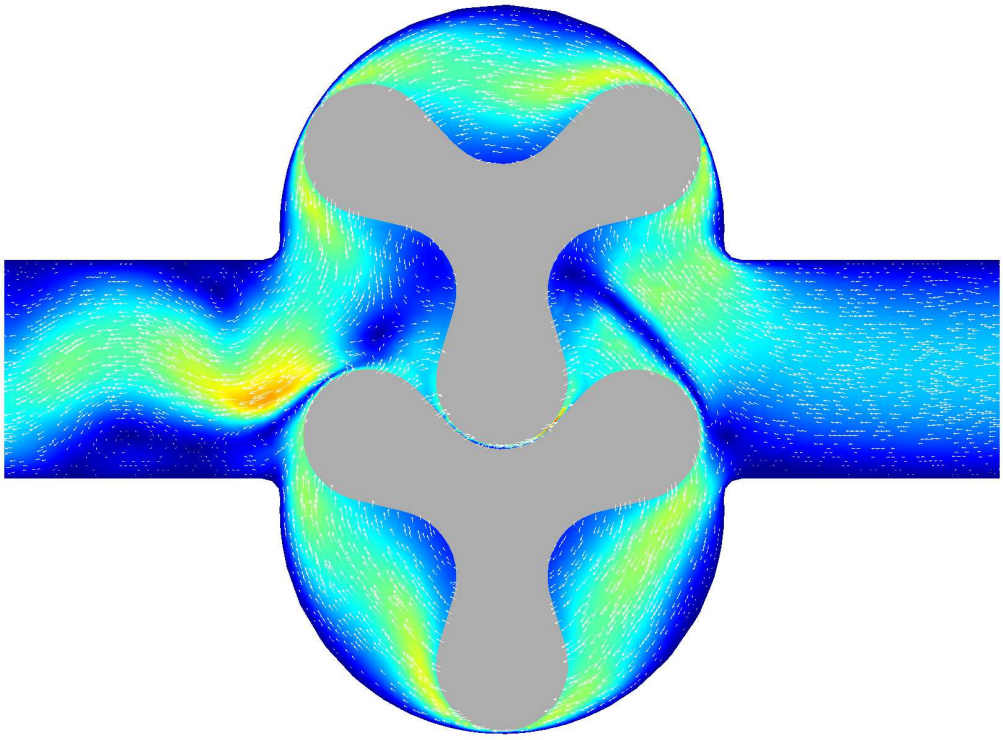

Figure 5.11: Lobe pump - velocity field for $t = 100$.

6 CONCLUSIONS AND OUTLOOK

In this work discretization schemes, to approximate time dependent problems by a numerical approach, have been introduced and studied. Moreover, a fast solver for the arising linear systems has been formulated and analyzed by using the so called local Fourier mode analysis. The main difference of the presented approach of this work to the more common time stepping schemes is, that in this work the discrete solution is obtained by decomposing the space-time domain $Q = \Omega \times (0,T)$ into finite elements. This results in an approach which allows the use of almost arbitrary space-time decompositions for the space-time domain Q. For moving spatial domains $\Omega = \Omega(t)$ these space-time methods lead to a continuous approximation for the motion of the domain Ω. This results in the advantage, that bigger time step sizes can be used for approximating the exact solution. Moreover these methods allow the use of local refinements in the space-time domain Q.

In particular, a space-time discretization scheme for the heat equation, as a model problem, has been derived by using a discontinuous Galerkin approach. For the discretization of the Laplace operator an interior penalty Galerkin approach has been used, whereas for the first order time derivative an upwind scheme in time has been applied. This discretization scheme has been analyzed in Chapter 2, where error estimates with respect to the energy norm have been proven. Moreover, several numerical examples confirmed these error estimates.

Based on the discontinuous Galerkin space-time discretization of Chapter 2, a hybrid space-time formulation has been introduced in Chapter 3 by defining a new unknown variable λ_h on the interface of the space-time subdomains. With this formulation the unknowns on each space-time subdomain can be eliminated, which results in the Schur complement system (3.10), where the unknowns of the Schur complement system are given by the introduced interface variable λ_h. This allows the use of parallel solution algorithms in space and time. Furthermore, error estimates for the related energy norms have been proven and numerical examples confirm the proven estimates.

In the main part of this work a space-time multigrid approach has been analyzed by applying the local Fourier mode analysis. This multigrid approach is based on so called space-time slabs, which are natural, if a standard discretization scheme in space and time is used. Under the assumption of periodic boundary conditions the two-grid cycle for this approach has been studied, where the asymptotic convergence rates have been computed for arbitrary polynomial degrees with respect

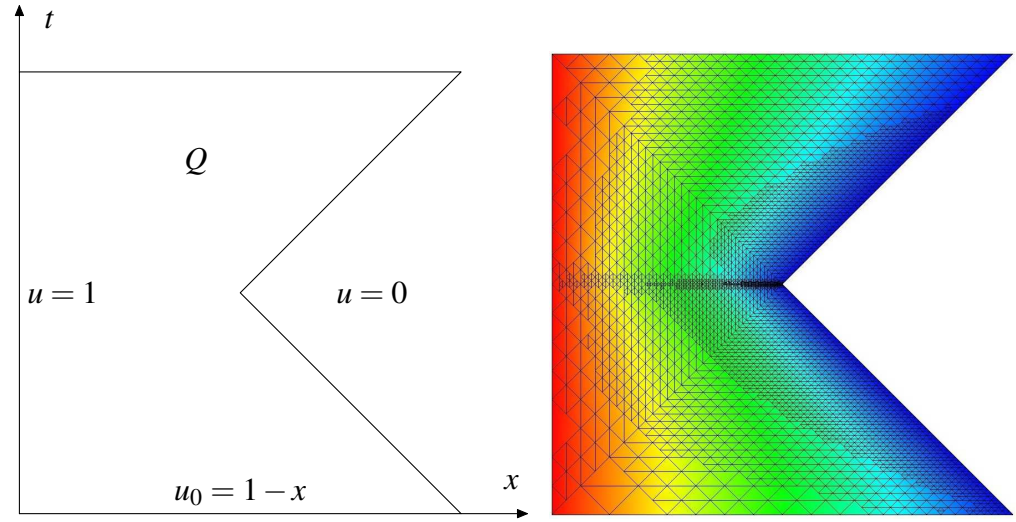

(a) Space-time domain Q for a moving domain Ω.

(b) Adaptive space-time mesh.

Figure 6.1: Space-time domain Q for a moving one-dimensional spatial domain Ω and the resulting adaptive space-time mesh.

to time. The measured convergence rates completely agree with the theoretical results which have been obtained by the local Fourier mode analysis. One advantage of this multigrid approach is, that each space-time slab can be solved separately. Hence, the linear systems resulting from the space-time discretizations can be solved in parallel with respect to time. For a tensor product space-time discretization the parallel performance of this approach has been studied at the end of Chapter 4.

In Chapter 5 the space-time discretization schemes introduced in Chapter 2 and Chapter 3 have been applied to the Navier-Stokes equations. Here numerical examples also showed the expected order of convergence with respect to the energy norm. Further, to show the advantage of this discretization schemes, this approach has been applied to simulate the flow in a two-dimensional pump.

To apply these methods to more complicated three-dimensional geometries, one has to implement a four-dimensional mesh generator. For spatial domains Ω which do not change in time one can simply generate a four-dimensional decomposition, by decomposing the tensor product space-time elements into simplices. For moving three-dimensional spatial domains the decomposition of a four-dimensional space-time domain is more complicated, but not impossible.

Another advantage of the presented approach is, that it is possible to apply mesh refinements local in the space-time domain. For example, singularities in the solution can occur local in the space-time domain Q, if the spatial domain is moving in time. For the moving spatial domain $\Omega(t) = (0, \frac{1}{2} + \left|t - \frac{1}{2}\right|)$ the heat

equation has been solved with the data as given in Figure 6.1(a). A simple residual error estimator has been used to apply adaptive refinements in space and time. The resulting adaptive space-time mesh is given in Figure 6.1(b), where most of the refinements take place near the singularity and almost uniform refinement has been used where the solution is smooth enough.

An interesting research topic would be the application of these space-time methods to other partial differential equations with first or second order time derivatives, as for example the bidomain equations, which are used to simulate the electrical activity of the heart. Further, one may study the coupling of this approaches with other discretization schemes, as for example the coupling with boundary element methods, where the coupling interface is in general a complex four-dimensional manifold.

REFERENCES

[1] R. Abedi, M.A. Hawker, R.B. Haber, and K. Matouš. An adaptive space-time discontinuous Galerkin method for cohesive models of elastodynamic fracture. *Internat. J. Numer. Methods Engrg.*, 81:1207–1241, 2010.

[2] J.M. Alam, N.K.-R. Kevlahan, and O.V. Vasilyev. Simultaneous space-time adaptive wavelet solution of nonlinear parabolic differential equations. *J. Comput. Phys.*, 214:829–857, 2006.

[3] T. Apel. *Anisotropic finite elements: local estimates and applications.* Advances in Numerical Mathematics. B. G. Teubner, Stuttgart, 1999.

[4] D.N. Arnold, F. Brezzi, B. Cockburn, and L.D. Marini. Discontinuous Galerkin Methods for Elliptic problems. *Numer. Methods Partial Differential Equations*, 16:365–378, 2000.

[5] D.N. Arnold, F. Brezzi, B. Cockburn, and L.D. Marini. Unified Analysis of Discontinuous Galerkin Methods for Elliptic Problems. *SIAM J. Numer. Anal.*, 39:1749–1779, 2002.

[6] E. Bacry, S. Mallat, and G. Papanicolaou. A wavelet based space-time adaptive numerical method for partial differential equations. *RAIRO Modél. Math. Anal. Numér.*, 26:793–834, 1992.

[7] G. Bal. On the convergence and the stability of the parareal algorithm to solve partial differential equations. *Lect. Notes Comput. Sci. Eng., Springer, Berlin*, 40:425–432, 2005.

[8] F. Bassi and S. Rebay. A High-Order Accurate Discontinuous Finite Element Method for the Numerical Solution of the Compressible Navier–Stokes Equations. *J. Comput. Phys.*, 131:267–279, 1997.

[9] C.E. Baumann and J.T. Oden. A discontinuous hp finite element method for convection-diffusion problems. *Comput. Methods Appl. Mech. Engrg.*, 175:311–341, 1999.

[10] M. Behr. Simplex space-time meshes in finite element simulations. *Internat. J. Numer. Methods Fluids*, 57:1421–1434, 2008.

[11] J. Bey. Simplicial grid refinement: on Freudenthal's algorithm and the optimal number of congruence classes. *Numer. Math.*, 85:1–29, 2000.

[12] A. Brandt. Multi-level adaptive solutions to boundary-value problems. *Math. Comp.*, 31:333–390, 1977.

[13] A. Brandt. Rigorous quantitative analysis of multigrid. I. Constant coefficients two-level cycle with L_2-norm. *SIAM J. Numer. Anal.*, 31:1695–1730, 1994.

[14] S. Börm and R. Hiptmair. Analysis of tensor product multigrid. *Numer. Algorithms*, 26:219–234, 2001.

[15] C.E. Castro, M. Käser, and E.F. Toro. Space-time adaptive numerical methods for geophysical applications. *Philos. Trans. R. Soc. Lond. Ser. A Math. Phys. Eng. Sci.*, 367:4613–4631, 2009.

[16] F.H. Chipman. A-stable Runge-Kutta processes. *Nordisk Tidskr. Informationsbehandling (BIT)*, 11:384–388, 1971.

[17] B. Cockburn, J. Gopalakrishnan, and R. Lazarov. Unified hybridization of discontinuous Galerkin, mixed, and continuous Galerkin methods for second order elliptic problems. *SIAM J. Numer. Anal.*, 47:1319–1365, 2009.

[18] M. Delfour, W. Hager, and F. Trochu. Discontinuous Galerkin methods for ordinary differential equations. *Math. Comp.*, 36:455–473, 1981.

[19] D.A. Di Pietrov and A. Ern. Analysis of a discontinuous Galerkin method for heterogeneous diffusion problems with low-regularity solutions. *Numer. Methods Partial Differential Equations*, 28:1161–1177, 2012.

[20] D.A. Di Pietrov and A. Ern. *Mathematical Aspects of Discontinuous Galerkin Methods*. Springer, Berlin, Heidelberg, 2012.

[21] H. Egger and J. Schöberl. A hybrid mixed discontinuous Galerkin finite-element method for convection–diffusion problems. *IMA J. Numer. Anal.*, 30:1206–1234, 2010.

[22] H. Egger and C. Waluga. hp analysis of a hybrid DG method for Stokes flow. *IMA J. Numer. Anal.*, 33:687–721, 2013.

[23] B.L. Ehle. *On Padé approximations to the exponential function and A-stable methods for the numerical solution of initial value problems*. PhD thesis, Technical Report CSRR 2010, Dept. AACS Univ. of Waterloo Ontario Canada, 1969.

[24] K. Eriksson and C. Johnson. Adaptive finite element methods for parabolic problems. I. A linear model problem. *SIAM J. Numer. Anal.*, 28:43–77, 1991.

[25] K. Eriksson and C. Johnson. Adaptive finite element methods for parabolic problems. II. Optimal error estimates in $L_\infty L_2$ and $L_\infty L_\infty$. *SIAM J. Numer. Anal.*, 32:706–740, 1995.

[26] K. Eriksson, C. Johnson, and A. Logg. *Adaptive computational methods for parabolic problems.* Encyclopedia of Computational Mechanics, 2004.

[27] K. Eriksson, C. Johnson, and V. Thomée. Time discretization of parabolic problems by the discontinuous Galerkin method. *RAIRO Modél. Math. Anal. Numér.*, 19:611–643, 1985.

[28] R.D. Falgout, J.E. Jones, and U.M. Yang. The design and implementation of hypre, a library of parallel high performance preconditioners. *Lect. Notes Comput. Sci. Eng.*, 51:267–294, 2006.

[29] R.D. Falgout and U.M. Yang. hypre: A Library of High Performance Preconditioners. *Proceedings of the International Conference on Computational Science-Part III*, pages 632–641, 2002.

[30] C. Farhat and M. Chandesris. Time-decomposed parallel time-integrators: theory and feasibility studies for fluid, structure, and fluid-structure applications. *Internat. J. Numer. Methods Engrg.*, 58:1397–1434, 2003.

[31] P. Fischer, F. Hecht, and Y. Maday. A parareal in time semi-implicit approximation of the Navier-Stokes equations. *Lect. Notes Comput. Sci. Eng., Springer, Berlin*, 40:433–440, 2005.

[32] H. Freudenthal. Simplizialzerlegungen von beschränkter Flachheit. *Ann. of Math.*, 43:580–582, 1942.

[33] M.J. Gander and S. Vandewalle. Analysis of the parareal time-parallel time-integration method. *SIAM J. Sci. Comput.*, 29:556–578, 2007.

[34] I. Garrido, M.S. Espedal, and G.E. Fladmark. A convergent algorithm for time parallelization applied to reservoir simulation. *Lect. Notes Comput. Sci. Eng., Springer, Berlin*, 40:469–476, 2005.

[35] I. Garrido, B. Lee, G.E. Fladmark, and M.S. Espedal. Convergent iterative schemes for time parallelization. *Math. Comp.*, 75:1403–1428, 2006.

[36] M. Griebel and D. Oeltz. A sparse grid space-time discretization scheme for parabolic problems. *Computing*, 81:1–34, 2007.

[37] M.D. Gunzburger and A. Kunoth. Space-time adaptive wavelet methods for optimal control problems constrained by parabolic evolution equations. *SIAM J. Control Optim.*, 49:1150–1170, 2011.

[38] W. Hackbusch. Parabolic multigrid methods. *Computing methods in applied sciences and engineering, VI*, page 189–197, 1984.

[39] W. Hackbusch. *Multi-Grid Methods and Applications.* Springer, Berlin, 1985.

[40] E. Hairer, C. Lubich, and G. Wanner. *Geometric numerical integration. Structure-preserving algorithms for ordinary differential equations.* Springer Series in Computational Mathematics, 31. Springer, Heidelberg, 2010.

[41] E. Hairer, S. P. Nørsett, and G. Wanner. *Solving ordinary differential equations. I. Nonstiff problems.* Springer Series in Computational Mathematics, 8. Springer-Verlag, Berlin, 1993.

[42] E. Hairer and G. Wanner. *Solving ordinary differential equations. II. Stiff and differential-algebraic problems.* Springer Series in Computational Mathematics, 14. Springer-Verlag, Berlin, 2010.

[43] I. Heppner, M. Lampe, A. Nägel, S. Reiter, M. Rupp, A. Vogel, and G. Wittum. Software Framework ug4: Parallel Multigrid on the Hermit Supercomputer. *High Performance Computing in Science and Engineering*, 12:435–449, 2013.

[44] G. Horton. The time-parallel multigrid method. *Comm. Appl. Numer. Methods*, 8:585–595, 1992.

[45] G. Horton and S. Vandewalle. A space-time multigrid method for parabolic partial differential equations. *SIAM J. Sci. Comput.*, 16:848–864, 1995.

[46] G. Horton and S. Vandewalle. Fourier mode analysis of the multigrid waveform relaxation and time-parallel multigrid methods. *Computing*, 54:317–330, 1995.

[47] G. Horton, S. Vandewalle, and P. Worley. An algorithm with polylog parallel complexity for solving parabolic partial differential equations. *SIAM J. Sci. Comput.*, 16:531–541, 1995.

[48] T.J.R. Hughes and G.M. Hulbert. Space-time finite element methods for elastodynamics: formulations and error estimates. *Comput. Methods Appl. Mech. Engrg.*, 66:339–363, 1988.

[49] S. Hussain, F. Schieweck, and S. Turek. Higher order Galerkin time discretizations and fast multigrid solvers for the heat equation. *J. Numer. Math.*, 19:41–61, 2011.

[50] S. Hussain, F. Schieweck, and S. Turek. A note on accurate and efficient higher order Galerkin time stepping schemes for the nonstationary Stokes equations. *Open Numer. Methods J.*, 4:35–45, 2012.

[51] H.B. Keller. Numerical methods for two-point boundary-value problems. *Blaisdell, Waltham, MA*, 1968.

[52] C.M. Klaij, J.J.W. van der Vegt, and H. van der Ven. Space–time discontinuous Galerkin method for the compressible Navier–Stokes equations. *J. Comput. Phys.*, 217:589–611, 2006.

[53] P. Lasaint and P.-A. Raviart. On a finite element method for solving the neutron transport equation. *Mathematical aspects of finite elements in partial differential equations (Proc. Sympos., Math. Res. Center, Univ. Wisconsin, Madison, Wis., 1974)*, pages 89–123. Publication No. 33, Math. Res. Center, Univ. of Wisconsin–Madison, Academic Press, New York, 1974.

[54] C. Lehrenfeld. Hybrid Discontinuous Galerkin methods for incompressible flow problems. Master's thesis, RWTH Aachen, 2010.

[55] J.-L. Lions, Y. Maday, and G. Turinici. A "parareal" in time discretization of PDE's. *C. R. Acad. Sci. Paris Sér. I Math.*, 332:661–668, 2001.

[56] J.-L. Lions and E. Magenes. *Non-homogeneous boundary value problems and applications. Vol. II.* Springer-Verlag New York, 1972.

[57] C. Lubich and A. Ostermann. Multigrid dynamic iteration for parabolic equations. *BIT*, 27:216–234, 1987.

[58] Y. Maday. A parareal in time procedure for the control of partial differential equations. *C. R. Math. Acad. Sci. Paris*, 335:387–392, 2002.

[59] Y. Maday and G. Turinici. The parareal in time iterative solver: a further direction to parallel implementation. *Lect. Notes Comput. Sci. Eng., Springer, Berlin*, 40:441–448, 2005.

[60] A. Masud and T.J.R. Hughes. A space-time Galerkin/least-squares finite element formulation of the Navier-Stokes equations for moving domain problems. *Comput. Methods Appl. Mech. Engrg.*, 146:91–126, 1997.

[61] T.P.A. Mathew. *Domain decomposition methods for the numerical solution of partial differential equations.* Springer, Berlin, 2008.

[62] D. Meidner and B. Vexler. Adaptive space-time finite element methods for parabolic optimization problems. *SIAM J. Control Optim.*, 46:116–142, 2007.

[63] P. Monk, J. Schöberl, and A. Sinwel. Hybridizing Raviart-Thomas elements for the Helmholtz equation. *Electromagnetics*, 30:149–176, 2010.

[64] A.D. Mont. *Adaptive unstructured spacetime meshing for four-dimensional spacetime discontinuous Galerkin finite element methods.* PhD thesis, University of Illinois, 2011.

[65] J. Nam, M. Behr, and M. Pasquali. Space-time least-squares finite element method for convection-reaction system with transformed variables. *Comput. Methods Appl. Mech. Engrg.*, 200:2562–2576, 2011.

[66] M. Neumüller. Eine Finite Elemente Methode für optimale Kontrollprobleme mit parabolischen Randwertaufgaben. Master's thesis, TU Graz, 2010.

[67] M. Neumüller and O. Steinbach. Refinement of flexible space-time finite element meshes and discontinuous Galerkin methods. *Comput. Visual. Sci.*, 14:189–205, 2011.

[68] M. Neumüller and O. Steinbach. A DG space–time domain decomposition method. *Domain Decomposition Methods in Science and Engineering XX (R. Bank, M. Holst, O. Widlund, J. Xu eds.). Lecture Notes in Computational Science and Engineering, vol. 91, Springer, Heidelberg*, pages 623–630, 2013.

[69] N.C. Nguyen, J. Peraire, and B. Cockburn. An implicit high-order hybridizable discontinuous Galerkin method for linear convection-diffusion equations. *J. Comput. Phys.*, 228:3232–3254, 2009.

[70] N.C. Nguyen, J. Peraire, and B. Cockburn. A hybridizable discontinuous Galerkin method for Stokes flow. *Comput. Methods Appl. Mech. Engrg.*, 199:582–597, 2010.

[71] J. Nievergelt. Parallel methods for integrating ordinary differential equations. *Comm. ACM*, 7:731–733, 1964.

[72] D. Orden and F. Santos. Asymptotically efficient triangulations of the d-cube. *Discrete Comput. Geom.*, 30:509–528, 2003.

[73] C. Pechstein. *Finite and Boundary Element Tearing and Interconnecting Solvers for Multiscale Problems*. Springer, Berlin, Heidelberg, 2013.

[74] A. Quarteroni and A. Valli. *Domain decomposition methods for partial differential equations*. The Clarendon Press, Oxford University Press, New York, 1999.

[75] W.H. Reed and T.R. Hill. Triangular mesh methods for the neutron transport equation. *Tech Report LAUR73479 Los Alamos National Laboratory*, Technical, Issue: LA-UR-73-479:1–23, 1973.

[76] O. Reichmann. Optimal space-time adaptive wavelet methods for degenerate parabolic PDEs. *Numer. Math.*, 121:337–365, 2012.

[77] T. Richter. Discontinuous Galerkin as Time-Stepping Scheme for the Navier–Stokes Equations. *Modeling, Simulation and Optimization of Complex Processes, Proceedings of the Fourth International Conference on High Performance Scientific Computing, March 2-6, 2009, Hanoi, Vietnam.*

H.G. Bock, H.X. Phu, R. Rannacher and J.P. Schlöder (eds.), Springer, 2012.

[78] T. Richter, A. Springer, and B. Vexler. Efficient numerical realization of discontinuous Galerkin methods for temporal discretization of parabolic problems. *Numer. Math.*, 124:151–182, 2013.

[79] B. Rivière. *Discontinuous Galerkin Methods for Solving Elliptic and Parabolic Equations*. Cambridge University Press, 2008.

[80] D. Ruprecht and R. Krause. Explicit parallel-in-time integration of a linear acoustic-advection system. *Comput. & Fluids*, 59:72–83, 2012.

[81] Y. Saad and M.H. Schultz. GMRES: a generalized minimal residual algorithm for solving nonsymmetric linear systems. *SIAM J. Sci. Statist. Comput.*, 7:856–869, 1986.

[82] O. Schenk, M. Bollhöfer, and R.A. Römer. On large-scale diagonalization techniques for the Anderson model of localization. *SIAM Rev.*, 50:91–112, 2008.

[83] O. Schenk, A. Wächter, and M. Hagemann. Matching-based preprocessing algorithms to the solution of saddle-point problems in large-scale nonconvex interior-point optimization. *Comput. Optim. Appl.*, 36:321–341, 2007.

[84] C. Schwab and R. Stevenson. Space-time adaptive wavelet methods for parabolic evolution problems. *Math. Comp.*, 78:1293–1318, 2009.

[85] J. Schöberl. NETGEN An advancing front 2D/3D-mesh generator based on abstract rules. *Computing and Visualization in Science*, 1:41–52, 1997.

[86] D. Schötzau and C. Schwab. An hp a priori error analysis of the DG time-stepping method for initial value problems. *Calcolo*, 37:207–232, 2000.

[87] G.A. Staff and E.M Rønquist. Stability of the parareal algorithm. *Lect. Notes Comput. Sci. Eng., Springer, Berlin*, 40:449–456, 2005.

[88] O. Steinbach. *Lösungsverfahren für lineare Gleichungssysteme. Algorithmen und Anwendungen*. B.G. Teubner, Stuttgart, Leipzig, Wiesbaden, 2005.

[89] O. Steinbach. *Numerical Approximation Methods for Elliptic Boundary Value Problems*. Springer, New York, 2008.

[90] K. Stüben and U. Trottenberg. *Multigrid methods: fundamental algorithms, model problem analysis and applications*. GMD-Studien [GMD Studies], 96. Gesellschaft für Mathematik und Datenverarbeitung mbH, St. Augustin, 1985.

[91] J.J. Sudirham, J.J.W. van der Vegt, and R.M.J. van Damme. Space–time discontinuous Galerkin method for advection–diffusion problems on time-dependent domains. *Appl. Num. Math.*, 56:1491–1518, 2006.

[92] T.E. Tezduyar. Interface-tracking and interface-capturing techniques for finite element computation of moving boundaries and interfaces. *Comput. Methods Appl. Mech. Engrg.*, 195:2983–3000, 2006.

[93] T.E. Tezduyar, M. Behr, and J. Liou. A new strategy for finite element computations involving moving boundaries and interfaces—the deforming-spatial-domain/space-time procedure. I. The concept and the preliminary numerical tests. *Comput. Methods Appl. Mech. Engrg.*, 94:339–351, 1992.

[94] T.E. Tezduyar, M. Behr, S. Mittal, and J. Liou. A new strategy for finite element computations involving moving boundaries and interfaces—the deforming-spatial-domain/space-time procedure. II. Computation of free-surface flows, two-liquid flows, and flows with drifting cylinders. *Comput. Methods Appl. Mech. Engrg.*, 94:353–371, 1992.

[95] T.E. Tezduyar and S. Sathe. Enhanced-discretization space-time technique (EDSTT). *Comput. Methods Appl. Mech. Engrg.*, 193:1385–1401, 2004.

[96] S. Thite. Adaptive spacetime meshing for discontinuous Galerkin methods. *Comput. Geom.*, 42:20–44, 2009.

[97] V. Thomée. *Galerkin Finite Element Methods for Parabolic Problems*. Springer, New York, 2006.

[98] A. Toselli and O. Widlund. *Domain decomposition methods—algorithms and theory*. Springer-Verlag, Berlin, 2005.

[99] U. Trottenberg, C. W. Oosterlee, and A. Schüller. *Multigrid*. Academic Press, Inc., San Diego, 2001.

[100] J.J.W. van der Vegt and H. van der Ven. Space–Time Discontinuous Galerkin Finite Element Method with Dynamic Grid Motion for Inviscid Compressible Flows: I. General Formulation. *J. Comput. Phys.*, 182:546–585, 2002.

[101] S. Vandewalle and E.V. de Velde. Space-time concurrent multigrid waveform relaxation. *Ann. Numer. Math.*, 1:347–360, 1994.

[102] S. Vandewalle and R. Piessens. Efficient parallel algorithms for solving initial-boundary value and time-periodic parabolic partial differential equations. *SIAM J. Sci. Statist. Comput.*, 13:1330–1346, 1992.

[103] P.S. Vassilevski. *Multilevel block factorization preconditioners*. Springer, New York, 2008.

[104] J. Česenek and M. Feistauer. Theory of the Space-Time Discontinuous Galerkin Method for Nonstationary Parabolic Problems with Nonlinear Convection and Diffusion. *SIAM J. Numer. Anal.*, 50:1181–1206, 2012.

[105] N.J. Walkington. Compactness properties of the DG and CG time stepping schemes for parabolic equations. *SIAM J. Numer. Anal.*, 47:4680–4710, 2010.

[106] T. Warburton and J.S. Hesthaven. On the constants in hp-finite element trace inverse inequalities. *Comput. Methods Appl. Mech. Engrg.*, 192:2765–2773, 2003.

[107] T. Weinzierl and T. Köppl. A geometric space-time multigrid algorithm for the heat equation. *Numer. Math. Theory Methods Appl.*, 5:110–130, 2012.

[108] P. Wesseling. *An Introduction to Multigrid Methods*. John Wiley & Sons Ltd., 1992. Corrected Reprint. Philadelphia: R.T. Edwards, Inc., 2004.

[109] T.P. Wihler and B. Rivière. Discontinuous Galerkin methods for second-order elliptic PDE with low-regularity solutions. *J. Sci. Comput.*, 46:151–165, 2011.

[110] J. Xu and J. Zou. Some Nonoverlapping Domain Decomposition Methods. *SIAM Rev.*, 40:857–914, 1998.

[111] A. Üngör and A. Sheffer. Tent-Pitcher: A Meshing Algorithm For Space-Time Discontinuous Galerkin Methods. *Proceedings, 9th International Meshing Roundtable, Sandia National Laboratories*, pages 111–122, 2000.

Monographic Series TU Graz

Computation in Engineering and Science

Vol. 1 Steffen Alvermann

Effective Viscoelastic Behaviour of Cellular Auxetic Materials
2008
ISBN 978-3-902465-92-4

Vol. 2 Sendy Fransiscus Tantono

The Mechanical Behaviour of a Soilbag under Vertical Compression
2008
ISBN 978-3-902465-97-9

Vol. 3 Thomas Rüberg

Non-conforming FEM/BEM Coupling in Time Domain
2008
ISBN 978-3-902465-98-6

Vol. 4 Dimitrios E. Kiousis

Biomechanical and Computational Modeling of Atherosclerotic Arteries
2008
ISBN 978-3-85125-023-7

Vol. 5 Lars Kielhorn

A Time-Domain Symmetric Galerkin BEM for Viscoelastodynamics
2009
ISBN 978-3-85125-042-8

Vol. 6 Gerhard Unger

Analysis of Boundary Element Methods for Laplacian Eigenvalue Problems
2009
ISBN 978-3-85125-081-7

Monographic Series TU Graz

Computation in Engineering and Science

Vol. 7 Gerhard Sommer

Mechanical Properties of Healthy and Diseased Human Arteries
2010
ISBN 978-3-85125-111-1

Vol. 8 Mathias Nenning

Infinite Elements for Elasto- and Poroelastodynamics
2010
ISBN 978-3-85125-130-2

Vol. 9 Thanh Xuan Phan

Boundary Element Methods for Boundary Control Problems
2011
ISBN 978-3-85125-149-4

Vol. 10 Loris Nagler

Simulation of Sound Transmission through Poroelastic Plate-like Structures
2011
ISBN 978-3-85125-153-1

Vol. 11 Markus Windisch

Boundary Element Tearing and Interconnecting Methods for Acoustic and Electromagnetic Scattering
2011
ISBN: 978-3-85125-152-4

Monographic Series TU Graz

Computation in Engineering and Science

Vol. 12 Christian Walchshofer

Analysis of the Dynamics at the Base of a Lifted Strongly Buoyant Jet Flame Using Direct Numerical Simulation
2011
ISBN 978-3-85125-185-2

Vol. 13 Matthias Messner

Fast Boundary Element Methods in Acoustics
2012
ISBN 978-3-85125-202-6

Vol. 14 Peter Urthaler

Analysis of Boundary Element Methods for Wave Propagation in Porous Media
2012
ISBN 978-3-85125-216-3

Vol. 15 Peng Li

Boundary Element Method for Wave Propagation in Partially Saturated Poroelastic Continua
2012
ISBN 978-3-85125-236-1

Vol. 16 Jörg Schriefl

Quantification of Collagen Fiber Morphologies in Human Arterial Walls
2012
ISBN 978-3-85125-238-5

Vol. 17 Thomas S. E. Eriksson

Cardiovascular Mechanics
2013
ISBN 978-3-85125-277-4

Monographic Series TU Graz

Computation in Engineering and Science

Vol. 18 Jianhua Tong

Biomechanics of Abdominal Aortic Aneurysms
2013
ISBN 978-3-85125-279-8

Vol. 19 Jonathan Rohleder

Titchmarsh–Weyl Theory and Inverse Problems for Elliptic Differential Operators
2013
ISBN 978-3-85125-283-5

Vol. 20 Martin Neumüller

Space-Time Methods
2013
ISBN 978-3-85125-290-3